**Universidade de Aveiro**
**2017**
Departamento de Engenharia de Materiais e Cerâmica

**Aleksey Lisenkov**

# Síntese eletroquímica de filmes de óxido finos em superfícies de titânio e alumínio usando anodização a altas tensões.

# Electrochemical synthesis of thin oxide films on titanium and aluminium surfaces using high voltage anodisation technique.

**Universidade de Aveiro**
**2017**
Departamento de Engenharia de Materiais e Cerâmica

**Aleksey Lisenkov**

# Síntese eletroquímica de filmes de óxido finos em superfícies de titânio e alumínio usando anodização a altas tensões.

# Electrochemical synthesis of thin oxide films on titanium and aluminium surfaces using high voltage anodisation technique.

Tese apresentada à Universidade de Aveiro para cumprimento dos requisitos necessários à obtenção do grau de Doutor em Ciência e Engenharia de Materiais, realizada sob a orientação científica do Doutor Mário G.S. Ferreira, Professor Catedrático do Departamento de Engenharia de Materiais e Cerâmica da Universidade de Aveiro

Apoio financeiro da FCT, referência SFRH/BD/78628/2011

Dedicated to my mother Iryna and to the memory of my father Dmitry for their immense love and care

**o júri**

presidente

Prof. Doutor Vasile Staicu
professor catedrático de Departamento de Matemática da Universidade de Aveiro

Prof. Doutor Mário Guerreiro Silva Ferreira
professor catedrático de Departamento de Engenharia de Materiais e Cerâmica da Universidade de Aveiro

Prof. Doutor João C. Salvador Fernandes
professor associado de Departamento de Engenharia Química da Instituto Superior Técnico

Prof. Doutor Christopher M.A. Brett
professor catedrático de Departamento de Química da Faculdade de Ciências e Tecnologia da Universidade de Coimbra

Prof. Doutor Carlos Manuel Melo Pereira
professor auxiliar da Faculdade de Ciências da Universidade do Porto

Prof. Doutor Jorge Ribeiro Frade
professor catedrático de Departamento de Engenharia de Materiais e Cerâmica da Universidade de Aveiro

**agradecimentos**

I would like to express sincere gratitude to my supervisors Professor Mário Ferreira and Dr. Mikhail Zheludkevich for inviting me in Portugal, their help, guidance and advises during my PhD studies.
I address many thanks to Dr. Syargei Poznyak for his help with the experimental work, guidance, interesting and motivating discussions. I am particularly thankful to my colleagues and friends Dr. Silvar Kalip, Dr. Joao Tedim, Dr. Dmitry Ivanou, Dr. Kiryl Yasakau, Alena Kuznetsova, Maksim Starykevich, Claudio Almeida, Jorge Carneiro, Dr. Andrei Salak, Dr. Tiago Gavão, Dr. Isabel Sousa, Dr. Alexandre Bastos, Dr. Ricardo Serra, Dr. Alexei Yaremchenko, Dr. Fred Maia, Olga Karavai, Dr. Andrey Kavaleuski, Dr. Sergey Mikhalev, Ana Caetano, Diogo Almeida, Kiryl Zakharchuk who helped in my work. Also, I would like to express gratitude to Prof. Dr. M. Fátima Montemor and Prof. Dr. M.J. Carmezim for thier help during my visits to IST.
Many thanks go to people in DEMaC that assisted and helped me during all those years. I personally to thank Marta Ferra for opening me the world of electron microscopy. Many thanks to Luísa, Alexandra, Paulo, Sophia, Carla from secretary of DEMaC.
Specially I would like to thank Zinaida for her love, bringing joy to my life and supporting me during these years.

**palavras-chave**

anodização, fimes finos de óxidos, alumínio, titânio, oxidação por descarga pulsada de alta tensão, EIS, SKPFM, revestimentos sem impurezas

**resumo**

A síntese eletroquímica de filmes finos de óxido usando a técnica de oxidação de alta tensão e a investigação da estrutura, propriedades físicas e químicas dos filmes obtidos são os principais objetivos desta tese. A anodização de metais sob a ação de vários kilovolts produz filmes com espessura pequena (até 180 nm) e com propriedades diferentes dos filmes formados usando técnicas eletroquímicas convencionais. As camadas de óxido depositadas desta forma conferem, frequentemente, melhores propriedades de proteção, semicondutoras e fotoeletroquímicas. No âmbito deste trabalho filmes finos sobre titânio e alumínio foram preparados em diferentes eletrólitos, incluindo soluções de ácidos e sais, bem como em água desionizada e peróxido de hidrogénio. Mostra-se que os filmes preparados por oxidação com descarga pulsada de alta tensão têm estrutura superficial e propriedades elétricas mais uniformes em comparação com os obtidos por anodização convencional.

Outro objetivo do trabalho é a dopagem dos filmes anódicos com diferentes dopantes, por incorporação de espécies do eletrólito durante a formação do filme. Os filmes preparados por oxidação de descarga pulsada de alta tensão no titânio mostram uma melhor resposta de fotocorrente a comprimentos de onda pequenos e uma concentração mais baixa de dadores ionizados, relativamente aos filmes obtidos por anodização convencional. Os filmes preparados por descarga no alumínio e titânio são formados por uma camada compacta. Estudos sobre o processo de descarga revelaram que o principal fator que influencia a cinética de crescimento do filme de óxido é a concentração de defeitos pontuais, que por sua vez é determinada pela composição do eletrólito. Também se mostrou que as técnicas usando alta tensão permitem preparar filmes anódicos não só em soluções convencionais, mas igualmente em outros meios, tal como água desionizada, água destilada e peroxido de hidrogénio, onde a anodização por métodos convencionais (potenciostático ou galvanostático) é impossível. Além disso é revelado que a técnica da descarga pulsada de alta tensão é um método eficiente para encapsulação de nanocilindros de metal, preliminarmente depositados em nanoporos de titânia e alumina alinhados verticalmente.

**keywords**

anodisation, thin oxide films, aluminium, titanium, powerful pulsed discharge oxidation, EIS, SKPFM, impurity-free coatings

**abstract**

Electrochemical synthesis of thin oxide films by using the high-voltage oxidation technique and investigation of structure, physical and chemical properties of the obtained films are the main objectives of this thesis. Anodisation of metals under action of several kilovolts allow to produce films with rather low thickness (up to 180 nm) and with properties different from the films created by using conventional electrochemical approaches. The oxide layers deposited in this way often confer advanced protective, semiconductor and photoelectrochemical properties. In the frame of this thesis thin films on titanium and aluminium were prepared in several electrolytes, including solutions of acids and salts as well as in deionised water and hydrogen peroxide. It is shown that the films prepared by powerful pulsed discharge oxidation are characterized by more uniform surface structure and electrical properties in comparison to those obtained by conventional anodization. Another aim of the work is doping of the anodic films with different dopants by incorporation of species from the electrolyte during the film formation. Films prepared by powerful pulsed discharge oxidation technique on titanium demonstrate a significantly improved photocurrent response at short wavelengths and an essentially lower concentration of ionized donors as compared with the films obtained by conventional anodization. The discharge-prepared films on both aluminium and titanium are composed by one compact layer. Studies of the discharge processes revealed that the main factor influencing the kinetics of the oxide film growth is the concentration of point defects which, in turn, is determined by the composition of electrolyte. Also, it was shown that the high voltage techniques allow to prepare anodic films not only in conventional solutions, but also in other media such as deionised water, distilled water and hydrogen peroxide, where anodisation by conventional (potentiostatic or galvanostatic) methods is impossible. Furthermore, the powerful pulsed discharge technique is shown as efficient method for encapsulation of metal nanorods preliminarily deposited into the vertically aligned titania and alumina nanopores.

# Table of Contents

# List of figures:

**Figure 4.1.9.** Evolution of the ionized donor concentration, $N_d$, calculated from the Mott-Schottky plots, with thickness of the anodic oxide films prepared by the conventional galvanostatic oxidation and the pulsed discharge method.

**Figure 4.1.10.** Photocurrent spectra of the anodic oxide films with different thickness prepared by the pulsed discharge method (a) and conventional galvanostatic anodizing (b). Electrode potential: 0.8 V vs. SCE.

**Figure 4.2.1.** Time evolution of the current through aluminium electrode during first 4 μs. Inset shows schematically a profile of the pulsed discharge as a whole. Dashed area represents the total charge passed through the electrode.

**Figure 4.2.2.** (Color online) Bode plots of the oxide films formed on aluminium surface as a result of pulsed discharge anodisation; solid lines represent the fitting results.

**Figure 4.2.3.** TEM cross sections of the aluminium samples anodized by application of 3 (a) and 10 (b) discharge pulses.

**Figure 4.2.4.** Maps of the surface topography (left) and Volta potential difference (right) of the aluminium sample before (a, b) and after (c, d) the pulsed discharge anodisation procedure (10 pulses applied).

**Figure 4.2.5.** Volta potential difference *versus* thickness of the alumina films prepared by pulsed discharge anodisation method before (solid squares) and after (open circles) annealing at 300°C. The inset shows magnification of the plot for the thickness range of 1-45 nm. The reference levels corresponding to the measured VPD values for the untreated aluminium sample and non-anodized sample thermally oxidized at 300°C are indicated.

**Figure 4.2.6.** Schematic representation of charge distribution in alumina film polarized as a result of anodisation: after *N*th pulsed discharge (a), during the 1st step of the discharge (in a field of ~ $10^9$ V/cm) (b), and after $(N+1)^{th}$ pulsed discharge (c). Provided the same charge is embedded, the induced potential is proportional to the film thickness, *d*. Charge distribution in the pulsed discharge films is suggested to be essentially similar to that in the films produced by combination of the galvanostatic and potentiostatic methods.

**Figure 4.3.1:** Cross-section TEM image of the anodic film on titanium prepared by high voltage method in 1M $H_3PO_4$ after 5 discharges (thickness of the film is about 120 nm).

**Figure 4.3.2:** Fitting model (a) and EIS spectra of $TiO_2$ films prepared in 2M $H_3PO_4$ solution recorded at different polarizations (from +0.8V to -0.4V vs. $Hg/HgSO_4$ reference electrode with step 0.2V) with thicknesses of the oxide films 70nm (b) and 120 nm (c).

**Figure 4.3.3:** Fitting results of 70 nm (a) and 120 nm (a) titanium oxide films under -0.2V polarization.

**Figure 4.3.4:** Mott-Schottky plots calculated from the SCR capacitance on titania films (with thickness 70 nm (a) and 120 nm (b)) obtained in electrolytes with different concentrations.

**Figure 4.3.5:** Ionized donor concentration, $N_d$ (a), and photocurrent spectra (b) of $TiO_2$ films prepared in $H_3PO_4$ solutions with different concentrations.

**Figure 4.3.6:** Topology (top) and measured potential distribution (bottom) on titania films with thickness 95 nm prepared by pulsed discharge anodisation in phosphoric acid electrolytes with different concentrations ( 1M (a), 2M (b) and 4M (c)).

**Figure 4.3.7:** Volta potential measured on the titanium oxide films prepared by PPDO method in $H_3PO_4$ solutions with different concentrations.

**Figure 4.3.8**: Influence of the concentration of $H_3PO_4$ on the current profiles during pulse oxidation.

**Figure 4.4.1**: SEM images of the film breakdown on the oxides prepared at applied voltage of 2000 V by the potentiostatic (A) and discharged (B) methods.
**Figure 4.4.2**: (A) Discharge plots for the aluminium anodisation by discharge method at different potentials applied to the Al electrodes. (B) Discharge plots for the aluminium anodisation by discharge method at 1000 V applied to the electrode covered with oxide film with different thicknesses.
**Figure 4.4.3**: TEM cross sectional images (A, B) and SEM images (C, D) of aluminium oxide prepared by high-voltage potentiostatic (A, C) and discharge (B, D) methods.
**Figure 4.4.4**: SKPFM images of aluminium samples with oxide thickness of 15 nm anodised by high-voltage anodisation at applied voltage of 1600V by potentiostatic (A) and discharge (B) methods. Volta potential difference versus thickness of the alumina films (different number of discharges) prepared by discharge method at an applied voltage of 1600V (C).
**Figure 4.4.5** The impedance spectra recorded on as-polished Al with a native oxide film (black solid) and anodized aluminium in different conditions: Al with: 10 nm thick oxide prepared by potentiostatic method in deinonized water (red dashed line); oxide with thickness of 20 nm prepared by discharged method in deionised water (blue dotted line); oxide with thickness of 20 nm prepared by conventional anodisation in ammonium pentaborate solution (green dash-dot). Experimental: points; Fitting: lines.
**Figure 4.5.1.** SEM images of the pure porous titania (A, C) and alumina (B, D) before (A, B) and after (C, D) application of 5 discharge pulses with a potential of 1600V.
**Figure 4.5.2.** Typical CVA of aluminium deposition into titania nanopores at sweep rate of 50 mV/s
**Figure 4.5.3.** SEM image of the titania pores filled with aluminium in potentiostatic mode (A) and by potential cycling (B)
**Figure 4.5.4.** Discharge plots of the nanoporous alumina (A) and titania (B) filled with Ti-Al and Al, respectively.
**Figure 4.5.5.** Cross-section of the film (A) and top view (B) of the alumina pores filled with Ti-aluminium alloy after action of 10 discharge pulses applied at 1600V (A) and 1800V (B).
**Figure 4.5.6.** Surface of the titania nanotubes filled with aluminium after action of 10 discharge pulses at 1600V (A) and 1800V (B).
**Figure 4.6.1.** Typical discharge plots on the aluminium electrodes in hydrogen peroxide, water and ammonium pentaborate at 1400V. The inset shows magnification of the plot for the period up to 0.1 ms after discharge.
**Figure 4.6.2.** Comparison of current plots on $1^{st}$ and $10^{th}$ discharges on the aluminium electrode in water at different potentials at 1600V (a) and 2000V (b).
**Figure 4.6.3.** Discharge plots in the titanium obtained in different electrolytes (a) and charge evolution in hydrogen peroxide obtained at 1400V (b) and 2000 V (c).
**Figure 4.6.4.** SEM image of the titania film obtained by applying of 5 discharge pulses at 2000V.
**Figure 4.6.5.** EIS spectra of the alumina obtained in water (black, solid) and hydrogen peroxide (red, dash) electrolytes prepared by powerful pulsed discharge oxidation at 1400V. Experimental: points; Fitting: lines.
**Figure 4.6.6.** Cross-section TEM image of the anodic film on aluminium prepared in hydrogen peroxide by action of 5 discharges at 1400V.

**Figure 4.6.7.** Impedance spectra of the 120 nm thick anodic oxide films under polarization formed on titanium in water (A) and hydrogen peroxide (B) electrolytes. Equivalent circuit used for fitting (C).

**Figure 4.6.8.** Topology (A,B) and measured potential distribution (C,D) on alumina films with thickness 60 nm prepared by pulsed discharge anodisation in water (A,C) and hydrogen peroxide (B,D); obtained at 1400V.

**Figure 4.6.9.** Dependence of Volta potential from the thickness on the aluminium oxides prepared in water (a) and hydrogen peroxide (b) electrolytes.

**Figure 4.6.10** Topology (left) and measured potential distribution (right) on titania films with thickness 60 nm prepared by pulsed discharge anodisation in hydrogen peroxide.

**Figure 4.6.11.** Dependence of Volta potential on the thickness of the titania prepared at different potentials and electrolytes

**Figure 4.6.12.** Dependence of Volta potential on the thickness of titania after 1, 4 and 24 hours of film preparation. Titania was prepared by pulsed discharge anodisation at 1400V in hydrogen peroxide.

## List of tables:

## List of abbreviations and symbols:

| | |
|---|---|
| A | Surface area |
| AES | Auger Electron Spectroscopy |
| AFM | Atomic Force Microscopy |
| α | Fractional exponent of equivalent circuit responsible for CPE |
| C | Capacitor in equivalent circuits |
| C, *Cox , Cred* | Concentration of oxidative and reductive species |
| CE | Counter electrode |
| CPD | Contact potential difference |
| CPE | Constant phase element |
| d | Distance, thickness |
| DC- polarization | Direct current polarization |
| *E* | Field strength |
| E | Electrode potential |
| $E_{eq}$ | Equilibrium potential |
| EEC | Equivalent electric circuits |
| $e_{CB-}$ | Electron in conduction band |
| EDS | Energy Dispersive Spectroscopy |
| EIS | Electrochemical Impedance Spectroscopy |
| ε | Dielectric constant |
| $ε_0$ | Permittivity of free space |
| GS | Galvanostatically deposed films |
| $h_{VB+}$ | Hole in valence band |
| *I* | Current |
| F | Faraday constant |
| *ω* | Frequency |
| Φ | Work function |
| *j* | Current density |
| $j_{crit}$ | Critical current |
| $j_p$ | Passive current density |
| PD | Pulsed deposed films |
| PPDO | Powerful pulsed discharge oxidation |
| L | Inductor in equivalent circuits |
| $N_d$ | Ionized donor concentration |
| n | Number of electrons involved in electrochemical process |
| nm | Nanometer |
| Q | Parameter of equivalent circuit responsible for CPE |
| R | Resistor in equivalent circuits |
| RE | Reference electrode |
| SCE | Saturated calomel electrode |
| SEM | Scanning Electron Microscopy |

| | |
|---|---|
| SKPFM | Scanning Kelvin Probe Microscopy |
| SHE | Standard Hydrogen Electrode |
| *T* | Time |
| T | Temperature |
| TEM | Transmission Electron Microscopy |
| XPS | X-ray Photoelectron Spectroscopy |
| U | Voltage |
| $U_p$ | Passivation potential |
| $U_{ocp}$ | Open circuit potential |
| VPD | Volta potential difference |
| *Y* | Admittance |
| *Z* | Impedance |

# 1. Introduction

Electrochemical anodizing of valve metals (aluminium, tantalum, niobium, zirconium, titanium, zinc etc.) is a very important process that is widely used for capacitor manufacturing, enhancing the corrosion protection and modification of the metal surface properties, such as wear-resistance, friction, hardness, and aesthetic properties. Usually anodic films are prepared using dc polarization of a metal under potentiostatic, galvanostatic or combined (galvanostatic and then potentiostatic) control [1]. Electrochemical oxidation (anodisation) of many metallic materials provides thick oxide layers demonstrating improved protective and functional properties [2].

A great interest has recently arisen to a relatively new electrochemical technique called micro-arc oxidation (MAO) or plasma electrolytic oxidation (PEO)[3]. This technique operates at enhanced voltages when anodizing is accompanied by film breakdown, and is characterized by multiple arcs moving over the treated surface. Under these conditions, owing to plasma thermochemical interactions during the local surface discharges, the formation of not only oxides but more complicated composite inorganic coatings, exhibiting a set of excellent protective, mechanical and dielectric properties, is possible as well. However, this method does not allow preparing relatively thin anodic films (nanometers and tens of nanometers).

Recently the application of the high-voltage pulsed discharge technique for creation of thin anodic films on titanium[4] was suggested. Under the action of single powerful electric discharges in electrolyte, extremely high rates (40-150 μm/s) of the oxide film growth were reached on the titanium anode. The growth rate is the fastest ever reported. The results of elemental analysis showed that the oxide films prepared by the pulsed discharge method are characterized by high stoichiometry and more homogeneous distribution of basic elements (Ti and O) through the film thickness in comparison to the films grown by the conventional galvanostatic anodisation. Moreover, enhanced photoelectrochemical activity was revealed for the pulse discharge-prepared films motivating their further investigation[4-5].

The novelty of this method and the possibility to prepare thin uniform films, with unique properties are the main driving forces for deeper research of the powerful pulsed discharge high voltage oxidation technique. Preparation of the oxide films, studies of the anodisation kinetics and properties of the obtained films are the main aims of the current PhD work. Possibility of impurity-free anodic oxide films preparation on valve metals, particularly aluminium, by high-voltage anodization (both discharge and galvanostatic) in deionized water was also demonstrated. The obtained films were studied by different methods, including electrochemical impedance spectroscopy (EIS), electron microscopy (SEM, TEM), photocurrent spectroscopy, scanning Kelvin probe force microscopy (SKPFM) among others. Taking into account the novelty of the technique, a big part of the work is aimed at revealing the mechanism of the oxidation during the discharge. For comparison reasons, corresponding studies of films grown by conventional galvanostatic or potentiostatic oxidation in the same electrolytes are also discussed.

# 2. State of the art.

## 2.1 Anodisation of titanium

### 2.1.1 Native oxide film on titanium.

Owing to the excellent mechanical properties and the high corrosion resistance, titanium and titanium alloys are widespread applied in aircraft, automotive and chemical industry, as well as in medical implants.

Titanium is known as a highly reactive metal, which is readily oxidized in the different media. Oxidation kinetics are extremely fast, thus oxidation can take few nanoseconds[6]. Due to the high reactivity of titanium and the short time scales, titanium is almost always covered by an oxide layer. In practice, pure metallic titanium surfaces can only exist under certain artificial conditions, under ultra-high vacuum. In most cases the oxidized surface layer consists mainly of the most stable titanium oxide, titanium dioxide ($TiO_2$). When the oxidation process takes place in an oxygen-free medium, other surface layers can be formed (e.g. nitrides, carbides etc.) However, even in this case the coating will convert into oxides after exposure to air or water in most of the cases.

In contrast to titanium, $TiO_2$ is a stable compound, which is resistant to chemical attack by most of the substances. In can be dissolved only by a few acids, such as HF. Due to presence of this oxide titanium has excellent chemical and corrosion resistance[7]. However, chemical stability of the titania doesn't mean its chemical inertness. $TiO_2$ surfaces can react with aqueous solutions, resulting in its changes, they can irreversibly adsorb and dissociate the organic molecules from air. It is also well known in the surface science community that $TiO_2$ surfaces act as catalysts for a certain number of chemical reactions[8].

The main part of the physical and chemical properties of any material surface strongly depends of the conditions under which it is formed. This is also true for titanium, because of its reactivity combined with the chemical activity of its oxides leads to a variety of possible surface reactions and products. The oxidation kinetics and the final surface oxide properties are influenced by surface pretreatment, temperature, and type and concentration of oxidizing species. In addition, certain impurities have a catalysing or an inhibiting effect on the oxidation. For further studies of the oxide film formation it is important to understand kinetics of native film formation. One of the most convenient and widely used method is based on use of polarization curves[9]. A schematic semilogarithmic polarization curve is shown in Figure 2.1.1. In current case only the anodic direction of polarization, i.e. towards positive potential is presented. During sweeping of the potential to the positive direction, from the open circuit potential ($U_{ocp}$), the current will increase quickly to considerably high values. It should be mentioned that shape of the curve is often characterized by Tafel equation[10]. In these conditions oxide film forms, and current will reach a critical value ($j_{crit}$). In this case passivation of the metal will take place. This

oxide formation is manifested by a dramatic drop of current in the polarization curve at the passivation potential ($U_p$). The anodic current density in this region is lower for several orders of magnitude and is called the passive current density ($j_p$). Minor currents in this region relate to some conductivity of the thin film[11]. With a continuous sweep towards higher potential, current will start to rise. This region, where the current rapidly increases as the potential rise, is the trans-passive region. It can be associated essentially to the following processes: further oxidation or decomposition of the film, oxygen evolution or other electrolyte decomposition reactions[1].

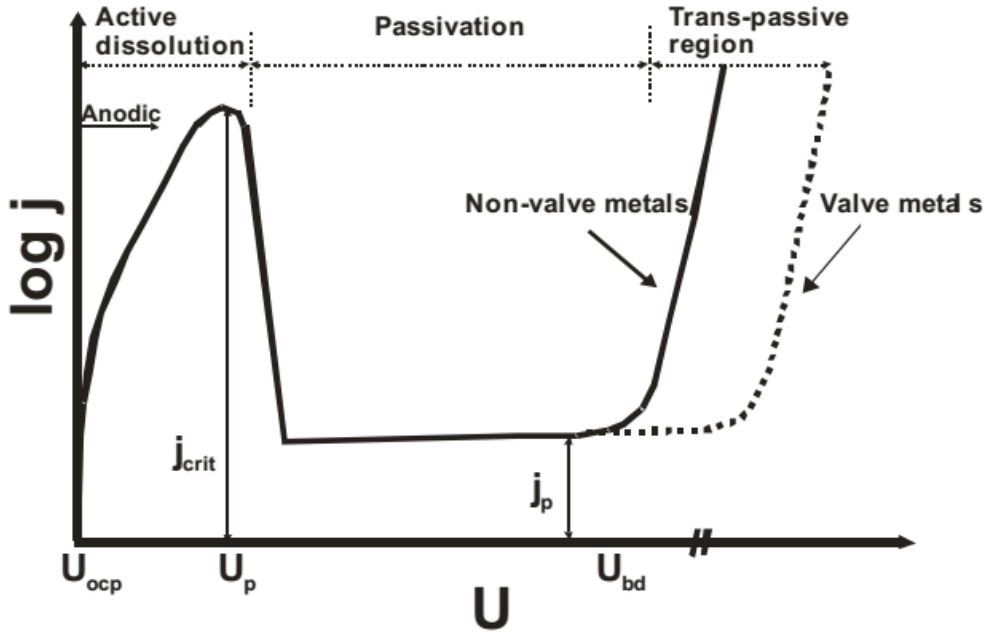


**Figure 2.1.1** Schematic anodic polarization curve for a metal electrode[11].

It should be mentioned that depending on the metal, the width of passivation region may vary significantly. For all valve metals, including Ti, this region is usually very wide can achieve values of dozens of volts. In the case of non-valve metals it is smaller and, for instance, for Fe it is less than 2V[12].

Once the passive film is formed, it cannot be described as a rigid layer, but instead the system is in dynamic equilibrium between film dissolution and growth. Chemical composition and the thickness of electrochemically formed passive films depend on a number of parameters, such as the electrolyte composition, temperature, time, positive potential, etc. For titanium and other valve metals, the passive film thickness increases linearly with the positive potential.

### 2.1.2 Growth of anodic film on titanium

The spontaneously formed passive films on titanium are thin and dense. However, they are not always suitable for the modern technologies. In many cases a thicker film is required to increase corrosion stability of different structures, decorative reasons, enhancement of photovoltaic properties, etc. Typical approaches to grow thick $TiO_2$ layers usually include two different techniques[1]: an anodic oxidation of Ti, where an applied electric field controls the ion

($O^{2-}$, $Ti^{4+}$) movement during the oxide growth, and a thermal oxidation of Ti, at which the oxygen ion diffusion controls the $TiO_2$ layer thickness. There are some other methods of preparation of titania such as sol–gel [13], chemical vapour deposition (CVD) [14], physical vapour deposition (PVD). However, these methods are usually used for a special reason and they will not be discussed in the frame of current work. The stability and electrochemical properties of the $TiO_2$ layer depend on its preparation mode but also on the mode of preparation of the titanium substrate itself. In order to perfectly control the Ti/$TiO_2$ interface, a sophisticated procedure of mechanical and electrochemical polishing has to be carried out[15]. Different properties of the grown oxides, such as structure, concentration of ionized donors, permittivity, conductivity, are important in different fields of industry and technology.

Both conventional processes are time-dependent: in the case of galvanostatic anodisation, applied potential results in an electric field that is reciprocal of thickness and decreases following the logarithmic kinetic law, whereas in the case of thermal oxidation the oxygen diffusion rate is proportional to the square root of time[16]. One should also mention that Ti is a typical example of a valve metal (as well as Al, Ta, etc.). Valve metals represent a class of metals that can be anodized to grow considerably thicker oxide layers (several hundred nm), whereas on the other common metals (e.g. Fe, Ni), only a few nm thick oxide layers can be achieved. On the other hand, there are a number of approaches to decrease the thickness of the oxide layer, or to completely remove it. In addition to the mechanical and physico-chemical methods such as polishing, or sputtering, purely chemical approaches can also be used. Typical compounds that can chemically dissolve $TiO_2$ are namely acidic HF and $H_2O_2$ solutions and high alkaline hydroxide solutions (via a formation of soluble complexes). Immersion of Ti / $TiO_2$ substrates in these agents may lead to complete $TiO_2$ removal, but the Ti surface after such treatment will again immediately reoxidize and form a thin native $TiO_2$ layer, as soon as it has access to the atmosphere, or moisture.

**Classification of anodic films**

Usually the anodic films which can be obtained on metals can be classified as noncontinuous, continuous and duplex[17] . Noncontinuous films are the coatings which have various pores or defects in their structure. They grow under an positive potential near the equilibrium potential of the metal. Usually, they are crystalline and precipitated from the reaction of ionized metal and electrolyte. Sometimes the coatings can detach from the metal substrate. As a typical example of such film $MnO_2$ deposited on a stainless-steel anode from manganese sulphate electrolyte can be mentioned. Very often these films are semiconductive [18-24]In contrast to noncontinuous, continuous films may be either electronic conductors or insulators. In the first case, passive films on Ni, Cr, stainless steel, show usually semiconductive nature and cannot be prepared thick [25-26]. On the second case, anodisation of the valve metals (Al, Ta, Nb, etc.) results in preparation of a continuous coating. In these metals, very thin films of about 5 nm covers the metal surface completely and usually consist of amorphous oxide. These films can be prepared with thickness of 1 μm, however this requires very high anode polarization, which can reach up several hundred volts [22, 27-30].

Duplex film can be obtained when a continuous film is partially transformed into a noncontinuous film. A typical example is the thick anodic coating on aluminium.

**Kinetics of titanium anodisation**

Anodic oxidation is a widely used method for producing different types of protective oxide films on metals, especially on aluminium. The main technological use of titanium anodisation is connected with improving adhesive bonding, in particular in the aerospace industry. It can also be used for producing oxides with high thicknesses, coloration, and porous coatings. The physical and chemical properties of the anodic oxides on titanium can be varied in wide range by controlling the process parameters, such as anode potential, electrolyte composition, temperature and current. Different acids ($H_2SO_4$, $H_3PO_4$, acetic acid and others), as well as alkalis are commonly-used electrolytes for anodic oxidation of titanium.

The main reactions leading to oxidation at the anode can be presented as:

$$Ti = Ti^{2+} + 2e^- \qquad (2.1)$$

$$Ti^{2+} + 2O^{2-} = TiO_2 + 2e^- \qquad (2.2)$$

The titanium and oxygen ions formed in these redox reactions are driven through the oxide by the applied electric field, leading to growth of the oxide. The anodic titanium oxides have a high resistivity in comparison with the electrolyte and the metallic parts of the electrical circuit, thus the applied voltage drop will occur mainly through the oxide film on the anode. Kinetics of titania formation can be described through mass transfer[9, 31]. In such case one of the ionic species has to migrate through the oxide. During anodisation Ti oxidation and migration of $O^{2-}$ ions towards the Ti/oxide interface and $Ti^{4+}$ ions to the opposite direction takes place. Due to their recombination a continued growth of the film occurs. As long as the electric field is strong enough to drive the ions through the oxide, the current will flow and the oxide will continue to grow. According to this, the final oxide thickness, d, is almost linearly dependent on the applied voltage, U:

$$d \approx \alpha U, \qquad (2.3)$$

where α is a growth constant which is usually in range of 1.5-6 $nmV^{-1}$. This linear relationship can be observed below the dielectric breakdown limit of oxide, which is around 100 V depending on electrolyte and other process conditions. Anodisation can be performed either at constant current (galvanostatic anodisation) or at constant potential (potentiostatic anodisation). If the anodisation is carried out at voltages above the breakdown limit, conventional anodisation will no longer take place and at such conditions the process will lead to increased gas evolution and frequently also sparking. This type of anodizing is usually called plasma electrolytic oxidation (PEO) or spark anodizing. It results in less uniform and more porous oxide films than conventional anodisation below the dielectric breakdown limit.

Many anodic oxides, including $TiO_2$, are semiconductors. The defects that exist in the structure may strongly influence the ionic and electronic transport[32]. Models for the oxide growth consider different processes to be rate determining[31-32].

The presented high-field models are relevant for the $TiO_2$ growth, as well as for any other valve metal oxides. The first experiments regarding the ionic conductivity of oxide films on

aluminium have been performed in 1934 Günterschultze and Betz[33],followed by Verwey in 1935[34]. In the first work it was realized that current density *j* was exponentially dependent on the field strength *F* according to:

$$j = \alpha \exp(\beta . E), \qquad (2.4)$$

where *j* represents the current density, *α* and *β* are constants and *E* is the field strength across the oxide. They provided values *α* and *β* for a variety of valve metals based on the thickness obtained from capacitance measurements. The metal/oxide interface was firstly taken in account in works of Mott and Cabrera[35-36]. Later, Dewald[37] took into account semiconductive nature of titania and made the extension to their theory by including the effects of the space charge layer. It was shown that in the presence of sufficiently high fields (> $10^6$ V / m) at low or moderate temperatures pure diffusion of ionic species results in negligible contribution for the film growth. The field strength *E* across the oxide film can be estimated from the potential drop across the oxide (∆U) and the thickness of the oxide *d* by the following equation:

$$E = \Delta U / d \qquad (2.5)$$

Thus, the thickness of the barrier layer is in reverse proportion to the logarithm of current density (*j*) for a given anodisation potential *U*. When positive potential is applied to the working electrode, oxide film starts to grow and this results in exponential decrease of the current density, because the field strength across the oxide continuously decreases[38]. Thus film growth (at constant voltage) is self-limiting as *F* is lowered with increasing film thickness. This thickness of the obtained film can be described as:

$$d^{-1} = A - B \log(t), \qquad (2.6)$$

where *A* and *B* are constants and *t* is time.

According to this equation an infinite oxide growth would take place, however, usually the limiting situation can be reached, when the formation rate of the oxide has dropped to the value of the chemical dissolution rate in the electrolyte.

In reality, metallic substrate has a lot of defects (dislocations, scratches, etc.) and non-homogenous current flow through these areas takes place. Schultze et al.[39-40] studied influence of the field effects on the oxide film thickness and they has found that oxide thickness almost does not change, and fluctuations of films thickness usually are less than few percent. It shows that if current flows at one moment through a thinner oxide area, this area will get thicker and the current will likely find again another (easier) path to flow and thicken the oxide film there. As a result at the end of anodisation substrate is covered with an oxide layer of homogenous thickness.

The most well-studied anodic oxide films on titanium are formed by galvanostatic anodisation below the breakdown potential [24, 27, 41-45]. The oxide thickness can easily be varied since it is linearly dependent on anodizing voltage. Growth rates for films formed in $H_2SO_4$ are typically around 2 nm $V^{-1}$ [24, 27, 44], however values ranging from 1.5 to 6 nm $V^{-1}$ have also been reported.

## 2.1.3 Structure and properties of anodic $TiO_2$

It is known that titanium dioxide can exist in three different crystalline forms, namely rutile, anatase, and brookite[46].The most stable form is rutile. All three polymorphs can be easily synthesised in the laboratory, and the metastable anatase and brookite can slowly transform into the thermodynamically more stable rutile, especially during the calcination at temperatures higher than 600 °C[47]. The main difference in polymorphs is related to their structures, thus in rutile the octahedra share edges at (0 0 1) planes to give a tetragonal structure (Fig. 2.1.2a), while anatase is composed of corner sharing octahedra which form (0 0 1) planes (Fig. 2.1.2b) resulting in a tetragonal structure. In brookite both edges and corners are shared to give an orthorhombic structure (Fig. 2.1.2c) [48]. In all forms, titanium ($Ti^{4+}$) atoms are co-ordinated with six oxygen ($O^{2-}$) atoms, forming octahedral [$TiO_6$].

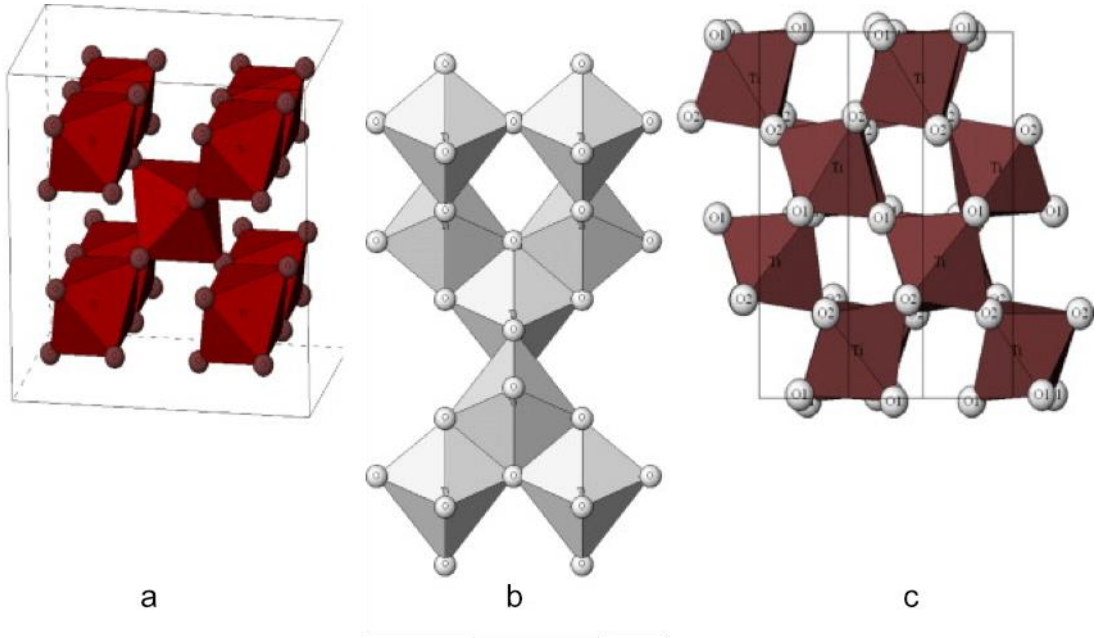


**Figure 2.1.2.** Different forms of titanium dioxide: rutile (a), anatase (b) and brookite (c)

Titania obtained by conventional methods (like electrochemical anodisation, thermal oxidation, etc.) is typically an n-type semiconductor due to the deficiency of oxygen atoms [49]. The band gap varies for the different forms of oxide and has a values of 3.2 eV for anatase, 3.0 eV for rutile, and ~ 3.2 eV for brookite [50]. The most widely investigated polymorphs of the titania are anatase and rutile due to their high photo-activity, low cost, low toxicity and good chemical and thermal stability [50-51].

The influence of crystallographic orientation of substrates has been approached by single crystals for a long time. Such experiments, however, do not represent the reality of polycrystalline metals, since the concentration of impurities differ, the surfaces are atomically flat and the role of typical defects such as screw dislocations (1D), grain boundaries (2D), and twins and inclusions (3D) cannot be simulated. On the other hand, the real metal surfaces could not be analysed in a microscopic scale for a long time. But progress in electrochemical

microsystem technologies as well as in surface analysis now allows direct measurements on single grains down to grain sizes of some micrometres [52]. Crystallographic orientation of large grains can be determined by anisotropy-micro-ellipsometry (AME) for metals with an anisotropic lattice system, like titanium for example, which has a hexagonal crystal structure [52]. Also it was shown that the density of surface atoms does not only determine the oxide film formation, but in addition to that it has a very strong influence on the rate of electron transfer reactions as well [53]. The effects, however, differ. In case of Ti, a low reactivity of ion transfer reactions activity is combined with a high doping of the oxide film causing a high reactivity for electron transfer reactions. On the loosely packed oxide films, the electron transfer reactions activity is almost negligible at lower overpotentials. Oxide films on different grains show a homogeneous film thickness up to the grain boundaries. This is indicated by constant interference colours. The electron transfer reactions activity, however, depends on the distance from the grain boundary.

According to XPS analysis the composition of the anodic films on titanium consists mainly of $TiO_2$ [24]. However, it is also reported[44] a more complex composition, for example, the presence of an oxygen-enriched surface layer. Anions from the electrolyte can be frequently observed at the surface, and in the bulk of the oxide films[24, 27, 43]. RBS and other nuclear interaction-based techniques also show that near-surface regions of the oxide can also contain significant amounts of hydrogen[24, 44].

Anodic oxide films on titanium and titanium alloys usually have a complex surface morphology and microstructure. It depends of the oxide thickness, and usually the roughness increases with increasing of the coating thickness. Various types of defects (pits and sometimes pores) are frequently observed [27, 41]. The microstructure of films formed on polished surfaces replicates the substrate microstructure[24, 27]. According to the diffraction studies obtained films can be either amorphous or partly crystalline. Anatase and/or rutile are the most frequently reported phases, however brookite has been also reported.

### 2.1.4 Breakdown of oxide and PEO anodisation.

Under certain conditions, oxide layer of metal tends to have localized instabilities of electronic nature (leading e.g. to dielectric breakdown) or due to the chemical reactivity (leading to e.g. enhanced localized oxide dissolution). The reasons for these local instabilities are precipitates, inclusions, grain boundaries, dislocations on substrate or properties of passive films itself, such as electrostriction, local composition and structural differences. Under specific conditions, namely in the case of high field strength local destruction of the passive film or breakdown, occurs.[22, 27, 31, 54-57]. The dielectric breakdown of an oxide layer takes place at comparably high voltages, when extra charge carriers are generated either by tunneling of electrons (Zener mechanism), or by collision of electrons (avalanche mechanism)[22, 27, 55]. Resistivity of the film plays a main role for the appearance of breakdown and it is influenced by the band gap size, structure and impurities. During the breakdown, the resistivity of the layer drops by several orders of magnitude. Ikonopisov proposed that for $TiO_2$ the avalanche mechanism involving electron injection from the electrolyte into the conduction band is most likely responsible for dielectric breakdown[56]. In further works, he reported that composition and concentration of the electrolyte also play an important role, whereas the current density, temperature and roughness of the surface are less significant. Breakdown is usually accompanied by sparking, or acoustic crackling noise. Anodisation using potentials above the

breakdown voltage of the oxide film growing on the anode surface, is widely used and usually called plasma electrolytic oxidation (PEO) [30, 58]

Preparation of oxide films on a wide range of valve metals (Nb, Ta, Zr, Hf, Al, Ti, W, Mo) by PEO technique has been investigated for years by many researchers[31, 54, 56, 59-60]. In the case of Ti, it has been mainly investigated in sulfuric acid electrolytes[31, 55, 60]. However, for all valve metals it has been shown that breakdown is dependent on the growth mode (galvanostatic, potentiostatic) and on the rapidity of voltage rise[52, 54]. In comparison with conventional (galvanostatic, potentiostatic) anodisation, PEO is accompanied by oxygen evolution and in some cases also by crystallization[54]. There has been a lot of discussion in literature on the exact reasons for the breakdown phenomena. Generally, it can be stated that it is connected with film damage, oxygen evolution and change in the electrical characteristics. Furthermore, it is still a subject of debate, whether the quality of the metal substrate will play any role in the PEO. Breakdown of the passive film will happen at high voltages on both rough surface, as well as on a perfectly polished surface. With further anodisation at high voltages, the breakdown spots may appear all over the surface. It leads to a surface covered with a well adherent, hard, ceramic-like coatings[30, 58] with thickness that varies depending on the breakdown potential from hundreds of nanometers up to few micrometers. Although in electrochemistry the dielectric breakdown of valve metal oxides is the most investigated case, there is the second reason for the local destruction of passivity – presence of aggressive ions that may penetrate into the oxide film. These ions most typically chloride anions, whereas effects of fluorides are less studied.

### 2.1.5 Photoelectrochemical properties of $TiO_2$

In the past few decades, the works concerning the photoactivity of titanium dioxide were under intensive investigation. One of the first important works in this field was done in 1972 by Fujishima and Honda, who investigated the photoelectrochemical decomposition of water using titania anode and a Pt counter electrode[61]. Afterwards, in 1977 Frank and Bard have reported a work concerning titanium dioxide photocatalysis where the reduction of $CN^-$ in water was observed[62]. As a result of this work the potential for water and air purification through utilization of “free” solar energy attracted attention for the titania and a dramatic increase in the research in this area has started[50]. Another milestone in the research of the titanium oxide was reached by Graetzel and O’Regan in 1991[63] who used nanosized titanium dioxide in an efficient dye sensitized solar cell. Later, in 1997, another wave of interest for titanium dioxide appeared due to the work of Wang et al. (1997), who reported $TiO_2$ surfaces with excellent anti-fogging and self-cleaning abilities [64].

The photocatalytic transformation of different substances (e.g. pollutants) is possible when a material, usually a semiconductor, interacts with the light of certain energy and produces the reactive oxidizing species. During the photocatalytic reaction, at least two events must occur simultaneously: the first is connected with oxidation of adsorbed $H_2O$ by photogenerated holes in the valence band, and the second reaction with the reduction of an

electron acceptor (usually dissolved oxygen) by electrons from the conduction band. These two reactions lead to the production of a hydroxyl and a superoxide radical anion, respectively [65].

Photocatalysis implies photon-assisted generation of catalytically active species rather than the action of light as a catalyst in a reaction[66]. Usually photocatalysis is described by two mechanisms: catalysed photoreaction and sensitized photoreaction. According to the first mechanism, an initial photoexcitation process occurs in an adsorbate molecule, which then interacts with the ground state of the catalyst substrate. The reaction goes under the second mechanism if the initial photoexcitation takes place in the catalyst substrate and the photoexcited catalyst then interacts with the ground state of an adsorbed molecule[65].

For the process of electron transfer from the valence band to the conduction band energy of light should be greater than the band gap of the semiconductor. In the case of anatase, the band gap is 3.2 eV, thus UV light ($\lambda \leq 387$ nm) is required. The equation according to which absorption of the photon excites an electron to the conduction band ($e_{CB}^-$) generating a positive hole in the valence band ($h_{VB}+$) is the following:

$$TiO_2 + hv \rightarrow h_{VB}^+ + e_{CB}^- \qquad (2.7)$$

Charge carriers can be trapped as $Ti^{3+}$ and $O^-$ defect sites in the $TiO_2$ lattice, or they can recombine, dissipating energy. Though they can migrate to the titania/electrolyte interface and initiate redox reactions with adsorbed substancies[67]. Positive holes can react with $OH^-$ or water producing *OH radicals which are known as extremely powerful oxidants. Also the hydroxyl radicals can oxidize organic species producing mineral salts, $CO_2$ and $H_2O$ and in this case photocatalysis can be used for pollution removal[68]. Furthermore electrons in the conduction band can react with the molecular oxygen adsorbed on the titania particle, resulting superoxide radical anion ($*O_2^-$) that may further react with $H^+$ to generate hydroperoxyl radical (*OOH) and further electrochemical reduction yields $H_2O_2$[69]. These reactive oxygen species may also be involved to the oxidative pathways such as the degradation of a pollutant[70].

Recombination of the photogenerated charge carriers is the major limitation of the semiconductors in photoelectrochemistry as it reduces the overall quantum efficiency[71]. When recombination occurs, the excited electron reverts to the valence band without reacting with the adsorbed species. This process can occur non-radiatively or radiatively, i.e. dissipating the energy as light or heat [72]. The recombination may occur either on the surface or in the bulk of the semiconductor. It is connected with the nature of the material as well as with impurities, defects, and every factor which introduces bulk or surface imperfections into the crystal[71]. It is shown that trapping of excited electrons by holes in the valence band ($Ti^{3+}$ species) can occur in a time scale of ~ 30 ps and that about 90% or more of the photogenerated electrons recombine within 10 ns. The doping with ions, the heterojunction coupling or the preparation of the semiconductor as nanosized crystals promote the separation of the electron–hole pair, reducing the recombination and improving the photoelectrochemical activity. For example, in the titania crystallites which contain a combination of anatase (~ 80%) and rutile (~ 20%) the conduction band level of rutile is more positive than that of anatase, and, thus, the rutile phase may act as an electron sink for the photogenerated electrons from the conduction band of the anatase phase. Many researchers attribute the high photoelectrochemical activity of this material to the intimate contact between two phases, enhancing the separation of the photogenerated electrons and holes, and resulting in reduced recombination.

## 2.2 Anodisation of aluminium

### 2.2.1 General information about aluminium anodisation, its history and use

During the last century, aluminium became one of the most important materials. In the end of 19$^{th}$ century, it was clear that it is lighter and has a better corrosion resistance in comparison with steel, however its lower mechanical strength was limiting the use of aluminium. There was a big number of attempts to overcome these difficulties which resulted in the appearance of a great number of aluminium alloys. Thus, alloys with copper have higher mechanical strength, addition of Si improves their castability, doping with Mg and Zn enhances the weldability. Electrochemical modification of the aluminium (especially anodisation) can result in obtaining a variety of desirable surface properties, such as abrasion and corrosion resistance, increase in surface hardness, and dye-absorption properties. Thin films of aluminium oxide have found important applications in the electronic industry and corrosion protection due to their relatively high dielectric constant, ultra-low conductivity as well as high corrosion resistance and good thermal and mechanical stability [73]. The above properties also make aluminium oxide films promising for novel applications in microelectronics. Nowadays, thin alumina layers are used as dielectrics in integrated capacitors with ultrahigh capacitance density [74]. Films of $Al_2O_3$ are also considered as replacements for $SiO_2$ in semiconductor devices [75-76].

The history of aluminium anodisation is closely allied with electrochemical studies of its properties. In 1857, H. Buff[77] tried to find an improved primary cell. During his research it was found that when Al is coupled with Pt in dilute sulphuric acid, Al becomes anode and a large current flows, significantly higher in comparison with classical Volta cell. However, the current in immediately reduced to very small values, soon after the beginning of the process. A similar phenomenon was found in 1864 by Wheatstone[78], who published his observations in the Philosophical Magazine. He suggested that this effect is connected with a Si layer formed on the Al surface, because Al at that time contained some amounts of silicon. In later works, Wohler and Buff[79] found that the current is not reduced for aluminium in chloride solutions. Ducretet[80] suggested that current drop occurs due to the formation of $Al_2O_3$. Also, he has found that if this anode becomes the cathode, a large amount of current would immediately flow. He suggested that this behaviour could be used in electric circuits. In further works, in 1899, Norden[81] suggested that an Al-anode/film/electrolyte system could be described as an electrolytic capacitor. In addition, he succeeded to separate anodic oxide films from the aluminium substrate by polarizing Al sequentially anodicaly and cathodicaly in dilute sulphuric acid. He confirmed that the anodic oxide film could not be reduced during cathodic polarization by measuring the hydrogen gas evolution. In the next year, 1900, the first industrial capacitors based on Norden's ideas was constructed in Siemens and Halske AG.

## 2.2.2 Kinetics of aluminium anodisation

During electrochemical reaction, aluminium from the anode reacts with the oxygen from the electrolyte and form $Al_2O_3$. Under polarization, when the aluminium is set as the anode in electrolytes of certain concentration and when direct current is passing through cell, aluminium metal starts to convert into oxide through the following electrochemical reaction：

Anode:

$$Al \rightarrow Al^{3+} + 3e^- \qquad (2.8)$$

$$2Al^{3+} + 3O^{2-} \rightarrow Al_2O_3 \qquad q = -1675.7\ kJ.mol^{-1} \qquad (2.9)$$

$$2Al + 6OH^- \rightarrow Al_2O_3 + 3H_2O + 6\ e^- \qquad (2.10)$$

Cathode:

$$2H_2O + 2e^- \rightarrow H_2 + 2OH^- \qquad (2.11)$$

$$2H^+ + 2e^- \rightarrow H_2\ (2) \qquad (2.12)$$

Thus, when electrical field is applied, $Al^{3+}$ ions start to go from aluminium and start to move towards the anodic oxide layers through the metal anode/oxide interface, and then continue to move outwards. Meanwhile, the $O^{2-}$ formed on the electrolyte/oxide interface is moving inwards with the opposite direction, until both of them meet each other, forming anodic oxide ($Al_2O_3$) ("high-field" ionic conduction). As a result, a compact and adherent film deposits on the electrode surface. In this case oxidation proceeds strictly according to Faraday's law, thus a definite amount of oxide is produced by a certain quantity of charge. With passing the charge of 3 Faraday, 1 mole of aluminium oxidizes and produces 51 g of alumina.

Also, it should be mentioned that this reaction is exothermic. However, alumina is an electric insulator without free electrons in the conduction band, thus, according to the above reaction should stop after a monomolecular film is formed. In case the film is very thin (within 2nm) quantum tunnelling of electrons is also possible however this current is very small in comparison with the ionic. For constant current anodizing, the voltage-time behaviour reveals an initial voltage surge of about 2.0 V, indicating the presence of an air formed film on the electropolished aluminium surface with thickness of 2.5 nm. Further, the voltage rises linearly with time as the relatively compact film thickens. The driving force for film growth is high-field ionic conduction, which may be simply expressed as

$$j = A \exp(BE) \qquad (2.13)$$

where $j$ is the current density, A and B are temperature dependent constants, and E is the field strength (the ratio of the potential drop across the anodic oxide film to the film thickness). Clearly, films grown at constant current density develop at constant field strength. In the work of Walkenhorst[82] it was found that the growth rate under the high-field ionic conduction equals 1,4 nm/V what corresponds to a high electric field of about $10^7$ V/cm. Further, the reciprocal of the field strength for anodizing of aluminium reveals that the film thickens at a constant rate. In order to maintain the constant field strength, the voltage must increase as the film thickens.

The anodic film which thickness linearly depends on the applied voltage is called the "barrier layer". This layer is insulator with dielectric constant in the range 8-9. In comparison with other dielectric materials this value is not very high, however the film thickness can be easily controlled in a wide range to obtain the required capacity. This is the reason why electrolytic capacitors are so important and widely used[83].

When the film becomes too resistive to pass anodic current its growth terminates. Uniform film thickening is terminated eventually by dielectric breakdown, with visible sparking observed frequently over the anodic film surface. Therefore, for the film growth, it is important to increase the positive potential. Furthermore, composition of the electrolyte plays an important role in the film growth. If there is no effect of dissolution of the depositing film (as in ammonium borate solution), the voltage can be theoretically raised up to 700 V, resulting in a film with the thickness about 1μm (1.4nm * 700V). At a certain limit, which depends upon the nature, concentration, and temperature of the electrolyte, the random arcing could occur on the film surface resulting in film breakdown. In such case the electronic current will predominate but will not make any influence in the film growth.

Using inert marker experiments, locations of the film growth are defined[84]. A transmission electron image of the cross-section shows the typical barrier type film have relatively flat metal/oxide and oxide/electrolyte interfaces and shows behaviour of mainly amorphous anodic oxide films, as it is shown in Figure 2.2.1. During the studies of barrier films formation with inert marker experiments, a critical current density may be defined for many electrolytes at which point directly measured cation transport number approaches to zero. In such cases no solid oxide growth can be observed above the marker layer, which stays close to the oxide/electrolyte interface. Further analysis of the electrolyte after anodizing reveals the presence of $Al^{3+}$ ions which shows that cation transport number is equivalent to that measured under conditions of high current efficiency when converted to equivalent anodic oxide film thickness. Thus, during oxide growth both ions ($Al^{3+}$ and $O^{2-}$/OH-) are mobile. Further formation of the film at the film/electrolyte interface depends on specific anodizing conditions. At the critical current density, little or no oxide film formation is possible at that interface.

To understand deeply the behaviour of outwardly mobile $Al^{3+}$ ions, anodizing was performed at current densities below critical current density, where no solid oxide formation at the oxide/electrolyte interface is possible[85] (Figure 2.2.2 (a)). In this case uniform oxide dissolution proceeds during the anodizing at relatively low current efficiency, thus, the original oxide film material containing the marker layer is expected to be completely lost to the electrolyte (Figure 2.2.2 (b)). It should be noted that presence of the marker layer is always close to the oxide/electrolyte interface, although it is lost in local regions owing to undermining of film material by pore initiation by field-assisted dissolution at preferred sites (Figure 2.2.2 (c))

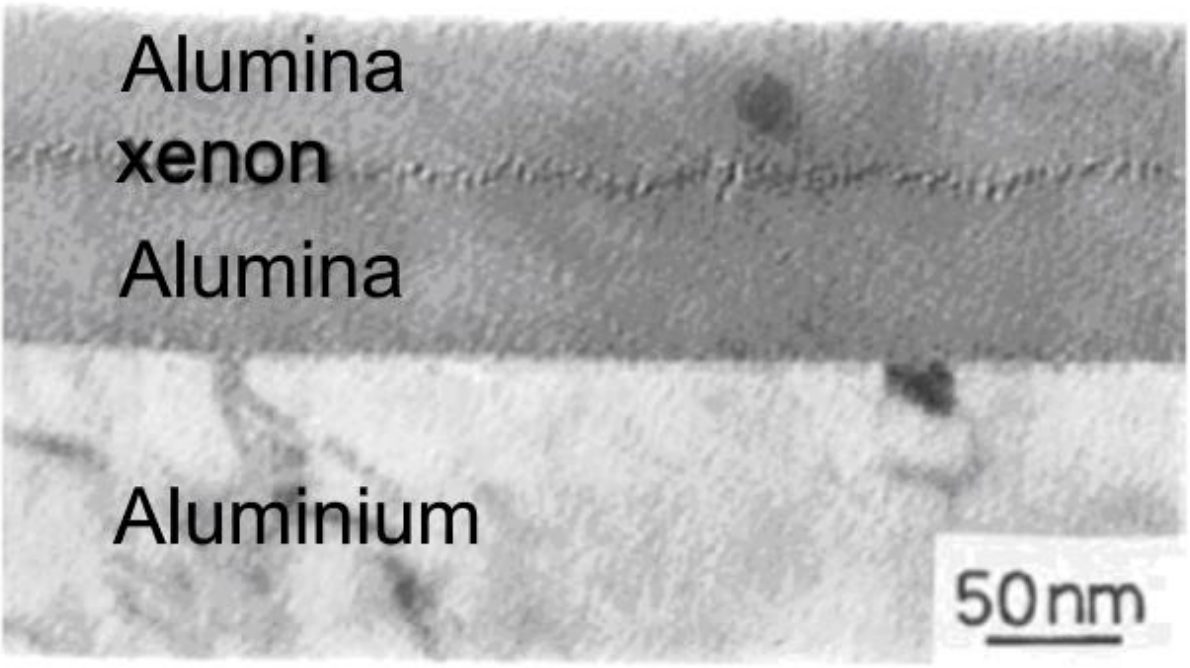


**Figure 2.2.1** TEM micrograph of cross session of Al substrate and anodic film, formed at a constant current density of 10A $m^{-2}$ to 100 V in near-neutral potassium phosphate electrolyte at 298K. This reveals the xenon implant, originally retained within a relatively thin pre-formed anodic film[86].

When aluminium is anodized in a near neutral solution, the dissolution of oxide is usually very slow. In such case the thickness of the oxide layer will continuously increase. The electric field in such system can be written as E = U/d. In the case of constant applied voltage, U, to the oxide layer, the electric field strength E in the oxide layer is inversely proportional to the thickness of the oxide layer, d. Therefore, E will drop when the thickness of the oxide layer increases, reducing the migration rate of the anions. The oxidation process will eventually stop when d approaches a critical value ($d_c$), which depends of the anodizing conditions, while the corresponding electric field strength ($E_c$) becomes too weak to drive the oxygen containing anions through the oxide barrier layer. When the thickness of the oxide layer is smaller than $d_c$, and the field strength $E > E_c$, the migration of ions takes place and the oxide layer grows. In this case constant electric field strength will be established in the whole barrier layer.

The system becomes more complicated in the case when electrolyte can dissolve the deposited film. In this case, the restoration of the barrier layer occurs resulting in a thickness limit. During the anodisation simultaneous formation and dissolution of the oxide occurs resulting in the development of an oxide cells array with cylindrical pores. When the balance is established the film formation results in the increase of the thickness of the porous layer. In this type of coating (duplex film) the outer region is porous since it contains a big amount of hexagonal pores which can be observed with the electron microscope. In this type of anodic oxide film, the porous layer can grow at constant voltage, and its parameters depend from the relationship between formation and dissolution in pores.

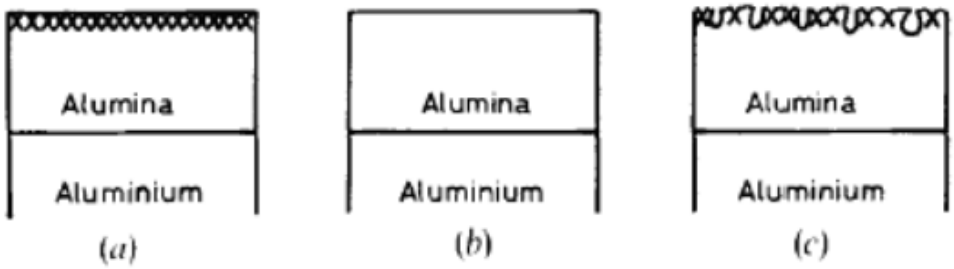


**Figure 2.2.2** Schematic illustration of cross sessions of barrier type films formed at various current densities in chromate electrolyte: (a) films formed at critical current density; (b) film formed at a current density below critical density, when dissolution of the outer film regions is expected to remove the marker layer;(c) films formed at current density below current density, revealing location of the marker layer and pore initiation at preferred sites[85]

In general, several types of processes can be considered during the anodic polarization of aluminium. During anodisation at constant voltage (potentiostatic) the current rapidly drops to nearly zero value and only a small current flows which is called "leakage current" (electronic current through impurities, etc.). In the case of anodisation with constant current (galvanostatic), the positive potential rises linearly with the time resulting a barrier film. This can occur in electrolytes where the film is not dissolved. In the case of use of electrolyte, that can dissolve the film (sulphuric and oxalic acid), during anodisation in galvanostatic mode the voltage becomes constant. In this case, deposit film consists from the barrier plus the porous layer. If concentrated strong acids or in alkaline solutions with a strong solvent action-sulphuric and phosphoric acids, sodium phosphate solutions[87], and sodium or potassium hydroxide solutions are used during galvanostatic anodisation the voltage can fluctuate. The anodic surface in this case is brightly polished (electropolishing).

During the anodisation the heat of reaction can accumulate when the film becomes thicker, resulting in increase of the dissolution. Thus, the film cannot grow infinitely and there is a maximum thickness which can be obtained.

### 2.2.3 Plasma electrolytic anodisation on aluminium

Similarly, to titanium, plasma electrolytic oxidation (PEO) is a method which allows to prepare relatively thick, dense, ceramic-like coatings. During PEO process complex physical, chemical, electrochemical and plasma thermo-chemical reactions occurs.

There are a few studies that suggest coating formation mechanisms. Based on the voltage-time response the PEO anodisation can be divided into several stages where different processes occur. At the beginning of the PEO process the voltage increase linearly and rapidly and a very thin insulating oxide film is formed on the surface of metal. In this stage, the mechanism of conventional anodisation occurs which is described above. Eventually, when voltage reaches a critical value, the breakdown voltage, dielectric breakdown occurs. Usually it

appears in weak sites across the oxide film accompanied by the formation of a large number of fine, uniform, micro-discharges on the surface of the sample. Sparks are typical of the PEO process and play a main role in the formation of the coating. When the breakdown voltage is reached, many discharge channels are created as a result of micro-regional instability in the coating. The discharge temperature is estimated to be in the range of 4000-10000 K [88-89]. The low temperature range corresponds to small discharges happening in the early stages, i.e. immediately after the breakdown voltage is reached. The high temperature range corresponds to strong, long-lasting discharges happening in the final stages of the process. The local plasma temperature is high enough to ionize all the species that exist close to the discharge channels, and the induced electron collapse makes the coating materials move into these channels. Anionic species present in the electrolyte, can enter the channels. The high temperature and pressure inside the discharge channels melt the substrate elements which diffuse into the channels. In next stage, after breakdown occurred, the voltage slowly increases while oxide film growth rate decreases. This molten material is ejected from the coating/substrate interface and solidifies when cooled by the surrounding electrolyte, whose temperature is controlled using an external heat exchanger. This solidified oxide increases the coating thickness in areas close to the discharge channels. In following stage, the rate of voltage change increases slightly, micro-discharges become more intensive and start to last longer while their spatial density decreases. The gases produced escape through the discharge channels resulting in the formation of circular areas with a hole in the centre, resembling the structure of a crater in a volcano. These volcano-like morphologies are often referred to as either a 'pancake structure' [90-92], or a 'crater'[93-96] . In next step, the rate of voltage increase starts to decrease, and the sparks become stronger. In PEO process discharges play an important role in the coating growth mechanism. Since discharge events are very short, it is very difficult to catch them instantaneously to analyse the physical and chemical processes which occur in the discharge channels[97]. During PEO, melting, solidification, sintering and densification of oxide layer occur usually in relatively weak regions of the coating surface leading to a uniform increase in overall coating thickness[89, 97-100]. Due to the high cooling rate caused by the cold substrate, the molten oxide at the coating/substrate interface rapidly solidifies, creating a thin crystalline layer with small uniform nano-sized grains. TEM studies confirm presence of this layer in PEO coatings on aluminium[101-102]. The nano-crystalline layer is formed during PEO and moves inwards and is considered as the main inner growth mechanism [97, 100]. During the PEO process different types of discharge are considered to occur. There are a number of models proposed to describe micro-discharge formation during PEO such as glow discharge electrolysis[103], electronic avalanche [104], electronic tunneling[105] and the model by Yerokhin et al.[99] which assumes the possibility of free electron generation and glow discharge ignition in the gaseous media at the oxide-electrolyte interface.

# 3 Experimental part

This chapter describes the experimental procedures related to the fabrication and characterization of aluminium and titanium oxides which was performed in the frame of present work, including materials selection, specimen preparations, anodizing and electrodeposition procedures, as well as characterization methods.

## 3.1 Construction of an experimental setup for performing the pulsed anodizing and studying the kinetics of the process.

High-voltage experimental setup for performing the pulsed anodizing and for studying the kinetics of the process was mounted according to the scheme shown in Figure 3.1.1.

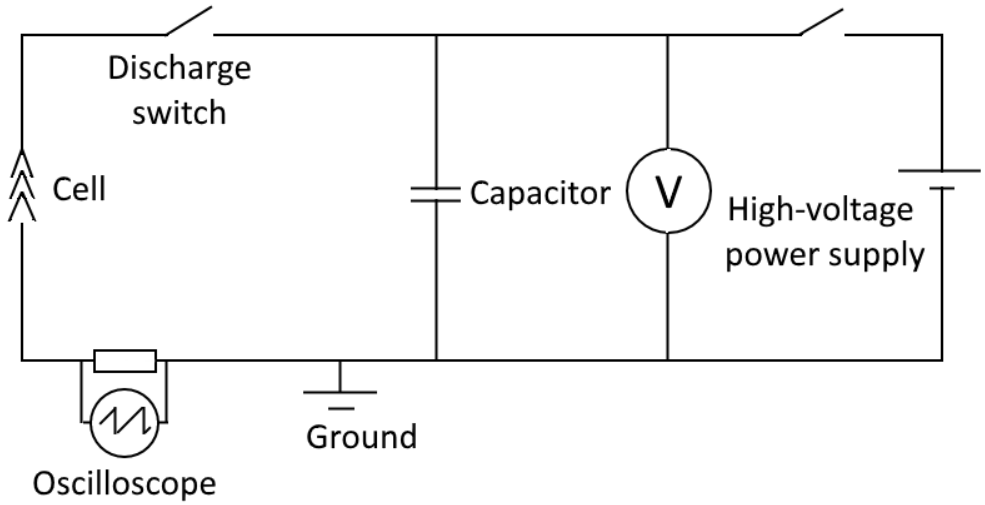


**Figure 3.1.1** Principal scheme of high-voltage experimental setup.

The main parts of experimental setup are high-voltage power supply, a capacitor bank with a stepped variation of capacity, a commutation system, voltmeter, oscilloscope and discharge cell. The capacitor bank charged by the high-voltage power supply to definite voltage. High Voltage Source Measuring Unit Keithley 237 as a voltmeter controls voltage. Then the charge accumulated by the capacitor bank was injected into the electrochemical cell by means of a low-inertial switch triggered by a synchronizing pulse. This setup allows applying a high voltage up to 3000 V to the metal electrode at a fixed value of the injected charge up to 1 C per impulse. To reduce ohmic losses in the system, the electrochemical cell is connected to the capacitor bank by low-impedance cables of minimal length. To reduce inductance flat cables were used, to reduce influence of skin-effect. The registration system permits recording several

parameters of the anodizing process such as the applied voltage and the evolution of the pulse current in the circuit. To measure the transient current in the electrode system, a precision resistor is connected to the circuit. A multi-channel digital phosphor oscilloscope Tektronix DPO 7054 records the current flow through the resistor. Changing capacitor banks can vary capacitance and highest voltage.

All parts of the setup are installed in a rack, so the system is mobile and multifunctional (Figure 3.1.2). Galvanostatic anodisation can also be carried out on this installation. In this case the High Voltage Source Measuring Unit Keithley 237 is used as a current source.

**Figure 3.1.2** Photo of the high-voltage experimental setup.

The electrochemical cell is constructed from thick (2.5 mm) polyethylene terephthalate because of its hardness and chemical stability. The shape and construction of the cell was designed to reduce possibility of destruction of the cell (Figure 3.1.3a).


**Figure 3.1.3.** Photo of the cell (a) and titanium cathode (b)

The counter electrode (cathode) is made of chemically polished titanium (Figure 3.1.3b). Titanium is used as a hard, chemically stable material, which wouldn't influence the composition of electrolyte during the experiment. The shape of counter electrode is cylindrical, to make electrical field inside the cell as uniform as possible. The counter electrode has a slit, for further optical measurements of the pulse electrodeposition process.

Electric discharges between the electrodes were generated using a low-inductance 100 μF capacitor bank, charged to a defined voltage. In order to prepare films with different thicknesses, the capacitor was discharged through the electrochemical cell in the range between 1 and 30 times.

## 3.2 Material selection and preparation

In this work, 99.999% (Alfa Aesar and Goodfellow) high purity aluminium foils with dimensions of 100x80x1 mm were used for the formation of alumina anodic films. For the

formation of titania, Ti 99.999% plates (Goodfellow) with dimensions of 100x80x1 mm were used.

In order to remove lubricant and other contaminants from the surface, the specimens were initially ultrasonically cleaned in acetone bath, and then rinsed with deionised water before dried in dry air.

Electropolishing of aluminium was always performed as an important surface treatment prior to anodizing. Electropolishing is able to selectively decrease macroscopic heterogeneities, thus develop relatively smooth surfaces. Smooth surface is necessary for the formation of porous anodic films on pure aluminium substrate. Further, electropolishing give rise to fine nano-textures on the treated aluminium surfaces, which also facilitate pore nucleation at the initiation stage of anodizing. A mixture of perchloric acid and ethanol in the proportion of 1:4 (vol) was used for electropolishing. Electropolishing was carried out at 20 V for 180 s at 5 °C using an aluminium sheet as counter electrode, in a fume cupboard with highly carefulness since perchloric acid is a strong oxidative and corrosive acid. Immediately after electropolishing, the specimens were rinsed in ethanol for 30 s first, then in deionised water for 30 s, and finally dried in dry air.

Titanium plates were polished mechanically and then chemically in HF:$HNO_3$ mixture to mirror finish and finally rinsed with deionised water.

Heat treatment of aluminium specimens, here specified as annealing treatment was carried out before electropolishing. Degreased aluminium specimens were annealed at 400◦C for one hour. Grain size became significantly larger after heat treatment, since recrystallization and grain coarsening occur during annealing treatment [106]. The large grains favour self-ordering process during the formation of porous anodic oxide films.

## 3.3 Techniques: brief description and specific equipment used

### 3.3.1 Transmission electron microscopy

Transmission electron microscopy (TEM) is a microscopy technique in which a beam of electrons is transmitted through a specimen to form an image. In this case the much smaller wavelength makes possible to achieve resolution significantly better than that with a light microscope. High energy electrons, which pass through ultra-thin samples, allow image resolutions to reach values of 0.05 nm or less.

In TEM electron source generates electrons that travel through the vacuum in the column of the microscope. Instead of glass lenses that focus the light in the conventional light microscope, TEM uses electromagnetic lenses to focus electrons into a very fine beam which passes through the specimen, screen, sensor or microphotographic film. Depending of the density and properties of the material, some of the electrons can be scattered or absorbed. At the bottom of the microscopes the unscattered electrons hit a fluorescent screen, sensor or microphotographic film, where it forms a "shadow image" of the specimen with its different parts displayed in varied brightness based on their density. The image can be studied directly by the operator or recorded. Variations in the intensity of electron diffraction across a crystalline

specimen, called “diffraction contrast,” is useful for making images of defects such as dislocations, interfaces, and second phase particles.

Although this technique is much more time consuming than many other common analytical tools, the amount of information available from TEM is impressive. It is possible to obtain not only outstanding image resolution, it is also possible to characterize crystallographic phase, crystallographic orientation (both by diffraction mode experiments), produce elemental maps (using EDS), and images that highlight elemental contrast (dark field mode). All of this information can be obtained in nm sized areas that can be precisely located. Compared to SEM, TEM has better spatial resolution, is capable of additional analytical measurements.

In current work TEM study was carried out using a Hitachi H9000 transmission electron microscope at an acceleration voltage of 300 kV.

### 3.3.2 Scanning electron microscopy

In Scanning electron microscopy (SEM), a focused electron beam is scanned across a sample surface and provides images of the sample surface. In comparison with conventional light microscopy images have significantly higher resolution (0.5 nm and more) and increased depth-of-field. Similarly, to the TEM electron beam follows a vertical path through the column of the microscope where it passes through electromagnetic lenses which focus and direct the beam down towards the sample. Once it hits the sample, other electrons (backscattered or secondary) are ejected from the sample. Detectors collect the secondary or backscattered electrons, and convert them to a signal and forms an image on the computer. Microscopes used in current work use several detectors which are installed perpendicularly and laterally to the sample and help to form pseudo 3D image. Scanning electron microscope produces images of the sample surface morphology. All specimens are required to be conductive for SEM examination, thus the anodic oxide specimens were always carbon coated before SEM examination. Scanning electron microscopy is extensively used in this work to obtain morphology details of anodic oxides.

In the frame of current work SEM studies were performed on a Hitachi S-4100 and a Hitachi SU-70 scanning electron microscopes.

### 3.3.3 Energy dispersive X-ray spectroscopy

Energy dispersive X-ray spectroscopy (EDS or EDX) is a technique that provides elemental analysis on areas as small as nanometers in diameter during scanning electron microscopy and transmission electron microscopy. The impact of electron beam on the sample produces X-rays that are characteristic of the elements in specimens.

During the qualitative analysis, the X-ray energy values from the EDS spectrum are compared with known characteristic X-ray energy values allowing to determine the presence of an element in the sample. Elements with atomic numbers ranging from that of beryllium to uranium can be detected. The minimum detection limits may vary from approximately 0.1% to a few atomic percentages, depending on element, sample matrix, acceleration voltage and current of the electrons.

Quantitative results can be obtained from the relative X-ray counts at characteristic energy levels for the sample. Semi-quantitative results are easily available without standards by using mathematical corrections based on the analysis parameters and sample composition. However, the accuracy of such analysis depends on the sample composition and structure. In practice, relatively good accuracy can be obtained using samples with similar structure and composition to known standards. Currently elemental mapping where characteristic X-ray intensity is measured relative to position on the sample is also available. During line profile analysis, the SEM electron beam is scanned along a pre-selected line across the sample while X-rays are detected for discrete positions along the line. Variations in the X-ray intensity at any characteristic energy value indicate relative concentration for the element across the surface. One or more maps can be recorded simultaneously using image brightness intensity as a function of the local relative concentration of the element(s) present. Elemental concentration for each element on every position along the line is also available and widely used. For thin samples on TEM elemental resolution of 1 nm is possible.

In the frame of current work, a Hitachi SU-70 scanning electron microscope coupled with an Brucker energy dispersive spectrometer (EDS) was used.

### 3.3.4 Atomic force microscopy

Atomic force microscopy (AFM) is one of the forms of scanning probe microscopy (SPM) where a small probe is scanned across the sample to obtain information about the material surface. The information gathered from the probe interaction with surface can be interpreted as physical topography. Depending of the probe composition and scanning technique information about materials physical, electrical, magnetic, or chemical properties can be also obtained. These data are collected as the probe is scanned in a raster pattern across the sample to form a map of the measured property relative to the X-Y position.

Unlike SEM which provides two-dimensional image of a sample, AFM provides a true three-dimensional surface profile. Additionally, samples examined by AFM do not require any special treatments (such as metal/carbon coatings for insulator samples) which would irreversibly change or damage the sample. While an electron microscope needs a vacuum environment for proper operation, most AFM modes can work perfectly well in the ambient air or even a liquid environment. However, AFM could not scan images as fast as SEM.

In the frame of the present work, AFM studies were performed by a Molecular Imaging PicoSPM and Digital Instruments Nanoscope III atomic force microscopes.

### 3.3.5 Scanning Kelvin probe force microscopy

SKPFM is a promising method to study the surface electrical properties [107]. Scanning Kelvin probe force microscopy (SKPFM) operates in noncontact mode of AFM[108]. The work function of the sample surface can be recorded by SKPFM at atomic scale.

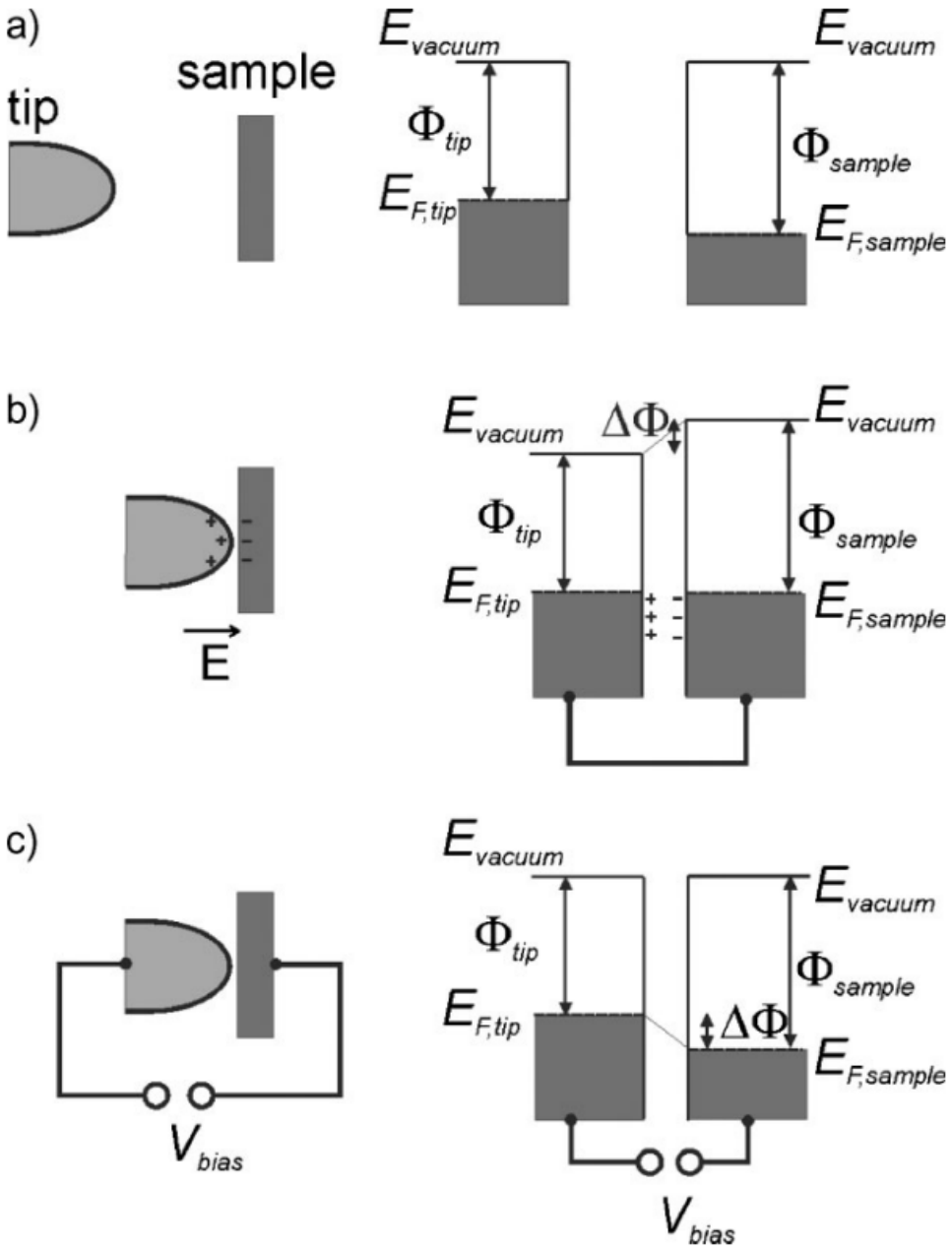


Fig. 3.3.1 Schematic image of a tip sample contact and the associated energy levels: a) tip and sample are separated, b) tip and sample are in contact, and c) upon applying an additional external potential[109].

When two metals with a different work function Φ are separated, their energy levels are different (fig. 3.3.1a). After electrical contact of them occurs their Fermi levels align. Thus, electrons flow from the metal with lower work function ($\Phi_{sample}$) into to the metal with higher ($\Phi_{tip}$). The charges accumulate on the surface, resulting in a space charge. Afterwards, their electric field start to push the electrons back, until an equilibrium is reached (fig. 3.3.1b)[109]. In the equilibrium, the separated space charges result in a potential difference, which is called Volta potential difference (VPD) (fig. 3.3.1c) which equals:

$$VPD = (\Phi_{sample}-\Phi_{tip})/e \qquad (3.7.1)$$

In a metal, the work function is defined as the energy difference between the vacuum state and the Fermi energy, which is also the minimal energy required to remove an electron from the metal to vacuum. For semiconductors, the work function can be regarded as the difference in energy between the vacuum energy level and the most loosely bounded electron. SKPFM is a useful technique for study of surface structure[110], doping and band-bending of semiconductors[111].

The method of contact potential difference measurement was developed for more than a century ago by Lord Kelvin in 1898[112], called Kelvin probe method.

In comparison with the conventional Scanning Kelvin Probe (SKP), it combines capabilities of both SKP and atomic force microscopy and provides much higher resolution when mapping the local electrical properties of a surface. The Kelvin probe methods are based on the measurement of the VPD between the surface and a reference electrode. A conductive cantilever is used for KPFM. The cantilever is a reference electrode that forms a capacitor with the sample surface, and the cantilever scans above the sample at a constant height. The cantilever oscillates but not driven at its resonance frequency while an AC bias VAC is applied at the resonance frequency.

The (DC) bias voltage is modulated with an AC voltage. If the DC components not equal to the CPD, the AFM will be excited also at the modulation frequency and oscillate with a certain amplitude. A DC bias VDC forms between the cantilever and the sample when the cantilever and the sample are close, since electrons will flow from the material with a lower work function to the material with a higher work function. The AC and DC bias will cause the cantilever to vibrate.

This oscillation can be detected through the photo detector. A null circuit is used to apply a DC potential to minimize the oscillation. This DC potential is recorded and produces an image of the work function of the sample.

The Lock-in technique and a feedback on the DC bias can be used to keep the minimal AC amplitude. This method can be applied while scanning an image in AFM mode, resulting both AFM image and map of CPD.

In the SKPFM technique, VPD corresponds to the voltage that nulls the oscillations of a cantilever, while in a SKP method it is equal to the voltage applied to null the induction currents between the electrode and the surface [113-114]. It was shown [115-116] that the VPD distribution observed in some metals correlates with their corrosion potential. Thus, in spite of some restrictions of the technique related to the impact of the topography, probe-surface interactions and others [117], SKPFM is a valuable tool for nano-scale surface studies.

The measured potential consists of the contact potential and that induced by embedded charges (induced potential). Opposite charges localized near the counter interfaces, create polarization of a film. The character of the charge distribution and, as result, the magnitude of the polarization of the anodic alumina films have been found to be affected by the anodisation conditions [118]. In particular, Hickmott has shown [119] that the charge contributing to the polarization depends on the nature of the anodizing electrolyte. Lambert *et al*. [118] associated the permanent polarization of thin anodic alumina layers with charges trapped by structural defects created during the anodisation process. An atomic force microscope and a Kelvin probe were applied to measure the potential induced by these embedded charges [118]. It was found that application of potentiostatic polarization to the layers prepared using galvanostatic anodisation results in significant increase of their polarization. Scanning Kelvin probe force microscopy (SKPFM) has recently been used to study electrical properties of oxidized aluminium surfaces,

since changes in the Volta potential difference (VPD) measured by SKPFM are caused by changes in the inducted potential [120].

In the frame of the present work, SKPFM studies were performed by Digital Instruments Nanoscope III atomic force microscope and Cr-Pt tips (Budget sensors).

### 3.3.6 Electrochemical impedance spectroscopy

Electrochemical impedance spectroscopy (EIS) is a powerful technique for the investigating the mechanisms of electrochemical reactions, surface and bulk properties and structure of different electrode materials. It is widely used to characterize cell limitations and study processes occurring on different time-scales. EIS is based on the current response when a small sine wave is applied to the system. The EIS characterization technique has been widely used in corrosion, electrode kinetics, membranes, batteries and solar cells, biochemistry, solid state electrochemistry, in development and characterization of fuel cells. The main feature of this technique is based on its ability to distinguish, in the frequency domain, the individual contributions of charge-transfer, mass-transfer and ohmic losses[121-122]. However, despite its high potential and applicability to many fields of electrochemistry, data interpretation is sometimes difficult. Interpretation of the EIS data requires a model representing physically meaningful parameters relevant to system, and assessment of the stochastic error structure. The most common approach to simulate experimental data is based on the development of equivalent circuits, which consist from an arrangement of different electrical elements and having the same frequency response than the one obtained by EIS measurements. The most commonly used equivalent circuit elements are:

Resistors (R) - The impedance of a resistor is independent of frequency and has no imaginary component. The current through a resistor stays in phase with the voltage across the resistor.

Capacitors (C) - A capacitor's impedance decreases as the frequency is raised. Capacitors also have only an imaginary impedance component

Warburg Element - Diffusion can create an impedance known as the Warburg impedance. At high frequencies the Warburg impedance is small since diffusing reactants don't have to move very far. At low frequencies the reactants have to diffuse farther, thereby increasing the Warburg impedance. On a Nyquist plot, it appears as a line with a slope of 0.5

Constant phase element (CPE): For the solid electrode solution interface, the situation is complicated by apparently non-capacitive properties of the interface. In modelling this system, the capacitance should be replaced by a distributed electrical element. Usually this is a constant phase element CPE. CPE is characterised by two parameters, neither of them being a capacitive one. The origin of CPE behaviour at the interface has been a subject of many papers [123-125]. This phenomenon is also called ‘frequency dispersion of capacitance’. Its physicochemical nature are still not clear.

The admittance, *Y*, of the CPE element can be alternatively defined by the phenomenological equations:

$$Y_{CPE(a)} = Q_a(i\omega)^{\alpha} \qquad (3.8.1)$$

$$Y_{CPE(b)} = Q_b(i\omega)^{\alpha} \qquad (3.8.2)$$

where i is the imaginary unit and $\omega$ is the angular frequency. The coefficient $Q$a or $Q_b$. and fractional exponent, α, are the parameters of the CPE. Generally, -1 ≤ α ≤ 1. A CPE cannot be described by a finite number of discrete elements (R, C and L) with frequency-independent values. However, for some values of α, it simplifies to discrete elements: for α = -1, it is an inductance ($Q$a = $L^{-1}$), for α = 1, it is a capacitance ($Q$a = $Q_b$ = C), for α =0, it is a resistance ($Q$a = $R^{-1}$), and for α = 0.5, it is a Warburg element.

The impedance of the CPE, $Z_{CPE}$, depends on frequency, ω, according to the following equation[123, 125]:

$$Z_{CPE} = [Q(j\omega)^n]^{-1} \qquad (3.8.3)$$

where Q is a parameter numerically equal to the admittance ($|Z|^{-1}$) at $\omega$= 1 rad $s^{-1}$ and $n$ (≤ 1) is a power coefficient calculated as the ratio of the measured maximum phase angle and -90 degrees. The value of effective capacitance, $C_{eff}$, can be estimated by assuming a normal time-constant distribution through a surface layer by Brug's equation (5) derived by Hirschorn et al.[126]:

$$C_{eff} = Q^{1/n} R^{(1-n)/n} \qquad (3.8.4)$$

In the frame of current work, the electrochemical impedance spectroscopy measurements were performed using a Gamry FAS2 Femtostat with a PCI4 Controller in a frequency range from $10^5$ to $10^{-3}$ Hz with 7 points per decade. The measurements were carried out at room temperature in a conventional three-electrode cell consisting of a mercury–mercurous sulphate reference electrode, a platinum foil as a counter electrode and the working electrode with an exposed area of 1 $cm^2$. Impedance spectra were recorded applying a 10 mV (RMS) sinusoidal perturbation at an open circuit potential. The cell was placed in a Faraday cage to avoid interferences with external electromagnetic fields. 0.1 M acetic buffer solution (pH=6.03) and 0.1 M ammonium pentaborate ($(NH_4)_2B_{10}O_{16}$) aqueous solution was used as electrolyte for EIS measurements. Before recording the spectra, the system was allowed to attain a stable open circuit potential. At least two samples prepared in the same conditions were tested to ensure reproducibility of the results. The impedance plots were fitted using equivalent circuits by means of the Echem Analyst software from Gamry Inc.

# 4 Results and discussion

## Introduction

The present work aims at deposition of anodic oxide films with advanced properties on different metallic substrates using a high voltage pulse anodisation technique. The most important distinction of this technique in comparison with the known galvanostatic (or potentiostatic) anodizing or micro-arc oxidation is an extremely high rate of the film growth realized under the action of short powerful high-voltage electric discharges in electrolyte. Anodisation by this method allows preparing both doped and non-doped coatings. The doping of the anodic films can result in essentially different properties desirable for particular applications such as improved corrosion resistance, photosensitive properties, biocompatibility etc.

To prepare films by powerful pulsed discharge oxidation (PPDO) technique a special setup was developed (3.1). In comparison with conventional anodisation, which is widely used for more than a century, setup for PPDO is relatively unique and has several nuances. This setup is based on accumulation of charge by a low latency capacitor bank, which is injected into the electrochemical cell by means of a low-inertial switch triggered by a synchronizing pulse. It allows to study kinetics of the pulsed discharges without limitation from the equipment side. This system allows to produce compact films with desired thickness by controlling the number of pulses, capacitance and applied voltage. ). It was found that also applying pulses to a porous oxide produced by traditional methods results in melting of the top layer of the pores and creates a complex composite porous film with closed porosity. Aluminium and titanium were the substrates in focus in this work.

In the frame of current PhD thesis four articles were published and two more are currently under submission. In a first work (“Impedance behavior of anodic $TiO_2$ films prepared by galvanostatic anodisation and powerful pulsed discharge in electrolyte”) anodic titania films were prepared on titanium by the novel powerful pulsed discharge technique, which confers extremely high rates of film growth. Electrochemical impedance spectroscopy (EIS) has been used as a main method to study the structure and semiconductive properties of the anodic oxide films grown in sulphuric acid electrolyte. In this work the EIS results were supported with microscopic observations and photoelectrochemical measurements. For comparison, the properties of the anodic films prepared by the conventional galvanostatic anodisation in the same electrolyte were also examined. For modeling of the impedance spectra, different equivalent circuits taking into account the effects of space charge region and film structure were proposed. It was shown that thinner anodic films (d ≈ 25 nm) prepared by both methods demonstrate a similar behavior characteristic of amorphous barrier-type oxide, whereas a very significant difference in the properties of the films produced by the two different approaches was revealed for thicker films (d = 70-120 nm). The discharge-prepared films in this range of thickness are composed by one compact layer with a relatively low concentration of ionized donors ($N_d$ = $1.3\times10^{18}$ $cm^{-3}$) estimated from Mott-Schottky plots, while the conventional galvanostatic method leads to the development of two-layer films consisting of an inner compact layer and a nanoporous outer one. The latter samples exhibit a significantly reduced

photocurrent response at short wavelengths and an essentially higher concentration of ionized donors as compared with the films obtained by the pulsed discharge method.

In another paper (“Anodic alumina films prepared by powerful pulsed discharge oxidation”) a novel powerful pulsed discharge anodisation technique has been applied to prepare dense, homogeneous oxide films of 16 to 180 nm thickness on aluminium surface. The Volta potential difference of the obtained films was studied by scanning Kelvin probe force microscopy. It was shown that the measured VPD values were correlated with the films thicknesses and compared with the same correlation for the anodic alumina films prepared by the conventional galvanostatic and potentiostatic methods. The anodic films carry an induced polarization due to the embedded charges localized near the film interfaces. It was shown that despite the apparent differences in the respective anodisation processes, the pulsed discharge films demonstrate the magnitude of polarization entirely comparable with that of the conventional anodic alumina films of the same thickness. At the same time, the pulsed discharge films are characterized by more uniform surface structure and electrical properties. The characteristic features of the films such as their fast growth and homogeneity have been considered in terms of the processes occurring during the powerful pulsed discharge.

In a third paper (“Titania films obtained by powerful pulsed discharge oxidation in phosphoric acid electrolytes”) thin $TiO_2$ films were prepared on the titanium surface using the powerful pulsed discharge oxidation method in phosphoric acid based electrolytes. The obtained films were characterized with electrochemical impedance spectroscopy, photocurrent spectroscopy, scanning Kelvin probe force microscopy, and Mott-Schottky plot analysis. The potential dependence of the space charge layer capacitance demonstrated that the ionized donor concentration in the oxide is strongly influenced by the electrolyte concentration used during the pulsed anodisation. It is also shown that the main factor influencing the kinetics of the oxide film growth is the concentration of point defects, which, in turn is determined by the composition of electrolyte. SKPFM results show a non-linear evolution of the Volta potential of the anodized surface with the film thickness reaching a plateau after the film thickness exceeds 100 nm. The results obtained in this paper clarify the mechanisms of titania film formation under high-voltage pulses and allow tuning the semiconductive properties of thin oxide layers on titanium surfaces.

In the paper “Aluminium anodisation in deionised water as electrolyte” thin oxide films were prepared electrochemically on the aluminium surface using the high-voltage discharge and high-voltage potentiostatic methods in deionised water as an electrolyte. In contrast to the high-voltage discharge anodisation in highly conductive electrolytes [4-5, 127], the process in deionised water cannot be explained by the same mechanism and has a significant difference in duration. As it was shown previously [127] in highly conductive electrolytes, such as 0.1 M ammonium pentaborate, the full discharge takes less than 0.5 s. In deionised water, the applied voltage decays down to 100 V over a period of more than 100 s. Also in deionised water, the measurements do not reveal the presence of plasma since besides the time elapsed, the current is low compared to previous works [127-128]. Taking into account the growth rate of the films, their composition and structure, it can be suggested that the growth mechanism is similar to that obtained in potentiostatic method in conventional solutions where plasma is not similarly formed during film growth[115].

It was found that the growth of continuous films occurred only at potentials lower than the breakdown potential. The films obtained by the discharge method are more uniform and can grow to a higher thickness in comparison to those formed by the potentiostatic mode, as

demonstrated by electrochemical impedance spectroscopy, transmission electron microscopy, and scanning Kelvin probe force microscopy.

In a following work (“Aluminium and titanium-aluminium nanorods encapsulated into oxide matrix by powerful pulsed discharge method”) metal nanostructures, formed in porous alumina and titania coatings, were encapsulated using the powerful pulsed discharge method. The metal nanorods were deposited in the pores by direct electrodeposition from 1-ethyl-3-methylimidazolium chloride-based ionic liquids. The deposition process was characterized by cyclic voltammetry. Morphology of the encapsulated structures was studied by SEM. It was found that the most efficient method for electrodeposition of pure aluminium into titania nanotubes is the potential cycling method, while for deposition of the Al-Ti alloy in alumina pores a pulsed method with three different steps is preferable. It was shown that closing the titania nanotubes is possible both with empty and metal-filled channels, whereas for the alumina matrix this procedure can be performed only when pores are filled with conductive material.

Finally, in the work “Powerful pulsed discharge oxidation of aluminium and titanium in hydrogen peroxide and distilled water” thin oxide films were prepared electrochemically on the aluminium and titanium surfaces using the high-voltage powerful pulsed discharge oxidation method in distilled water and hydrogen peroxide as electrolytes. It was found that growth of the continuous film on the aluminium is possible in both electrolytes at potentials 1400V-2000V. In the case of titanium in distilled water growth of the films is possible until a certain limit, which decreases with increment of the potential. The films obtained by the discharge method are uniform and have lower number of defects compared to those obtained by conventional methods as demonstrated by several different techniques.

## 4.1 Impedance behavior of anodic $TiO_2$ films prepared by galvanostatic anodisation and powerful pulsed discharge in electrolyte

Electrochimica Acta 76 (2012) 453–461

Contents lists available at SciVerse ScienceDirect

Electrochimica Acta

journal homepage: www.elsevier.com/locate/electacta

### Impedance behaviour of anodic $TiO_2$ films prepared by galvanostatic anodisation and powerful pulsed discharge in electrolyte

S.K. Poznyak[a,b,*], A.D. Lisenkov[a], M.G.S. Ferreira[a], A.I. Kulak[c], M.L. Zheludkevich[a]

[a] University of Aveiro, CICECO, Dep. Ceramics and Glass Eng., 3810-193 Aveiro, Portugal
[b] Research Institute for Physical Chemical Problems, Belarusian State University, 220030 Minsk, Belarus
[c] Institute of General and Inorganic Chemistry, National Academy of Sciences of Belarus, 220072 Minsk, Belarus

ARTICLE INFO

*Article history:*
Received 5 February 2012
Received in revised form 15 May 2012
Accepted 19 May 2012
Available online 29 May 2012

*Keywords:*
Anodic films
Titanium dioxide
Pulsed discharge
EIS
Photocurrent

ABSTRACT

Anodic titania films were prepared on titanium by novel powerful pulsed discharge technique which confers extremely high rates of the film growth. Electrochemical impedance spectroscopy (EIS) has been used as a main method to study the structure and semiconductive properties of the anodic oxide films grown in sulphuric acid electrolyte. The EIS results are supported with microscopic observations and photoelectrochemical measurements. For comparison, the properties of the anodic films prepared by the conventional galvanostatic anodisation in the same electrolyte were also examined. For modeling of the impedance spectra, different equivalent circuits taking into account the effects of space charge region and film structure were proposed. Thinner anodic films ($d \approx 25$ nm) prepared by both methods demonstrate a similar behaviour characteristic of amorphous barrier-type oxide, whereas a very significant difference in the properties of the films produced by the two different approaches was revealed for thicker films ($d = 70–120$ nm). The discharge-prepared films in this range of thickness are composed by one compact layer with a relatively low concentration of ionised donors ($N_d = (1–3) \times 10^{18}$ cm$^{-3}$) estimated from Mott–Schottky plots, whilst the conventional galvanostatic method leads to the development of two-layer films consisting of an inner compact layer and a nanoporous outer one. The latter samples exhibit a significantly reduced photocurrent response at short wavelengths and an essentially higher concentration of ionised donors as compared with the films obtained by the pulsed discharge method.


#### 1. Introduction

Titanium and its alloys are widely used in different applications owing to their good mechanical properties and a high corrosion resistance in various media [1–3]. The latter is provided by a chemically stable oxide film which spontaneously forms on titanium. Electrochemical oxidation (anodisation) of titanium and its alloys provides thicker oxide layers demonstrating improved protective and functional properties [4,5]. Thin films of titania have very high potential to be used for fabrication of memristors [6]. The memristance arises naturally in nanoscale systems in which solid-state electronic and ionic transport are coupled under an external bias voltage [7]. The thickness and defect structure of the titania films has a significant effect on the memristance properties [6].

It has been shown that the properties of the anodic films on titanium depend greatly on the conditions at which the film is grown [8–16]. One of the important factors affecting the characteristics of the anodic films is their growth rate. Blackwood and Peter reported that the relative dielectric constant, $\varepsilon$, and defect concentration profiles in the oxide film depend markedly on the film growth rate [11]. Ohtsuka and Otsuki revealed that the $\varepsilon$ value increases and the ionised donor concentration decreases with increasing the growth rate of the anodic film on titanium [14]. The refractive index of the anodic $TiO_2$ films was also found to be smaller with the higher growth rate [13].

Recently we have demonstrated the application of the high-voltage pulsed discharge technique for creation of thin anodic films on titanium [17]. Under the action of single powerful electric discharges in electrolyte, extremely high rates (400–700 μm/s) of the oxide film growth were reached on the titanium anode. The growth rate is the fastest ever reported. The results of Auger depth profiling showed that the oxide films prepared by the pulsed discharge method are characterised by higher stoichiometry and more homogeneous distribution of basic elements (Ti and O) through the film thickness in comparison to the films grown by the conventional galvanostatic anodisation [17]. Moreover, enhanced photoelectrochemical activity was revealed for the pulse discharge-prepared films motivating their further investigation. Also preparation of oxide films on pure aluminium electrodes using the powerful

* Corresponding author. Permanent address: Research Institute for Physical Chemical Problems, Belarusian State University, 220030 Minsk, Belarus.
*E-mail addresses:* poznyak@bsu.by, poznyak@ua.pt (S.K. Poznyak).

0013-4686/$ – see front matter © 2012 Elsevier Ltd. All rights reserved.
http://dx.doi.org/10.1016/j.electacta.2012.05.064

Contribution to this paper:
Fitting of the EIS obtained data, electron microscopy, partial sample preparation, reproducibility experiments, preparation of all images, partial text preparation.

### 4.1.1 Introduction

Titanium and its alloys are widely used in different applications owing to their good mechanical properties and a high corrosion resistance in various media[129]. The latter is provided by a chemically stable oxide film which spontaneously forms on titanium. Electrochemical oxidation (anodisation) of titanium and its alloys provides thicker oxide layers demonstrating improved protective and functional properties [2, 24]. Thin films of titania has very high potential to be used for fabrication of memristors[130]. The memristance arises naturally in nanoscale systems in which solid-state electronic and ionic transport are coupled under an external bias voltage[131]. The thickness and defect structure of the titania films has a significant effect on the memristance properties[130].

It have been shown that the properties of the anodic films on titanium depend greatly on the conditions at which the film is grown [22, 25, 27, 132-138]. One of the important factors affecting the characteristics of the anodic films is their growth rate. Blackwood and Peter reported that the relative dielectric constant, ε, and defect concentration profiles in the oxide film depend markedly on the film growth rate[134]. Ohtsuka and Otsuki revealed that the ε value increases and the ionized donor concentration decreases with increasing the growth rate of the anodic film on titanium[25]. The refractive index of the anodic $TiO_2$ films was also found to be smaller with the higher growth rate[136].

Recently we have demonstrated the application of the high-voltage pulsed discharge technique for creation of thin anodic films on titanium[4]. Under the action of single powerful electric discharges in electrolyte, extremely high rates (400-700 μm/s) of the oxide film growth were reached on the titanium anode. The growth rate is the fastest ever reported. The results of Auger depth profiling showed that the oxide films prepared by the pulsed discharge method are characterized by higher stoichiometry and more homogeneous distribution of basic elements (Ti and O) through the film thickness in comparison to the films grown by the conventional galvanostatic anodisation[4]. Moreover, enhanced photoelectrochemical activity was revealed for the pulse discharge-prepared films motivating their further investigation. Also preparation of oxide films on pure aluminium electrodes using the powerful pulsed discharge technique was studied[127]. It was found that dense one-layer alumina films with thicknesses up to 200 nm can be created on the Al surface. Scanning Kelvin Probe Force Microscopy (SKPFM) measurements showed that the anodic alumina films prepared by the pulsed discharge method have more uniform surface structure and electrical properties which are less dependent on the initial surface conditions than those of the films prepared by the conventional anodisation methods.

Electrochemical impedance spectroscopy (EIS) is a powerful technique for *in situ* characterization of various oxide films on metal surfaces. This technique was successfully applied to examine anodic oxide films on different valve metals such as Al[139-141], Zr[142], Nb[143]. EIS was also used to characterize oxide films on titanium surface [17, 144-158] . Blackwood [144] investigated the impedance response from very thin (several nanometers) passive oxide films on titanium and showed that the contribution of the space charge region (SCR) formed in the oxide layer must be taken into account when interpreting the impedance data. In a number of EIS studies[17, 149-150], impedance spectra of thin anodic films on titanium exhibit a single time constant, which is indicative of a uniform compact layer, whereas thicker films tend to reveal a second time constant in the impedance spectra. In the latter case, the interpretation of the EIS data was based on a two-layer model of the oxide film composed by a thin intact inner layer and a porous outer layer [17, 145, 149-151, 158].

In the present work, electrochemical impedance spectroscopy has been used as the main method for characterization of the structural features and semiconductive properties of novel anodic oxide films formed on titanium at extremely high growth rates under the powerful pulsed discharges (hereafter referred to as PD films). For comparison reasons, impedance spectra recorded on the films grown by the conventional galvanostatic oxidation (hereafter referred to as GS films) are also discussed. The photoelectrochemical method as well as transmission electron microscopy (TEM) accompanied with electron diffraction were also applied for studying the anodic oxide films to support the selection of the equivalent circuits and the conclusions drawn from the EIS measurements.

## 4.1.2 Experimental

Titanium plates (0.8×70 mm; 99.999% Ti) used as working electrodes were polished mechanically and then chemically in $HF:HNO_3$ (1:3 by volume) mixture to mirror finish and finally rinsed with deionised water. Part of the surface was isolated with epoxy resin, giving electrode working area of 6 $cm^2$.The electrochemical cell used for the pulsed discharge oxidation of Ti was constructed from high-impact polystyrene and consisted of a titanium anode placed in the center of a cylindrical Ti cathode with 20 times larger surface area. 1 M H2SO4 aqueous solution (T = 25±1°C ) was used as an electrolyte. Electric discharges in the electrode system were generated using a low-inductive 100 μF capacitor bank charged to a definite voltage (1350 V) which was commutated with a low-inertial relay triggered by a synchronizing pulse. Duration of discharge was less than 10 μs Conventional galvanostatic anodisation of the titanium electrodes was performed in the same cell at a current density of 10 mA $cm^{-2}$ using a controllable dc power supply.

The EIS measurements were performed using a Gamry FAS2 Femtostat with a PCI4 Controller in a $10^5$ down to $10^{-2}$ Hz frequency range with a step of 10 points per decade. Impedance spectra were recorded applying a 10 mV sinusoidal perturbation at open circuit potential or at different potentials in the range from 0.8 V to -0.4 V vs SCE. The EIS measurements were carried out at room temperature in a conventional three-electrode cell consisting of a saturated calomel reference electrode (SCE), a platinum foil as the counter electrode and the working electrode with an exposed area of 1 $cm^2$. The cell was placed in a Faraday cage to avoid interferences with external electromagnetic fields. The working solution was 0.1 M acetate buffer (pH 6). To remove oxygen, the solution was purged with argon. Before the spectra recording, the system was allowed to attain a stable open circuit potential or a quasi-stationary current under potentiostatic polarization. At least two samples prepared under the same conditions were tested to ensure reproducibility of the results. The impedance plots were fitted using different equivalent circuits by means of the Elchem Analyst software from Gamry Inc.

Photocurrent spectra were recorded in a quartz cell having an optical quality window. A setup equipped with a high-intensity grating monochromator, a 1000 W xenon lamp and a slowly rotating light chopper (0.3 Hz) was used for monochromatic irradiation of the working electrode. Photocurrent spectra were corrected for the spectral intensity distribution at the monochromator output measured by a calibrated thermocouple power meter.

TEM measurements were performed on a Hitachi H9000 transmission electron microscope at an acceleration voltage of 300 kV. Electron transparent sections for TEM with a thickness of 15 nm were cut using a Leica Reichert Supernova ultramicrotome. To prepare the

samples, titanium electrodes with an oxide film were embedded into resin and polished from the metal side up to a thickness of 10-15 μm, and then they were re-embedded into resin. A cut with a width of 10 μm was then made using an ultramicrotome with a glass knife. Obtained microrod (10-15μm × 10μm × 3-4mm, oxide is on the one of faces) was embedded once more into resin, perpendicular to the cut, and finally was sliced with a diamond knife (Diatome 45°).

### 4.1.3 Anodic oxide film formation

Upon the action of powerful electric discharge on the electrode system, the extremely rapid growth of the oxide film on titanium anode surface is observed. An electric charge of 0.0225 C $cm^{-2}$ was passed through the Ti electrode – electrolyte interface during one discharge, resulting in the formation of 25 nm thick anodic film as shown in our previous work [4]. The subsequent discharges lead to step-wise increase in the film thickness visually observed as a characteristic change of the interference color. The color properties of anodic oxide films on titanium have been previously shown to originate from light interference[159]. The average thickness of the obtained anodic films was estimated by the depth profile analysis using Auger electron spectroscopy as described in detail in our previous work[4]. For relatively thick films (120-170 nm) the thickness values were also confirmed by TEM observations (Fig. 4.1.1.). The films obtained by the discharge approach appear to be intact and uniform.

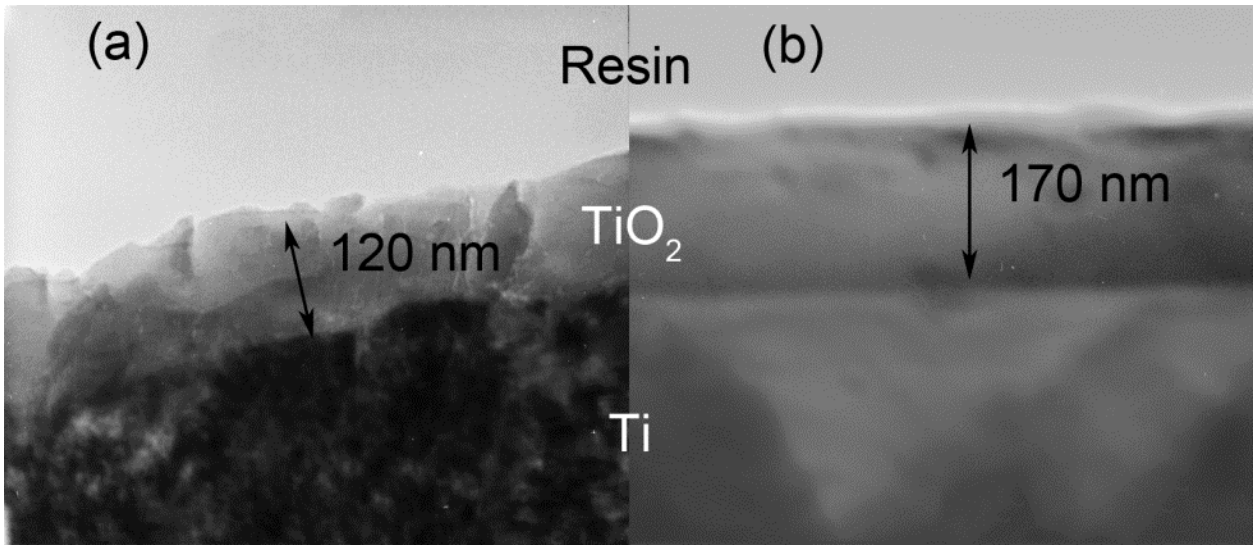


**Figure 4.1.1.** Transmission electron micrographs of a cross section of the anodic $TiO_2$ films on titanium prepared by the powerful pulsed discharge method. Five (A) and ten (B) discharges (U = 1350 V; C = 100 μF) were passed through the electrode system.

For comparison, the anodic films on titanium were also prepared by the conventional galvanostatic anodisation in the same electrolyte at a current density (j) of 10 mA $cm^{-2}$. The duration of the galvanostatic anodisation was chosen so that the thickness of the GS films was coincident with that of the PD films. This makes possible more correct comparison of the properties of the anodic films prepared by these two methods. The anodizing ratio (the ratio between the oxide film thickness, d, and the maximum film formation voltage, Umax) calculated

for the galvanostatic growth of anodic $TiO_2$ films was about 2.78 nm/V and slightly decreased down to 2.65 nm/V for the films with d > 120 nm. This estimate is in a good agreement with the anodizing ratio values (2.5-3 nm/V) more commonly reported in literature for the titania anodic films grown in sulphuric acid solutions [27, 156, 159-162].

### 4.1.4 EIS measurements

Figure 4.1.2 shows the Bode plots obtained on the titanium electrodes covered with GS and PD anodic oxide films with different thickness. The impedance spectra presented in Fig. 4.1.2 were measured at anodic bias (0.6 V vs SCE). In this potential region the EIS spectra of the anodic films, as will be shown below, are insignificantly changed with electrode potential. In a wide range of thickness, impedance spectra of the PD films exhibit an almost pure capacitive response (one time constant) illustrated by a phase angle close to -90º over a wide frequency range from 103 to 0.1Hz originated from capacitance of the formed titania film (Fig. 4.1.2a). Only at lower frequencies does the phase angle starts to increase demonstrating the onset of the resistive response originated from the resistance of the oxide layer.

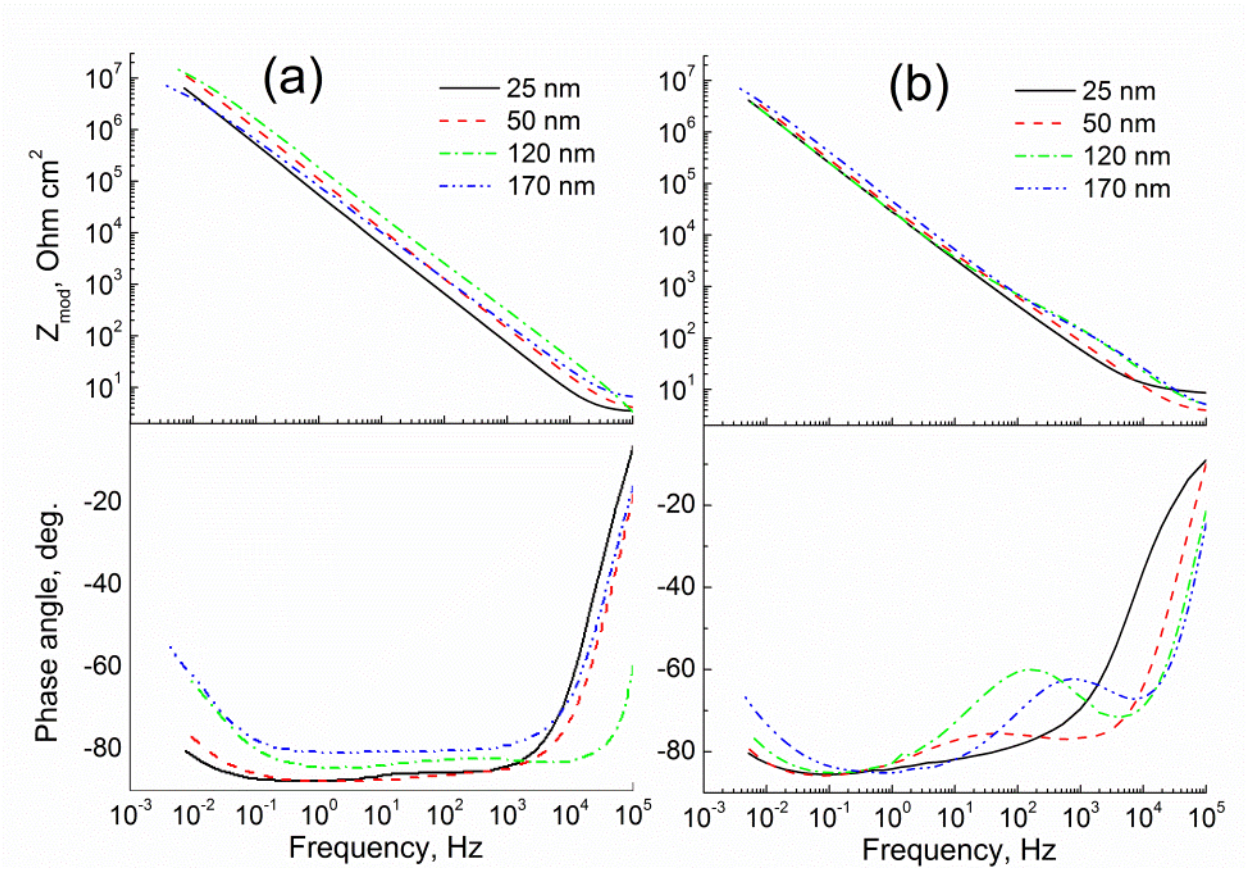


**Figure 4.1.2.** Impedance spectra of the anodic oxide films with different thickness formed on titanium by pulsed discharge method (a) and galvanostatic anodising (b). The spectra were measured at a potential of 0.6 V.

The Bode plot of the thinnest (d ≈ 25 nm) anodic film produced by the conventional galvanostatic technique exhibits quite similar behavior and impedance values as compared with those of the pulse discharge-prepared one with the same thickness (Fig. 4.1.2b). As the film thickness grows, a second time constant begins to appear in the EIS spectra of the GS films at intermediate frequencies. This relaxation process starts to be more pronounced and shifts gradually to higher frequencies with film thickening (Fig. 4.1.2b).

According to the literature [17, 145, 149-151], the first time constant can be assigned to the response from compact inner layer. Another time constant at intermediate frequencies is related to the outer porous layer. The formation of bilayer structure for the GS films is also supported using cross-sectional TEM analysis (Fig. 4.1.3). The bright field image (Fig. 4.1.3a) demonstrates a porous outer layer. Two layers are well distinct on the dark field (Fig. 4.1.3b): outer layer is composed almost completely by amorphous oxide, while clearly defined crystallites (bright spots) can be found in inner layer. These electron microscopy data are in good agreement with the TEM observations presented by Jaeggi et al. [149]. Taking into account this consideration, one may assume that the anodic films grown on titanium by the pulsed discharge method in a wide range of thickness is constituted by only one compact uniform oxide layer. This suggestion is confirmed by TEM as shown in Fig. 4.1.1.

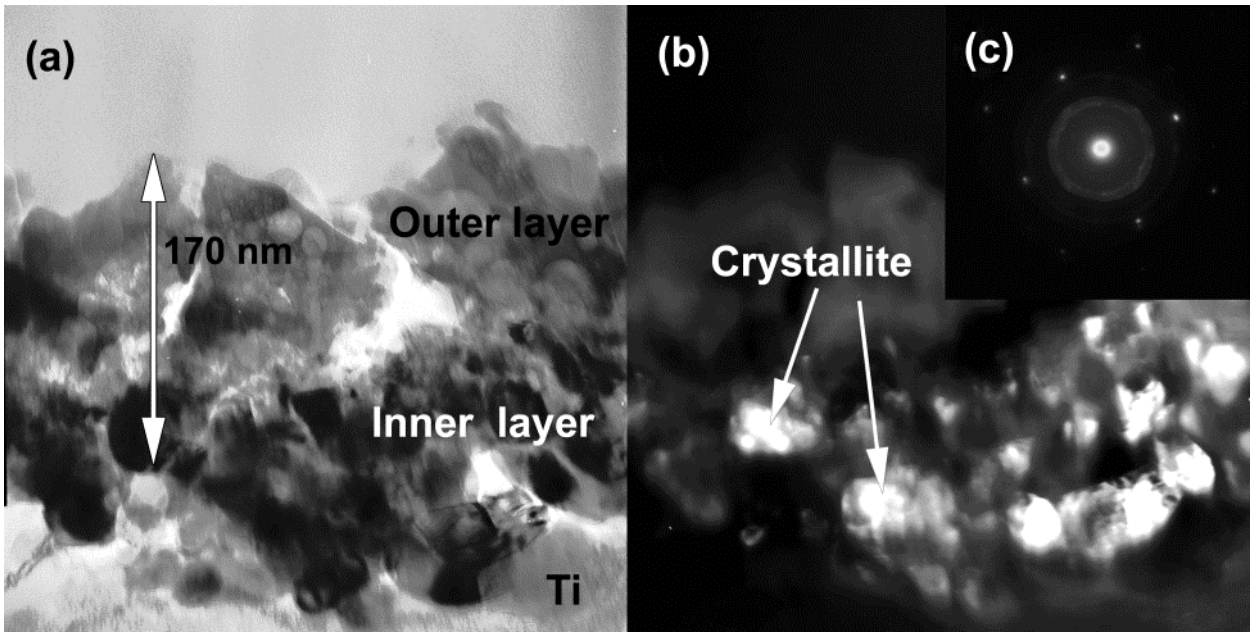


**Figure 4.1.3.** Bright field (A) and dark field (B) transmission electron micrographs of a cross section of the anodic $TiO_2$ film prepared by galvanostatic anodizing ($U_{max}$ = 64 V). Bright parts on the dark field TEM image show $TiO_2$ nanocrystallites. (C) shows electron diffraction pattern from the $TiO_2$ nanocrystallites.

It is known that titanium dioxide films prepared by anodisation are not simply a dielectric, but demonstrate well defined semiconductive behavior[163-164]. Therefore, for these materials the influence of a space charge region (SCR) formed at the oxide – electrolyte interface on the electrochemical impedance spectrum can be appreciable [144, 151, 158]. To clarify this point for both PD and GS anodic films, the effect of the applied potential on the impedance spectra was studied. It is well known that polarization of a semiconductive film leads to variation of its

capacitance and, in turn, to modulation of the corresponding part of the impedance spectra. The modulation of the capacitance response under the variable polarization is used as a proof of correct assignment of the corresponding part of the spectra to the SCR[158]. The impedance spectra for the films with different thicknesses were acquired in a potential range from -0.4 to 0.8 V for GS and PD films where the current values are very low (≤ 1-2 μA $cm^{-2}$), moving from positive to negative potentials with a 0.2 V step.

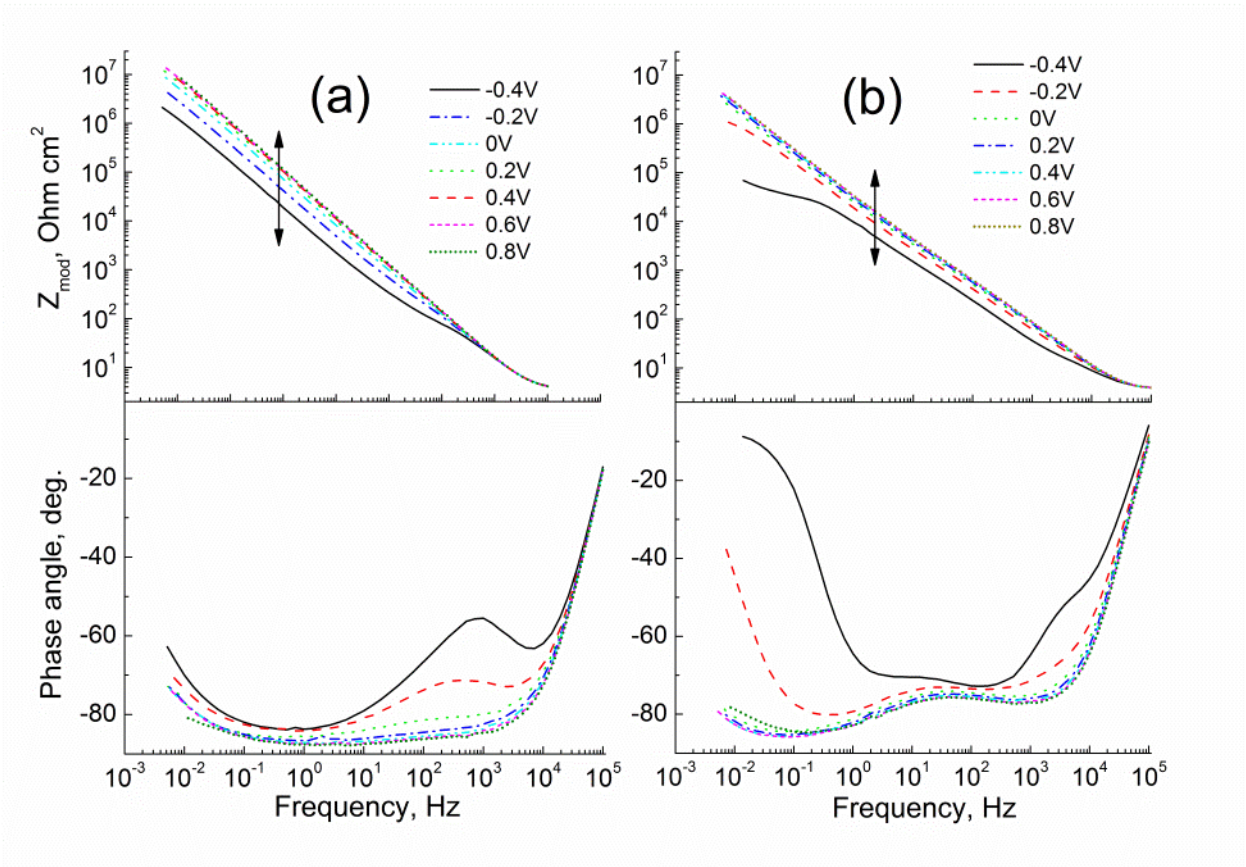


**Figure 4.1.4.** Impedance spectra of the 50 nm thick anodic oxide films formed on titanium by pulsed discharge method (a) and galvanostatic anodizing (b). The spectra were measured at different potentials.

The impedance spectra of 50 nm thick PD and GS anodic films taken at different potentials are shown in Fig. 4.1.4. The spectra depend slightly on the electrode potential in the region of positive bias. At potentials below 0 V vs SCE, a distinct second time constant appears in the spectra of the PD films and a third time constant – in the spectra of the GS ones (Fig. 4.1.4). This additional time constant is gradually shifted to lower frequencies with increasing film thickness. It is important to notice that the variation of the impedance spectra with electrode potential is reversible, i.e. after negative polarization similar spectra can be observed again at positive potentials. It is evident that this relaxation process modulated by the applied potential is originated from the SCR response.

In order to take into account the structure of the anodic oxide films formed on titanium and possible contribution of the space charge region, different equivalent electric circuits (EEC) were tested for fitting the experimental impedance spectra. When choosing an appropriate EEC

describing the obtained impedance spectra with a minimum error and a minimum number of EEC elements, physical significance of the EEC parameters as well as their correct evolution with changing the electrode potential and $TiO_2$ film thickness were taken into consideration.

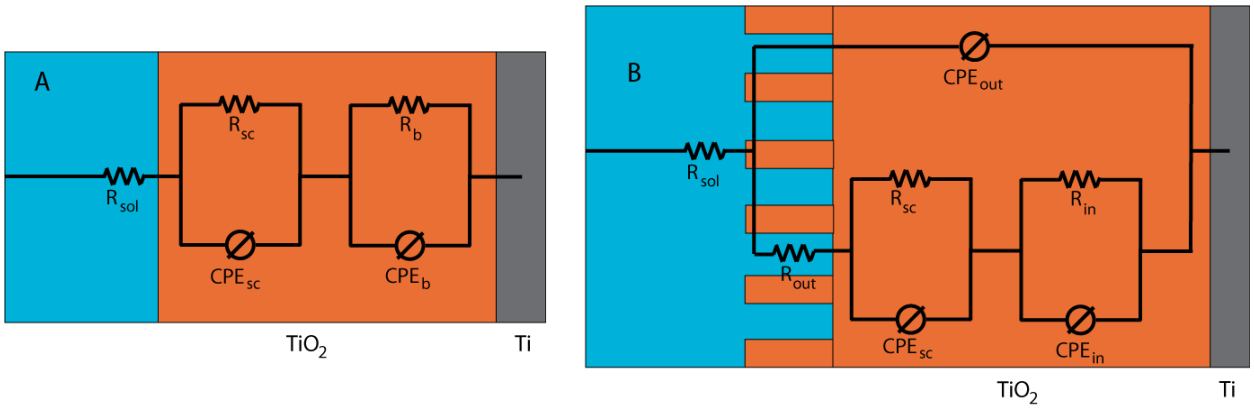


**Figure 4.1.5.** Equivalent circuits used for fitting the impedance spectra of the anodic films formed on titanium by pulsed discharge method (a) and galvanostatic oxidation (b).

The whole set of EIS data for PD films can be satisfactorily fitted using the circuit (Fig. 4.1.5a) corresponding to the Voight model[163], where CPEsc and CPEb represent the space charge layer and bulk film constant phase elements and Rsol, Rsc and Rb – the resistances of electrolyte, space charge layer and bulk film, respectively. Impedance spectra of the GS films were fitted using a more complex EEC shown in Fig. 4.1.5b, where CPEout and CPEin represent the constant phase elements of the outer nanoporous layer and inner compact layer and Rout and Rin – the resistance of the outer nanoporous layer and inner compact layer of the film, respectively. These equivalent circuits were already reported in the literature as adequate for fitting the EIS spectra of anodic titania layers obtained at different conditions[158].

A constant phase element (CPE) instead of a capacitor was used in all fittings presented in the work. Such modification is needed when the phase angle of the capacitor is different from -90 degrees. The physical origin of the CPE has been widely discussed in literature[125, 165]. The impedance of the CPE, $Z_{CPE}$, depends on frequency, ω, according to the following equation:

$$Z_{CPE} = [Q(j\omega)^n]^{-1} \qquad (4.1.1)$$

where Q is a parameter numerically equal to the admittance ($|Z|^{-1}$) at $\omega$= 1 rad $s^{-1}$ and n ≤ 1 is a power coefficient calculated as ratio of the phase angle at maximum of the corresponding time constant to -90 degrees. The capacitance values for the capacitive elements in the equivalent circuit were calculated as described previously[166].

As seen from Figure 4.1.6, the fitting curves show good agreement with the experimental impedance spectra.

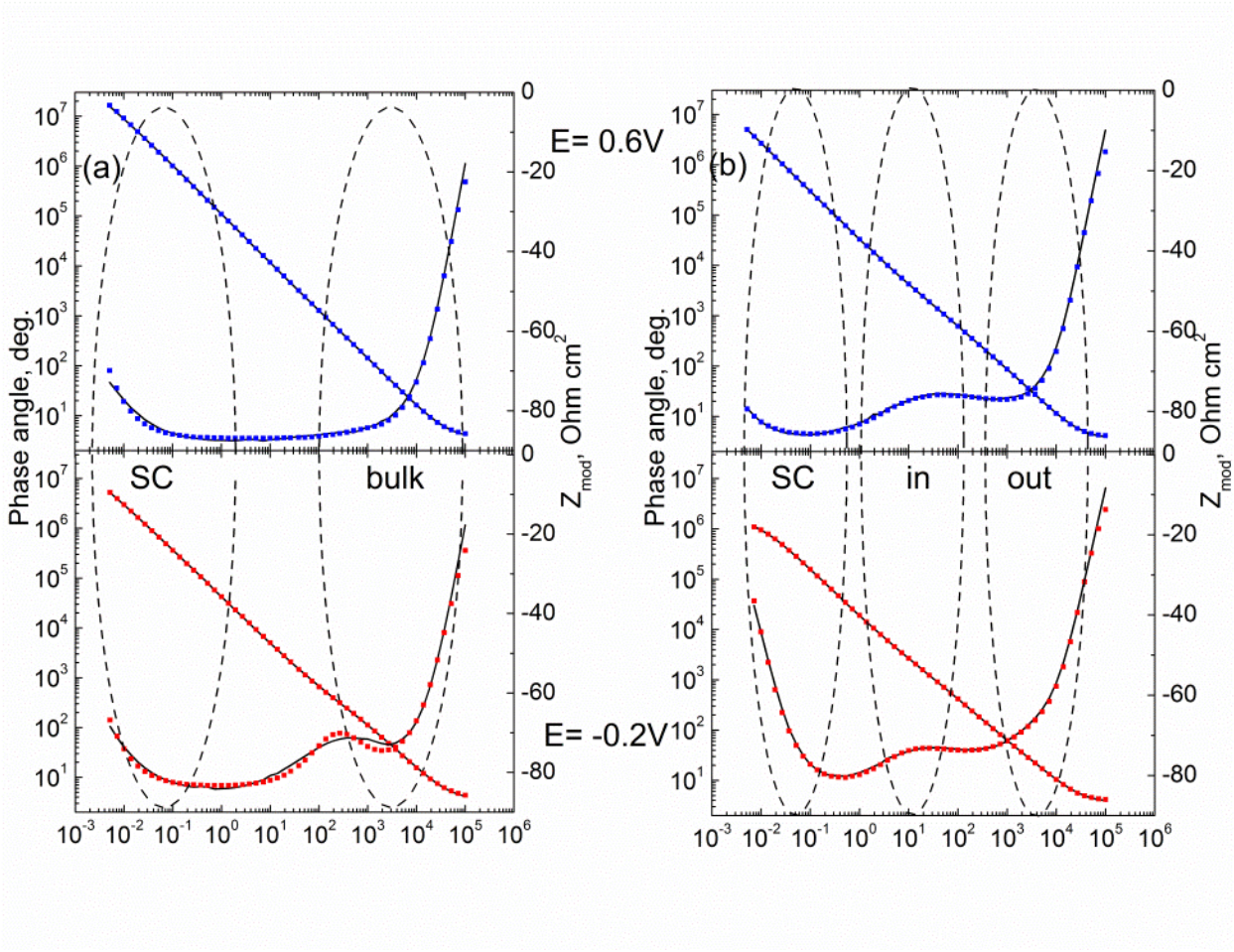


**Figure 4.1.6.** Impedance spectra measured at electrode potentials of 0.6 and -0.2 V for 50 nm thick anodic titania films formed by pulsed discharge method (a) and galvanostatic anodizing (b). Symbols are the experimental points; lines present the fitting curves obtained using the equivalent circuits shown in Fig. 4.1.5.

**Table 4.1.1.**
Equivalent circuit parameters and respective errors (in percents) obtained after fitting the impedance spectra of 50 nm thick PD film (Figs. 4.1.4 and 4.1.6) polarized at different potentials. $n_{sc}$ and $n_b$ are the power coefficients for the constant phase elements of SCR and bulk layer, respectively.

| Applied potential (V) | $R_{sol}$ (Ohm cm$^2$) | $R_{sc}$ ×10$^{-6}$ (Ohm cm$^2$) | $CPE_{sc}$ ×10$^6$ (S s$^n$ cm$^{-2}$) | $n_{sc}$ | $R_b$ (Ohm cm$^2$) | $CPE_b$×10$^6$ (S s$^n$ cm$^{-2}$) | $n_b$ |
|---|---|---|---|---|---|---|---|
| -0.2 | 3.7 ±2.4% | 18 ±7.8% | 4.3 ±0.70% | 0.92 ±0.24% | 140 ±9.3% | 9.2 ±14% | 0.88 ±1.7% |
| 0 | 3.8 ±2.4% | 40 ±9.5% | 2.4 ±0.71% | 0.95 ±0.24% | 110 ±21% | 22 ±31% | 0.87 ±3.4% |
| 0.6 | 3.9 ±2.1% | 56 ±7.9% | 1.6 ±0.69% | 0.97 ±1.9% | 8.0 ±11% | 27 ±20% | 1.0 ±19%* |

**Table 4.1.2.**
Equivalent circuit parameters and respective errors (in percents) calculated by fitting the impedance spectra of 50 nm thick GS film (Figs. 4.1.4 and 4.1.6) polarized at different potentials. $n_{sc}$, $n_{out}$ and $n_{in}$ are the power coefficients for the constant phase elements of SCR, outer nanoporous layer and inner compact layer, respectively.

| Applied potential (V) | $R_{sol}$ (Ohm cm$^2$) | $R_{out}$ (Ohm cm$^2$) | $CPE_{out}\times10^6$ (S s$^n$ cm$^{-2}$) | $n_{out}$ | $R_{in}\times10^{-3}$ (Ohm cm$^2$) | $CPE_{in}\times10^6$ (S s$^n$ cm$^{-2}$) | $n_{in}$ | $R_{sc}\times10^{-6}$ (Ohm cm$^2$) | $CPE_{sc}\times10^6$ (S s$^n$ cm$^{-2}$) | $n_{sc}$ |
|---|---|---|---|---|---|---|---|---|---|---|
| -0.2 | 4.0 ±0.38% | 31 ±9.4% | 1.6 ±9.4% | 1.0±7.3%* | 2.1 ±17% | 37 ±26% | 0.66 ±5.5% | 1.5 ±3.7% | 8.1 ±1.9% | 0.92 ±0.96% |
| 0 | 4.0 ±0.45% | 36 ±17% | 1.5 ±12% | 1.0 ±11%* | 3.7 ±6.5% | 34 ±32% | 0.60 ±7.5% | 26 ±2.4% | 5.6 ±4.1% | 0.93 ±0.84% |
| 0.6 | 3.9 ±0.41% | 62 ±9.4% | 1.5 ±14% | 1.0±8.2%* | 5.5 ±6.6% | 28 ±36% | 0.58 ±8.4% | 41 ±2.7% | 3.9 ±3.8% | 0.95 ±1.2% |

*High value of error was obtained due to the limitation of the n. Maximum value of CPE exponent is 1, so higher values have no physical meaning.

The representative results of impedance data fitting for different electrode potentials are presented in Tables 4.1.1 and 4.1.2 for 50 nm thick PD and GS films, respectively. These data show that all the elements of the equivalent circuits behave in a consistent manner. The resistance of the space charge region of both PD and GS films is highest and ranges from 10 to 70 MOhm cm$^2$ under positive bias, decreasing significantly at negative polarization. The outer layer of the GS films has more than three orders of magnitude lower resistance, suggesting the porous structure of this layer. The capacitance of the outer and inner layers depend noticeably less on the applied potential in comparison with parameters of the space charge region. The electrolyte resistance (several Ohms cm$^2$) remains constant over the whole potential range. The values of the exponent n range from 0.8 to 1 (except nin for the GS film), conforming thereby mainly capacitive character of the CPE elements.

The main objective of the performed impedance analysis was to elucidate how the extremely fast growth of the titania films can influence the structure and semiconducting properties of the anodic layers. The results clearly show that PD films are constituted by a single layer while the conventional GS films are constituted of outer porous and inner dense oxide layers. The semiconductive properties of the anodic layers can be assessed by analyzing the impedance response from the space charge layer.

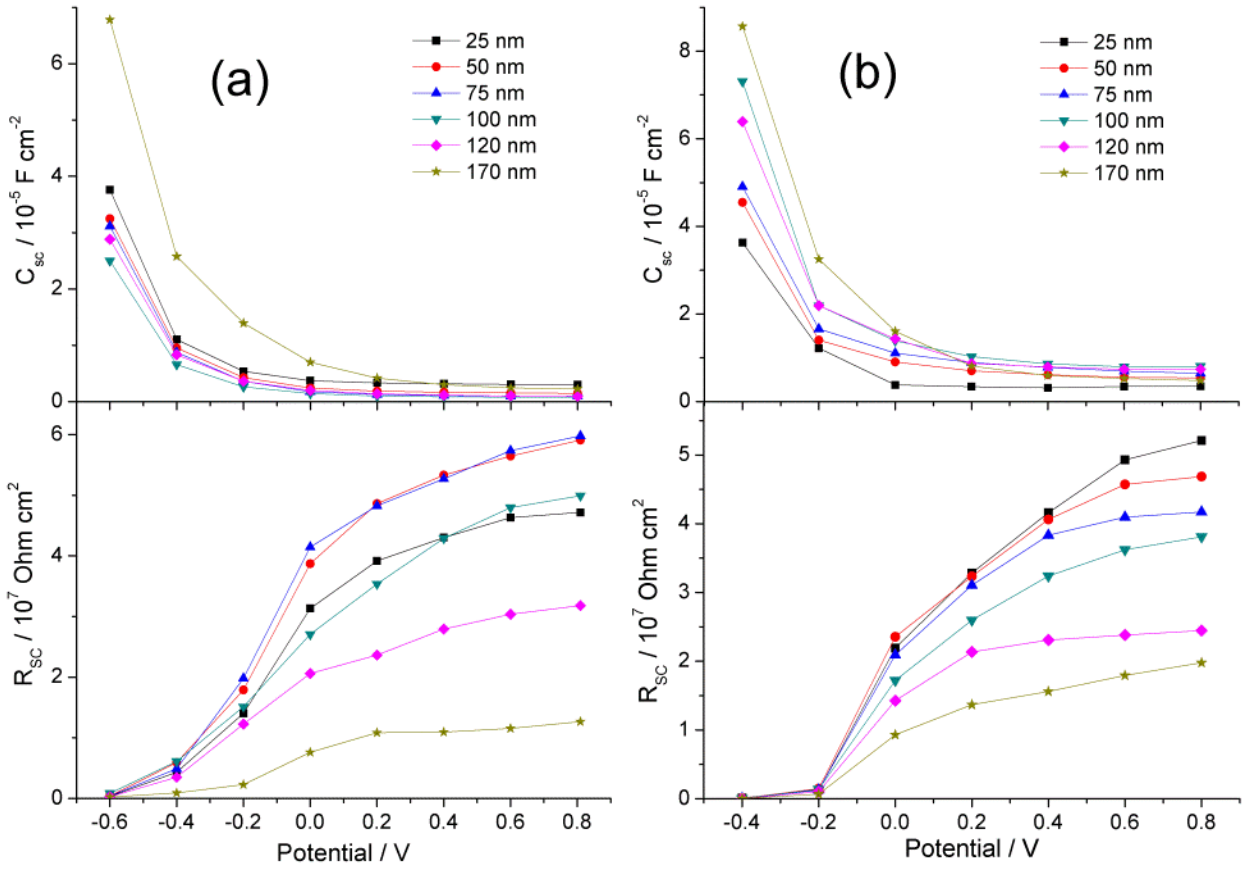


**Figure 4.1.7.** Capacitance and resistance of the SCR for anodic titania films formed by pulsed discharge method (a) and galvanostatic anodizing (b) as a function of the electrode potential for different thicknesses of the films.

Figures **4.1.**7 presents the dependencies of the equivalent circuit parameters related to the SCR for the PD and GS anodic films with different thicknesses on the electrode potential. As seen from this figure, the values of SCR resistance and SCR capacitance decrease and increase, respectively, with decreasing electrode potential. As expected the sharpest variation of the Rsc and Ccs values is observed in the negative potential region near the flat band potential, Efb, in accordance with the well known Mott-Schottky equation:

$$\frac{1}{C_{sc}^2} = \frac{2}{eN_d\varepsilon\varepsilon_0}\left(E - E_{fb} - \frac{kT}{e}\right) \qquad (4.1.2)$$

where $N_d$ is the ionized donor concentration for a n-type semiconductor, ε the relative dielectric constant of the anodic film, $\varepsilon_0$ the permittivity of free space, E the electrode potential, k the Boltzmann constant, T the temperature and e the charge of an electron.

It should be noted that the validity of the simple Mott-Schottky analysis is unambiguously confirmed only for classical single crystal or polycrystalline semiconductors. For thin anodic oxide films on valve metals, which are usually amorphous, the validity of this analysis is controversial [167-168]. Notwithstanding this fact, the Mott-Schottky relationship has been used by a great number of researchers for estimating semiconductive parameters of thin anodic oxide films on various valve metals such as titanium[25, 134, 144, 151, 156-158, 163], niobium [169-170], tin[171],

tungsten[172] and others. All things considered, in the present work we used the Mott-Schottky analysis for comparative reason to compare the semiconductive characteristics of the two types (GS and PD) of the anodic titania films having similar thickness.

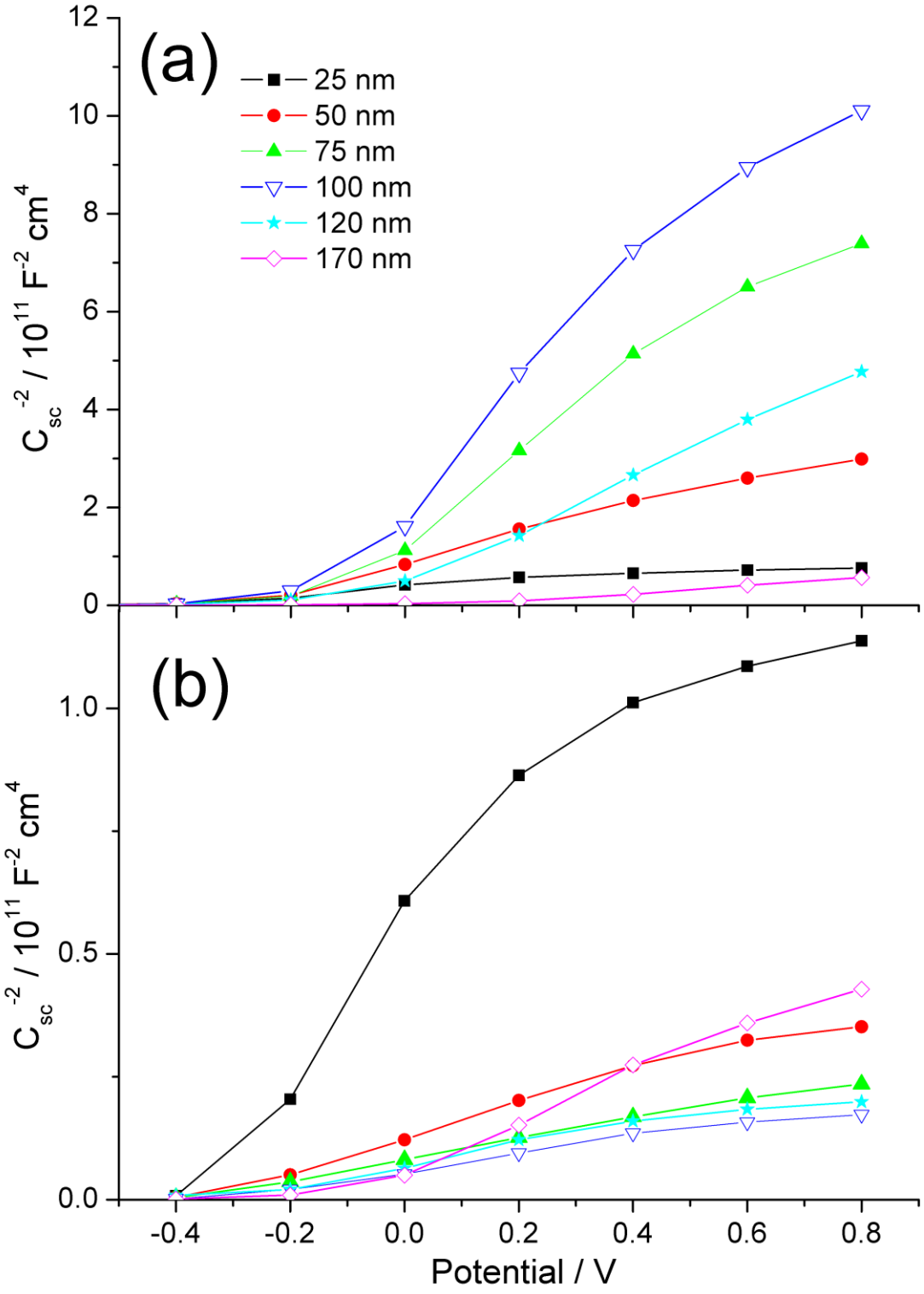


**Figure 4.1.8.** Mott-Schottky plots, constructed from the data shown in Fig. 4.1.7, for anodic titania films formed by pulsed discharge method (a) and galvanostatic anodizing (b).

As seen from Fig. 4.1.8, the calculated $Csc^{-2}$ – E plots for both GS and PD films demonstrate a loss of linearity in the whole potential range studied, and some decrease in the slope is observed at higher potentials. Such nonlinearity of the Mott-Schottky plots has been previously found for titania anodic films and discussed by a number of researchers [25, 134, 144, 151, 156-158, 163, 173-176]. Different hypotheses have been proposed to rationalize this behavior: uniform distribution of the donor concentration through the film thickness [144], existence of multiple donor levels within the bandgap of the oxide film [174] and field dependence of the relative dielectric constant of the oxide [175]. Moreover, at high positive potentials the passive film can be totally depleted of charge carriers when the space charge region becomes comparable with the film thickness [170, 177]. Taking into account the heterogeneity and complexity of the electronic structure of anodic films on titanium, probably not a single, but several above-mentioned factors can be responsible for the nonlinearity of the Mott-Schottky plots.

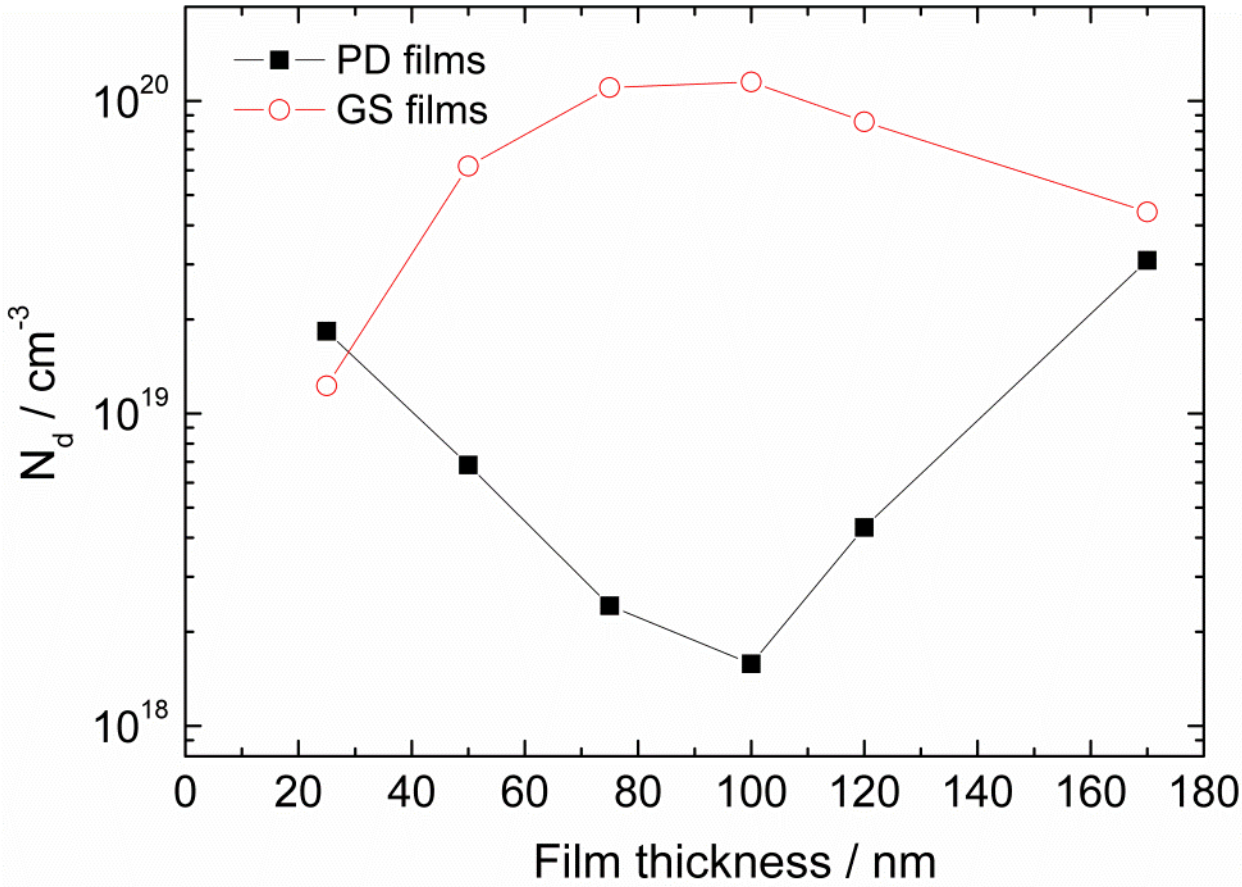


**Figure 4.1.9.** Evolution of the ionized donor concentration, $N_d$, calculated from the Mott-Schottky plots, with thickness of the anodic oxide films prepared by the conventional galvanostatic oxidation and the pulsed discharge method.

For estimation of the ionized donor concentration we used a linear portion of the $C_{cs}^{-2}$ - E plots observed in the potential region from -0.2 to 0.4 V. It is worth to mention that the SCR capacitance values were obtained using analysis of the impedance spectra in a wide range of frequencies. Moreover, the non-ideality of the capacitance was taken into account employing the constant phase element approach. Figure 4.1.9 summarizes the $N_d$ values for the anodic titania films with different thicknesses, which was estimated from the Mott-Schottky plots

assuming ε = 57 (the average of frequently reported ε values for anodic oxide films [25, 134, 144, 151, 156-158, 163, 173-176]).

High $N_d$ values observed for galvanostatically grown $TiO_2$ films (> 1019 cm-3) are in good agreement with the literature data[25, 134, 144, 151, 156-158, 163, 173-176, 178]. The increase in the GS film thickness from 25 to 100 nm leads to some rise in the ionized donor concentration. On further thickening of these films the ionized donor concentration begins to decrease. An essentially different situation was revealed in the case of the anodic films prepared by the pulsed discharge method. Surprisingly the relatively thin PD films become less defective with increasing their thickness in contrast to the GS ones (Fig. 4.1.9). The ionized donor concentration for the 100 nm thick PD film is about two orders lower than that for the GS film with the same thickness. The further thickening of the PD films leads to the increase in Nd, which could correlate with the onset of the film crystallization[4].

### 4.1.5 Photoelectrochemical spectroscopy measurements

Photocurrent spectroscopy is the other useful *in situ* technique which was repeatedly applied to examine semiconducting characteristics of titania anodic films[144, 163-164] and can be used to support the conclusions drawn from EIS results. We applied this technique to gain complementary information on the structural and semiconducting properties of the PD and GS anodic oxide films under study. The photocurrent spectra recorded under anodic polarization on two different types of the films are shown in Figure 4.1.10.

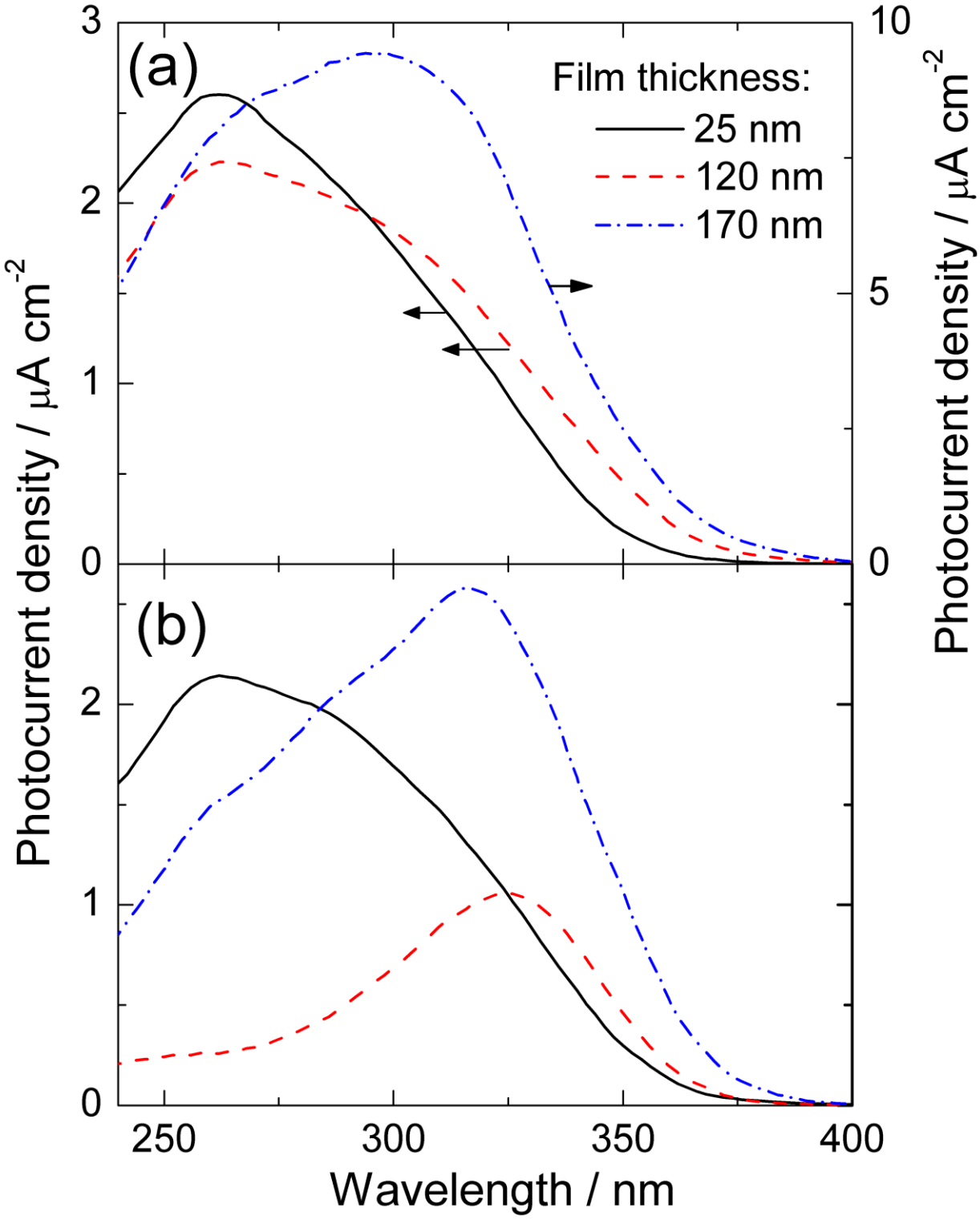


**Figure 4.1.10.** Photocurrent spectra of the anodic oxide films with different thickness prepared by the pulsed discharge method (a) and conventional galvanostatic anodizing (b). Electrode potential: 0.8 V vs. SCE.

For thinnest films, apart a small difference in the photocurrent density, the spectrum for the GS films is similar to that for the PD films exhibiting a peak at 260 nm. Further thickening of the GS film results in a significant drop of the photocurrent in the short-wavelength region of spectrum, and the photocurrent maximum is shifted to 325 nm (Fig. 4.1.10b). The similar short-

wavelength decay in the photocurrent spectra was reported previously for anodic $TiO_2$ films [144, 163-164, 178-179] and associated with a sharp change in the film structure (so called “film breakdown”) occurring in a definite thickness range during the film growth on titanium[163, 178, 180]. Since short-wavelength light with high-energy photons is absorbed close to the film surface, the photocurrent drop in the short-wavelength region can be related to the increased rate of recombination and trapping of the photogenerated charge carriers in the more defective outer layer formed after the breakdown of the anodic film. In contrast to the GS films, the PD films demonstrate considerably smaller drop of photocurrent in the short-wavelength region of spectrum (260-300 nm) and the photocurrent peak remains at 260 nm (Fig. 4.1.10a). These results indicate that the PD films are essentially more uniform and less defective than the GS films, which is in good agreement with the EIS data.

For relatively thick GS films (d ≥ 170 nm), the photocurrent increases considerably, especially in the short-wavelength region, and the photocurrent spectra again becomes to be similar to those of the PD films (Fig. 4.1.10). Crystallization of thicker GS and PD films, which was previously evidenced by Raman measurements[4], and related transformation of their semiconductor properties may be responsible for this effect and for the observed changes of the EIS spectra. TEM measurements also testify that crystallization of the anodic titania films occurs with increasing of their thicknesses (Fig. 4.1.3). On the dark field image (Fig. 4.1.3b) there are a lot of fine crystallites that appeared as a result of crystallization of the amorphous oxide. According to the electron diffraction patterns (Fig. 4.1.3c) the crystalline phase is anatase. Habazaki et. al. have reported that anatase crystallites develop in the inner anodic film region, formed by inward migration of oxygen species[181] .

## 4.1.6 Conclusions

The EIS measurements on the titania anodic films prepared by novel high-voltage pulsed discharge method and the conventional galvanostatic anodisation have demonstrated that the impedance spectra are sensitive both to the space charge region developed in the oxide and to the anodic film structure changing with the film thickness. The pulsed discharge technique leads to the formation of single-layer compact anodic oxide films up to a thickness of 170 nm. In contrast, the EIS spectra of the anodic films grown by the conventional galvanostatic method exhibit several time constants under anodic polarization for the film thickness above 25 nm, indicating a film with two layers: a dense inner layer and a nanoporous outer one. These films show a significantly lower photoelectrochemical activity at short wavelengths as compared with the films prepared in the pulsed regime. The concentration of the ionized donors estimated from Mott-Schottky plots for the relatively thin galvanostatically grown $TiO_2$ films (70-120 nm) is significantly higher (by two orders of magnitude) than that in the coatings obtained by the pulsed discharge method. Only at thickness above 170 nm, crystallization of both types of the films leads to the fact that their semiconducting properties become similar.

The powerful pulsed discharge method can be considered as a very promising approach for preparation of thin anodic films on titanium offering lower defectiveness and enhanced photoelectrochemical response at short wavelengths.

# 4.2 Anodic alumina films prepared by powerful pulsed discharge oxidation.

THE JOURNAL OF PHYSICAL CHEMISTRY C

ARTICLE

pubs.acs.org/JPCC

## Anodic Alumina Films Prepared by Powerful Pulsed Discharge Oxidation

Aleksey D. Lisenkov,[†] Andrei N. Salak,[†] Sergei K. Poznyak,[‡] Mikhail L. Zheludkevich,[*,†] and Mário G. S. Ferreira[†]

[†]Department of Ceramics and Glass Engineering/CICECO, University of Aveiro, 3810-193, Aveiro, Portugal

[‡]Institute for Physical Chemical Problems, Belarusian State University, 220050, Minsk, Belarus

**ABSTRACT:** A novel powerful pulsed discharge anodization technique has been applied to prepare dense, homogeneous oxide films of 16−180 nm thick on aluminum surface. The Volta potential difference (VPD) of the obtained films was studied by scanning Kelvin probe force microscopy. The VPD value was measured as a function of the film thickness and was compared with the similar dependences for the anodic alumina films prepared by the conventional galvanostatic and potentiostatic methods. The anodic films present polarization because of the embedded charges localized near the film interfaces. It was shown that despite the apparent differences in the respective anodization processes, the pulsed discharge films demonstrate the magnitude of polarization which is entirely comparable with that of the conventional anodic alumina films of the same thickness. At the same time, the pulsed discharge films are characterized by more uniform surface structure and electrical properties. The characteristic features of the films such as their fast growth and homogeneity have been considered in terms of the processes occurring at the powerful pulsed discharge.

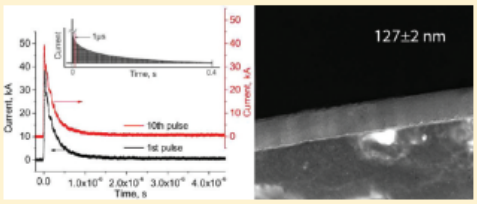


### 1. INTRODUCTION

Thin films of aluminum oxide have found important applications in electronic industry and corrosion protection because of their relatively high dielectric constant and ultralow conductivity as well as high corrosion resistance and good thermal and mechanical stability.[1] These properties also make aluminum oxide films promising for novel applications in microelectronics. Thin alumina layers are used as dielectrics in integrated capacitors with ultrahigh capacitance density.[2] Films of $Al_2O_3$ are also considered as replacements for $SiO_2$ in semiconductor devices.[3,4]

The conventional anodization methods allow production of alumina films of controlled thickness and quality.[5−7] In some cases, for example, in production of electrolytic capacitors and anticorrosion protection of aluminum and its alloys, anodization is combined with other oxidation methods.[8,9]

The relatively new electrochemical treatment technique being widely applied to lightweight metals is plasma electrolytic oxidation (PEO).[10] PEO operates at potentials above the breakdown voltage of an oxide film growing on the metal surface (typically, 120−350 V for aluminum). In the course of a PEO process, the multiple discharge channels, where the oxidation actually occurs, are created. Continuous formation and healing of pores and cracks (which are the natural discharge channels) is the essential feature of the process.[11,12] Therefore, the porous outer layer is the typical attribute of a PEO coating at any stage of its growth. Owing to the features of the technique, PEO coatings grow nonuniformly and are characterized by high roughness. Moreover, it was revealed from study of coating formed by PEO of aluminum that even the densest inner (next to the metal) alumina layer contains numerous defects.[13] PEO is certainly promising for corrosion and wear protection of aluminum and alloys and is inapplicable for production of thin (nanoscale) dielectric alumina films.

A new electrochemical technique of powerful pulsed discharge oxidation of metals has recently been reported.[14] In this technique, electrochemical reaction occurs at the metal−electrolyte interface under the action of single high-voltage (>1.3 kV) pulses. The most important difference of this technique from the conventional galvanostatic and potentiostatic anodization methods is an extremely high rate of the film growth. In principle, owing to plasma−thermochemical interactions at the electrode/electrolyte interface during a high-voltage electric discharge, both pure oxide films and doped ones can be easily produced (which is similar to the features of PEO). Only titania films prepared using the powerful pulsed discharge oxidation have been reported.[14] Since anodic $TiO_2$ is semiconductor and $Al_2O_3$ is dielectric, the surface properties of the respective films are expectedly different.

The potential measured on a metal surface is known to be an important characteristic of the covering oxide film since the potential reflects its physical properties.[15−18] The measured potential consists of the contact potential and that induced by embedded charges (induced potential). Opposite charges

Received: May 30, 2011
Revised: August 8, 2011
Published: August 22, 2011





dx.doi.org/10.1021/jp2050542 | J. Phys. Chem. C 2011, 115, 18634–18639

Contribution to this paper:
Conception of the work, preparation of all samples, fitting of the obtained data, electron microscopy, atomic force microscopy, reproducibility experiments, preparation of images, partial text preparation.

## 4.2.1 Introduction

Thin films of aluminium oxide have found important applications in electronic industry and corrosion protection due to their relatively high dielectric constant, ultra-low conductivity as well as high corrosion resistance and good thermal and mechanical stability [73]. The above properties also make aluminium oxide films promising for novel applications in microelectronics. Nowadays, thin alumina layers are used as dielectrics in integrated capacitors with ultrahigh capacitance density[74]. Films of $Al_2O_3$ are also considered as replacements for $SiO_2$ in semiconductor devices[75-76].

The conventional anodisation methods allow to produce alumina films of controlled thickness and quality[182-184]. In some cases, e.g., in production of electrolytic capacitors and anti-corrosion protection of aluminium and its alloys, anodisation is combined with other oxidation methods[185-186].

A new electrochemical technique of powerful pulsed discharge oxidation of metals has recently been reported[4]. In this technique, electrochemical reaction occurs at the metal-electrolyte interface under the action of single high voltage (> 1 kV) pulses. The most important difference of this technique from the conventional galvanostatic and potentiostatic anodisation methods is an extremely high rate of the film growth. In principle, owing to plasma-thermochemical interactions at the electrode/electrolyte interface during a high-voltage electric discharge, both pure oxide films and doped ones can be easily produced. The titania films prepared using the powerful pulsed discharge oxidation have only been reported so far[4]. Since anodic $TiO_2$ is semiconductor and (undoped) $Al_2O_3$ is dielectric, the surface properties of the respective films are expectedly different.

The potential measured on a metal surface is known to be an important characteristic of the covering oxide film, since reflects its physical properties[113, 117, 187-188]. The measured potential consist of the contact potential and that induced by embedded charges (induced potential). Character of the embedded charge distribution and, as result, the induced permanent polarization of anodic alumina films have been found to be affected by anodisation conditions[76, 118-120, 182]. In particular, Hickmott has shown [76, 119] that the charge contributing to the polarization depends on nature of the anodizing electrolyte. Lambert *et al*.[118] associated a permanent polarization of thin anodic alumina layers with the charges trapped by the structural defects created during the anodisation process. An electrostatic force microscope and a Kelvin probe were applied to measure the potential induced by these embedded charges [118]. It was found that application of potentiostatic stage to the layers prepared using galvanostatic anodisation results in significant increase of their polarization. Scanning Kelvin probe force microscopy (SKPFM) has recently been used to study electrical properties of oxidized aluminium surface, since changes in Volta potential difference (VPD) measured by SKPFM can be correlated to changes in the induced polarization[120].

SKPFM is a promising method to study surface electrical properties[107, 189]. In comparison with the conventional Scanning Kelvin Probe (SKP), it combines capabilities of both SKP and atomic force microscopy and provides much higher resolution when mapping the local electrical properties of a surface. The Kelvin probe methods are based on measurement of VPD between a surface and a reference electrode. In the SKPFM technique, VPD corresponds to the voltage that nulls the oscillations of the cantilever, while in SKP method it is equal to the voltage applied to null inducted currents between electrode and surface [113-114]. It was shown[115, 117, 190] that the

VPD distribution observed in some metals correlates with their corrosion potential. Thus, in spite of some restrictions of the technique related to impact of topography, probe-surface interactions and others[113, 188], SKPFM is a valuable tool for nano-scale surface studies.

In the present work, thin oxide films on aluminium surface were prepared by the powerful pulsed discharge anodisation. Peculiarities of the pulsed discharge process and their impact on the growth and the resulting properties of the alumina films were considered. Morphology and VPD of the films were characterized using transmission electron microscopy (TEM) and SKPFM facilities respectively. VPD measured as a function of the film thickness was analyzed in comparison with the 'VPD-thickness' dependences previously reported for the alumina films prepared using the conventional galvanostatic and potentiostatic methods.

## 4.2.2 Experimental

The electrochemical cell used for the pulsed discharge oxidation of aluminium was made of high-impact polystyrene and consisted of a plate Al anode (Goodfellow, 99.999%) with a working surface of 5 $cm^2$ placed inside a cylindrical Ti-foil cathode (Alfa Aesar, 99.7%) with 20 times larger surface area. Titanium was chosen as a cathode material due to its high strength and chemical stability. Both electrodes were mechanically polished using emery papers up to grid 4000. Then the titanium electrode was chemically polished in a $HF:HNO_3$ (1:3 by volume) mixture, while aluminium plate was electrochemically polished in a $C_2H_5OH:HClO_4$ (4:1 by volume) electrolyte in potentiostatic regime at 20 V to mirror finish. After polishing both electrodes were rinsed with deionised water.

0.1 M ammonium pentaborate ($(NH_4)_2B_{10}O_{16}$) aqueous solution was used as electrolyte for comparison reasons since alumina films prepared by the conventional anodisation methods in that electrolyte are well-studied. Electric discharges between the electrodes were generated using a low-inductivity 100 μF capacitor bank charged to a definite voltage (1400 V). The capacitor was commutated to the cell using a low-inertial relay triggered by a synchronizing pulse. In order to prepare the films with different thicknesses the capacitor was discharged through the electrochemical cell from 1 to 15 times. Time-current characteristics of discharges were recorded using a Tektronix DPO7054 oscilloscope connected to the system and synchronized with trigger.

The electrochemical impedance spectroscopy (EIS) measurements were performed using a Gamry FAS2 Femtostat with a PCI4 Controller in a frequency range from $10^5$ to $10^{-3}$ Hz with 7 points per decade. The measurements were carried out at room temperature in a conventional three-electrode cell consisting of a mercury – mercurous sulfate reference electrode, a platinum foil as the counter electrode and the working electrode with an exposed area of 1 $cm^2$. Impedance spectra were recorded applying a 10 mV sinusoidal perturbation at the open circuit potential. The cell was placed in a Faraday cage to avoid interferences with external electromagnetic fields. The testing electrolyte was 0.1 M ammonium pentaborate. Before recording the spectra, the system was allowed to attain a stable open circuit potential. At least two samples prepared at the same conditions were tested to ensure reproducibility of the results. The impedance plots were fitted using equivalent circuits by means of the Echem Analyst software from Gamry Inc.

Some of the anodized samples were annealed at 300°C for 3 hours followed by quenching in air down to room temperature. A heating rate of 5°C/min was applied. SKPFM measurements were performed on all the samples both before and after heat treatment.

TEM study was carried out using a Hitachi H9000 transmission electron microscope at acceleration voltage of 300 kV. Electron transcendent sections of the samples for TEM were cut with a Leica Reichert Supernova ultramicrotome.

Digital Instruments Nanoscope III atomic force microscope with conductive Pt-Cr probes (Budget Sensors) was used for SKPFM measurements. The measurements were performed in several areas of at least two samples of the same thickness. The obtained VPD values are presented versus the Volta potential values measured on Ni as a reference.

### 4.2.3 Results

A series of samples with the pulsed discharge anodic alumina layers was prepared applying 1, 2, 3, 5, 10 and 15 pulses. Typical current pulse through the electrochemical cell during the discharge oxidation of aluminium is shown in Figure 4.2.1. As opposed to pulsed oxidation of titanium [4], no change in the discharge profiles recorded during the first microseconds of each pulse is observed: the first and the following discharge peaks are essentially similar.

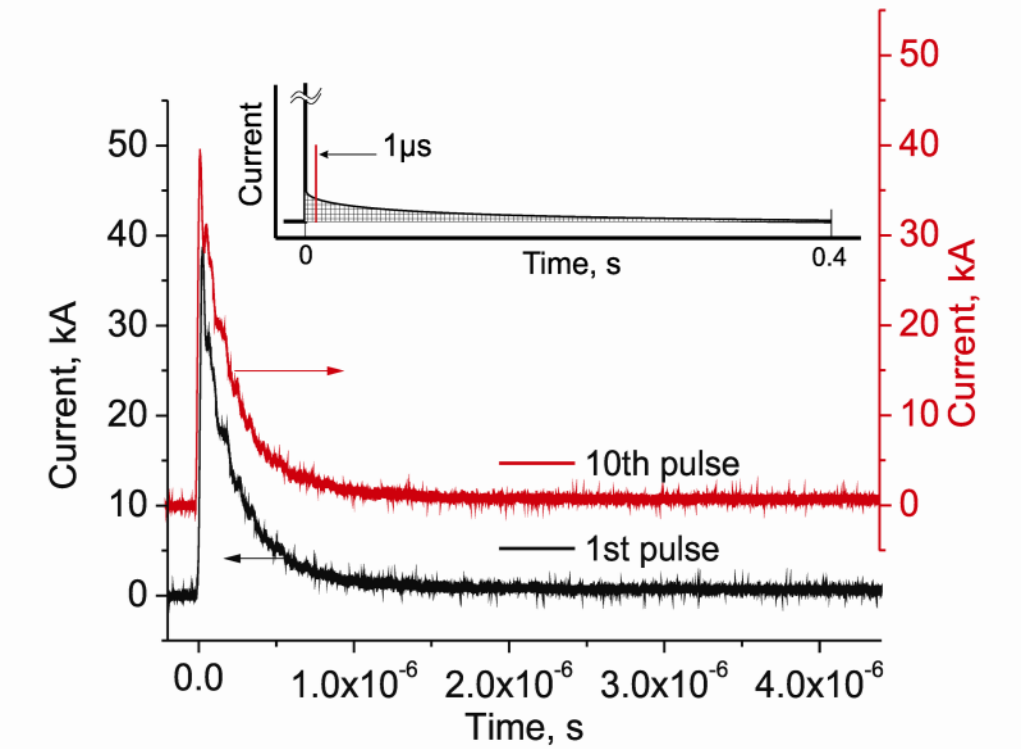


**Figure 4.2.1.** Time evolution of the current through aluminium electrode during first 4 μs. Inset shows schematically a profile of the pulsed discharge as a whole. Dashed area represents the total charge passed through the electrode.

Thickness of the alumina films prepared by the pulsed discharge anodisation was evaluated from EIS measurements. EIS spectra of the obtained films are shown in Figure 4.2.2. All the spectra demonstrate a broad relaxation process described by one time constant. This relaxation can be assigned to capacitance of the dielectric oxide films. The spectra were fitted

using a simple equivalent circuit with one parallel R-C element for description of oxide film and an additional R element connected is series for the electrolyte resistance. High quality fit was achieved as seen in Figure 4.2.2. Thickness of the films was calculated using the capacitance values derived from the EIS spectra. The dielectric constant value of alumina for the calculations was taken to be 9.

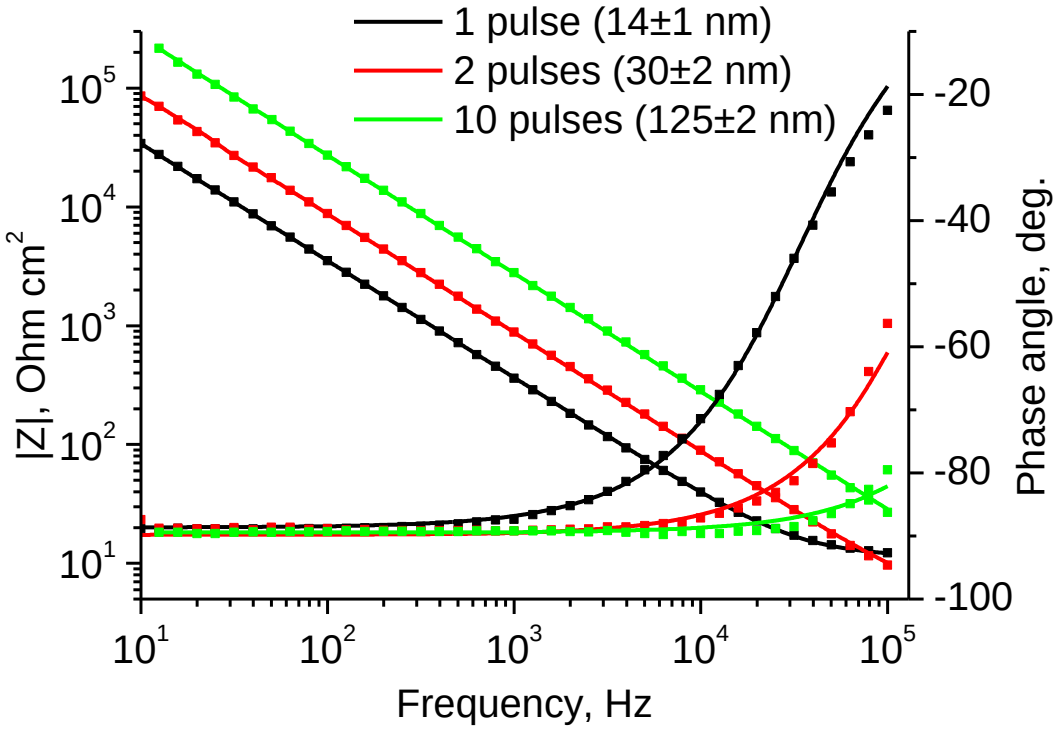


**Figure 4.2.2.** (Color online) Bode plots of the oxide films formed on aluminium surface as a result of pulsed discharge anodisation; solid lines represent the fitting results.

It was found that the thickness (*d*) of the pulsed discharge films as a function of number of applied pulses (*N*) obeys well an empirical equation:

$$d = d_0 N^{\alpha}, \qquad (4.2.1)$$

where $d_0$ = 16 nm and α= 0.9. A power law is known to describe a constant growth rate process: the relative increment $\Delta d/d$ of the film thickness is proportional (with a factor of 0.9) to the relative increase $\Delta N/N$ of the number of pulsed discharges.

The thickness values calculated from the EIS spectra were verified by the TEM measurements. Figure 4.2.3 shows the cross sections of the aluminium electrodes anodized by application of 3 and 10 discharge pulses. The obtained alumina films were measured to be 46±2 and 127±2 nm thick, respectively (cf. 45±2 and 125±2 nm found from the EIS data) and uniform along the sections. It was also revealed from the TEM study that all the films obtained by high-voltage pulsed discharge anodisation (1-15 pulses) are smooth, dense and free of microdefects. However, attempts to produce thicker alumina films were failed. The films formed by application of 20 and more pulsed discharges demonstrated typical signs of point electrical breakdown. In those points, the underlying aluminium surface was also affected. Thus, the

maximal thickness of a dense and homogeneous alumina film which can be produced using the pulsed discharge anodisation method at the above-described conditions is about 200 nm.

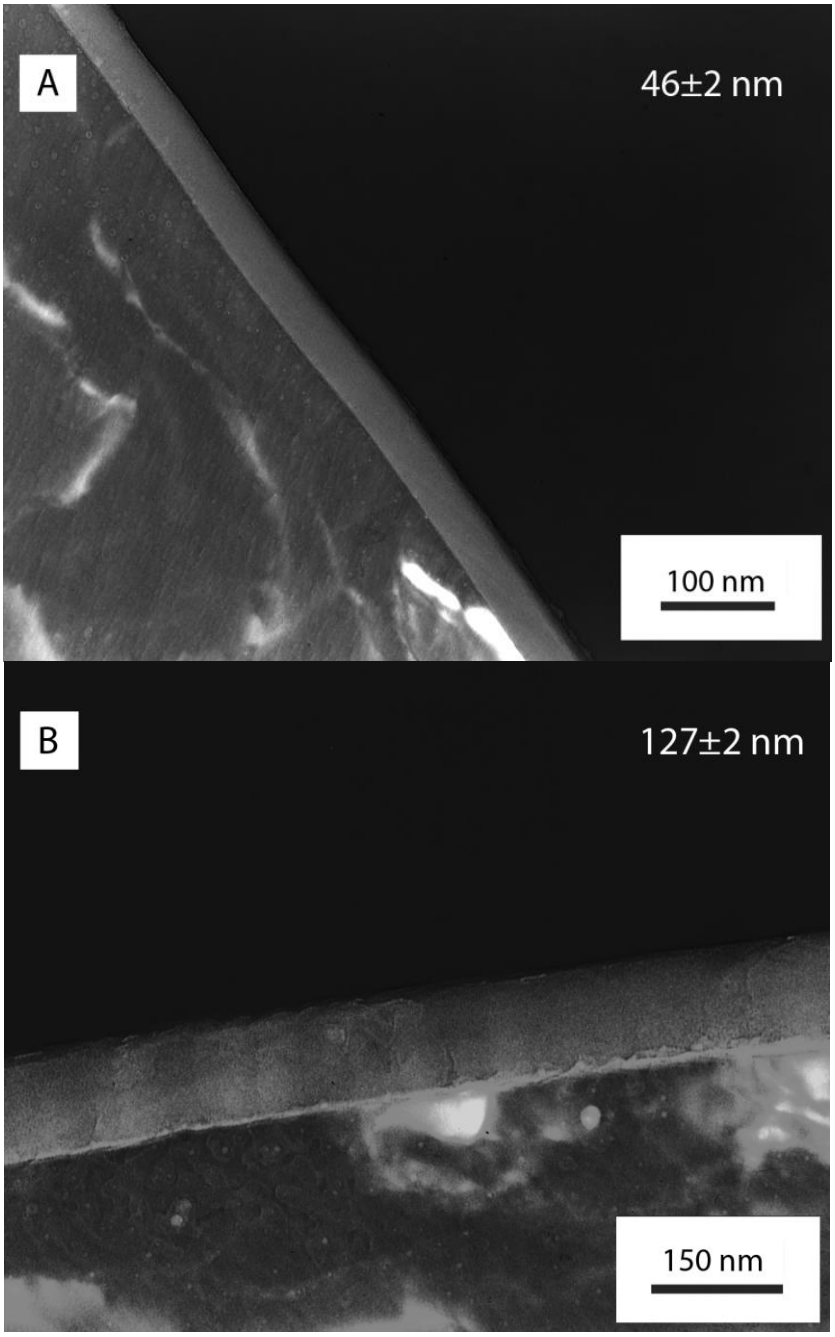


**Figure 4.2.3.** TEM cross sections of the aluminium samples anodized by application of 3 (a) and 10 (b) discharge pulses.

Figure 4.2.4 shows typical surface topography and the VPD map of the aluminium sample before and after 10 pulsed discharges which correspond to a native alumina layer (about 1 nm thick) and an anodic film (~127 nm), respectively. One can see that no visible change of topography occurs as a result of the anodisation process, while the average VPD increases from about -1.28 V to +6.33 V (hereafter versus a Ni reference). It should be also noticed that scatter of the VPD values in the typical SKPFM scans of the alumina films prepared by pulsed discharge technique is generally smaller than that observed in the films produced by

the conventional anodisation methods[120]. The above suggests that in spite of the discrete character of the deposition methods (layer by layer) the pulsed discharge films have uniform properties. Furthermore, it follows from comparison of both surface topography and VPD maps of the anodic alumina films prepared by different methods that in the case of the pulsed discharge anodisation the resulting film quality is less dependent on initial state of aluminium surface. Pulsed discharges evidently smooth out imperfections of the charge distribution caused by surface defects.

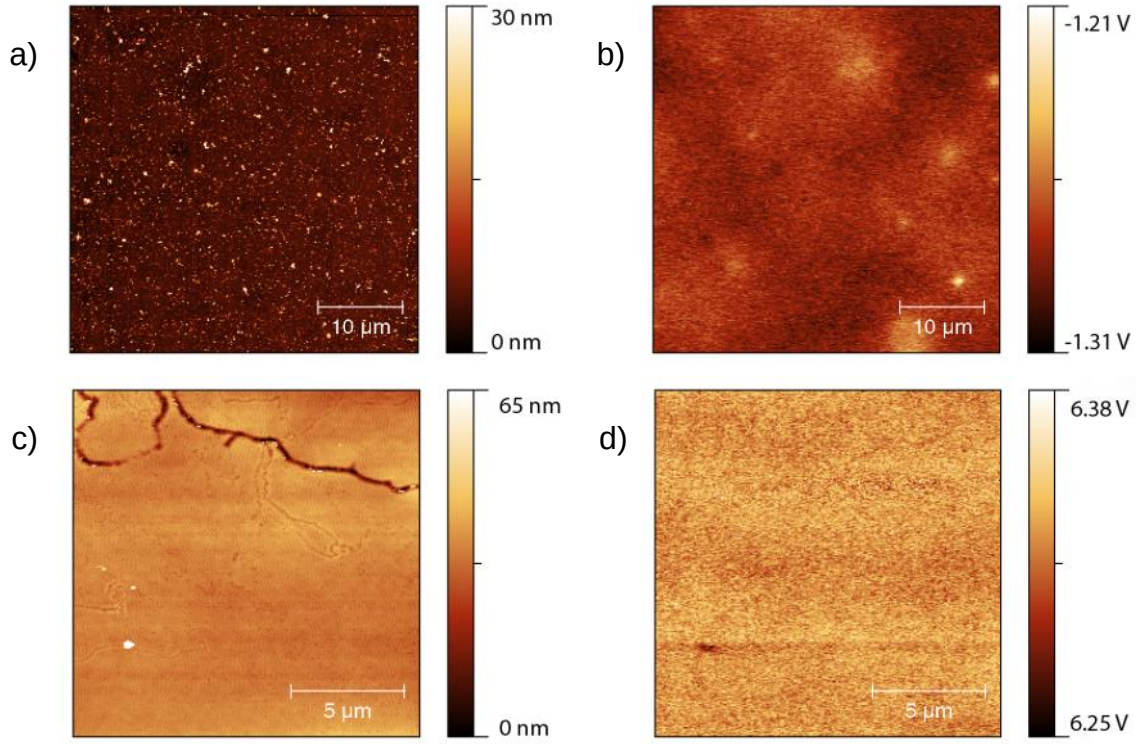


**Figure 4.2.4.** Maps of the surface topography (left) and Volta potential difference (right) of the aluminium sample before (a, b) and after (c, d) the pulsed discharge anodisation procedure (10 pulses applied).

Dependence of VPD on thickness of the pulsed discharge films is presented in Figure 4.2.5. As in the case of the anodic alumina films prepared by the conventional methods, this dependence is also described well with a linear function [118, 120]. The slope value ($\Delta V/\Delta d$) obtained for the pulsed discharge, 0.059±0.003 V/nm, is slightly higher than those previously found for the most polarized films produced by combination of the galvanostatic and potentiostatic methods (cf. ~0.052 and 0.055 V/nm reported by Lambert *et al*. [118] and Yasakau *et al*.[120], respectively). However, taking into account a typical data spread of SKFPM measurements, all the above-mentioned values $\Delta V/\Delta d$ are equal within the limits of experimental error. Thus, the induced polarization of the alumina films prepared by the pulsed discharge method is comparable with that observed in the conventional anodic films of the same thickness. It can be suggested that despite the apparent differences in the anodisation methods their film growth mechanisms and hence the associated effects which result in the induced polarization of the films are inherently the same.

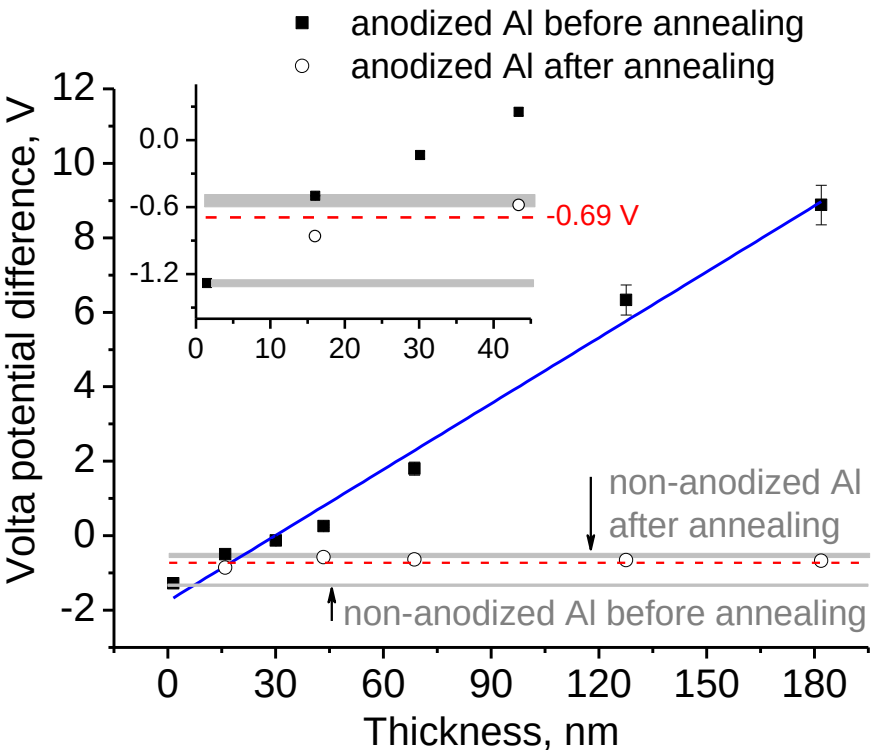


**Figure 4.2.5.** Volta potential difference *versus* thickness of the alumina films prepared by pulsed discharge anodisation method before (solid squares) and after (open circles) annealing at 300°C. The inset shows magnification of the plot for the thickness range of 1-45 nm. The reference levels corresponding to the measured VPD values for the untreated aluminium sample and non-anodized sample thermally oxidized at 300°C are indicated.

Due to the specificity of oxidation of a metal surface, the layers bordering the interfaces are characterized by structure imperfections: vacancies[76] and incorporated species (e.g. from electrolyte) [118], and thereby are the most defective regions of the oxide film. It has been accepted that polarization of an anodic film is caused by charge carriers (mainly by electrons and Al ions) trapped by these defects [118, 120]. These defects and, accordingly, the embedded charges are distributed throughout a film with the maximal charge density near the metal/oxide and oxide/air interfaces, as shown in Figure 4.2.6a,c.

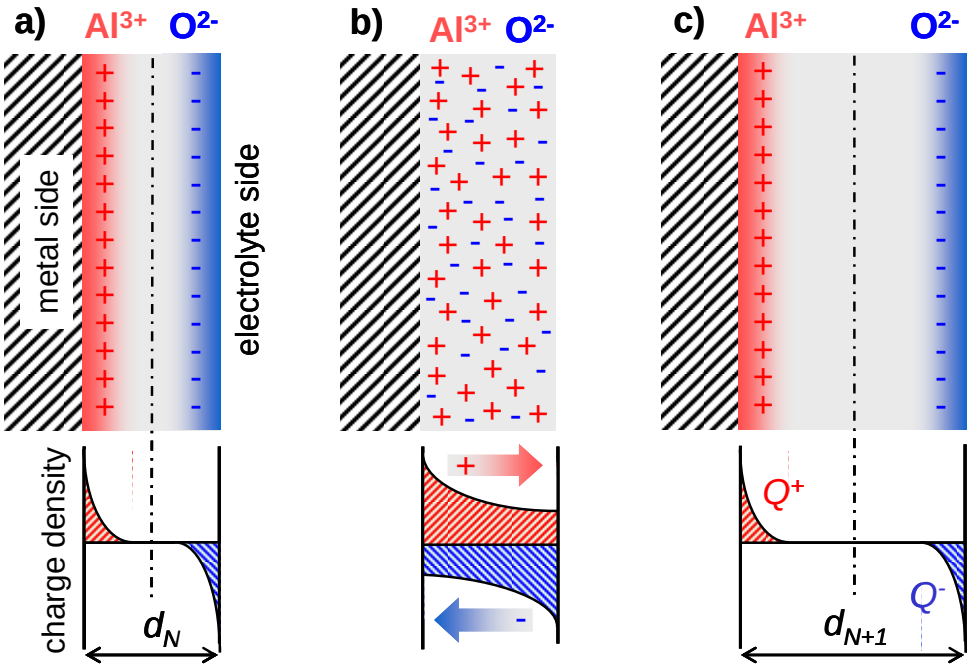


**Figure 4.2.6.** Schematic representation of charge distribution in alumina film polarized as a result of anodisation: after *N*th pulsed discharge (a), during the 1st step of the discharge (in a field of ~ $10^9$ V/cm) (b), and after (*N*+1)th pulsed discharge (c). Provided the same charge is embedded, the induced potential is proportional to the film thickness, *d*. Charge distribution in the pulsed discharge films is suggested to be essentially similar to that in the films produced by combination of the galvanostatic and potentiostatic methods [120].

Annealing of the as-prepared anodic alumina films was shown to lead to a release of their induced polarization owing to reduction of the number of defects [109] and the relaxation of the charge [191]. It has recently been revealed [120] that on annealing, the measured VPD of the anodic films tends to the certain (equilibrium) level independent on the film thickness. This level is suggested to be the VPD value for an alumina film formed by thermal oxidation in air at the given annealing temperature. VPD of the pulsed discharge films annealed at 300°C was found to be -0.69±0.07 V (Figure 4.2.5). This value is closer to the equilibrium level (which is around -0.55 V) measured in non-anodized aluminium sample annealed at 300°C than the respective values measured in the conventionally prepared anodic films annealed at the same temperature [120]. As suggested [120], the equilibrium level is not reached due to residual defects (which do not disappear after annealing). When the concentration of defects in some anodic film is higher and their distribution in is wider, the number of residual defects is also higher. Correspondingly, the VPD value of this film after annealing will be further from the equilibrium level at given annealing temperature.

## 4.2.4 Discussion

The presented results demonstrate certain differences in properties between the alumina films formed using the pulsed discharge anodisation and the respective anodic films prepared by the conventional methods. Their characteristic features are likely to result from specificity of

the used anodisation method. Thus the pulsed discharge anodisation process certainly needs to be considered in more detail.

Only 10% of the capacitor charge is consumed during the first microsecond (which corresponds to a current fall by more than 90% of the peak value) as follows from an analysis of the discharge profile (see inset in Figure 4.2.1). The remaining 90% of charge is used during subsequent stage which lasts up to 0.5 s (depending on the thickness of the film). Thus a pulsed discharge anodisation process can be conventionally divided into two stages where the first one (fast) is about 1 μs long, with the characteristic current magnitude of several kA/cm$^2$. It is believed that the main process during the first stage is ionization of an oxide film (either native film or that formed by previous oxidation). During the second long stage a new layer grows. In comparison to the conventional anodisation processes this growth occurs in much higher electrical field and a higher total charge is transferred in unit time. That is why at the pulsed discharge anodisation the film growth rate is higher than in the case of any conventional method.

It seems reasonable to suggest that the discharge profile is determined by the electrical conduction of a growing anodic oxide film. In particular, the discharge can be expected to terminate faster in the case of more conductive layer. Typical duration of the second stage at pulsed discharge anodisation of titanium (anodic $TiO_2$ is a semiconductor) was found to be several times shorter [4-5] than that observed when preparing the respective anodic alumina (which is dielectric). Thus during the second stage the pulsed discharge alumina film is likely to have a significant impedance, which suggests a low concentration of the point defects and the trapped charge carriers in at least the inner part of the film.

No boundary between the layers formed by subsequent pulsed discharges has been observed by TEM (Figure 4.2.3). The films were found to be homogeneous regardless whether they were obtained by application of one or a number of pulses. The respective EIS spectra characterized by one time constant (Figure 4.2.2) confirms uniformity of the properties across the coating suggesting no separation to internal sub-layers. Thus the ‘prehistory’ (amount of the previous pulsed discharges which is equal to the number of the deposited layers) seems to be inessential (Figure 4.2.6) when the film thickness is below the maximal value (~200 nm),.

This effect can be explained in terms of full ionization of the oxide films under conditions of high electrical potentials. The full ionization of the aluminium oxide can occur if the density of the electrostatic energy is higher or at least equal to the ionization energy of the oxide. The density of the electrostatic energy ($U_E$) in a film can be calculated using the following expression:

$$U_E = \frac{1}{2}\varepsilon_0 \varepsilon E^2 = \frac{\varepsilon_0 \varepsilon V^2}{2d^2} \qquad (4.2.2)$$

where $E$ is the electric field strength, $V$ is an applied voltage, $d$ is the film thickness, $\varepsilon$ is the dielectric constant of the film, $\varepsilon_0$ is the permittivity of the free space. The capacitor voltage and the dielectric constant of alumina mentioned previously in the text were used as the values of $V$ and $\varepsilon$ in the calculations.

The $U_E$ value found from Eq. (2) was compared with the value of ionization energy (per a volume unit) in the form of

$$\frac{\rho}{M} N_A W_t, \qquad (4.2.3)$$

where $\rho$ (2.8-3.0 g/cm$^3$ [192]) and $W_t$ (1.5 eV [193]) are density and (molecular) thermal ionization energy of amorphous alumina, respectively; $M$ is molar weight of $Al_2O_3$, $N_A$ is Avogadro’s

number. According to the estimations, when the film thickness does not exceed the value of an order of $10^2$ nm, the energy of electrostatic field in the first stage of pulsed discharge is enough to ionize the film over the whole volume (Figure 4.2.6b) supporting the assumption on the mechanism of the film growth during the first stage. At this stage of the pulsed discharge anodisation the existing defects and polarization do not matter since new defects are to be formed over again and consequently the respective polarization to be induced during the second longer stage.

A pulsed discharge film of about 200 nm thick represents already a substantial insulator. High-voltage discharge breaks down this insulator creating weakened paths within. This action destroys the film and makes further growth impossible.

The potential induced in an oxide film and registered by SKPFM is a function of both the total embedded charge and its distribution profile [120]. Provided the same charge is embedded, the bigger spacing is between positive and negative charges (i.e., the narrower the charge distribution profile and/or the thicker the film (cf. Figure 4.2.6a and 4.2.6c), the larger the respective induced polarization.

The VPD values measured in as-prepared pulsed discharge films are comparable with that of the films of the same thickness obtained by the conventional anodisation methods. At the same time, the VPD value of the annealed pulsed discharge films is closer to the equilibrium level than that of the conventionally anodized ones. This fact suggests that a smaller amount of the embedded charges located in narrower defect layers bordering the film interfaces contributes to the measured potential of discharge films. Thus the pulsed discharge films are less defective in their inner layers than the respective alumina films produced by the conventional anodisation methods.

## 4.2.5 Conclusions

A novel powerful pulsed discharge oxidation method allows to produce homogeneous low-defect anodic films up to ~200 nm thick on an aluminium surface. The thickness values estimated by independent methods (EIS and TEM) were found to be in excellent agreement which suggests a good homogeneity of these films.

A pulsed discharge anodisation process can be conventionally divided into two stages: ionization and growth of a film. Ionization of the film over the whole volume during the first microsecond of the process is essential feature of the pulsed discharge anodisation as it causes fast film growths and homogeneity. The film thickness can be controlled during the anodisation process since this parameter is a power function of the number of applied pulses with a scaling exponent 0.9.

# 4.3 Titania films obtained by powerful pulsed discharge oxidation in phosphoric acid electrolytes.

*Journal of The Electrochemical Society*, **161** (1) D73-D78 (2014) D73
0013-4651/2014/161(1)/D73/6/$31.00 © The Electrochemical Society

## Titania Films Obtained by Powerful Pulsed Discharge Oxidation in Phosphoric Acid Electrolytes

**Aleksey D. Lisenkov,[a,z] Sergey K. Poznyak,[b] M. Fátima Montemor,[c] M. J. Carmezim,[c] Mikhail L. Zheludkevich,[a] and Mário G. S. Ferreira[a,*]**

[a]*Department of Materials and Ceramic Engineering/CICECO, University of Aveiro, 3810-193 Aveiro, Portugal*
[b]*Institute for Physical Chemical Problems, Belarusian State University, 220050 Minsk, Belarus*
[c]*ICEMS, Instituto Superior Técnico, Universidade Técnica de Lisboa, 1049-001 Lisboa, Portugal*

Thin $TiO_2$ films were prepared on the titanium surface using the powerful pulsed discharge oxidation method (PPDO) in phosphoric acid based electrolytes. The obtained films were characterized with electrochemical impedance spectroscopy (EIS), photocurrent spectroscopy, scanning Kelvin probe force microscopy (SKPFM), and Mott-Schottky plot analysis. The potential dependence of the space charge layer capacitance has demonstrated that the ionized donor concentration in the oxide is strongly influenced by the electrolyte concentration used during the pulsed anodization. It is also shown that the main factor influencing the kinetics of the oxide film growth is the concentration of point defects which, in turn is determined by the composition of electrolyte. SKPFM results show a non-linear evolution of the Volta potential of the anodized surface with the film thickness reaching a plateau after film thickness exceeds 100 nm. The results obtained clarify the mechanisms of titania film formation under high-voltage pulses and allow tuning the semiconductive properties of thin oxide layers on titanium surfaces.
 [DOI: 10.1149/2.085401jes] All rights reserved.

Manuscript submitted September 6, 2013; revised manuscript received November 5, 2013. Published December 6, 2013.

Titanium and its alloys are materials widely used in many industrial applications such as aerospace and automotive industries, as well as in medicine due to their high corrosion resistance, hardness, high melting point and biomedical capability.[1–9] Titanium dioxide film which forms spontaneously on the metal surface brings high resistance against corrosion although is very thin (about 3–5 nm).[10] However additional surface modifications, such as injection of dopants, increasing the dense oxide layer thickness, forming porous layers are often needed to meet requirements of particular applications. Anodization of titanium is an attractive method that can be used for surface modification giving additional corrosion resistance, higher affinity to biological tissues, and advanced electronic properties when compared to the native thin oxide films.[11–14] The anodic films formed on Ti surface can have various morphologies from dense barrier layers to porous deposits composed by separated nanotubes[15,16]

Titanium anodization can be performed in different electrolytes including mineral acids. There are a number of publications, where anodization has been carried out in phosphoric acid.[17,18] The corrosive attack of phosphoric acid to titanium and its alloys is relatively mild probably due to the adsorption of phosphate ions on the surface of the native metal oxide.[19–21] Incorporation of phosphate ions in titanium oxide can result not only in an increase of corrosion stability in biological environment, but also in improved compatibility with biological tissues.

Recently a new electrochemical technique, namely powerful pulsed discharge oxidation (PPDO) of metals, has been suggested.[22–24] In this technique, electrochemical reaction occurs at the metal-electrolyte interface under the action of single high-voltage (>1 kV) pulses. Growth of the film under these conditions occurs at much higher rates than in the case of conventional galvanostatic or potentiostatic methods.[22] This results in the formation of oxide films with properties different of those obtained by conventional approaches. For example the anodic films prepared by the pulsed discharge method on Ti in sulfuric acid electrolytes are constituted by a single uniform dense amorphous oxide, while films of the same thickness prepared by the conventional galvanostatic method present more complex structure consisting of two layers: an inner crystalline and an outer amorphous one.[24–26]

Powerful pulsed discharge method was also used to produce anodic films on the aluminum substrate. The main difference of the anodization processes that occurring on these two metals originates from different electronic properties of the respective oxides. The oxide prepared on aluminum shows well pronounced dielectric properties, while the titania demonstrates typical semiconductor properties. In the case of aluminum the structure of the anodic films prepared by both the pulsed discharge technique and by the galvanostatic/potentiostatic method is rather similar. However PPDO films are less dependent on the starting metal surface conditions and show very uniform dielectric properties as demonstrated by the even distribution of Volta potential along the entire surface.[23] In this work a new two-stage mechanism of film growth under powerful discharge was also suggested. The full ionization of entire anodic film occurs in a first step during a few microseconds followed by a slower anodic faradaic process of film formation. The fact that the entire film is fully ionized during the first step leads to vanishing out the difference between different zones on the surface and confers creation of a very uniform layer.

However some mechanistic details of the processes which occurring on Ti during the anodization pulse and the main factors affecting the process are not clear yet. In the present paper the titania anodic films on titanium were prepared by the powerful pulsed discharge method in phosphoric acid solutions with different concentration. A set of electrochemical methods was used to clarify the effect of electrolyte concentration on the kinetics of anodization processes and on the electronic properties of the obtained film. This information is important for optimization of the PPDO method helping to predict the influence of the electrolyte and other experimental conditions on the final properties of the obtained films.

### Experimental

The electrochemical cell used for the pulsed discharge oxidation of titanium was made of high-impact polystyrene and consisted of a Ti anode plate (Goodfellow, 99.999%, dimensions: 100 × 0.8 × 1 mm) with a working surface of 4.4 $cm^2$ placed inside a cylindrical Ti cathode (Alfa Aesar, 99.7%) with about 20 times larger surface area. Titanium was chosen as a cathode material due to its high strength and chemical stability. Both electrodes were mechanically polished using abrasive papers up to grid 4000. Then the titanium electrodes were chemically polished in a HF:$HNO_3$ (1:3 by volume) mixture to mirror finish and finally rinsed with deionized water.

The anodization of titanium in phosphoric acid electrolytes with different concentrations (1, 2 and 4M) was performed. Electric discharges between the electrodes were generated using a low-inductance 100 μF capacitor bank, charged to a definite voltage (1400 V). The capacitor was commutated to the cell using a low-inertial relay triggered by a synchronizing pulse. In order to prepare films with different

*Electrochemical Society Active Member.
[z]E-mail: lisenkov@ua.pt

Contribution to this paper:
Conception of the work, preparation of all samples, fitting of the obtained data, electron microscopy, atomic force microscopy, reproducibility experiments, preparation of images, text preparation.

## 4.3.1 Introduction

Titanium and its alloys are materials widely used in many industrial applications such as aerospace and automotive industries, as well as in medicine due to their high corrosion resistance, hardness, high melting point and biomedical capability[129, 194-197] . Titanium dioxide film which forms spontaneously on the metal surface brings high resistance against corrosion although is very thin (about 3-5nm) [197]. However additional surface modifications, such as injection of dopants, increasing the dense oxide layer thickness, forming porous layers are often needed to meet requirements of particular applications. Anodisation of titanium is an attractive method that can be used for surface modification giving additional corrosion resistance, higher affinity to biological tissues, and advanced electronic properties when compared to the native thin oxide films[152, 198-199]. The anodic films formed on Ti surface can have various morphologies from dense barrier layers to porous deposits composed by separated nanotubes[200-201].

Titanium anodisation can be performed in different electrolytes including mineral acids. There are a number of publications, where anodisation has been carried out in phosphoric acid[135, 202]. The corrosive attack of phosphoric acid to titanium and its alloys is relatively mild probably due to the adsorption of phosphate ions on the surface of the native metal oxide [4-5, 127]. Incorporation of phosphate ions in titanium oxide can result not only in an increase of corrosion stability in biological environment, but also in improved compatibility with biological tissues.

Recently a new electrochemical technique, namely powerful pulsed discharge oxidation (PPDO) of metals, has been suggested[5, 127]. In this technique, electrochemical reaction occurs at the metal-electrolyte interface under the action of single high-voltage (> 1 kV) pulses. Growth of the film under these conditions occurs at much higher rates than in the case of conventional galvanostatic or potentiostatic methods[5, 127]. This results in the formation of oxide films with properties different of those obtained by conventional approaches. For example the anodic films prepared by the pulsed discharge method on Ti in sulfuric acid electrolytes are constituted by a single uniform dense amorphous oxide, while films of the same thickness prepared by the conventional galvanostatic method present more complex structure consisting of two layers: an inner crystalline and an outer amorphous one.

Powerful pulsed discharge method was also used to produce anodic films on the aluminium substrate. The main difference of the anodisation processes that occurring on these two metals originates from different electronic properties of the respective oxides. The oxide prepared on aluminium shows well pronounced dielectric properties, while the titania demonstrates typical semiconductor properties. In the case of aluminium the structure of the anodic films prepared by both the pulsed discharge technique and by the galvanostatic/potentiostatic method is rather similar. However PPDO films are less dependent on the starting metal surface conditions and show very uniform dielectric properties as demonstrated by the even distribution of Volta potential along the entire surface [127]. In this work a new two-stage mechanism of film growth under powerful discharge was also suggested. The full ionization of entire anodic film occurs in a first step during a few microseconds followed by a slower anodic Faradaic process of film formation. The fact that the entire film is fully ionized during the first step leads to vanishing out the difference between different zones on the surface and confers creation of a very uniform layer.

However some mechanistic details of the processes which occurring on Ti during the anodisation pulse and the main factors affecting the process are not clear yet. In the present paper the titania anodic films on titanium were prepared by the powerful pulsed discharge method in phosphoric acid solutions with different concentration. A set of electrochemical methods was used to clarify the effect of electrolyte concentration on the kinetics of anodisation

processes and on the electronic properties of the obtained film. This information is important for optimization of the PPDO method helping to predict the influence of the electrolyte and other experimental conditions on the final properties of the obtained films.

### 4.3.2 Experimental

The electrochemical cell used for the pulsed discharge oxidation of titanium was made of high-impact polystyrene and consisted of a Ti anode plate (Goodfellow, 99.999%, dimensions: 100x80x1 mm) with a working surface of 4.4 $cm^2$ placed inside a cylindrical Ti cathode (Alfa Aesar, 99.7%) with about 20 times larger surface area. Titanium was chosen as a cathode material due to its high strength and chemical stability. Both electrodes were mechanically polished using abrasive papers up to grid 4000. Then the titanium electrodes were chemically polished in a $HF:HNO_3$ (1:3 by volume) mixture to mirror finish and finally rinsed with deionised water.

The anodisation of titanium in phosphoric acid electrolytes with different concentrations (1, 2 and 4M) was performed. Electric discharges between the electrodes were generated using a low-inductance 100 μF capacitor bank, charged to a definite voltage (1400 V). The capacitor was commutated to the cell using a low-inertial relay triggered by a synchronizing pulse. In order to prepare films with different thicknesses, the capacitor was discharged through the electrochemical cell between 1 to 5 times. The thickness of the films was found to be a near linear function of the number of pulses with increment of 25 nm/pulse. Time-current responses of discharges were recorded using a Tektronix DPO7054 oscilloscope connected to the system and synchronized with trigger.

The electrochemical impedance spectroscopy (EIS) measurements were performed using a Gamry FAS2 Femtostat with a PCI4 Controller in a frequency range from $10^5$ to $10^{-3}$ Hz with 7 points per decade. The measurements were carried out at room temperature in a conventional three-electrode cell consisting of a mercury–mercurous sulphate reference electrode, a platinum foil as a counter electrode and the working electrode with an exposed area of 1 $cm^2$. Impedance spectra were recorded applying a 10 mV (RMS) sinusoidal perturbation at an open circuit potential. The cell was placed in a Faraday cage to avoid interferences with external electromagnetic fields. The electrolyte used for EIS measurements was 0.1 M acetic buffer solution (pH=6.03). Before recording the spectra, the system was allowed to attain a stable open circuit potential. At least two samples prepared in the same conditions were tested to ensure reproducibility of the results. The impedance plots were fitted using equivalent circuits by means of the Elchem Analyst software from Gamry Inc.

In the photoelectrochemical study the working electrode was illuminated through a quartz window with monochromatic light (beam area 0.12 $cm^2$). The optical instrumentation consisted of a 150 W Xe lamp (Oriel 6254), a 250 mm f18 monochromator (Oriel 77200), a stepper motor to control the wavelength and a mechanical chopper. The photocurrent was obtained by connecting the current output of the potentiostat (EG&G 273) to a lock-in amplifier (Brookdeal EG&G 5210) and recording the voltage output due to the signal at 19 Hz (the chopping frequency). The recorded values were then worked out to calculate the photocurrent and the quantum efficiency values using a spreadsheet software package.

TEM studies carried out using a Hitachi H9000 transmission electron microscope at an acceleration voltage of 300 kV. Electron transparent sections of the samples for TEM were cut with a Leica Reichert Supernova ultramicrotome. The main problem during preparation of the

titania samples was low stability of the oxide layer under high energy beams (especially ion milling). The high energy can lead to recrystallization of titania and misleading results. Taking into account that crystallization is an important part of this work, ultramicrotomy was chosen since it does not induce change in the crystallinity of the oxides. However titanium is known to react with the material of a diamond knife leading causing its degradation. To reduce the damaged area of the knife, small bars of the metal with oxide (less than 1x0.05x0.05 mm) were cut from the electrodes and embedded into resin. Then the typical procedures of trimming were performed resulting in locating the sample bar in the middle of the pyramid perpendicularly to the cutting-off side. Finally sectioning with diamond knife was performed. The sample thickness was about 15-20 nm.

Digital Instruments Nanoscope III atomic force microscope with conductive Pt-Cr probes (Budget Sensors) was used for SKPFM measurements. The measurements were performed in several areas in at least two samples with identical oxide thickness. The obtained Volta potential difference (VPD) values are presented versus the Volta potential values measured on a pure Ni as a reference.

### 4.3.3 TEM characterization

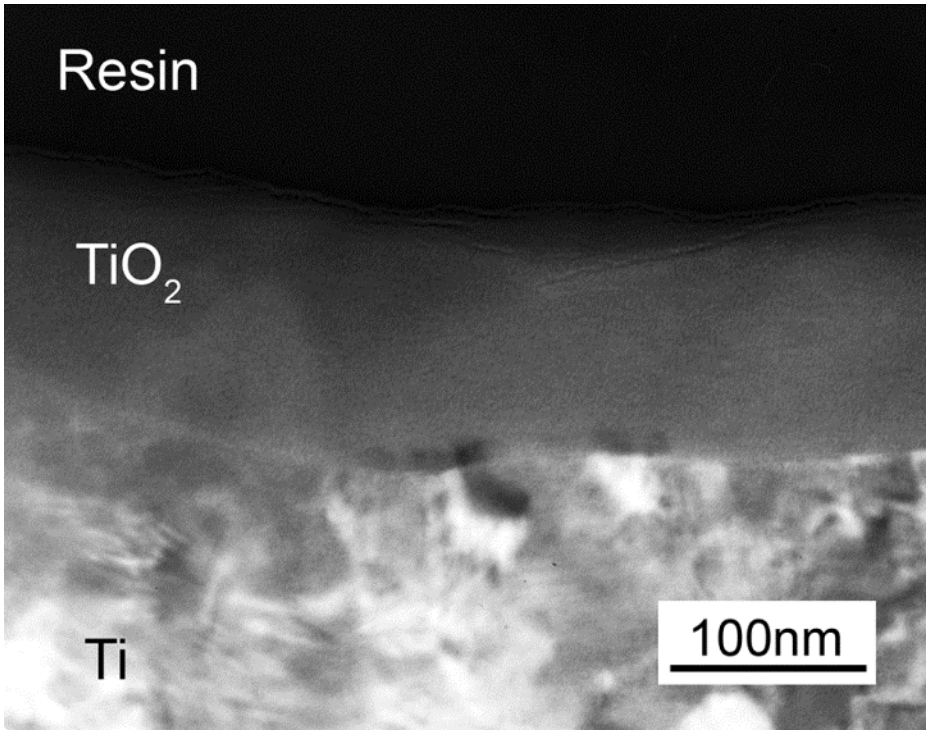


**Figure 4.3.1:** Cross-section TEM image of the anodic film on titanium prepared by high voltage method in 1M $H_3PO_4$ after 5 discharges (thickness of the film is about 120 nm).

Figure 4.3.1 shows a cross-section TEM image of titanium oxide film prepared by the high voltage pulse oxidation method in solution of 1M phosphoric acid on the titanium substrate. After 5 pulses a uniform oxide film with a thickness about of 120 nm is formed. Neither crystallites nor different layers can be observed in this film. The structure of the obtained film is similar to the one produced in sulphuric acid electrolyte as reported elsewhere[5].

## 4.3.4 Mott- Schottky analysis and photocurrent measurements.

Impedance measurements provide essential information about physical properties of oxide films measuring the electrochemical response in a wide frequency range. In the case of semiconductive surfaces the responses of the space charge region and the capacitance of bulk oxide can result in appearance of respective relaxation processes on the spectra[5]. However these time constants are often overlapped and cannot be easily discriminated. Application of external polarization can help to separate response from capacitance of space charge region since only this component is influenced by the applied electrical field. Thus acquisition of impedance spectra under electrical polarisation on the semiconductive electrode in this method can help to define the frequency ranges, corresponding to the different regions of the film (space charge region (SCR) and bulk oxide). In this way the capacitance of SCR can be accurately estimated and used for Mott-Schottky analysis to estimate electronic properties of the formed oxide layers. This approach accounts for the shifts of corresponding time constant in frequency domain conferring more adequate estimation of capacitance value when compared to conventional single frequency measurements.

A constant phase element (CPE) instead of a capacitor was used in all fittings presented in the work. Such modification is needed when the phase angle of the capacitor is different from -90 degrees. The impedance of the CPE, $Z_{CPE}$, depends on frequency, ω, according to the following equation:

$$Z_{CPE} = [Q(j\omega)^n]^{-1}, \qquad (4.3.1)$$

where Q is a parameter numerically equal to the admittance ($|Z|^{-1}$) at ω= 1 rad $s^{-1}$ and $n \leq 1$ is a power coefficient calculated as ratio of the maximum phase angle of the corresponding time constant to -90 degrees. The detailed description of the fitting on a similar system was previously discussed[5].

The impedance spectra of the titania film with two different thicknesses and obtained under different polarization values are presented in fig. 4.3.2. The frequency range $10^{-2}$-$10^{0}$ Hz corresponds to one time constant which can be interpreted as the space charge region (SCR) of the semiconductor film. The second time constant appears at frequencies $10^{1}$-$10^{3}$Hz, describing the bulk part of the film. The high-frequency range of the spectra is not changed significantly under polarization, showing that single frequency measurements (which are usually performed at $10^{3}$ Hz for Mott- Schottky analysis) cannot be directly related to semiconductive properties of the film. This fact is especially noticeable on the sample with 120 nm thickness (Fig. 4.3.2b).

At the first impression the EIS spectra of the 70 nm thick film seem to be composed by only one time constant. However detailed analysis of the spectra reveals an asymmetry in the phase angle plot which can be interpreted as the presence of a second relaxation process. The reason why this response is not well defined is that the space charge region in this case occupies almost all volume of the film leaving only a thin layer of bulk titania with a low resistance and a capacitance significantly higher than that of the SCR layer. In this situation the response of the bulk film is almost fully overlapping with the dominating low-frequency time constant. Fitting of these spectra (Fig. 4.3.3b) with two time constants model (Fig. 4.3.3a) results in a rather accurate estimation of R-C parameters for space charge (error is less than 10%). It is worth to notice that the fitting with one time constant equivalent circuit model gives a lower accuracy (error about 15-20%).

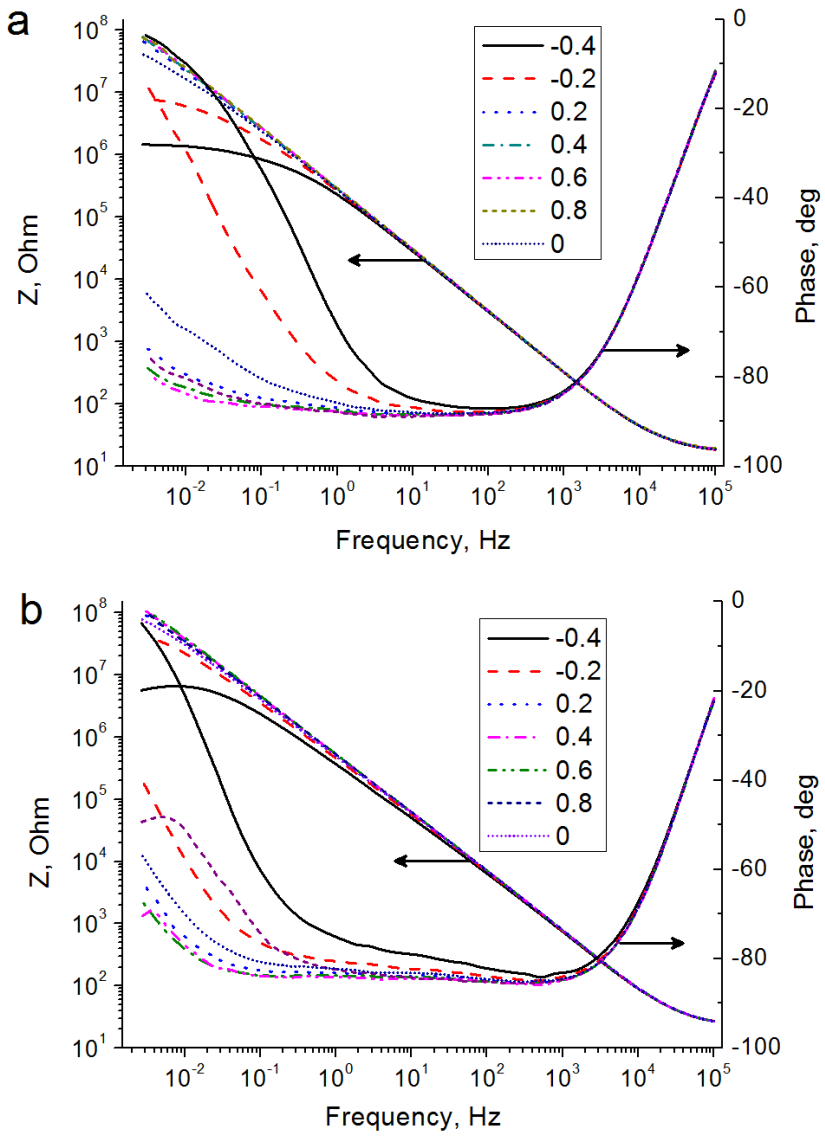


**Figure 4.3.2:** EIS spectra of $TiO_2$ films prepared in 2M $H_3PO_4$ solution recorded at different polarizations (from +0.8V to -0.4V vs. $Hg/HgSO_4$ reference electrode with step 0.2V) with thicknesses of the oxide films 70nm (a) and 120 nm (b).

The second time constant is better defined in the region from 10 Hz to 1000 Hz in the case of thicker films (Fig. 4.3.2b). The reason for this is that for thicker films the contribution of the bulk part of the coating becomes more important, resulting in a well-separated response. Fitting with two time constant model (Fig 4.3.3a) gives relatively good results (Table 4.3.1, Fig. 4.3.3c) while use of one RC equivalent circuit can be considered as unjustifiable oversimplification in this case. Calculation of the capacitance from the constant phase element was previously described [5].

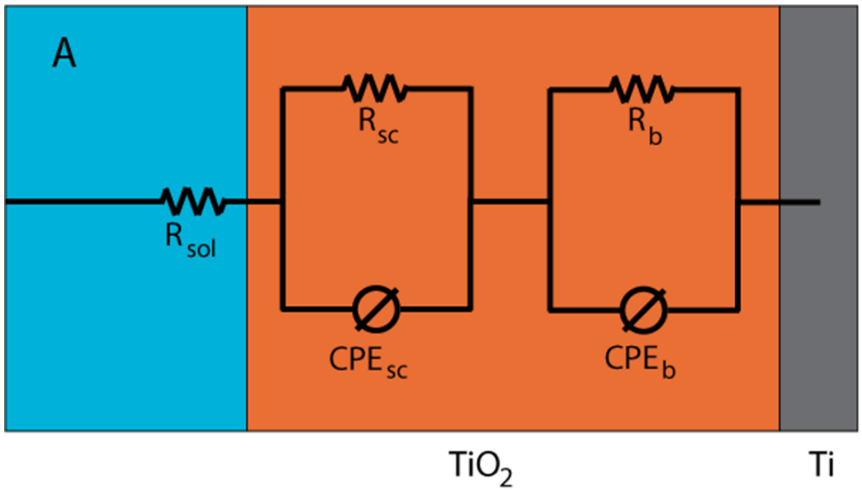


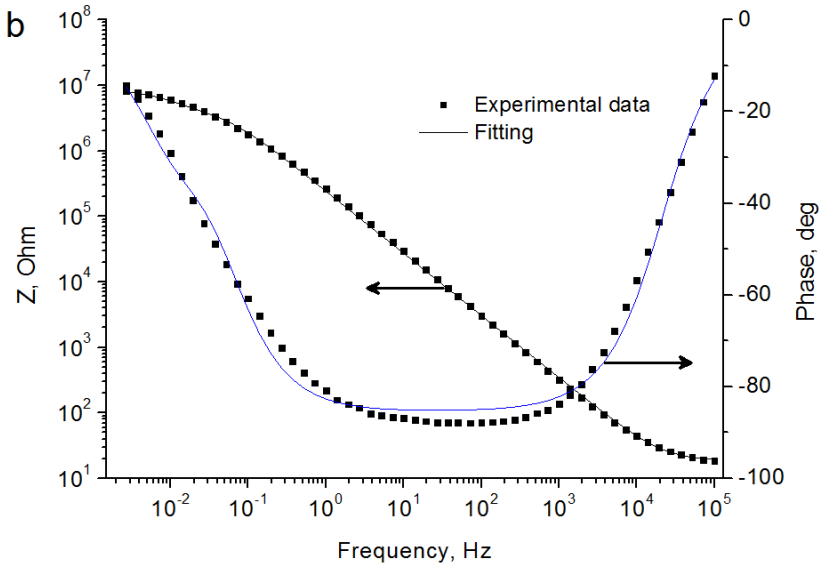


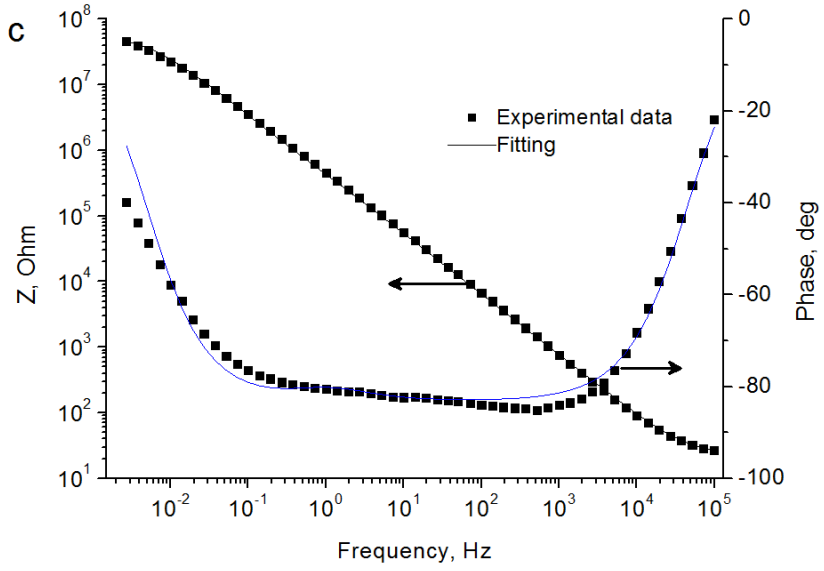


**Figure 4.3.3:** Fitting model (a) and fitting results of 70 nm (b) and 120 nm (c) titanium oxide films under -0.2V polarization.

**Table 4.3.1.** Equivalent circuit parameters and respective errors (in %) obtained for fitting the impedance spectra of 120 nm thick film (Fig. 4.3.3c) polarized at different potentials. $n_{sc}$ and $n_b$ are the power coefficients for the constant phase elements of SCR and bulk layer, respectively.

| Applied potential (V) | $R_{sol}$ (Ohm $cm^2$) | $R_{sc} \times 10^{-7}$ (Ohm $cm^2$) | $CPE_{sc} \times 10^6$ (S $s^n$ $cm^{-2}$) | $n_{sc}$ | $R_b \times 10^{-6}$ (Ohm $cm^2$) | $CPE_b \times 10^3$ (S $s^n$ $cm^{-2}$) | $n_b$ |
|---|---|---|---|---|---|---|---|
| -0.2 | 24±1.4% | 6.2 ±2.7% | 6.2 ±0.51% | 0.93 ±0.14% | 3.6 ±7.4% | 1.1 ±8.1% | 0.92 ±1.1% |
| 0 | 24 ±1.8% | 18 ±2.9% | 4.9 ±0.44% | 0.94 ±0.22% | 4.1 ±8.9% | 1.5 ±9.0% | 0.93 ±6.1% |
| 0.6 | 25 ±1.9% | 58 ±2.9% | 4.6 ±0.45% | 0.95 ±0.91% | 2.9 ±8.8% | 3.8 ±8.9% | 1.0 ±14%* |

*High value of error was obtained due to the limitation of the n. Maximum value of CPE exponent is 1, so higher values have no physical meaning.

The SCR capacitance for all studied samples at different potentials was calculated and used for the constructing Mott- Schottky analysis (Fig. 4.3.4). A correction for the Helmholtz layer and bulk region capacitance is not required in this situation, since fitting gives values of pure capacity of the space charge region. The obtained Mott-Schottky plots are typical for such systems and a linear part of the plots was used for calculation the ionized donor concentration.

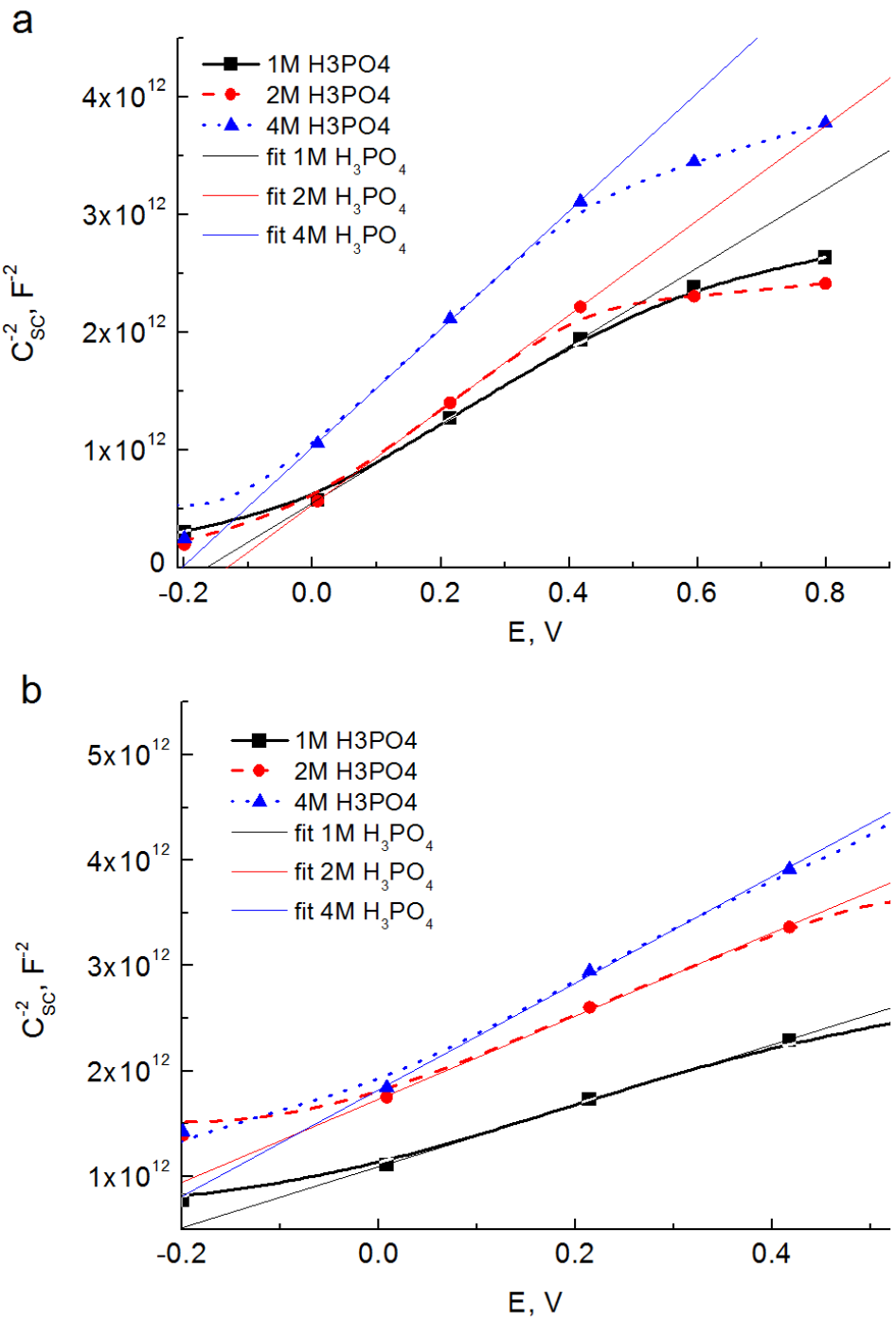


**Figure 4.3.4:** Mott-Schottky plots calculated from the SCR capacitance on titania films (with thickness 70 nm (a) and 120 nm (b)) obtained in electrolytes with different concentrations.

Figure 4.3.5a shows the dependence of the calculated ionized donor concentration on the film parameters. The $N_d$ increasing with the film thickness and with the electrolyte concentration. This can be explained by the fact that the increase of electrolyte concentration leads to a higher density of electron traps.

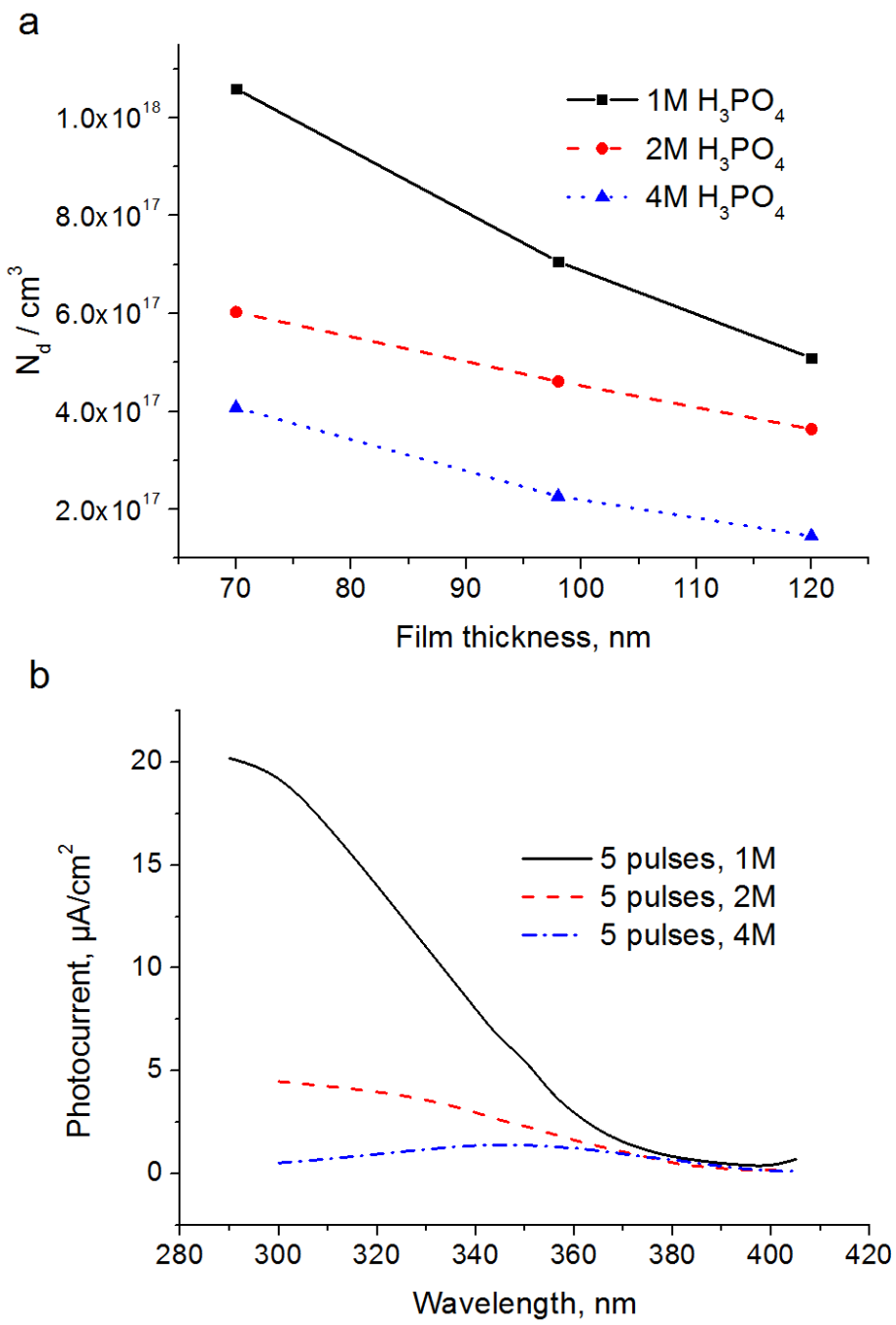


**Figure 4.3.5:** Ionized donor concentration, $N_d$ (a), and photocurrent spectra (b) of $TiO_2$ films prepared in $H_3PO_4$ solutions with different concentrations.

The photocurrent spectroscopy can be used as a complementary tool to characterize the obtained films for better understanding of their electronic structure. In the present work a qualitative analysis of the photocurrent response obtained from the electrodes 120 nm thick in the $H_3PO_4$ electrolytes with different concentrations are presented in Fig. 4.3.5b. The general observed trend shows a decrease in the photocurrent with increasing the electrolyte concentration. Taking into account that phosphor creates electron traps in titanium oxide, the drop of photocurrent response with $H_3PO_4$ concentration increment seems to be consistent (Fig. 4.3.5b). Higher concentration of phosphors should exist in the film grown in the more

concentrated electrolytes, thus a higher number of electron traps are formed in the film. It is also important to notice that the titania films prepared by PPDO in phosphoric acid have a lower photoresponse in comparison to those prepared in sulfuric acid[5].

### 4.3.5 Volta potential measurements.

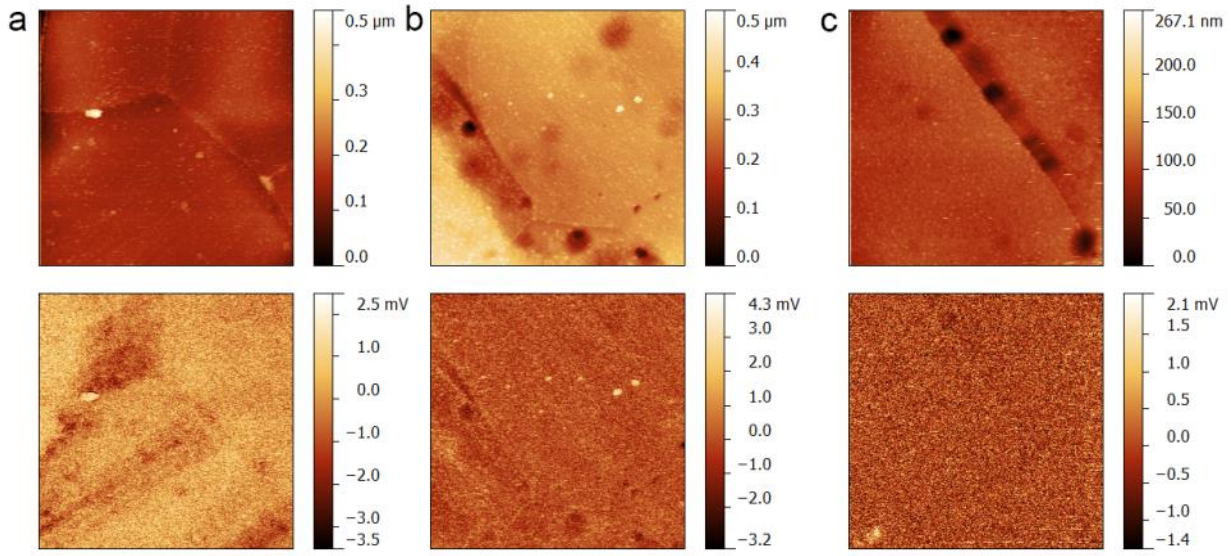


**Figure 4.3.6:** Topology (top) and measured potential distribution (bottom) on titania films with thickness 95 nm prepared by pulsed discharge anodisation in phosphoric acid electrolytes with different concentrations ( 1M (a), 2M (b) and 4M (c)).

Scanning Kelvin probe force microscopy (SKPFM) was used as an effective method for studying the electrical properties of the films. It was previously shown[127], that PPDO anodizing of aluminium results in a more smooth Volta potential map in comparison to conventional methods of anodisation. Figure 4.3.6 shows the topography and surface potential maps of the titania films with a thickness of 95 nm (4 pulses) prepared in $H_3PO_4$ solutions of different concentrations. The titania films prepared by PPDO demonstrate a very smooth Volta potential distribution (VPD) on the oxide surface similarly to the alumina. It is worth to notice that different topology effects, such as grain boundaries and cavities originating from the polishing procedure have almost no influence on the VPD. Furthermore, the Volta potential distribution becomes smoother when electrolyte concentration increases. Thus, for the sample prepared in solution of 1M phosphoric acid, fluctuation of the VPD is ±1.5 mV, while on the sample prepared in 4 M solution, the average deviation is even lower.

Figure 4.3.7 demonstrates the evolution of the average Volta potential values for 1M, 2M and 4M electrolytes with the increment of the oxide thickness. The observed growth of surface potential on titania is not linear in contrast to the results obtained on aluminium[127]. This non-linearity can be explained by the semiconductive nature of the titania film, where surface charges can spread into volume of the film much more easily than on an insulator film like alumina, avoiding high charging of the film surface.

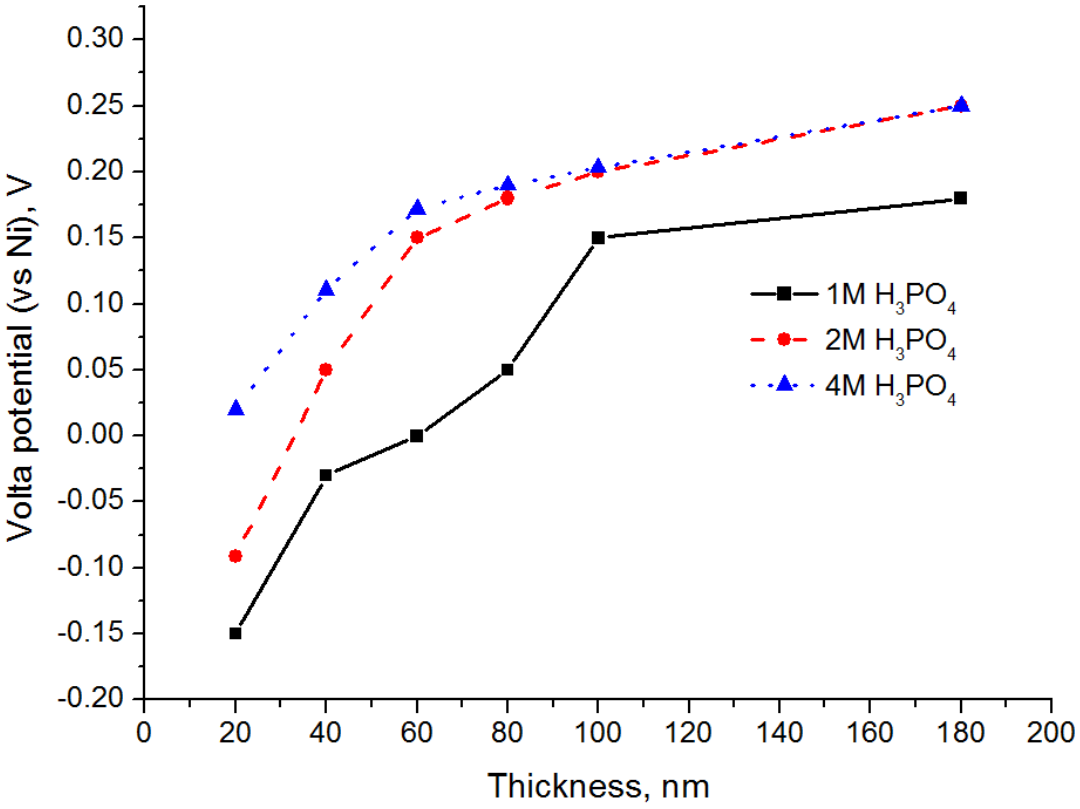


**Figure 4.3.7:** Volta potential measured on the titanium oxide films prepared by PPDO method in $H_3PO_4$ solutions with different concentrations.

The shift of the VPD values to higher potentials for higher electrolyte concentration can be explained as a result of better charge separation originated from lower electrical conductivity of the films, prepared in more concentrated solutions. However, it was not possible to obtain oxide films on titanium, with Volta potential higher than 0.30mV vs. Ni. Possible explanation of this fact can be that in semiconductive films a certain maximal charge can be achieved. Further charging is impossible because the stable charge separation is limited by the recombination processes. A similar effect was observed on aluminium samples, where after heat treatment the potential was also established at certain limit because of temperature-induced recombination[127]. The titania film does not need thermal activation for the charge recombination since mobility of charge carriers in the semiconductive film at room temperature is already sufficient. In contrast to the alumina films, it is also not possible to use the slope of the VPD vs. thickness plot for the characterisation of the film electronic properties. However, values of the Volta potential for the same thickness can be used to compare films obtained in electrolytes with different concentrations. Thus, for all studied systems the VPD increases with the electrolyte concentration until the plateau is reached. The influence of the dopant type, its concentration and film preparation conditions on the Volta potential still needs to be further investigated.

### 4.3.6 Discussion of the oxidation processes

In previous work [127]the mechanistic details of discharge on Al surface were investigated and growth model was proposed. In this section effect of the electrolyte concentration on the kinetics and mechanism of pulsed anodic film formation on Ti is discussed.

The pulsed discharge anodisation process on aluminium can be conventionally divided into two stages where the first one (short) is about 1μs long, with the characteristic current magnitude of several kA[127]. It has been proposed [127] that ionization of an oxide film (either native film or formed by previous oxidation) is the main process during the first stage. In pulse discharge under action of high field, the resistive oxide film fully ionizes giving plasma. During the second (long) stage the growth of a new part of the layer occurs due to migration of ions inside the plasma or destabilized film. In comparison to the conventional anodisation processes the oxide growth occurs in much higher electrical field and a higher total charge is transferred in an unit time leading to a higher film growth rate during the pulsed discharge anodisation in comparison to the conventional method. Opposite to aluminium, in the titanium case there is no sharp distinction between the two stages (Fig. 4.3.8) and the border is blurred.

As shown above, the amount of defect centres in the film rise with increment of the electrolyte concentration. However, in the beginning of discharge, these dopant atoms can play a role of ionization centres, resulting in a higher ionization degree on the first stage. In the second stage these dopants increase of the film growth speed as they play a role of charge carriers rising mobility of ions in the destabilized film. As a result higher values of instantaneous current in the second stage are observed. Thus the main factor, which play role in pulse duration, is the concentration of dopant atoms in the oxide film.

In the first period of discharge, which corresponds to the oxide ionization, the difference between current profiles obtained in different electrolytes can be seen in Fig. 4.3.8. The highest current is observed for the electrode in 4M solution of $H_3PO_4$. In the second period, which corresponds to the ion migration and film growth, differences also can be also seen. After 50 μs the current between electrodes in the solution of 4M $H_3PO_4$ drops almost to zero, while in the solution of 2M it still has a value around 40A and in 1M phosphoric acid it is almost 50 A.

The lower currents at the beginning of discharge are observed for the anodic films grown in 1M phosphoric acid since the amount of defects in these films is lower in comparison to more concentrated electrolytes giving lower currents at the beginning of discharge. The first stage is better defined in this case being close to the situation obtained on aluminium. , The ion transport also occurs with lower speed due to the low amount of the defects increasing duration of the second stage. In the case of current profile obtained in 4M solution, higher concentration of the defects results in higher currents in the first stage and also higher speed of film growth on the second one. These factors bring to superposition of both stages, so it is almost impossible to determine a border between two parts of the profile. In the other two electrolytes the effect of two phases superposition is not so evident.

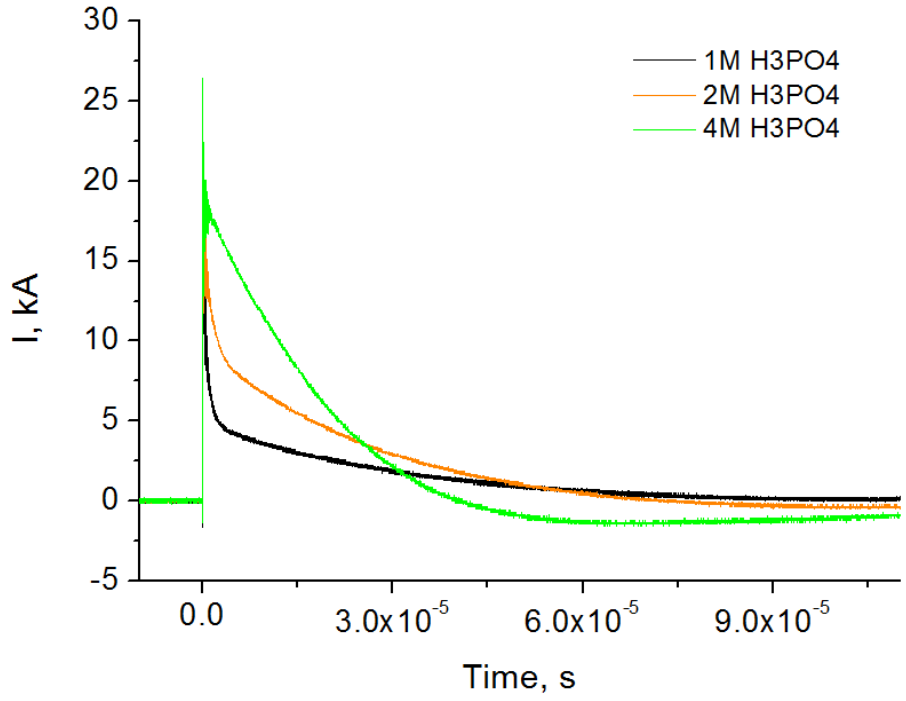


**Figure 4.3.8**: Influence of the concentration of $H_3PO_4$ on the current profiles during pulse oxidation.

It is known that solution conductivity becomes higher with increasing the phosphoric acid concentration. Taking into account that the current after the first stage is lower for the solutions with higher conductivity, we can consider that the solution conductivity doesn't play a main role in the discharge process.

## 4.3.7 Conclusions

Powerful Pulsed Discharge Oxidation (PPDO) is a novel method of thin film preparation, which allows producing oxide films with tailored properties, quite different of those obtained by other conventional methods. Higher number of defects concentration in the film with increased of phosphoric acid concentration in electrolyte was confirmed by non-direct results, obtained from several complementary methods (Mott- Schottky analysis, photocurrent spectroscopy, SKPFM).

SKPFM studies show uniformity of charge distribution on the films prepared by PPDO. In contrast to the results obtained on aluminium, it was observed that the dependence of Volta potential on the film thickness is not linear, which can be explained by the semiconductive nature of the titanium oxide.

Studies of the time evolution of current on titanium electrodes in phosphoric acid solutions with different concentrations show that the shape of the current profile does not depend on the electrolyte conductivity. The main role in the discharge profile is played by the dopant concentration in the oxide film. Oxides with lower concentration of dopants have well defined stages of ionization and film growth, while in the case of films with a higher dopant concentration, the two stages merge. The growth of the oxide also occurs with a higher rate for

the films with a higher concentration of dopants. Thus varying the concentration of electrolyte the electronic properties of resulting titatnia films and the kinetics of their growth can be tuned for specific applications.

# 4.4 Aluminium anodisation in deionised water as electrolyte

C364 *Journal of The Electrochemical Society*, **163** (7) C364-C368 (2016)

## Aluminum Anodization in Deionized Water as Electrolyte

**Aleksey D. Lisenkov,[a,*,z] Sergey K. Poznyak,[b] Mikhail L. Zheludkevich,[a,c] and Mário G. S. Ferreira[a,**]**

[a]*Department of Materials and Ceramics Engineering/CICECO, University of Aveiro, 3810-193 Aveiro, Portugal*
[b]*Institute for Physical Chemical Problems, Belarusian State University, 220050 Minsk, Belarus*
[c]*Institute of Materials Research, Helmholtz-Zentrum Geesthacht, 21502 Geesthacht, Germany*

Thin oxide films were prepared electrochemically on the aluminum surface using the high-voltage discharge and potentiostatic methods in deionized water as an electrolyte. The growth of continuous films occurred only at potentials lower than the breakdown potential. The films obtained by the discharge method are more uniform and can grow to a higher thickness in comparison to those formed by the potentiostatic mode, as demonstrated by electrochemical impedance spectroscopy (EIS), transmission electron microscopy (TEM), and scanning Kelvin probe force microscopy (SKPFM). The data herein obtained can be used as a reference to understand better the properties of the films produced in conventional electrolytes where apart from water other species are present.


Manuscript submitted January 29, 2016; revised manuscript received April 11, 2016. Published April 21, 2016.

Anodizing treatment is widely used on aluminum and its alloys in industrial practice to enhance surface performance (corrosion resistance, hardness and wear resistance) and to modify physical and chemical properties of the metal surface.[1,2] Anodization is a convenient and important method of oxide film formation owing to low cost, flexibility and easiness.[3–7] There are several anodization processes that are currently used: conventional anodic oxidation (potentiostatic or galvanostatic) and plasma electrolytic oxidation (PEO).[3–5,7] The conventional anodization is well studied and allows growing oxide films of controlled thickness and quality.[5,7] The films can be partially hydrated.[5] The other method, PEO, which utilizes potentials above the breakdown voltage of the oxide film growing on the anode surface, makes possible to prepare well adherent, hard, ceramic-like coatings.[3,4] Both methods are currently applied in industry although they are still under investigation. One of the problems, which appears when studying the anodic oxides, is related to the impossibility of preparing a pure oxide film without foreign atoms apart from metal atoms of the substrate, oxygen and hydrogen atoms. In all electrolytes used for anodization, different ionic species are added to increase the conductivity of solution and the foreign atoms are trapped into the growing oxide.[8] According to the literature, the concentration of the foreign atoms during anodic oxidation usually does not exceed 1%,[9] however, impact of them on anodic film parameters, such as concentration of ionized donors, conductivity and photosensitivity, is significant. It was shown that the electrolyte concentration used for anodization influences the dopant content in the oxide[8] and even small amount of ionic species in solution results in changes of the film properties. Thus, in order to have a reference point for further research it is important to obtain an oxide film with minimal influence of foreign atoms. One of the electrolytes that can help to decrease the amount of entrapped foreign atoms in the oxide is anodization in hydroxide solutions. Although the concentration of extraneous elements is lower than the elements entrapped from the conventional electrolytes (such as ammonium pentaborate), even in this case foreign cations will be entrapped to the bulk of the film. Of course, impurity-free oxide on the metal surface can be prepared by other methods, such as oxidation in oxygen atmosphere at high temperature[1] or in boiling water,[10] but the properties of the obtained films will be different of those prepared by electrochemical oxidation. This motivates the present work where only deionized water was used as an electrolyte.

The properties of the films obtained in the present work were studied by scanning (SEM) and transmission electron microscopies (TEM), electrochemical impedance spectroscopy (EIS) and scanning Kelvin probe force microscopy (SKPFM). SKPFM allows simultaneous mapping of topography and Volta potential distribution on passive surfaces in air.[11,12] The Kelvin probe methods are based on measurement of Volta potential difference (VPD) between a surface and a reference electrode. Several factors can influence the Volta potential measurements, i.e. composition and structure of the oxide film covering the aluminum surface and intermetallics, tip–sample distance and adsorption of different molecules at the surface. Previously it was shown[10,13] that the VPD distribution observed on some metal surfaces correlates, for example, with their corrosion properties.

The main aim of the present work is to demonstrate the possibility of preparing impurity-free anodic oxide films on valve metals, particularly aluminum, by high-voltage anodization in deionized water. The current paper is the first part of a research focused on the preparation of impurity-free oxides by electrochemical methods.

### Experimental

The electrochemical cell used for anodization consisted of an aluminum (Alfa Aesar, 99.999%) anode with a working surface of 4 $cm^2$ and Ti cathode (Alfa Aesar, 99.7%) with about 20 times larger surface area. Titanium was chosen as a cathode material due to its high mechanical strength and chemical inertness. The electrodes were abraded using abrasive papers up to grit 4000. Then the Ti electrode was chemically polished in a HF:$HNO_3$ (1:3 by volume) mixture. Aluminum was electrochemically polished in $C_2H_5OH$:$HClO_4$ (4:1 by volume) electrolyte in potentiostatic regime at 20 V to a mirror finish. After polishing, both electrodes were thoroughly rinsed with deionized water.

Deionized water ($18 \times 10^6$ $\Omega \cdot cm$) prepared from distilled water was used as an electrolyte for Al anodization. Preparation of the oxide film on Al was performed by two different ways: potentiostatic and high-voltage discharge methods. In the former, a constant voltage in the range from 1000 to 2000 V with 200 V step was applied to the electrodes using a Matsusada AU-3P400 high voltage power supply, and anodization was performed for different time intervals. The discharge method was another technique, in which a low-inductance 100-$\mu$F capacitor bank, with a measured internal resistance of $2.2 \times 10^3$ $\Omega$, charged to the same voltages as in the potentiostatic mode, was then discharged to the cell. In order to prepare films with different thicknesses, the capacitor was discharged sequentially through the electrochemical cell between 1 and 30 times to the residual voltage of 100 V. The length of discharge varied in the range of 200–350 s depending on the film thickness. The thickness of the oxide film was controlled by two parameters: initial voltage and number of

*Electrochemical Society Student Member.
**Electrochemical Society Member.
[z]E-mail: lisenkov@ua.pt

Contribution to this paper:
Conception of the work, preparation of all samples, fitting of the obtained data, electron microscopy, atomic force microscopy, reproducibility experiments, preparation of images, text preparation.

## 4.4.1 Introduction

Anodizing treatment is widely used on aluminium and its alloys in industrial practice to enhance surface performance (corrosion resistance, hardness and wear resistance) and to modify physical and chemical properties of the metal surface [24, 73]. Anodisation is a convenient and important method of oxide film formation owing to low cost, flexibility and easiness [2, 30, 58, 184, 203]. There are several anodisation processes that are currently used: conventional anodic oxidation (potentiostatic or galvanostatic) and plasma electrolytic oxidation (PEO) [2, 30, 58, 203] _ENREF_7. The conventional anodisation is well studied and allows growing oxide films of controlled thickness and quality [2, 203]. The films can be partially hydrated [2, 203]. The other method, PEO, which utilizes potentials above the breakdown voltage of the oxide film growing on the anode surface, makes possible to prepare well adherent, hard, ceramic-like coatings [30, 58]. Both methods are currently applied in industry although they are still under investigation. One of the problems, which appears when studying the anodic oxides, is related to the impossibility of preparing a pure oxide film without foreign atoms apart metal atoms of the substrate, oxygen and hydrogen atoms. In all electrolytes used for anodisation, different ionic species are added to increase the conductivity of solution and the foreign atoms are trapped into the growing oxide [128]. According to the literature, the concentration of the foreign atoms during anodic oxidation usually does not exceed 1% [204], however, impact of them on anodic film parameters, such as concentration of ionized donors, conductivity and photosensitivity, is significant. It was shown that the electrolyte concentration used for anodisation influences the dopant content in the oxide [128] and even small amount of ionic species in solution results in changes of the film properties. Thus, in order to have a reference point for further research it is important to obtain an oxide film with minimal influence of foreign atoms. One of the electrolytes that can help to decrease the amount of entrapped foreign atoms in the oxide is anodisation in hydroxide solutions. Although the concentration of extraneous elements is lower than the elements entrapped from the conventional electrolytes (such as ammonium pentaborate), even in this case foreign cations will be entrapped to the bulk of the film. Of course, impurity-free oxide on the metal surface can be prepared by other methods, such as oxidation in oxygen atmosphere at high temperature [73] or in boiling water [115], but the properties of the obtained films will be different of those prepared by electrochemical oxidation. This motivates the present work where only deionised water was used as an electrolyte.

The properties of the films obtained in the present work were studied by scanning (SEM) and transmission electron microscopies (TEM), electrochemical impedance spectroscopy (EIS) and scanning Kelvin probe force microscopy (SKPFM). SKPFM allows simultaneous mapping of topography and Volta potential distribution on passive surfaces in air [107, 189]. The Kelvin probe methods are based on measurement of Volta potential difference (VPD) between a surface and a reference electrode. Several factors can influence the Volta potential measurements, i.e. composition and structure of the oxide film covering the aluminium surface and intermetallics, tip–sample distance and adsorption of different molecules at the surface. Previously it was shown [115, 190] that the VPD distribution observed on some metal surfaces correlates, for example, with their corrosion properties.

The main aim of the present work is to demonstrate the possibility of preparing impurity-free anodic oxide films on valve metals, particularly aluminium, by high-voltage anodisation in deionised water. The current paper is the first part of a research focused on the preparation of impurity-free oxides by electrochemical methods.

## 4.4.2 Experimental

The electrochemical cell used for anodisation consisted of an aluminium (Alfa Aesar, 99.999%) anode with a working surface of 4 $cm^2$ and Ti cathode (Alfa Aesar, 99.7%) with about 20 times larger surface area. Titanium was chosen as a cathode material due to its high mechanical strength and chemical inertness. The electrodes were abraded using abrasive papers up to grit 4000. Then the Ti electrode was chemically polished in a $HF:HNO_3$ (1:3 by volume) mixture. Aluminium was electrochemically polished in $C_2H_5OH:HClO_4$ (4:1 by volume) electrolyte in potentiostatic regime at 20 V to a mirror finish. After polishing, both electrodes were thoroughly rinsed with deionised water.

Deionised water ($18\times10^6$ Ω·cm) prepared from distilled water was used as an electrolyte for Al anodisation. Preparation of the oxide film on Al was performed by two different ways: potentiostatic and high-voltage discharge methods. In the former, a constant voltage in the range from 1000 to 2000 V with 200 V step was applied to the electrodes using a Matsusada AU-3P400 high voltage power supply, and anodisation was performed for different time intervals. The discharge method was another technique, in which a low-inductance 100-μF capacitor bank, with a measured internal resistance of $2.2\times10^3$ Ω, charged to the same voltages as in the potentiostatic mode, was then discharged to the cell. In order to prepare films with different thicknesses, the capacitor was discharged sequentially through the electrochemical cell between 1 and 30 times to the residual voltage of 100V. The length of discharge varied in the range of 200-350 s depending on the film thickness. The thickness of the oxide film was controlled by two parameters: initial voltage and number of discharges. In both methods, the resistance of the electrolyte plays a very important role. During anodisation, the resistance of deionised water decreases from $8\times10^5$ Ω to $1\times10^5$ Ω, which could affect significantly the process. The electrolyte was replaced by fresh portions and all electrodes were carefully rinsed with deionised water after each two discharges or if the resistance of the water in the electrochemical cell, measured at the frequency of 1000 Hz, became lower than $6\times10^5$ Ω. To compare the properties of the obtained anodic oxides, anodisation of Al was also performed in galvanostatic mode at a current density of 10 $mA/cm^2$ followed by potentiostatic anodisation in a 0.1 M ammonium pentaborate ($(NH_4)_2B_{10}O_{16}$) aqueous solution.

Determination of the potential distribution in the electrolyte plays an important role for this work. Theoretically, the potential drop can be estimated by dividing the applied potential by the distance between electrodes, but several parameters, such as potential drop on the electrode surfaces, edge effects and nonuniformity of the electrolyte will result in significant error. A better way is the measurement of the potential between the counter electrode and a neutral point in the electrolyte. In this case it is possible to determine non-uniformities of the electrolyte conductivity and avoid errors connected with processes on the electrode (the current between the counter electrode and tip is negligible). However, in this case the geometry plays a role (flat electrode vs. point tip), thus modelling and calculations become difficult. To avoid this problem two electrodes with platinum tips (10 μm in diameter) were placed in the electrolyte bulk between the cathode and the anode. In this case the geometry is not relevant (point tip vs. point tip). The distance between tips can be varied, and they can be placed in different parts of the electrolyte bulk to determine the field distribution. To determine the potential at the electrode surface, E, the cell geometry was taken as two parallel electrodes in high-resistance electrolyte. Over the main part of the surface the potential distribution is uniform. Due to the high resistivity

of the electrolyte, the influence of the volume and distance to the walls of the cell can be ignored.

In highly resistive electrolytes, like deionised water, the anodic film thickness cannot be estimated by the applied voltage or by the charge passed through the cell during the discharge as in the case of the traditional anodisation. Electrochemical impedance spectroscopy (EIS) is an effective tool to estimate the thickness of oxide films as well as to obtain information about their structure, for example, crystallinity and defects. In the present work, the thickness of the alumina films was evaluated using EIS measurements and confirmed by TEM. For the sake of comparison, thickness of the oxide was also estimated for the discharge-prepared films from the voltage vs time plots.

The EIS measurements were performed using a Gamry FAS2 Femtostat with a PCI4 Controller in a frequency range from $10^5$ to $10^{-2}$ Hz with 7 points per decade. The measurements were carried out at room temperature in a conventional three-electrode cell consisting of a mercury–mercurous sulphate reference electrode, a cylindrical platinum foil as a counter electrode and the working electrode with an exposed area of 1 $cm^2$. Impedance spectra were recorded by applying a 10 mV (RMS) sinusoidal perturbation at the open circuit potential. The cell was placed in a Faraday cage to avoid interferences with external electromagnetic fields. A 0.1 M ammonium pentaborate solution was used as the electrolyte for EIS measurements. At least five samples prepared in the same conditions were tested to ensure reproducibility of the results. The impedance plots were fitted using equivalent circuits by means of the Echem Analyst software from Gamry Inc.

Transmission electron microscopy (TEM) was carried out using a Hitachi H9000 microscope at an acceleration voltage of 300 kV. Electron transparent sections of the samples for TEM were cut with a Leica Reichert Supernova ultramicrotome. Investigation of the surface topography was performed using a Hitachi SU-70 SEM.

A Digital Instruments Nanoscope III atomic force microscope with conductive Pt-Cr probes (AppNANO) was used for SKPFM measurements. The obtained VPD values are presented versus the VPD measured for pure Ni as a reference.

### 4.4.3 Results and Discussion

The results of Al anodisation in deionised water under high-voltage potentiostatic and discharge modes with applied voltages between 1000 and 2000 V (Table 4.4.1) showed that up to 1600 V in both cases oxide films with different properties can be obtained. For the first method the film thickness ranged from 5 to 12 nm (lower values are for lower voltages). Between 1000 and 1600 V the film was found to be uniform if anodisation was performed during 1-2 minutes depending on the applied potential (table 4.4.1). In the case of the lower voltage range (1000-1200 V) it was possible to generate films up to 2 minutes of anodisation. However, anodisation for a period less than 1 minute resulted in formation of thin films, which thickness was comparable with natural oxide. In the case of the higher voltages (1400-1600V) anodisation was performed for 1 or 1.5 minute. The film thickness is limited by two parameters: the thickness of the natural oxide from the lower side and the breakdown of the film from the higher one. Longer anodisation of the electrodes resulted in breakdown of the films. Application of potentials of 1800 and 2000V in the potentiostatic method also resulted in breakdown of the film (fig. 4.4.1A). For the discharge method, the film thickness was between 9 and 11 nm after 20 discharges and between 14 and 16 nm after 30 discharges for U = 1000-1200 V. When the

voltage increased up to 1400 -1600 V, the thickness rose to 15 nm after 10 discharges and 26 nm after 20 discharges. Under discharge mode the film still grew at 1800 V, reaching a maximum thickness of 16 nm after 5-7 discharges. At 2000V the oxide film cannot be prepared by either methods, since breakdown occurred (fig 4.4.1B). It should be noted, that in the case of the high-voltage potentiostatic method, the results show very poor reproducibility of breakdown events: even small fluctuations of parameters such as resistivity and amount of gases (oxygen and nitrogen) in the electrolyte, preparation and purity of the electrode surface can influence the process.

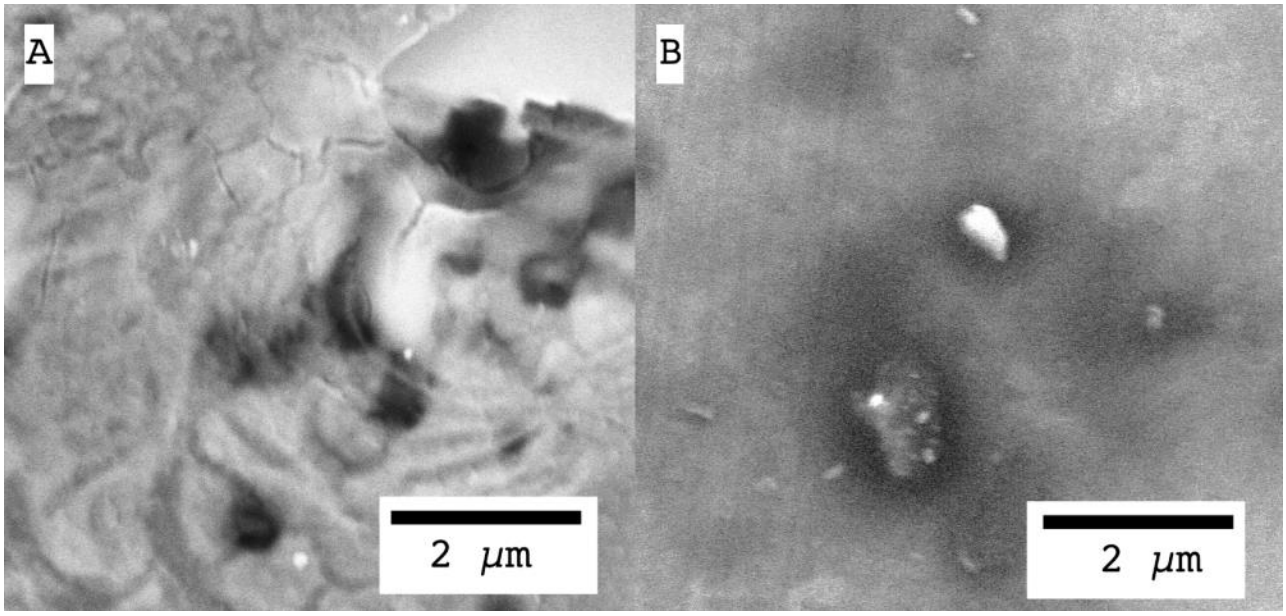


**Figure 4.4.1**: SEM images of the film breakdown on the oxides prepared at applied voltage of 2000 V by the potentiostatic (A) and discharged (B) methods.

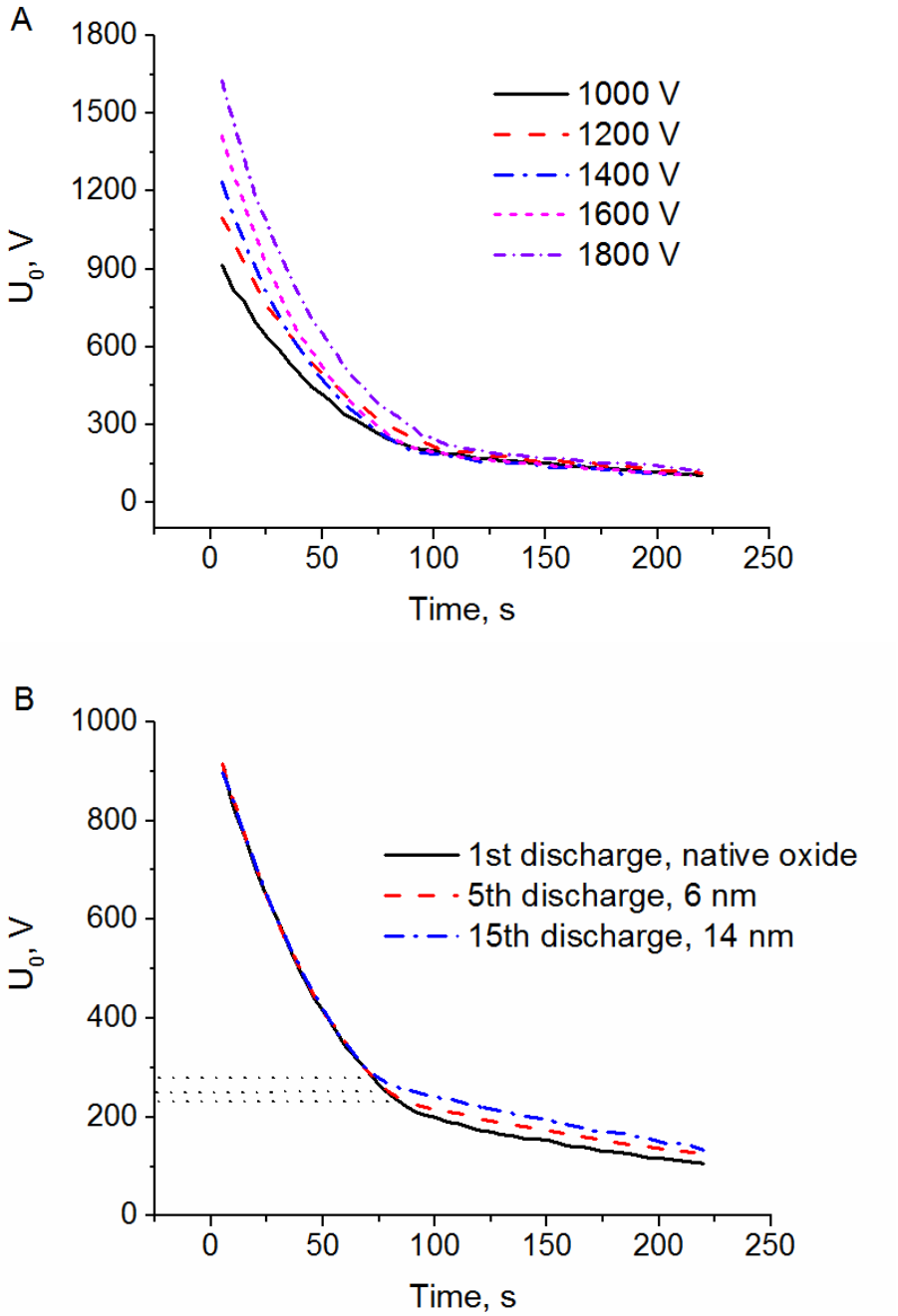


**Figure 4.4.2**: (A) Discharge plots for the aluminium anodisation by discharge method at different potentials applied to the Al electrodes. (B) Discharge plots for the aluminium anodisation by discharge method at 1000 V applied to the electrode covered with oxide film with different thicknesses.

In contrast to the high-voltage discharge anodisation in highly conductive electrolytes [4-5, 127], the process in deionised water cannot be explained by the same mechanism and has a significant difference in duration. As it was shown previously [127] in highly conductive electrolytes, such as 0.1 M ammonium pentaborate, the full discharge takes less than 0.5 s. In deionised water the applied voltage decays down to 100 V over a period of more than 100 s (Fig. 4.4.2). In deionised water, the measurements do not reveal the presence of plasma since besides the time elapsed, the current is low compared to previous works [127-128]. This is due to a large potential drop in the electrolyte bulk. In the conventional electrolyte, a plasma layer is formed on the anode surface and the oxide growth occurs in this layer [127-128]. Taking into

account the growth rate of the films, their composition and structure, it can be suggested that the growth mechanism is similar to that obtained in potentiostatic method in conventional solutions where plasma is not similarly formed during film growth[115].

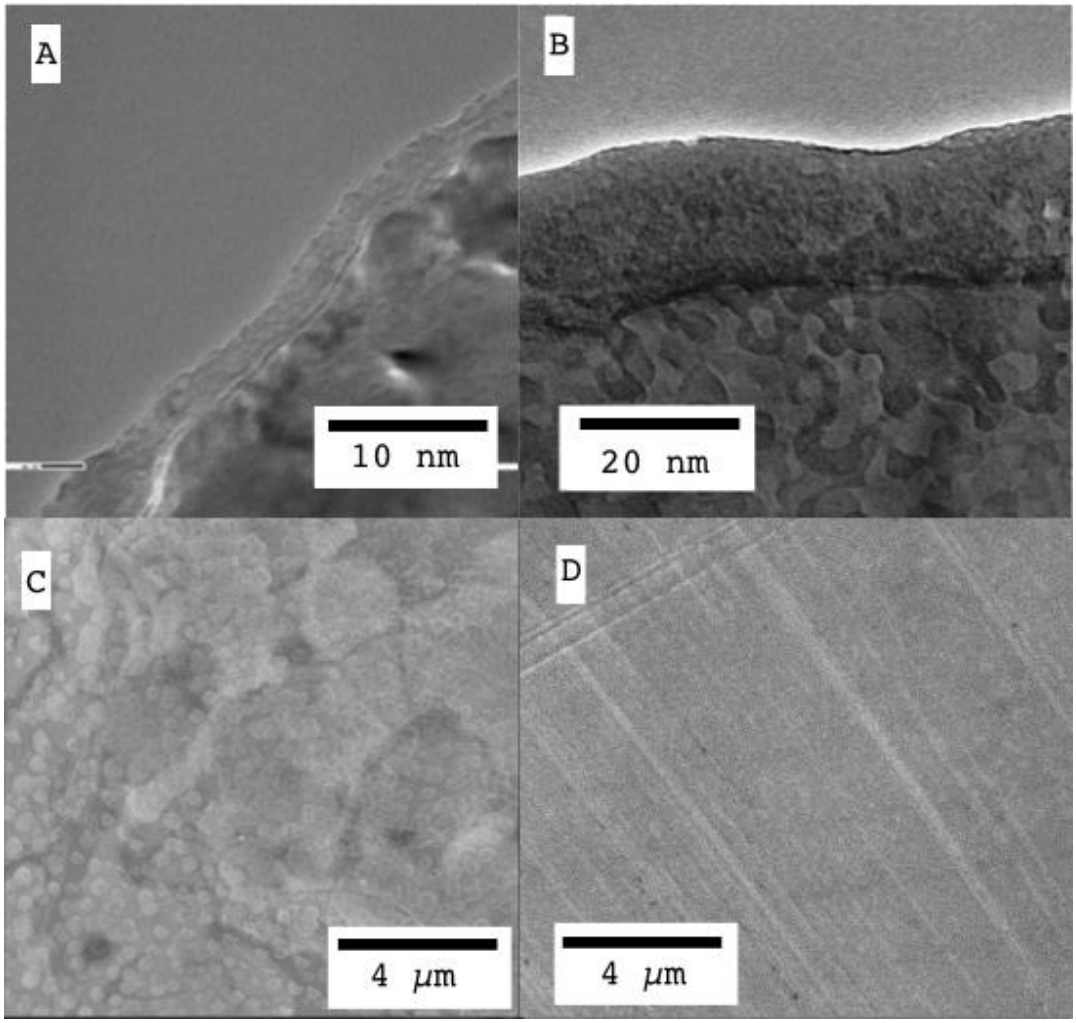


**Figure 4.4.3**: TEM cross sectional images (A, B) and SEM images (C, D) of aluminium oxide prepared by high-voltage potentiostatic (A, C) and discharge (B, D) methods.

In highly conductive solutions such as potassium hydroxide, an increase of the voltage to values higher than 100 V usually results in the formation of oxide film by PEO process, where a breakdown of the oxide followed by formation of plasma discharges and rapid growth of the porous anodic film occurs. However, in deionised water due to its high resistivity, no Faradaic processes take place up to voltages of 1000 V. Further increment of the voltage to higher values leads to the formation of a thin oxide film. The growth of the oxide under such conditions is limited to the range of 1000 kV–1800 kV (Table 4.4.1). At a certain voltage applied to the electrode, breakdown occurs only when a certain thickness of the oxide is reached. The same happens if the film is thick enough, but the voltage is lower than that required for filament formation (this voltage is the border between conventional anodisation and PEO). In the case of potentiostatic oxidation, a constant potential is applied to the electrode, resulting in breakdown of the oxide when the thickness is enough (critical thickness) for the filament formation. Thus the thickness of the oxide is a limiting factor for dense oxide growth in high voltage anodisation.

**Table 4.4.1**: Anodic film thickness, applied potential at the electrode after correcting for the ohmic drop in solution (E) and oxide growth parameters for aluminium anodized in deionised water at different applied voltages.

| $U_0$/ V | Potentiostatic method | | Discharge method | | | E/ V |
|---|---|---|---|---|---|---|
| | Time, min. | Thickness, nm | Number of discharges | Thickness, nm | Parameter $\beta \times 10^{-2}$ | |
| **1000** | 2 | 5±3 | 20 | 9±3 | 5.8 | 62 |
| | | | 30 | 14±4 | | |
| **1200** | 2 | 6±2 | 20 | 11±3 | 5.3 | 75 |
| | | | 30 | 16±4 | | |
| **1400** | 1.5 | 9±4 | 10 | 14±2 | 4.6 | 88 |
| | | | 20 | 24±2 | | |
| **1600** | 1 | 12±4 | 10 | 15±2 | 4.4 | 100 |
| | | | 20 | 26±2 | | |
| **1800** | - | Breakdown occurs from the beginning of the process. | 5-7 | 16±2 | 4.9 | 115 |
| **2000** | - | Breakdown occurs from the beginning of the process. | - | Breakdown occurs after the first discharge. | | 130 |

Electron microscopy (TEM and SEM) examination of the Al samples anodized by the potentiostatic method demonstrates a nonuniform oxide thickness distribution across the electrode surface (Fig. 4.4.3 A, C). However, the films prepared by the high-voltage discharge method were found to be more uniform, without defects and fluctuations of the thickness (Fig. 4.4.3 B, D). The oxide structure in the latter case is similar to the films previously prepared by powerful pulsed oxidation in ammonium pentaborate [127].

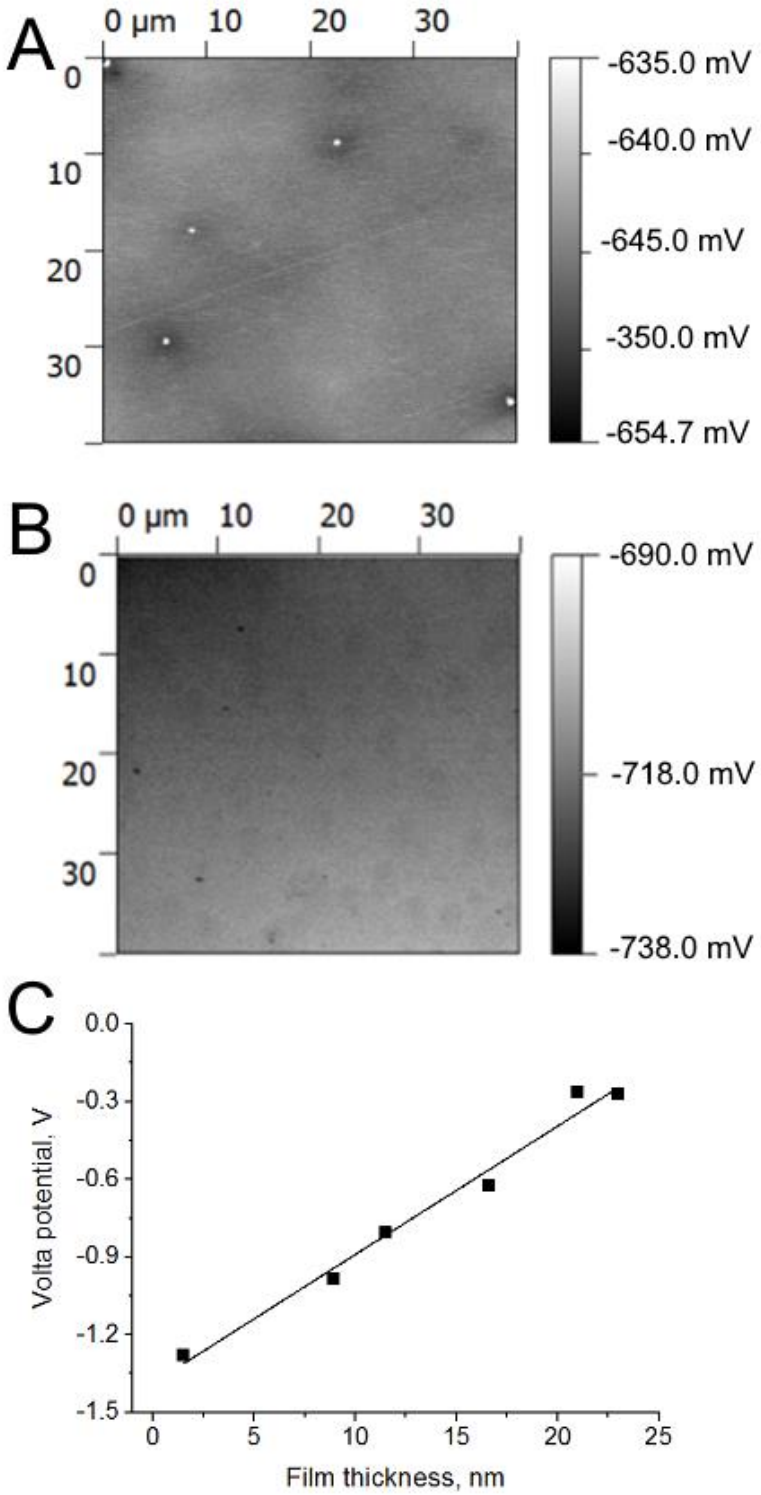


**Figure 4.4.4**: SKPFM images of aluminium samples with oxide thickness of 15 nm anodized by high-voltage anodisation at applied voltage of 1600V by potentiostatic (A) and discharge (B) methods. Volta potential difference versus thickness of the alumina films (different number of discharges) prepared by discharge method at an applied voltage of 1600V (C).

SKPFM measurements (Fig. 4.4.4A) on the Al surfaces treated in deionised water by potentiostatic oxidation demonstrate nonuniform charge distribution on the surface: the Volta potential changed across the film, rising in the most defected zones (up to +10 mV vs. Ni) and

decreasing in the intact areas (down to -9.7 mV vs. Ni). These results are a consequence of the nonuniform thickness of the oxide in the different areas [115, 127]. It was also observed that applying a constant high voltage to the electrochemical cell with deionised water (for periods longer than 1-2 min) led to the appearance of breakdown processes on the surface.

In contrast to the case of potentiostatically prepared samples, SKPFM studies of the discharge prepared ones (Fig. 4.4.4B) showed low fluctuation of the Volta potential. Furthermore, the surface potential rose as the oxide film thickness increased (Fig. 4.4.4C), which is in a good agreement with the observations reported previously [115]. In the case of this method, as the voltage was applied through discharge of a capacitor, the conditions for film breakdown were not met. The voltage applied to the electrodes was lower than the minimum needed for breakdown of the oxide film. Thus, the pulse method seems to be effective for preparing impurity free thin anodic oxide films in highly resistive electrolytes.

The current flowing through an electrode depends on the total overpotential, η, which can be divided [205] in the following components:

$$\eta = \eta_{res} + \eta_{conc} + \eta_{act} \qquad (4.4.1)$$

where $\eta_{res}$ describes the resistance overpotential resulting from the ohmic drop in the bulk of the electrolyte, $\eta_{conc}$ is the concentration overpotential which is related to mass transfer and $\eta_{act}$ is the activation overpotential. Due to the high resistivity of deionised water, the overpotential $\eta_{res}$ should be significantly higher in comparison to the conventional electrolytes. In order to estimate the $\eta_{res}$ value, two platinum tips were placed in the middle part of the cell and the voltage between them was measured. The distribution of the field in the bulk of the electrolyte was found to be uniform. The voltage available for the electrochemical process at the electrode for the initial voltage (time=0):

$$E = U - \eta_{res} \qquad (4.4.2)$$

can thus be estimated for the different applied potentials (Table 4.4.1).

During the film growth some ions can be injected from the electrode into deionised water (even in small amount), resulting in local fluctuations of the solution resistance. In such regions, the electrode potential can change. The film growth occurs preferentially in these areas and the amount of charge used for the oxide film growth on the rest of the surface will be lower. In the case of the discharge method, the electrolyte can homogenise and the layer near the electrode can be restored due to the diffusion process between the discharges, resulting in more uniform film growth (Fig. 4.4.3).

To understand better the processes, that occur during the discharge anodisation, the temporal evolution of the applied voltage was recorded (Fig. 4.4.2 A, B). It was found that the discharge plot consisted of two parts, both of which can be described by the equation of capacitor discharge [125], but with different resistance parameters:

$$U_t = U_0(e^{-\frac{t}{\beta C}}) \qquad (4.4.3)$$

where $U_t$ is the voltage after the time (s), $t$, from the beginning of the discharge, $U_0$ is the initial applied voltage, C is the capacitance and $\beta$ is the resistance parameter. Both parts of the plots can be easily separated (Fig. 4.4.2 A, B); the first part is highly influenced by the applied voltage and does not change with the oxide thickness, while the second part is displaced positively with the film thickness. Fitting the first part of the plots obtained at different applied voltages (Fig. 4.4.2A) using equation 3, the parameter $\beta$ can be estimated (Table 4.4.1). In the second part, the Faradaic process related to the oxide growth does not take place. The

resistance between electrodes becomes significantly higher than the internal resistance of the capacitor and the only process that takes place, is self-discharge of the capacitor. Thus the film growth occurs only during the first period of the discharge and only depends on the initial voltage applied. The change in the voltage $U_0$ in the second part of the plot is linearly related to the thickness of the oxide formed. Thus it is possible to estimate the thickness of the film using the value of $U_0$ obtained from the fitting of this section of the discharge plot.

Considering that the resistance parameter $\beta$ is the same for all the films and very close to the values found for self-discharge of a capacitor ($2.2\times10^3$ Ω), it is possible to fit the second part of the plot using equation 3 and reveal the parameter $U_0$ . Estimated values of thickness were found to be in good agreement (less than 5%) with values in Table 4.4.1 obtained from EIS and TEM measurements.

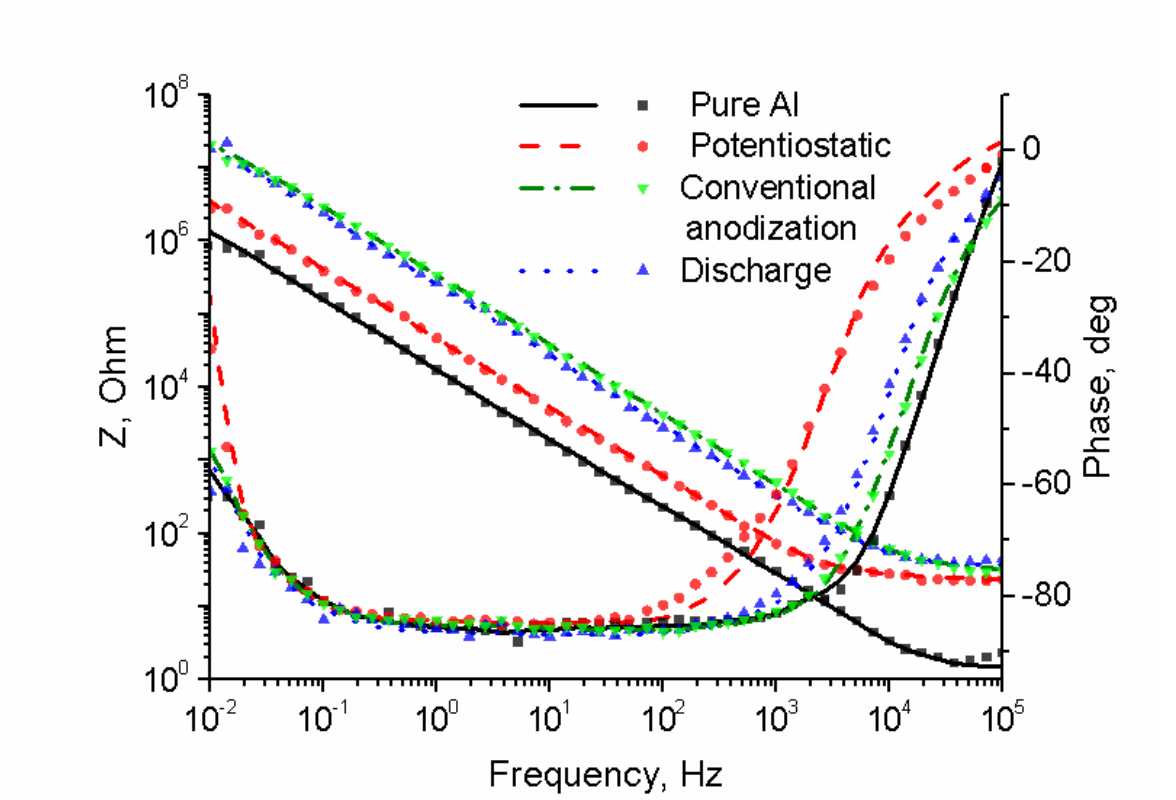


**Figure 4.4.5** The impedance spectra recorded on as-polished Al with a native oxide film (black solid) and anodized aluminium in different conditions: Al with: 10 nm thick oxide prepared by potentiostatic method in deinonized water (red dashed line); oxide with thickness of 20 nm prepared by discharged method in deionised water (blue dotted line); oxide with thickness of 20 nm prepared by conventional anodisation in ammonium pentaborate solution (green dash-dot). Experimental: points; Fitting: lines.

EIS measurements of the anodized aluminium samples with an oxide thickness of 20 nm prepared by different methods are displayed in Fig. 4.4.5. The impedance values of the specimens prepared by high-voltage potentiostatic anodisation (red dash line) are higher than those measured on the pure metal coated only by the native oxide (black solid line), but significantly lower in comparison with those prepared by the discharge method (dash dot green line) and conventional anodisation in ammonium pentaborate solution (dot blue line). This last film was prepared for the sake of comparison by galvanostatic followed by potentiostatic

anodisation in solution of ammonium pentaborate. The advantages of the two-step method of anodisation in comparison with pure galvanostatic are described in the literature [115, 183, 206]. Alumina films prepared in this way have been well studied and have a dense uniform structure [115, 127, 183, 206]. According to the data from electron microscopy (Fig. 4.4.3B, D) and SKPFM (Fig. 4.4.4B), the topography of the films prepared by the discharge method is similar to those obtained by the conventional method.

The EIS spectra were fitted with a model, that consists of a constant phase element (CPE) in parallel with a resistor (R) corresponding to the oxide film, in series with an additional resistor element, which describes the electrolyte. The physical origin of the CPE has been widely discussed in the literature [125]. The impedance of the CPE, $Z_{CPE}$, depends on frequency, ω, according to the following equation:

$$Z_{CPE} = [Q(j\omega)^n]^{-1} \quad (4.4.4)$$

where Q is a parameter numerically equal to the admittance ($|Z|^{-1}$) at $\omega$= 1 rad $s^{-1}$ and $n$ (≤ 1) is a power coefficient calculated as the ratio of the measured maximum phase angle and -90 degrees. The fitting of the spectra shows a high goodness (<$10^{-6}$ according to the Echem Analyst software) and low error (< 1% for all parameters) (Fig. 4.4.5). The value of effective capacitance, $C_{eff}$, was estimated by assuming a normal time-constant distribution through a surface layer by equation (5) derived by Hirschorn et al. [126]:

$$C_{eff} = Q^{1/n} R^{(1-n)/n} \quad (4.4.5)$$

The capacitances of all films prepared by the discharge method were higher by 5-10 % than for the films prepared by conventional method. Capacitance, $C$, is related to thickness, $d$, by the following equation:

$$C = \varepsilon\varepsilon_0 \frac{S}{d} \quad (4.4.6)$$

where $S$ is the surface area and $\varepsilon$ is the dielectric constant of the film and $\varepsilon_0$ is the vacuum permittivity ($8.854\times10^{-12}$ F·$m^{-1}$). Taking into account that the thickness of the samples prepared by both methods is similar (20 nm) and using eq. 6 it was found that the aluminium oxide prepared by electrochemical oxidation of Al in deionised water has a dielectric constant of 9.3-9.9 with a mean value of 9.8. This value is slightly higher than the value obtained for the alumina (9.0) produced by conventional anodisation.

## 4.4.4 Conclusions

The formation of oxide films on the aluminium surface in deionised water was demonstrated in the current work by several methods: TEM, EIS, SKPFM. Images and properties of the films are in good agreement with those widely presented in literature for different conditions.

Discharge and potentiostatic methods were used to prepare thin oxide films on the surface of aluminium in deionised water. The maximum thickness of the anodic film increased

with increasing the applied voltage, but at voltages over 1800 V oxide film cannot be prepared by either methods due to film breakdown. The maximum thickness of the film was 12 nm for the potentiostatic method and 26 nm for the discharge method. The alumina films obtained by the discharge method have also better uniformity in comparison to those prepared by the potentiostatic method. Both films have a dielectric constant comparable to that for the alumina films obtained in conventional electrolytes.

The data here obtained can be used as a reference for better understanding of the properties of anodic films prepared in conventional electrolytes. Further investigation allowing to obtain additional parameters, such as nature of defects, charge carriers concentration, etc., will be pursued.

## 4.5 Aluminium and titanium-aluminium nanorods encapsulated into oxide matrix by powerful pulsed discharge method. (under submission)

Contribution to this work:
Conception of the work, preparation of all samples, fitting of the obtained data, electron microscopy, atomic force microscopy, reproducibility experiments, preparation of images, text preparation.

### 4.5.1 Introduction

Core-shell nanostructures that consist of an inner core and an external shell of different chemical composition is part of the family of nanomaterials, that attract increasing research interest due to their unique structural properties[207-214]. These structural features allow the possibility of combining various properties of several materials[214]. Core-shell nanostructures show improved physical, chemical and mechanical properties in comparison to their single-component counterparts[210]. The created core-shell nanostructures are of great importance to a wide range of applications including electronics, magnetism, optics and catalysis[208, 210]. A wide variety of core-shell nanostructures have been successfully fabricated using different methods ranging from laser ablation and high-temperature evaporation to carbothermal reduction and hydrothermal methods[212-214]. Structural characterization of these nanostructures and determination of their unique properties for various applications have been well documented[213].

One of the methods for core-shell nanostructures preparation is based on the deposition of metals into a porous matrix. This method allows preparing metal particles coated with shells of oxide of different metals. In contrast to the physical methods, during electrodeposition metal fills the oxide pores from the bottom, providing substrate/nanostructure interface.

Recently a new electrochemical technique, namely powerful pulsed discharge oxidation of metals, has been suggested[127-128, 215]. In this technique, the electrochemical reaction occurs at the metal-electrolyte interface under the action of single high-voltage (> 1 kV) pulses. Powerful pulsed discharge method was also used to melt the surface of the porous alumina and titania resulting in sealing of the pores. In previous work a two-stage mechanism of powerful discharge was suggested. The full ionization of the film occurs in a first step during a few microseconds followed by a slower anodic Faradaic process of film growth [127-128]. The fact that the entire film is fully ionized during the first step leads to vanishing out the difference between different zones on the surface and allowing the formation of a very uniform layer. However, mechanistic details of the process, which occur on the surface during the pulse and the main factors affecting the process are not yet clear.

Developing of the methods which allow to prepare metal nanostructures encapsulated into oxide matrixes was the main aim of the present work. Porous titania and alumina films were treated by the powerful pulsed discharge method to study the possibility of pores sealing. To reveal the mechanism of closing of the pores, the influence of the metal deposited into pores

was studied. A set of electrochemical methods were used to clarify the effect of applied voltage on the kinetics of ionization, film morphology and level of pore sealing.

## 4.5.2 Experimental details

Both aluminium and titanium substrates were mechanically polished using abrasive papers up to grid 4000. Then Ti electrode was chemically polished in a $HF:HNO_3$ (1:3 by volume) mixture, while Al was electrochemically polished in a $C_2H_5OH:HClO_4$ (4:1 by volume) electrolyte in potentiostatic regime at 20 V to mirror finish. After polishing the electrodes were rinsed with deionised water. Two-step anodisation was used to form a well-ordered alumina template. The first and second anodisation steps were performed at a constant voltage of 40 V in 0.3 M oxalic acid for 1 h at a temperature of about 3º C. Between them the pre-structured alumina surface was dissolved in a mixture of phosphoric acid and $CrO_3$ at 70–80 ºC for 5 min. Afterwards pores were enlarged in a 0.3 M oxalic acid solution at 40 ºC for 2.5 h. Titania templates were prepared by anodisation of titanium (99.9%, Goodfellow) with platinum counter-electrode in electrolyte containing 0.75% $NH_4F$ and 2% $H_2O$ in ethylene glycol. Potential was increased from 0 to 20 V with 0.1 V/s rate, followed by anodisation at a constant potential of 20V for 20 min. In both cases vertical nanopores had a length of ~1 μm.

All experiments of metal deposition from ionic liquids were carried out in a glovebox filled with nitrogen (concentration of $O_2$ and $H_2O$ < 5ppm). Anhydrous aluminium chloride (Sigma-Aldrich, >99.9%) and anhydrous titanium (II) chloride (Aldrich, 99%) were used as received. The ionic liquid 1-ethyl-3-methylimidazolium chloride (Fluka, ≥99.0%) was heated at 140 ºC under dynamic vacuum during 24 h in order to dry it. The electrolyte was prepared by addition of 1.7moles of $AlCl_3$ to 1 mole of 1-ethyl-3-methylimidazolium chloride and stirred for 24 h. Reaction of $AlCl_3$ and EMIM-Cl is highly exothermic, therefore the temperature was controlled below 70 °C to avoid decomposition of the ionic liquid. 0.5 M solution of $TiCl_2$ in the EMIM-$AlCl_4$ ionic liquid was used as electrolyte for Ti-Al alloy deposition.

Electrochemical deposition was performed in a three-electrode cell. Aluminium wire (Alfa Aesar, 99.999%) and graphite rod were used as a reference and counter electrodes correspondently. Deposition, cyclic voltammetry and electrochemical impedance spectroscopy (EIS) were carried out using a Bio-Logic SP-300 potentiostat.

Electrochemical cell used for the pulsed discharge oxidation of titanium was made of high-impact polystyrene and consisted of a Ti anode plate (Goodfellow, 99.999%, dimensions: 100x80x1 mm) with a working surface of 4.4 $cm^2$ placed inside a cylindrical Ti cathode (Alfa Aesar, 99.7%) with about 20 times larger surface area. Titanium was chosen as a cathode material due to its high strength and chemical stability. 0.1 M ammonium pentaborate ($(NH_4)_2B_{10}O_{16}$) aqueous solution was used as electrolyte for pore sealing. Electric discharges between the electrodes were generated using a low-inductance 100 μF capacitor bank, charged to a fixed voltage (1400-1800 V). The capacitor was commutated to the cell using a low-inertial relay triggered by a synchronizing pulse.

Surface topography and composition of the films were investigated using a Hitachi SU-70 scanning electron microscope (SEM) coupled with an energy dispersive spectrometer (EDS).

## 4.5.3 Behaviour of the nanoporous alumina and titania films under action of powerful pulsed discharge

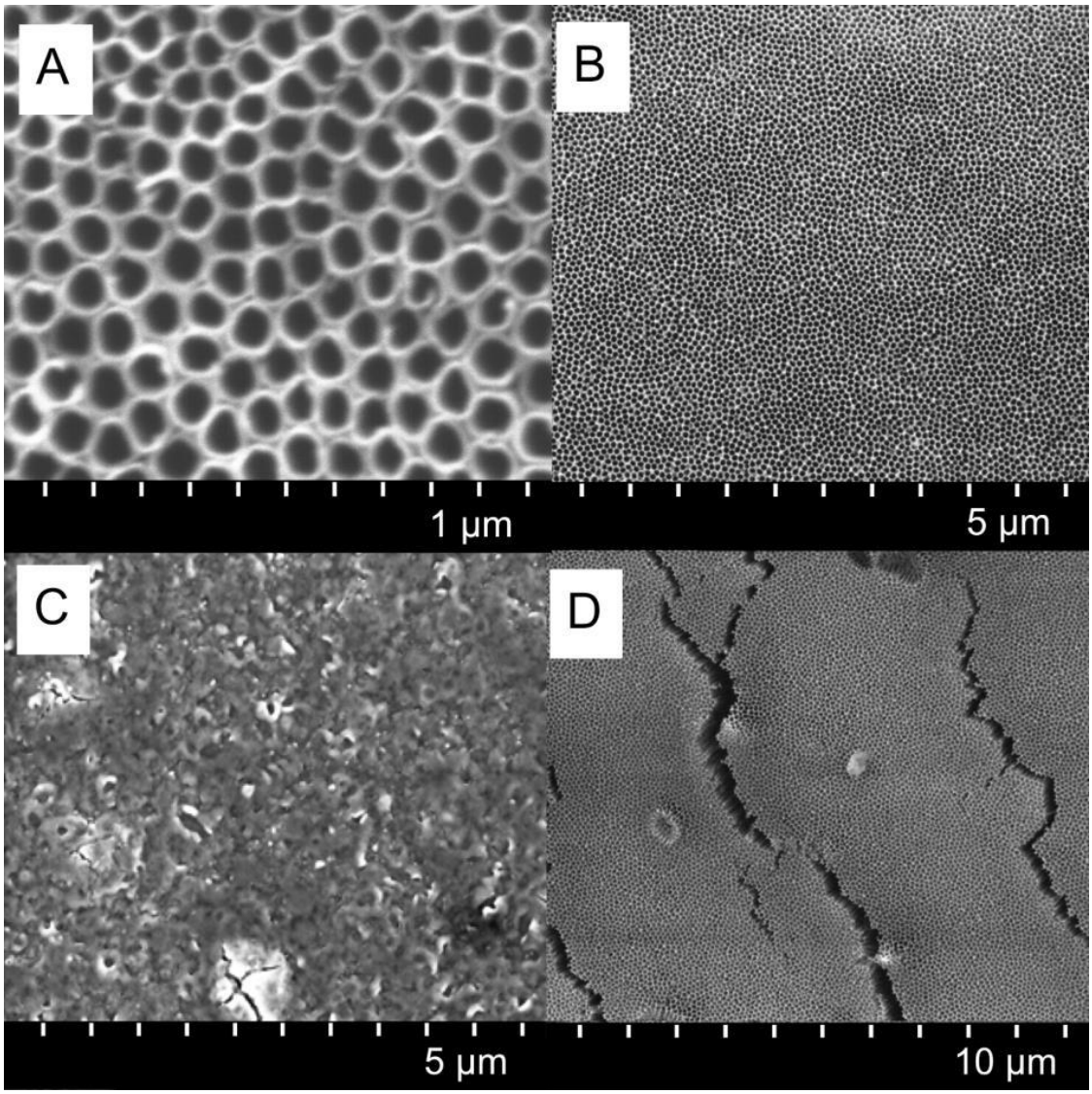


**Figure 4.5.1.** SEM images of the pure porous titania (A, C) and alumina (B, D) before (A, B) and after (C, D) application of 5 discharge pulses with a potential of 1600V.

Nanoporous alumina and titania films have essentially different nature. While aluminium oxide demonstrates hexagonal structure with a pore in the centre and no space between cells, titanium oxide mainly consists of nanotubeshaving thin walls in the top and thicker ones closer to the metal substrate which can be even separated [29, 216]. The conductivity of the porous oxides is also different: $TiO_2$ is known as a wide-bandgap semiconductor, while $Al_2O_3$ films can be considered as a dielectric material and have higher resistance.

To estimate the possibility of closing the oxide pores , porous titania and alumina films were studied under action of the discharge pulses before deposition of the metals into the pores (Figure 4.5.1 A, B). Figure 4.5.1 C, D shows the structure of the porous oxides after 5 pulses. The morphology of the discharge-treated titania film seems to be different from the unexposed one (Fig. 4.5.1 C). The cross-section of this film shows that the top part of the pores was melted, resulting in sealing of the nanotubes and encapsulation of their content. According to the processes described in the previous works [127-128], it can be suggested that plasma is formed on the top of the pores, resulting in their melting.

Behaviour of the alumina films under the same conditions was found to be different. After application of 5 pulses at 1600V, cracks in the film can be observed (Fig. 4.5.1D). Action of 40

pulses with a lower potential (1100V) leads to changes of the film structure, and at high magnification a minor melting of the pore walls can be seen (not shown). Examination of the film cross-section reveals signs of the wall melting near to the substrate and some sealing in the lowest part of the pores (10-25 nm). It can be suggested that closing the alumina pores under powerful pulsed discharges is incipient, and only minor part of pores can be closed. We can suggest that the electrical conductivity of the alumina is insufficient to transport charges through the oxide to the upper part of the film for further melting process.

### 4.5.4 Deposition of the metals into pores

To study the behaviour of the metal-filled titania and alumina nanotubes two types of electrodes were prepared: aluminium deposited into the titania film, and aluminium-titanium alloy deposited into the porous alumina.

Electrodeposition of aluminium into the titania tubes was performed from the respective ionic liquid using potential cycling, to avoid the growth of the metal crystals on the surface of the oxide coating. Vertex potentials were chosen in the range of -0.5 V and +0.35 V vs. Al quasi-reference electrode to avoid ionic liquid destruction from the cathodic side and significant but not complete metal dissolution from the anodic one. Typical cyclic voltammograms for different number of cycles are shown in Fig. 4.5.2.

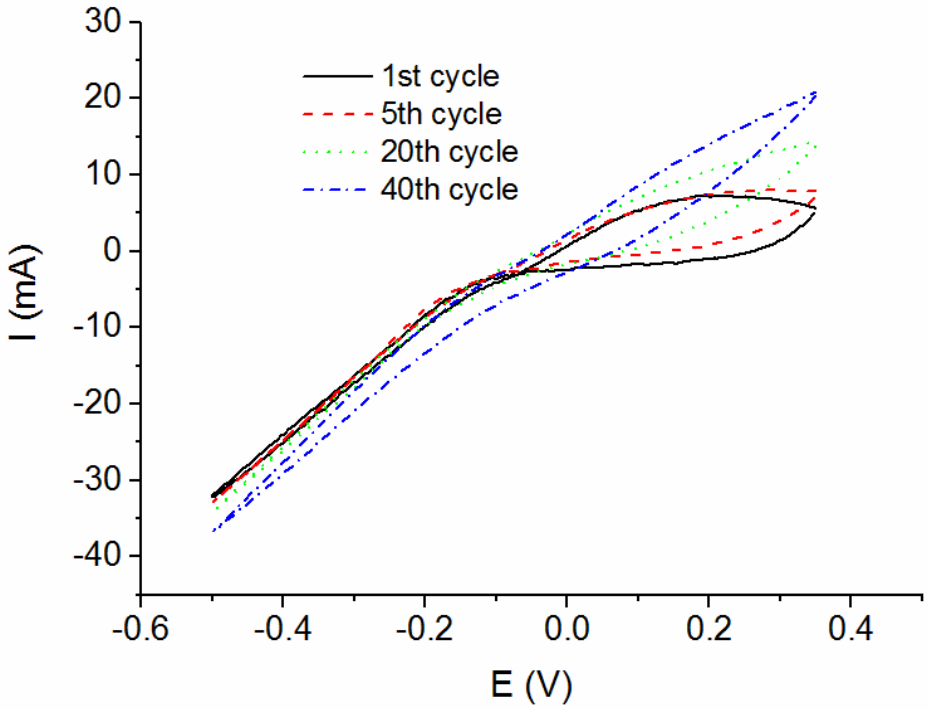


**Figure 4.5.2.** Typical CVA of aluminium deposition into titania nanopores at sweep rate of 50 mV/s

Careful analysis of the process evolution reveals its changing during potential cycling. Diffusion limitation of the oxidation processes and anodic current drop to almost zero at the reverse scan can be observed for the first cycle in the beginning of the process (Fig. 4.5.2, black solid line). Anodic oxidation can be described by the following processes[217]:

$Al(0) + 4Cl^- = AlCl_4^- + 3e^-$

$Al(0) + 3\ Cl^- + AlCl_4^- = Al_2Cl_7^- + 3e^-$

$Al(0) + 2Cl^- + 2AlCl_4^- = Al_3Cl_{10}^- + 3e^-$

etc.

Due to diffusion limitation through the pores, the amount of chloride anions is restricted and the possibility of aluminium dissolution is limited. Increasing the anion size (and the number of Al atoms in it) of the ionic liquid results in the drop of its solubility and, as a result, polymeric aluminium chloride structures deposit on the surface of the metal. In the following cycles the anodic current limitation becomes less distinct and almost disappears after the 20$^{th}$ scan (Fig. 4.5.2, green dotted line).

Electrodeposition in the potentiostatic mode results in a slow deposition of the aluminium in the pores. After filling the pore volume, aluminium nanostructures start to grow on the top of the nanotubes (Fig. 4.5.3A) as well covering whole surfaces with bulky deposits. Increase of the aluminium amount on the titania surface, where oxidation of the metal is not limited by diffusion and its dissolution is easier, results in a rise of the anodic current. In the case of cathodic reduction process there are almost no diffusion limitations taking into account that the ionic liquid contains aluminium chloride ions.

Sweep rate is a very important parameter for the aluminium formation in the pores. Aluminium deposition was studied at the following sweep rates: 20, 50, 100, 200 and 500 mV/s. It was found that metal particles are not deposited at the top of $TiO_2$ films when a sweep rate of 20mV/s is applied, though the fill factor remains low. Deposition at higher sweep rates, 50 and 100 mV/s, results in good filling of the pores with aluminium without further growth of metal structures on the surface (Fig. 4.5.3B). With increment of the sweep rate to 200 and 500 mV/s the number of empty pores increases and the deposition of metal on the surface starts.

Previously the possibility of aluminium-titanium alloy deposition from the solution of $TiCl_2$ in $AlCl_3$-EMIM-Cl (2:1) mixture was demonstrated [218]. The composition of the alloy is highly dependent on the applied potential. Deposition using the potential cycling mode in this case can produce a fluctuation in the nanorods composition. Recently Perrie et al. [219-220] have proposed a method based on pulsed deposition. It was shown that two pulses are important for metal nanowires formation: the first one with cathodic polarization for metal deposition and the second one, anodic, for relaxation processes in the pores. To avoid the formation of metal structures on the surface of the porous layer, we used a modified pulsed method, and three pulses instead of two were applied. The first one, which corresponds to metal growth, was applied for 50 ms at a potential of -0.3 V *vs* Al quasi-reference electrode. The partial dissolution of the deposit was performed at +0.2 V for 40 ms, and the final pulse at 0 V for 150 ms was used for the sake of ion migration and electrolyte renewal in the pores. The absence of the third pulse results in a high irregularity of the obtained nanowires.

EDS analysis of the obtained metal nanostructures in the pores shows the presence of a high content of titanium in the deposit.

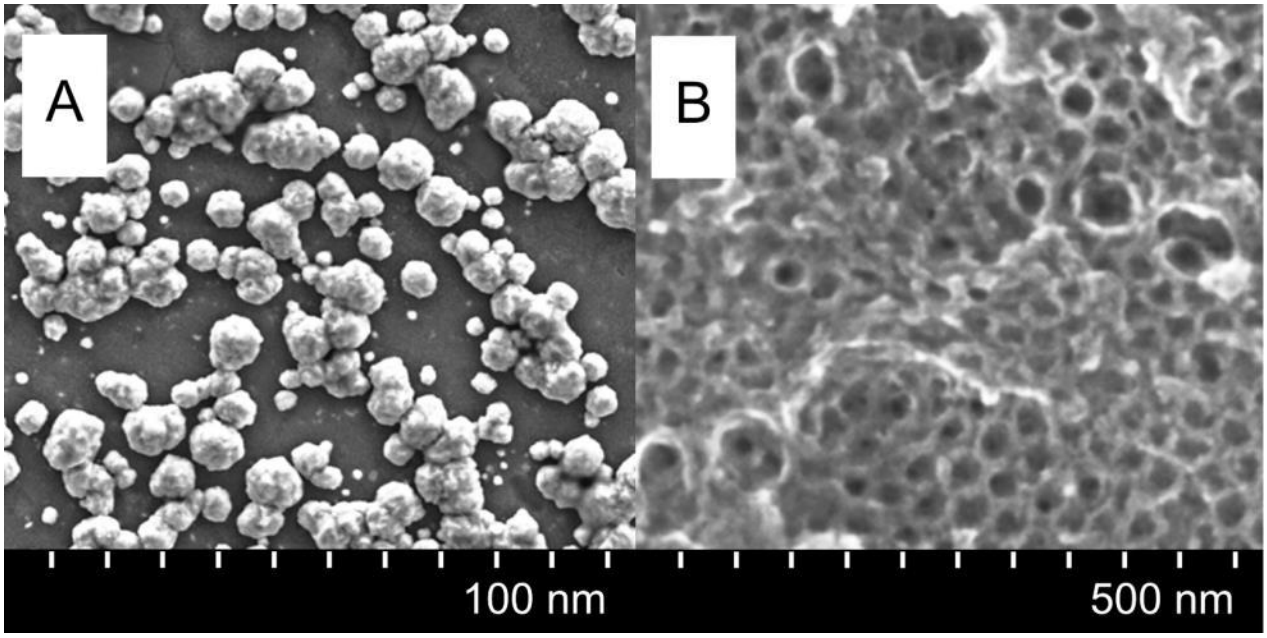


**Figure 4.5.3.** SEM image of the titania pores filled with aluminium in potentiostatic mode (A) and by potential cycling (B)

## 4.5.5 Closure of the metal-filled pores by applying Powerful Pulsed Discharge

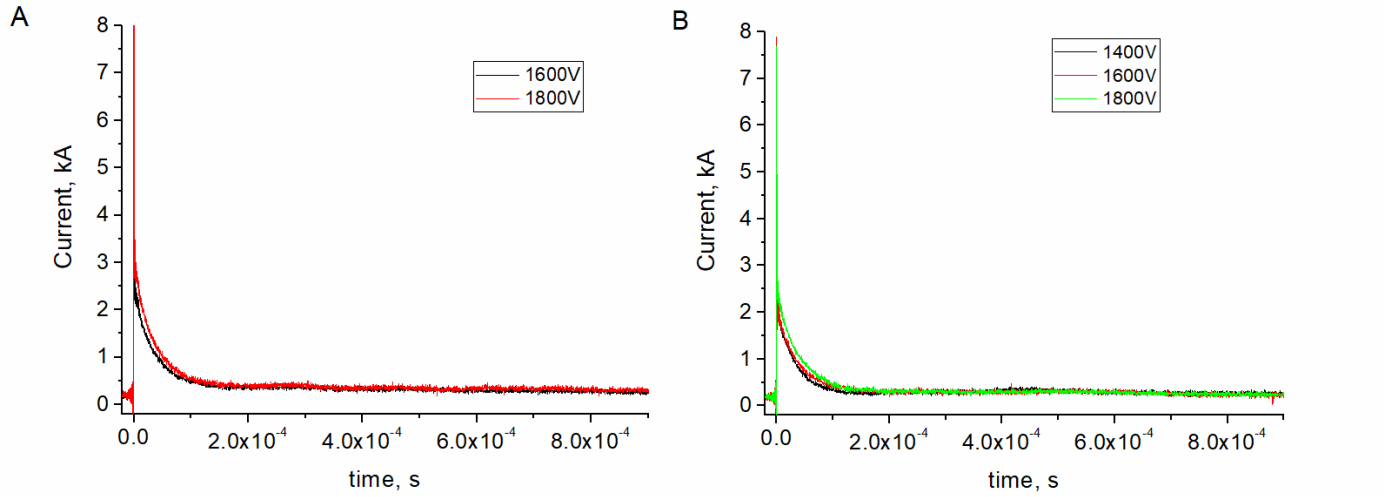


**Figure 4.5.4.** Discharge plots of the nanoporous alumina (A) and titania (B) filled with Ti-Al and Al, respectively.

The obtained structures were further treated with high voltage pulses. Analysis of the current *vs* time plots can throw light on the mechanism of processes that occur under the action of such discharge. As it was previously studied [127-128], the discharge process contains two steps. During the first, short one, which is characterized by relatively high currents, ionization and melting of the oxide occurs. In the second one with a significantly higher duration, the main process is the growth of the film. The key factor that corresponds to the charge distribution ratio between the first and second step is the amount of the defects in the coating. Figure 4.5.4 shows typical discharge curves obtained for porous titania and alumina electrodes filled with

aluminium and titanium-aluminium alloy, respectively. In comparison to the plots recorded on the pure metal electrodes, the shape of discharge profile is closer to that obtained on aluminium [127], oxide of which can be characterized by high resistance and low amount of defects. These plots contain a short first ionization part and a relatively long second one, and the two steps are well separated. However, detailed analysis of the plots reveals that the charge passed through the cell during the second period, which corresponds to the film growth, is negligible and consists only of about 1% of the capacitor charge. Moreover, according to the current integration, only 30% of charge is consumed by the ionization processes. It can be suggested that in such systems growth of the oxide does not occur, and the only process is ionization of the oxide with its further melting. Increasing of the discharge voltage does not result in changes in the plot shape, and only a current increment in the first step of the process can be observed.

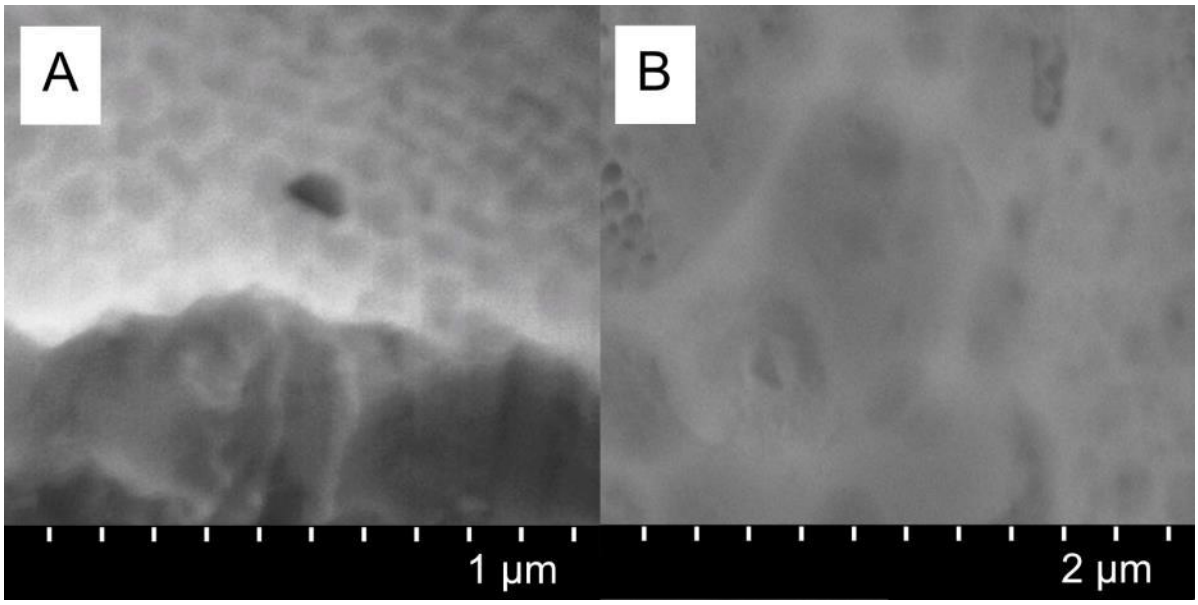


**Figure 4.5.5**. Cross-section of the film (A) and top view (B) of the alumina pores filled with Ti-aluminium alloy after action of 10 discharge pulses applied at 1600V (A) and 1800V (B).

Inspection of the electrode surface after applying the discharges reveals dependence of its morphology on the applied potential. Application of 1400V to the alumina electrode was found to result in destruction of the coating. In all the cases, the discharge curves have a shape different of that obtained previously, and further investigation by SEM shows a big amount of cracks on the porous oxide surface. Increasing the voltage up to 1600 and 1800 V leads to the sealing of the pores (Fig. 4.5.5). EDS analysis of the cross section (not shown) revealed that alumina is the main material of the melted part of the pore. Taking into account that the coating contains titanium-aluminium alloy inside, it can be assumed that the main source of the material for the sealed part of the pore is alumina from the nanotube walls. In contrast to the action of discharge on the empty pores, in this case encapsulation of the pore content takes place. Thus filling the channels in alumina with conductive material opens the possibility to close the pores in the same way as it occurs on titanium.

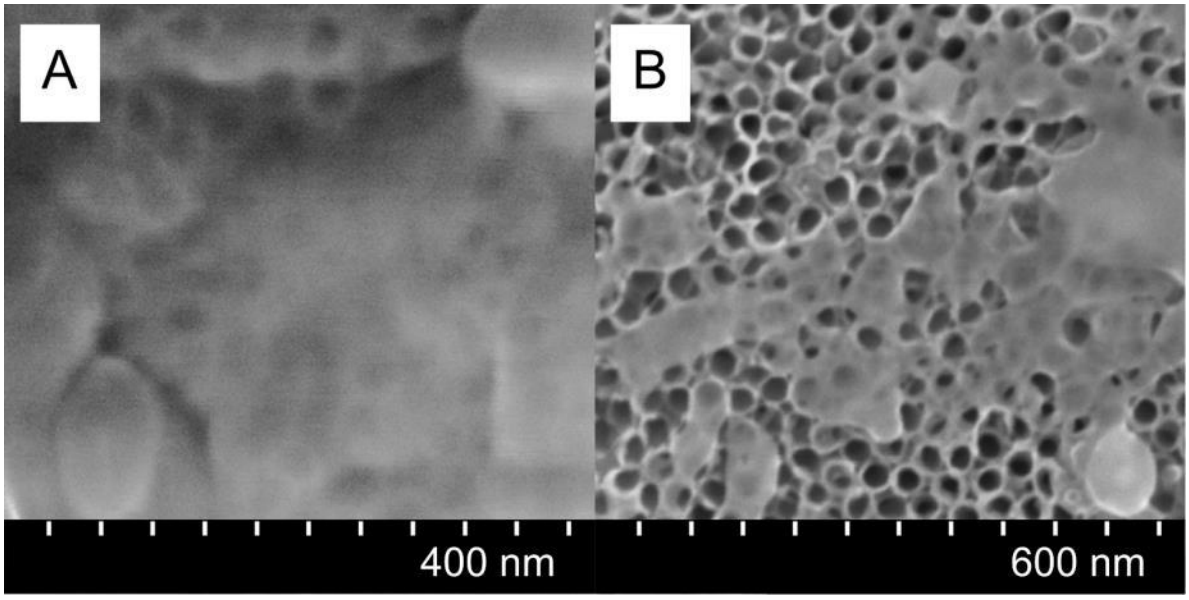


**Figure 4.5.6.** Surface of the titania nanotubes filled with aluminium after action of 10 discharge pulses at 1600V (A) and 1800V (B).

Application of powerful pulsed discharges to the aluminium-filled titania pores also causes closure of the pores. In contrast to alumina, at 1400V some nanotubes can be closed but the main amount of them remains open. Further increase of the potential to 1600V results in the entire encapsulation of the pore content (Fig. 4.5.6A). It was also found that the melts on the surface of the nanotubes consist mainly of titania, what is in good agreement with our previous assumption. It should be mentioned that further increase of the potential leads to the formation of islands of the melts on the surface and the major part of the pores seems to be still open (Fig. 4.5.6B).

## 4.5.6 Conclusions

Powerful Pulsed Discharge method offers unconventional approach not only for electrochemical synthesis of thin oxide layers, but also for modification of the oxide morphology. In the present study we proposed this method for efficient encapsulation of metal nanorods preliminarily deposited into the vertically aligned titania and alumina nanopores. Under action of the discharge with voltage less than 1600V, the top part of the titania tubes melts, resulting in closing of the pore volume. Closing the titania nanotubes by this method is possible irrespective of the pore content. In the case of alumina nanoporous layer, only minor part of the pores can be sealed if they are empty. However, filling of the channels with conductive metal provides the possibility of their closure starting from the top.

Studies of kinetics of the discharge process on the metal-filled porous titania and alumina electrodes show that the shape of temporal current evolution profile does not depend on the oxide matrix composition. Increasing the applied voltage results in a current increment without changing the profile shape. Analysis of the current *vs* time plots shows that only minor part of the charge is spent for the oxide growth and the main process is ionization of the oxide with its further melting.

We also demonstrated that the potential cycling method is efficient for electrodeposition of aluminium into titania nanotubes. In the case of Al-Ti alloy deposition into alumina pores, a

pulse method, where the potential is reversed during deposition, can be applied to avoid the growth of structures on the oxide surface and provides a high fill factor of the pores with metal.

# 4.6 Powerful pulsed discharge oxidation of aluminium and titanium in hydrogen peroxide and distilled water. (under submission)

Contribution to this work:
Conception of the work, preparation of all samples, fitting of the obtained data, electron microscopy, atomic force microscopy, reproducibility experiments, preparation of images, text preparation.

## 4.6.1 Introduction

Anodizing treatment is widely used on aluminium, titanium and their alloys in industrial practice to enhance surface performance (corrosion resistance, hardness and wear resistance) and to modify physical and chemical properties of the metal surface [24, 73, 194]. On both metals oxide film forms, spontaneously on the metal surface and brings resistance to atmospheric oxygen. However, corrosion resistance of such films is not enough in pure aggressive media. Anodisation is a convenient and important method of oxide film formation owing to low cost, flexibility and easiness [2, 30, 52, 58, 184, 198, 203]. Anodisation of titanium is an attractive method that can be used for surface modification giving additional corrosion resistance, higher affinity to biological tissues, and advanced electronic properties when compared to the native thin oxide films[52, 197-199]. Thin films of aluminium oxide have found important applications in electronic industry and corrosion protection due to their relatively high dielectric constant, ultra-low conductivity as well as high corrosion resistance and good thermal and mechanical stability.[73] The above properties also make aluminium oxide films promising for novel applications in microelectronics.[74] Nowadays, thin alumina layers are used as dielectrics in integrated capacitors with ultrahigh capacitance density. Films of $Al_2O_3$ are also considered as replacements for $SiO_2$ in semiconductor devices[75-76].

There are several anodisation processes that are currently used: conventional anodic oxidation (potentiostatic or galvanostatic) and plasma electrolytic oxidation (PEO) [2, 30, 58, 203]. The conventional anodisation is well studied and allows growing oxide films of controlled thickness and quality [2, 52, 197, 203]. The conventional anodisation methods allow to produce the alumina films of controlled thickness and quality[182-184]. In some cases, e.g., in production of electrolytic capacitors and anti-corrosion protection of aluminium and its alloys, anodisation is combined with other oxidation methods[185-186]. Using the other method, PEO, which occurs at potentials above the breakdown voltage of the oxide film growing on the anode surface, it is possible to prepare well adherent, hard, ceramic-like coatings[30, 58]. Both methods are currently applied in industry although they are still under investigation. One of the problems, which appear when studying the anodic oxides, is related to the impossibility of preparing a pure oxide film without foreign atoms apart metal atoms of the substrate, oxygen and hydrogen atoms. In all electrolytes used for anodisation, different ionic species are added to increase the conductivity of solution and foreign atoms are trapped into the growing oxide [128]. According to the literature, concentration of the foreign atoms during anodic oxidation usually does not

exceed 1% [204], however, the impact of them on anodic film properies, such as concentration of ionized donors, conductivity and photosensitivity, is significant. It was shown that the electrolyte concentration used for anodisation influences the dopant content in the oxide [128] and even low amount of ionic species in solution results in changes of the film properties. Thus, in order to have a reference point for further research it is important to obtain an oxide film with minimal influence of foreign atoms. Of course, impurity-free oxide on the metal surface can be prepared by other methods, such as oxidation in oxygen atmosphere at high temperature [73] or in boiling water [115], but the properties of the obtained films will be different of those prepared by electrochemical oxidation. This motivates the present work where only water and hydrogen peroxide were used as electrolyte. This gives the opportunity to clarify the mechanism/pattern of charge distribution in oxide films.

A new electrochemical technique using powerful pulsed discharge oxidation (PPDO) of metals has recently been reported[4-5, 127-128]. In the present work, the processes that occur in this method were studied. In PPDO the electrochemical reaction occurs at the metal-electrolyte interface under the action of single high-voltage (> 1 kV) pulses. The most important difference of this technique from the conventional galvanostatic and potentiostatic anodisation methods is an extremely high rate of film growth. During PPDO the oxide film ionizes completely[128]. Thus, as opposed to the plasma electrolytic oxidation process, the film grows not only near breakdown areas (channels), but also simultaneously over the whole surface of the electrode. This results in formation of oxide films with properties different from those obtained by other methods. Furthermore, in this technique, solutions with very high resistivity can be used.

Volta potential of the obtained anodic films prepared by pulsed discharge method was measured using Scanning Kelvin Probe Force Microscopy. It has been shown that the charge and polarization of alumina films is affected by anodisation conditions: in particular, the electrolyte composition. Structure and thickness of the films were studied using a transmission electron microscopy and electrochemical impedance spectroscopy methods. Films of different thicknesses up to 180 nm were obtained. It was found a relation between thickness and potential on the surface of these films.

Two types of films were studied using two different electrolytes. Films of the first type were prepared by pulsed method in solutions of only hydrogen peroxide. Second-type films were prepared in distilled water. For comparison, powerful pulsed discharge oxidation in solution of ammonium pentaborate was also examined. Assumptions on the processes, which occur on the surface under action of discharge pulse, were done based on the comparative analysis of the films characteristics.

## 4.6.2 Experimental

The electrochemical cell used for the pulsed discharge oxidation of aluminium and titanium was made of high-impact polystyrene and consisted of a plate Al anode (Goodfellow, 99.999%) with a working surface of 5 $cm^2$ placed inside a cylindrical Ti-foil cathode (Alfa Aesar, 99.7%) with 20 times larger surface area. Titanium was chosen as a cathode material due to its high strength and chemical stability. Both electrodes were mechanically polished using emery papers up to grid 4000. Titanium electrodes were chemically polished in a $HF:HNO_3$ (1:3 by volume) mixture, while aluminium plate was electrochemically polished in a $C_2H_5OH:HClO_4$ (4:1

by volume) electrolyte in potentiostatic regime at 20 V to mirror finish. After polishing both electrodes were rinsed with deionised water.

A 30% hydrogen peroxide solution (Sigma-Aldrich) and $10^{-8}$M solution of sodium hydroxide in deionised water were used as electrolytes. The diluted solution of NaOH was chosen to use instead of only distilled water for the sake of reproducibility. Assuming that the concentration of sodium ions in such electrolyte is low enough to consider that they will not incorporate into the oxide, this solution will be mentioned in text as water electrolyte. In comparison with pure deionised water the conductivity of the solution is three orders of magnitude higher. A 0.1 M ammonium pentaborate ($(NH_4)_2B_{10}O_{16}$) aqueous solution was used as electrolyte for comparison reasons since alumina films prepared by the conventional anodisation methods in this electrolyte are well-studied. In the case of titanium oxidation 1M phosphoric acid electrolyte will be used for comparison.

Electric discharges between the electrodes were generated using a low-inductivity 100 μF capacitor bank charged to definite voltages (1400-2000V). The capacitor was commutated to the cell using a low-inertial relay triggered by a synchronizing pulse. In order to prepare the films with different thicknesses the capacitor was discharged through the electrochemical cell from 1 to 15 times. Time-current characteristics of discharges were recorded using a Tektronix DPO7054 oscilloscope connected to the system and synchronized with the trigger.

The EIS measurements were performed using a Gamry FAS2 Femtostat with a PCI4 Controller in a frequency range from $10^5$ to $10^{-3}$ Hz with 7 points per decade. The measurements were carried out at room temperature in a conventional three-electrode cell consisting of a mercury – mercurous sulfate reference electrode, a platinum foil as the counter electrode and the working electrode with an exposed area of 4.4 $cm^2$ in solution of 0.1 M ammonium pentaborate as the electrolyte. Impedance spectra were recorded by applying a 10 mV sinusoidal perturbation at the open circuit potential. The cell was placed in a Faraday cage to avoid interferences with external electromagnetic fields. Before recording the spectra, the system was allowed to attain a stable open circuit potential. At least two samples prepared at the same conditions were tested to ensure reproducibility of the results. The impedance plots were fitted using equivalent circuits by means of the Echem Analyst software from Gamry Inc.

Constant phase elements (CPE) instead of capacitances were used in all fittings presented in the work. Such modification is needed when the phase angle of the capacitor is different from -90 degrees. The physical origin of the CPE has been widely discussed in literature[125, 165]. The impedance of the CPE, $Z_{CPE}$, depends on frequency, ω, according to the following equation:

$$Z_{CPE} = [Q(j\omega)^n]^{-1} \quad (4.6.1)$$

where Q is a parameter numerically equal to the admittance ($|Z|^{-1}$) at ω= 1 rad $s^{-1}$ and $n \leq 1$ is a power coefficient which is equal to 1 in the case of an ideal capacitor and lower in the case of a CPE element. The value of n can be calculated as the ratio of the phase angle at maximum of the corresponding constant phase element to -90 degrees. The value of effective capacitance, $C_{eff}$, can be estimated by assuming a normal time-constant distribution through a surface layer by equation[126]:

$$C_{eff} = Q^{1/n} R^{(1-n)/n} \quad (4.6.2)$$

The TEM study was carried out using a Hitachi H9000 transmission electron microscope at acceleration voltage of 300 kV. Electron transcendent sections of the samples for TEM were cut with a Leica Reichert Supernova ultramicrotome.

A Digital Instruments Nanoscope III atomic force microscope with conductive Pt-Cr probes (Budget Sensors) was used for SKPFM measurements. The measurements were performed in several areas of at least two samples of the same thickness. The obtained Volta potential difference (VPD) values are presented versus the Volta potential measured on Ni as a reference.

### 4.6.3 Oxidation of aluminium

The nature of the discharge oxidation in the present electrolytes is similar with previously shown and current profile of the process seems close to that described in conventional electrolytes[5, 127-128, 221]. In contrast to the oxides prepared in deionised water [221] conductivity of these electrolytes are 2-3 orders of magnitude higher, what results in significantly change of the growth mechanism to the typical rate for powerful pulsed discharge mechanism, which was described previously [5, 127-128]. Figure 4.6.1 shows typical discharge spectra for the aluminium electrodes in water, hydrogen peroxide and for comparison in ammonium pentaborate. Attempts to prepare films in the potentiostatic conditions result in breakdown of the oxide films with thicknesses 7-15 nm, similar to the previously described results in deionised water[221].

Previously[127] it was shown that the thickness (*d*) of the pulsed discharge films on aluminium could be described as a function of number of applied pulses (*N*) and thickness of the film after the first discharge ($d_0$) by the following empirical equation:

$$d = d_0 N^{\alpha}, \qquad (4.6.3)$$

Thickness of the alumina films prepared by the pulsed discharge anodisation was evaluated from EIS measurements as well as from TEM data. Detailed description of the thickness determination is described below. Application of the discharges in water and hydrogen peroxide solution also obeys to this equation. Thus thickness of the oxide film in low conductive electrolyte can be also controlled by the number of the applied pulses. To understand the influence of the electrolyte and applied voltage a series of samples was prepared applying 1, 2, 3, 5, 10 and 15 pulses at potentials from 1400 to 2000V with a step of 200V.

In water electrolyte the shape of the discharge plot seems different from that obtained in conventional electrolytes. One can see that the first part of the discharge seems to have higher currents and shorter duration in comparison with those prepared in ammonium pentaborate. The second part, which is responsible for the film growth, also has higher current values. Furthermore, its duration seems to be around 0.2s in comparison to 0.4s in conventional electrolyte. However, their differences don't contradict the process previously described and it is connected with the structure of the obtained oxide. The shape of the pulse was found to be similar at all the applied voltages while the current value rises respectively with growth of the potential. At 1400V (not shown) and 1600V (fig 4.6.2a) the discharge plot at the first and the last discharges seems to be identical. With further rise of the potential, the current starts to decrease during the film growth and at 2000V the difference in current between the first and 10$^{th}$ discharge after 5e-4 s was around 2 times (fig 4.6.2b).

The thickness of the oxide obtained from a single discharge was found to be influenced by the applied potential. The thickness doesn't change linearly and it was found that there is almost no difference in the growth rate per pulse at 1800 and 2000V. The values of $d_0$ and α obtained are shown in Table 4.6.1. However, in all the cases the influence of the number of pulses on the oxide thickness can be described by equation (1).

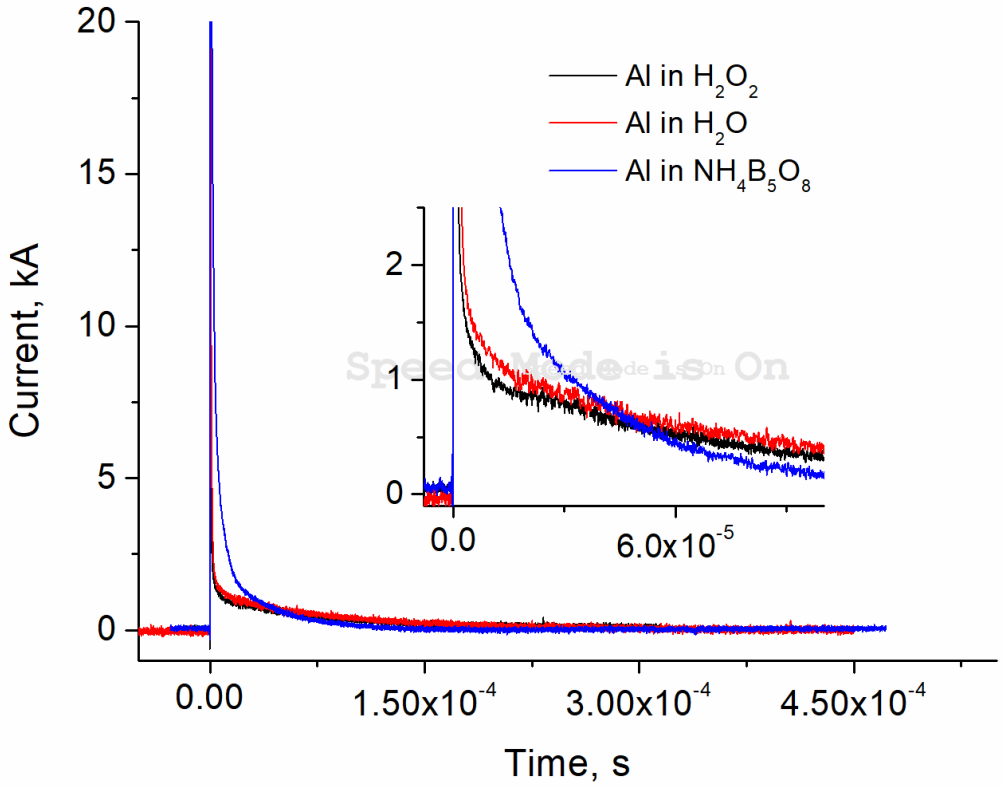


**Figure 4.6.1.** Typical discharge plots on the aluminium electrodes in hydrogen peroxide, water and ammonium pentaborate at 1400V. The inset shows magnification of the plot for the period up to 0.1 ms after discharge.

The structure of the discharge plot, the current values and the duration of every phase in hydrogen peroxide seems to be very similar to that obtained in ammonium pentaborate. The rise of the applied potential almost doesn't influence the discharge plot change up to 2000V. Thus the 1$^{st}$ and 10$^{th}$ discharges at 1400, 1600 and 1800V are similar, and only at 2000V the difference between them is 20%. Similarly, to the oxide growth in water electrolyte, the growth of the film in hydrogen peroxide solution can be described by equation (1) and parameters for the equation are also shown in table 4.6.1.

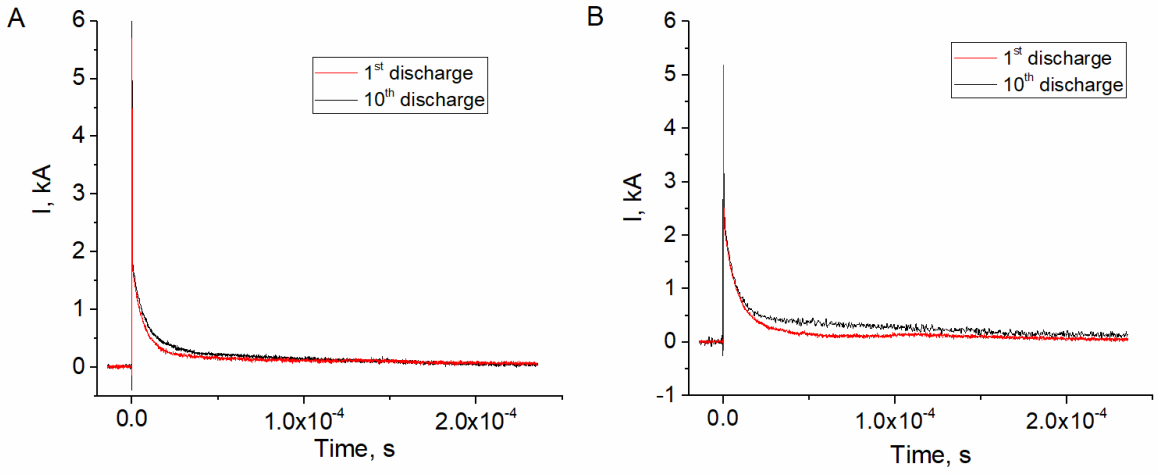


**Figure 4.6.2.** Comparison of current plots on 1$^{st}$ and 10$^{th}$ discharges on the aluminium electrode in water at different potentials at 1600V (a) and 2000V (b).

**Table 4.6.1.** Parameters of equation (1) for film growth on aluminium in water and hydrogen peroxide at different potentials.

| Electrolyte and potential | $d_0$, nm | A |
|---|---|---|
| **Water, 1400V** | 14 | 0.98 |
| **Water, 1600V** | 17 | 0.95 |
| **Water, 1800V** | 18 | 0.93 |
| **Water, 2000V** | 18 | 0.89 |
| **Hydrogen peroxide, 1400V** | 15 | 0.99 |
| **Hydrogen peroxide, 1600V** | 17 | 0.98 |
| **Hydrogen peroxide, 1800V** | 18 | 0.95 |
| **Hydrogen peroxide, 2000V** | 19 | 0.92 |

## 4.6.3 Oxidation of the titanium

The structure of the discharge plot on titanium has a different shape in comparison to aluminium. According to the previously described mechanism[128], aluminium discharge has two well defined phases responsible for film ionization and film growth respectively. In the case of titanium, due to the significantly higher oxide conductivity there is no defined border between the phases. The duration of the whole discharge process is highly dependent of the electrolyte composition and concentration, applied potential, etc. Furthermore, due to the increment of dopants in the oxide during the film growth, the shape of the discharge plot changes at every following discharge. In our previous work [128] the mechanism of the oxidation is described in detail.

The discharge plots (fig. 4.6.3a) obtained in $H_2O$ and $H_2O_2$ show a shape similar to that obtained in conventional electrolytes [5, 127-128]. However, the duration of the pulse was found to be shorter. This can be explained by the absence of dopant atoms, which play a role of charge traps, making difficult migration of the ions during the second phase.

During the first discharges, oxidation of the titanium in water electrolyte seems to be similar to previously performed in sulphuric and phosphoric acid [5, 128]. When thickness of the film achieves 120 nm following growth rate of the coating significantly drops. It was found that after applying 30-35 pulses the film in water electrolyte thickness was 180 nm, while in the solution of sulphuric acid the same thickness was obtained already after 10 pulse discharges[5]. The increment of the applied voltage resulted in decrease of the oxide thickness at which this phenomenon starts to appear. Thus, the growth rate at 1600V drops for an oxide thickness around 100nm, while at 2000V this thickness drops for 30-50nm (1-2 discharges). SEM studies of the samples show, that after this thickness, the oxide starts to grow on the grain boundaries of the substrate (fig. 4.6.4).

Preparation of the oxide in the solution of hydrogen peroxide doesn't encounter the same problems as in water electrolyte. The shape of the discharge plot seems to be similar for all applied potentials. The increase of the voltage results in a corresponding rise of the current and also to a minor increase of the pulse duration. In contrast to the pulse evolution with film growth

in conventional solutions, it was found that at 1400V the plot shape almost doesn't change up to the thickness of 120 nm (fig 4.6.3b). With increment of the applied voltage, the shape of the discharge plot starts to change with thickness(fig 4.6.3c), but even at 2000V the difference between the 1$^{st}$ and 15$^{th}$ discharges is significantly less in comparison to the current evolution for sulphuric acid[5]. This can be associated with absence of foreign dopant atoms, which can play a role of traps. While in conventional electrolytes the amount of defects increases with film growth, in hydrogen peroxide only atoms of Ti, O and H can be found and thus the possibility to have defect traps in the oxide structure is lower. The minor changes in this case can be associated with non-uniform distribution of the Ti and O atoms in the bulk of the film, resulting in local nonstable charge traps.

Increase of the applied potential in water almost doesn't influence the oxidation process. Thus, changing of potential from 1400V to 1600V results in minor increase of the thickness, which appears on the electrodes with oxide thickness of 80 nm. Similarly, further growth is difficult due to the growth of oxide on the grain boundaries. However the increase of potential doesn't influence the rate of oxide growth, and the limits were similar to those obtained at 1600V. Rise of potential results also in decrease of the potential at which the main process occurs is the growth of the oxide on grain boundaries. Furthermore, at 2000V it was not possible to obtain the film with thickness higher than 30-50 nm.

In the solution of hydrogen peroxide at all potentials can be found dependence of the growth rate on the applied voltage. Thus at 1800V the thickness of the oxide after 4 pulses was 110-130 nm, which is around 20% thicker than those obtained at 1400V. However, the growth efficiency is not linear with potential and drops as the potential increases. The difference between 1800 and 2000V is less than 3-5%.

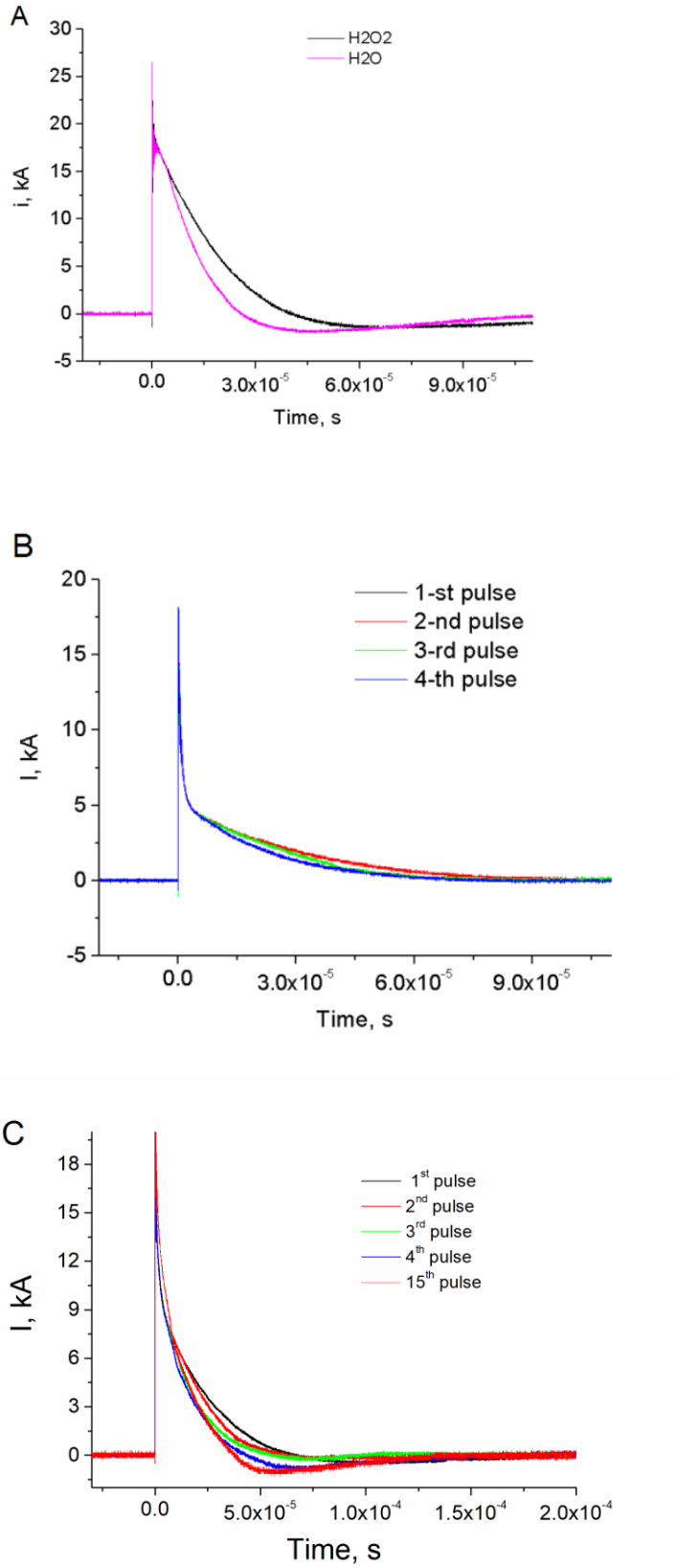


**Figure 4.6.3.** Discharge plots in the titanium obtained in different electrolytes (a) and charge evolution in hydrogen peroxide obtained at 1400V (b) and 2000 V (c).

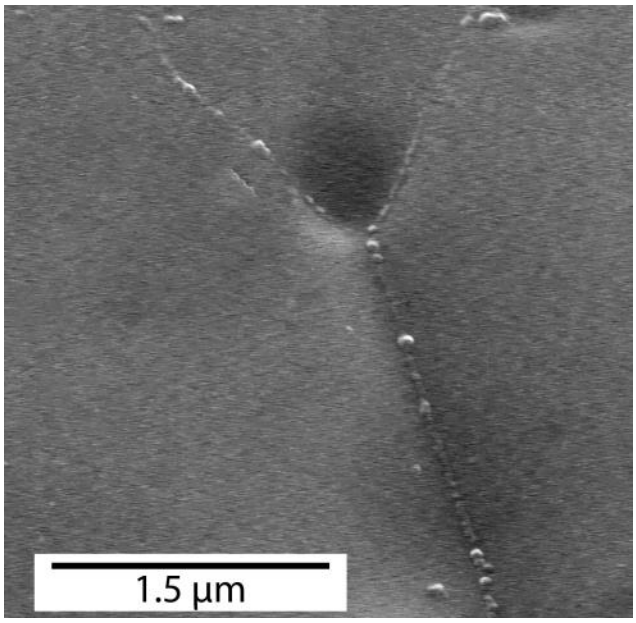


**Figure 4.6.4.** SEM image of the titania film obtained by applying of 5 discharge pulses at 2000V.

## 4.6.4 EIS studies of the aluminium oxide

EIS spectra of the films obtained in $H_2O_2$ and $H_2O$ are shown in Figure 4.6.5. All the spectra demonstrate a broad relaxation process described by one time constant. This relaxation can be assigned to the CPE of the dielectric oxide films. The spectra were fitted using a simple equivalent circuit with one parallel R-CPE element for description of oxide film and an additional R element connected is series for the electrolyte resistance.

To estimate the thickness of the alumina, film cross-sections were examined using TEM (fig. 4.6.6). The electron microscopy study revealed that all the films obtained by high-voltage pulsed discharge anodisation (1-15 pulses) are smooth, dense and free of microdefects. The comparison of the EIS spectra of the films prepared at 1400V with thickness of 120 nm as measured by TEM, shows that the impedance of the samples prepared by the discharge method (fig. 4.6.5) is slightly higher, in comparison to those prepared by conventional anodisation in ammonium pentaborate[120, 127]. This result was repeated on the alumina with other thicknesses.

Calculation of the dielectric constant from the CPE and the film thickness shows that aluminium oxide prepared by pulsed discharge in hydrogen peroxide has higher dielectric constant in the order of 9.9-10.3, while films prepared in water electrolyte have values of 9.4-9.9 in comparison with 9.0 obtained on for alumina made by conventional method. The values of the dielectric constant for alumina prepared in the two electrolytes at different applied voltages are presented in table 4.6.2.

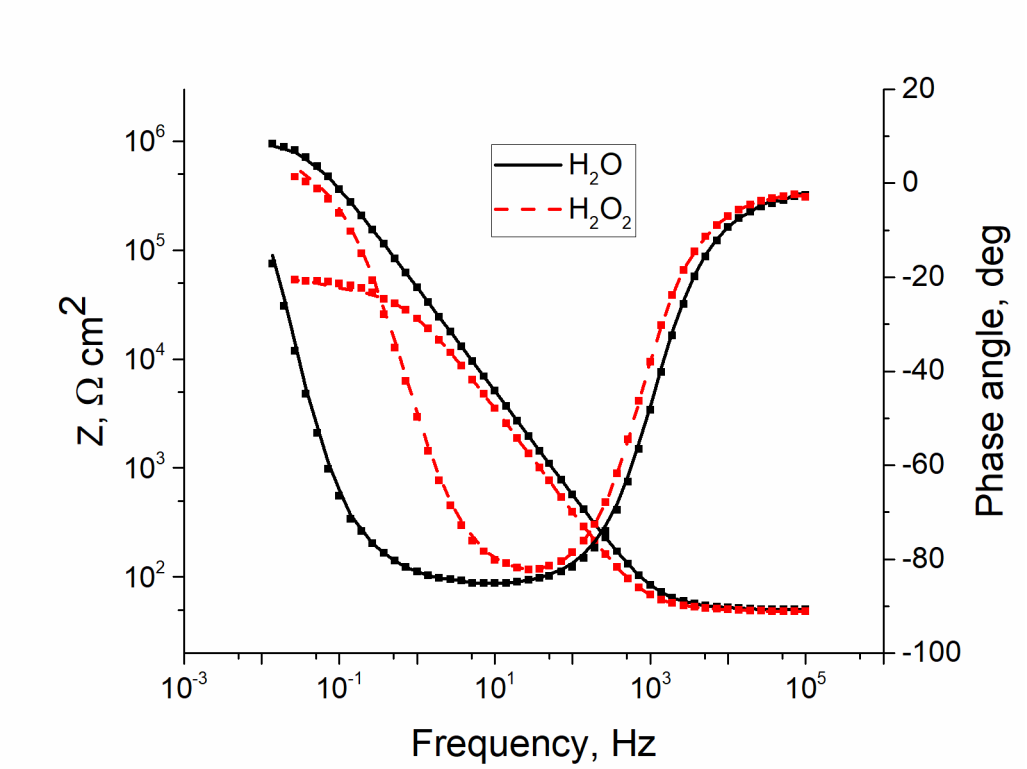


**Figure 4.6.5.** EIS spectra of the alumina obtained in water (black, solid) and hydrogen peroxide (red, dash) electrolytes prepared by powerful pulsed discharge oxidation at 1400V. Experimental: points; Fitting: lines.

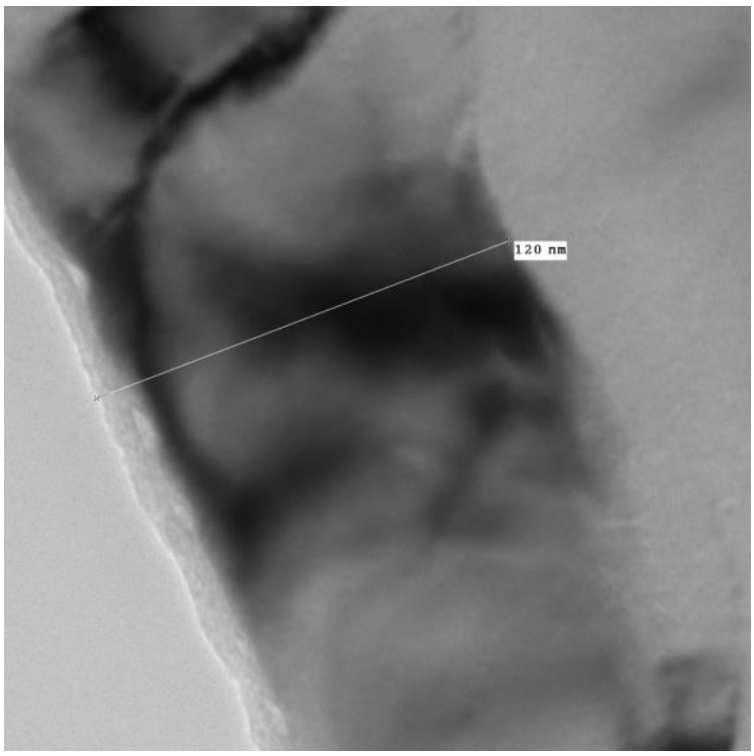


**Figure 4.6.6**. Cross-section TEM image of the anodic film on aluminium prepared in hydrogen peroxide by action of 5 discharges at 1400V.

**Table 4.6.2** Dielectric constant for the alumina prepared by PPDO in different electrolytes and different potentials

| Electrolyte and potential | Dielectric constant |
|---|---|
| Water, 1400V | 9.8 |
| Water, 1600V | 9.9 |
| Water, 1800V | 9.5 |
| Water, 2000V | 9.4 |
| Hydrogen peroxide, 1400V | 10.2 |
| Hydrogen peroxide, 1600V | 10.3 |
| Hydrogen peroxide, 1800V | 10.1 |
| Hydrogen peroxide, 2000V | 9.9 |

### 4.6.5 EIS studies of the titanium oxide

In contrast to aluminium, it is not possible to determine the thickness of the titanium oxide just from impedance spectra. However, EIS on the titania can help to reveal information about its structure and number of ionized donors. Impedance spectra of the titania films prepared in both water and hydrogen peroxide electrolytes have similar shape at low thicknesses and correlate well with the results obtained in previous works[5, 128]. Previously it was shown that in contrast to the oxide prepared by conventional galvanostatic anodisation, which consists of two layers and space charge region, the film obtained by PPDO contains only one dense part[5]. Spectra recorded on films prepared by pulsed discharge method contain two relaxation processes: the first responsible for the space charge region and the second, describing the bulk oxide. It is well known that polarization of a semiconductive film leads to variation of its capacitance and, in turn, to modulation of the corresponding part of the impedance spectra. The modulation of the capacitance response under the variable polarization is used to reveal parameters of the space charge region and bulk part of the film. The impedance spectra were taken at different polarizations from 0.8V to -0.4V with a step of 0.2 V vs. SCE (Fig. 4.6.7). Fitting the plots with two R-CPE and one R elements in series shows good results (Fig 4.6.7c). In comparison to the results obtained in sulphuric acid the resistance and capacitance of the bulk part of the film is lower. This can be explained by the lower number of defects, resulting in drop of the number of charge carriers. On the other hand, at anodic polarization the time constant corresponding to the bulk film is less evident, due to enlargement of the space charge region for the whole volume of the film.

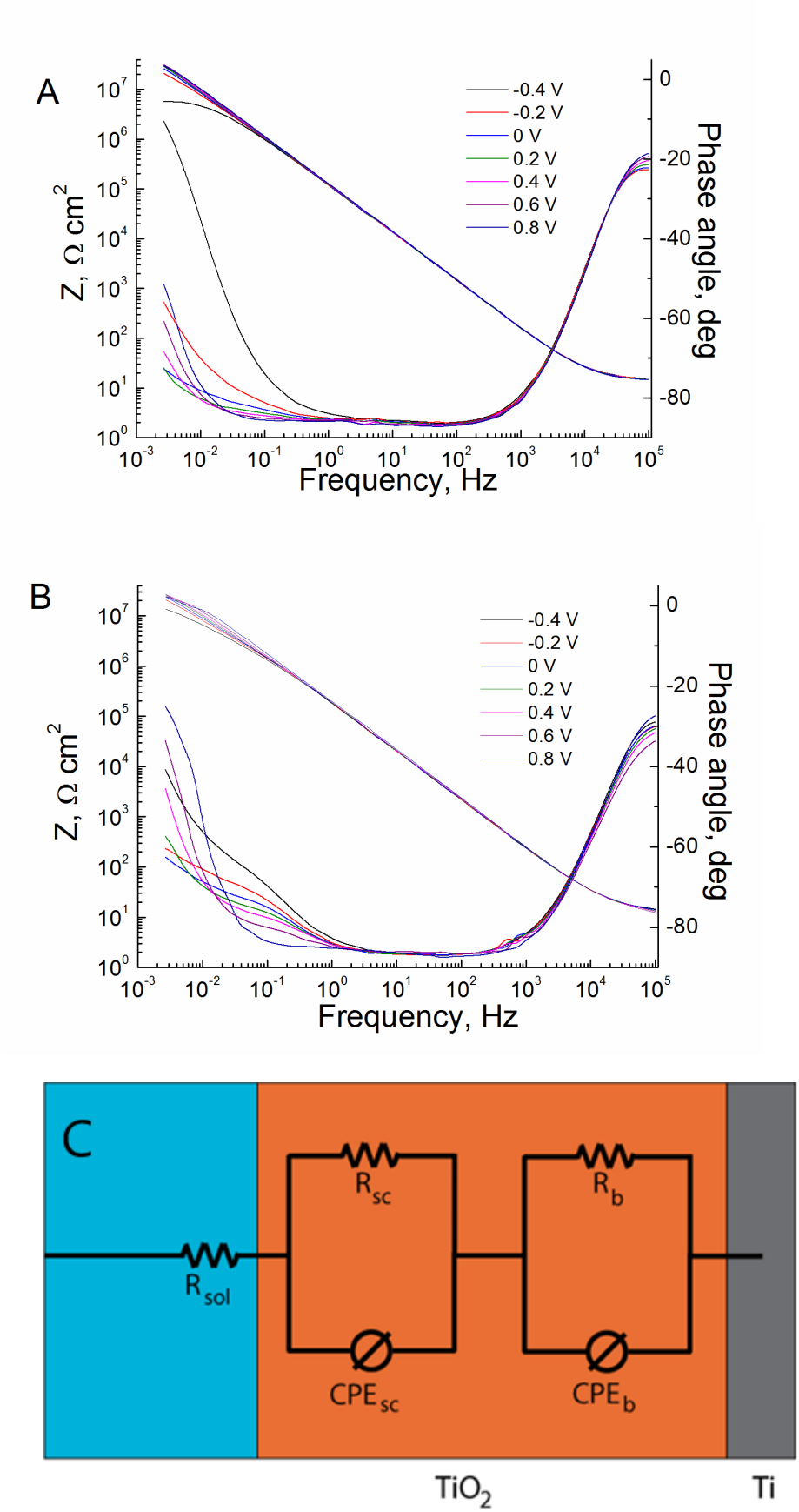


**Figure 4.6.7.** Impedance spectra of the 120 nm thick anodic oxide films under polarization formed on titanium in water (A) and hydrogen peroxide (B) electrolytes. Equivalent circuit used for fitting (C).

## 4.6.6 SKPFM studies of the aluminium oxide

One of the advantages of the oxide films prepared by the powerful pulsed oxidation method is the uniformity of the charge distribution on their surface. In comparison with the films prepared by galvanostatic anodisation, where defects and contamination of the electrode surface can highly influence the electrical properties of the film, in PPDO method the charge distribution uniforms after every discharge pulse due the processes which occurs during film growth. SKPFM studies obtained in water and hydrogen peroxide electrolytes show good and uniform charge distribution over the surface of the film for all the thicknesses and applied potentials (fig 4.6.8). As it was previously shown[127, 221], the Volta potential difference is highly dependent from the physical properties of the film as well as its thickness. Thus, the film can be characterised by the slope of the VPD-thickness plot. Figure 4.6.9 shows dependencies of Volta potential obtained on the aluminium at different voltages and different thicknesses. One can see that change of the Volta potentials on the surface of the film with change of the applied voltage correlates with changes of their dielectric constant obtained from EIS spectra. The slopes of the graphs are shown on the table 4.6.3. On the oxides prepared in the hydrogen peroxide solution the value of the slope was found to be up to 0,062V, which is higher than that described in literature[118, 120]. However, the samples prepared in water electrolyte have values of 0,059-0,061 which also exceed the values previously published. Taking into account that most of the films prepared in these electrolytes have similar structure to those obtained in conventional solutions, it can be suggested that it is possible to use the oxides prepared in contamination-free electrolytes as a reference for further studies of thin films on aluminium.

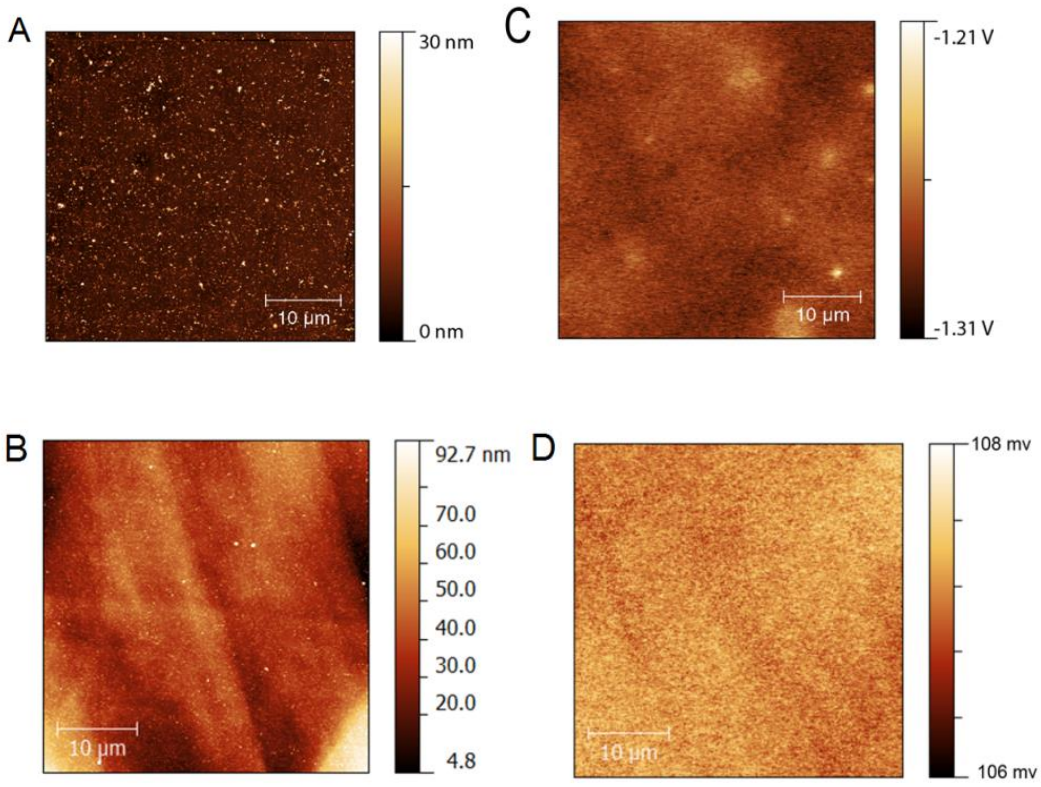


**Figure 4.6.8**. Topology (A,B) and measured potential distribution (C,D) on alumina films with thickness 60 nm prepared by pulsed discharge anodisation in water (A,C) and hydrogen peroxide (B,D). obtained at 1400V.

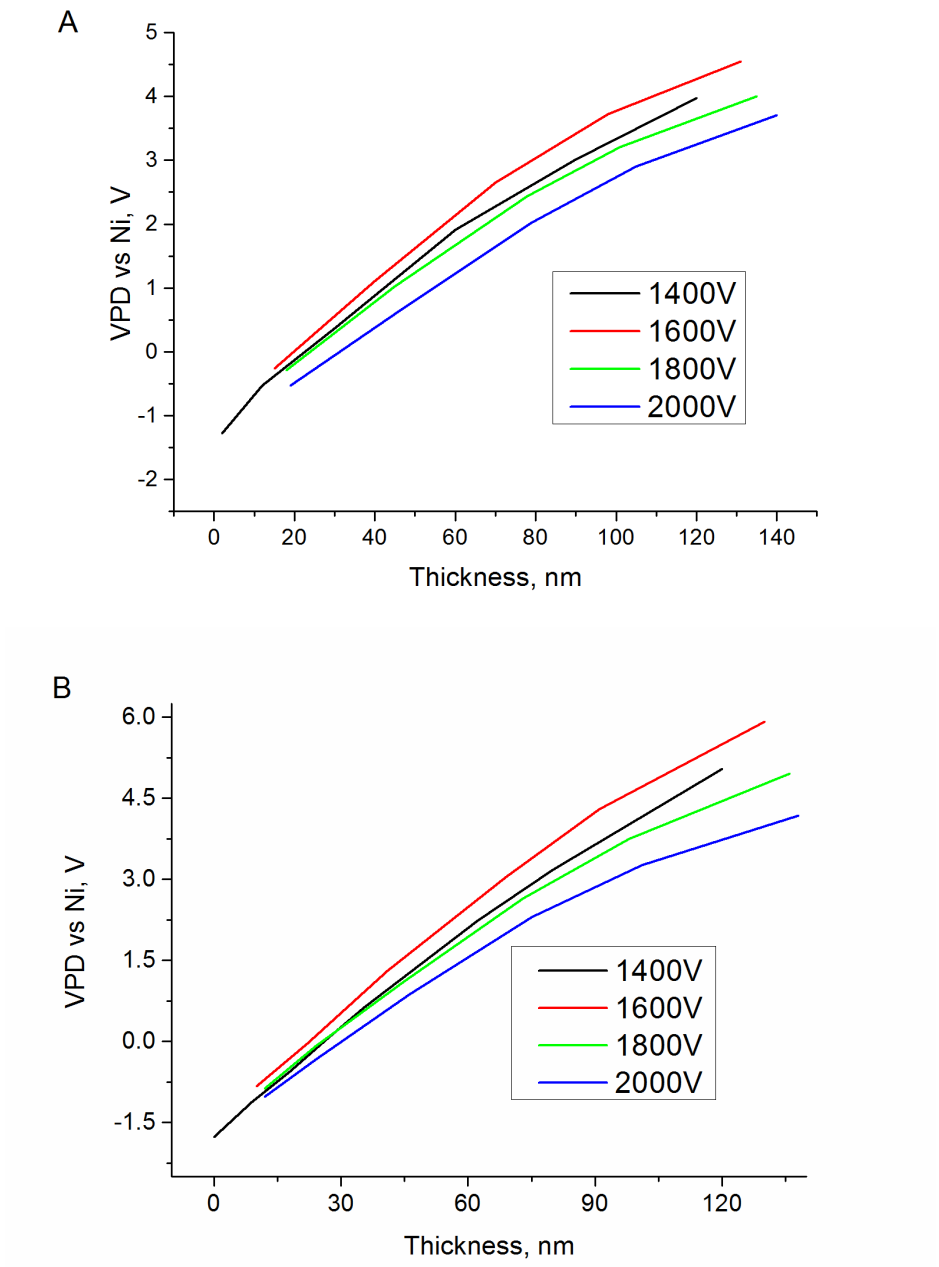


**Figure 4.6.9**. Dependence of Volta potential from the thickness on the aluminium oxides prepared in water (a) and hydrogen peroxide (b) electrolytes.

**Table 4.6.3**. Slopes of the graphs on the aluminium anodized in different conditions.

| Electrolyte and potential | Slopes |
|---|---|
| Water, 1400V | 0.061 |
| Water, 1600V | 0.061 |
| Water, 1800V | 0.060 |
| Water, 2000V | 0.059 |
| Hydrogen peroxide, 1400V | 0.061 |
| Hydrogen peroxide, 1600V | 0.062 |
| Hydrogen peroxide, 1800V | 0.061 |
| Hydrogen peroxide, 2000V | 0.060 |

### 4.6.7 SKPFM studies of the titania

In contrast to alumina, the relation VPD-thickness for titania is not linear and reaches a plateau. According to the previous works[128], the charges in the film bulk are separated.

On alumina, it was found that after annealing the VPD values tend to change and take a certain (equilibrium) level[120, 127]. This level is suggested to be the VPD value for an alumina film formed by thermal oxidation in air at the given annealing temperature. It is connected with low diffusion rate of ions in alumina at room temperature and increasing of it with temperature growth. In the case of titania, the ion migration rate seems to be higher in comparison to alumina, thus the values don't significantly differ from the equilibrium level[128].

SKPFM maps were found to be different for electrodes prepared in different electrolytes. In hydrogen peroxide the VPD distribution seems to be smooth and uniform, similar to that on aluminium (fig 4.6.10).

Increasing the applied voltage on the electrodes prepared in hydrogen peroxide doesn't significantly change the map of the SKPFM, but the values of the Volta potential rise. In fig. 4.6.11 the VPD-thickness plots are shown. It can be observed, that films prepared at potentials of 1400-1800V have approximately equal equilibrium level of Volta potential, while the films obtained at 2000V has the equilibrium VPD at higher level. Taking into account that preparation of the titania by the pulsed discharge method in the solutions of acids results in increment of the equilibrium level with rise of the dopant concentration[128], it can be suggested that the increase of applied voltage higher than 1800V results in rise of the defects.

Another effect which was found during the SKPFM studies of the titania was connected with aging of the oxide. On fig. 4.6.12 it can be found VPD-thickness plots obtained after 1, 4 and 24 hours after preparation. It was found that with aging the VPD values tend to change to the equilibrium potential. In comparison with titania obtained in phosphoric acid[128], oxides prepared in hydrogen peroxide tend to have faster relaxation speed. This can be connected with absence of dopant atoms and the corresponding number of defects that can play the role of charge traps. Furthermore, exposition under UV light for 10sec results in changing the Volta potential values. Thus, in the case of titania obtained in $H_2O_2$ the values were equal for all the

thicknesses, while on the samples prepared in $H_3PO_4$ there were minor differences. Influence of the aging on the VPD values of the samples prepared in different solutions will be discussed in later works. The results obtained on the samples above show that they can be used as a reference point for the study of surface properties of the titania.

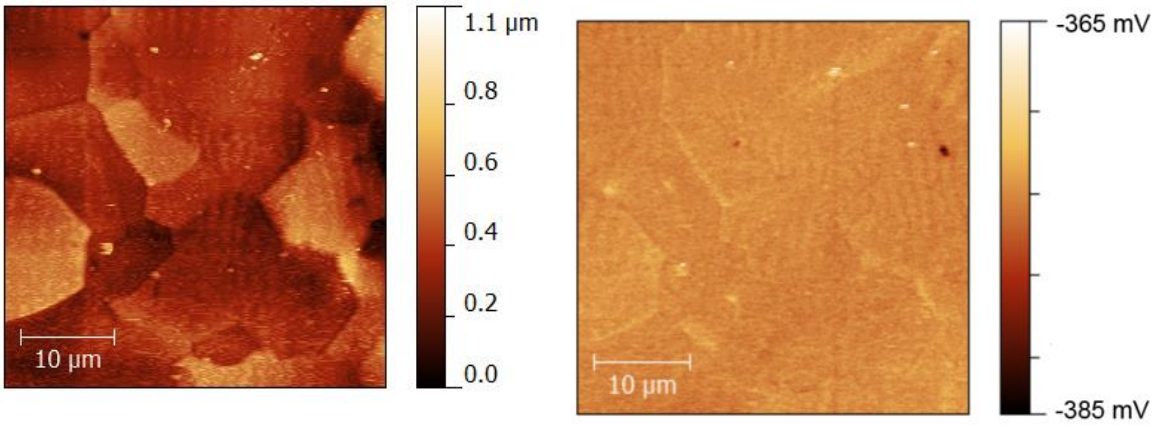


**Figure 4.6.10** Topology (left) and measured potential distribution (right) on titania films with thickness 60 nm prepared by pulsed discharge anodisation in hydrogen peroxide.

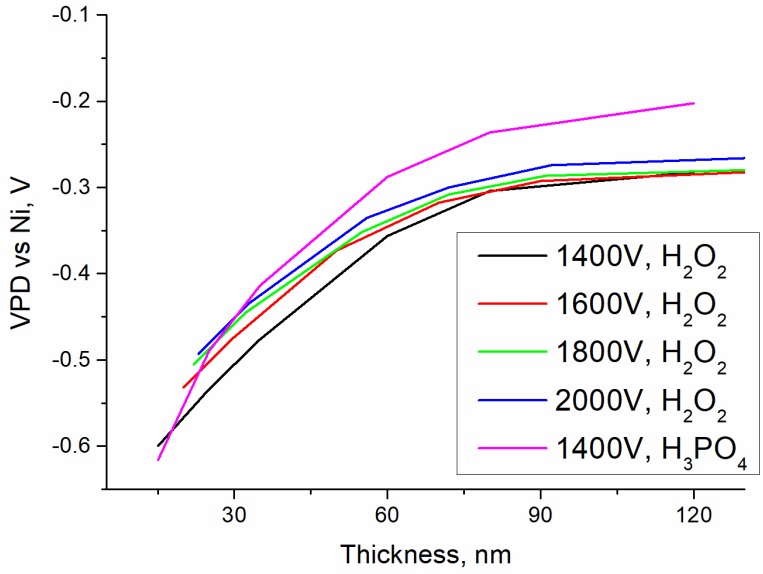


**Figure 4.6.11**. Dependence of Volta potential on the thickness of the titania prepared at different potentials and electrolytes

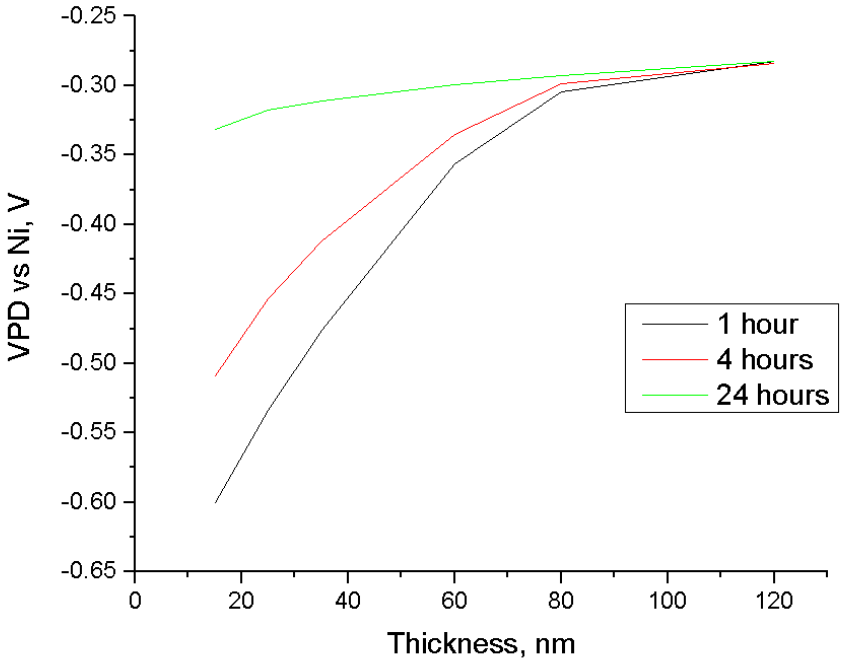


**Figure 4.6.12**. Dependence of Volta potential on the thickness of titania after 1, 4 and 24 hours of film preparation. Titania was prepared by pulsed discharge anodisation at 1400V in hydrogen peroxide.

## 4.6.8 Conclusions

The films prepared by PPDO methods in impurity-free electrolytes have very similar structure to those obtained in conventional solution. In comparison with traditional potentiostatic or galvanostatic methods, PPDO allows to produce films in high resistance electrolytes with the same thickness as in conventional electrolytes. These films can be interesting as a reference point for further research of thin oxides on aluminium and titanium and possibly also on other metals. In comparison to the films prepared in conventional electrolytes by galvanostatic anodisation the films have less defective structure and more uniform charge distribution over the surface.

Thin oxide films prepared on aluminium in water and hydrogen peroxide have s structure similar to that obtained in ammonium pentaborate. Alumina obtained in $H_2O_2$ at all the potentials have higher values of dielectric constant in comparison to those obtained in water. SKPFM shows uniform charge distribution over the surface. Such films can be interesting for the preparation of capacitors. Also, due to low number of defects and absence of dopant atoms they can be considered as reference point for further studies of alumina films.

Preparation of titanium oxide in both electrolytes shows similar behaviour during the first discharges. However when thickness of the film achieves a certain value the growth rate of the coating significantly drops in pure water. This oxide thickness decreases with the increase of the applied voltage. SEM studies of the samples show, that after this critical thickness, the oxide starts to grow at the grain boundaries of the substrate. In hydrogen peroxide behaviour of the film growth is similar to that in conventional electrolytes. The EIS measurements on the titania anodic films prepared in both electrolytes have demonstrated that the pulsed discharge oxidation leads to the formation of single-layer compact anodic oxide film.

# 5 General conclusions

Powerful Pulsed Discharge Oxidation (PPDO) is a novel method to prepare thin oxide films with properties quite different than those obtained by other conventional methods. It allows producing homogeneous low-defect anodic films up to ~200 nm thick on aluminium and titanium surface. The thickness values estimated by independent methods (EIS and TEM) were found to be in excellent agreement, which suggests a good homogeneity of these films.

The work developed in the framework of this thesis that gave origin to the different papers intended in general to include the following points:

1) Development and construction of the anodisation setup
2) Preparation of the films by the PPDO technique and their comparison with oxides prepared by conventional methods.
3) Study of the conditions (applied voltage, electrolyte concentration) that influence the characteristics of the obtained films.
4) Investigation of the film growth kinetics under action of discharge.
5) Preparation of films and structures by high voltage techniques that could not be obtained by conventional anodisation (due to high resistance of the electrolyte).

### Development and construction of the anodisation setup

To prepare films by the PPDO technique a special setup was developed (3.1). In comparison with conventional anodisation, which is widely used for more than a century, the setup for PPDO is relatively unique and has several specificities. The charge accumulated by the capacitor bank in this setup is injected into the electrochemical cell. Low latency of the capacitor and switch and wide possibilities of oscilloscope allows to study kinetics of the pulsed discharges without limitation from the side of equipment. This system allows to produce films with desired thicknesses by controlling the number of pulses, capacitance and applied voltage.

### Preparation of the films by PPDO technique and their comparison with oxides prepared by conventional method.

Thin films of titania and alumina were obtained by the PPDO technique in sulfuric acid and ammonium pentaborate respectively and compared with similar films obtained by conventional method. The EIS measurements on the titania anodic films prepared by the high-voltage pulsed discharge method and the conventional galvanostatic anodisation have demonstrated that the impedance spectra are sensitive both to the space charge region developed in the oxide and to the anodic film structure that changes with the film thickness. The pulsed discharge technique leads to the formation of single-layer compact anodic oxide films. In contrast, the EIS spectra of the anodic films grown by the conventional galvanostatic method exhibit several time constants: a dense inner layer and a nanoporous outer one. These films

show a significantly lower photoelectrochemical activity at short wavelengths as compared with the films prepared in the pulsed regime. The concentration of the ionized donors estimated from Mott-Schottky plots for the relatively thin galvanostatically grown $TiO_2$ films (70-120 nm) is significantly higher (by two orders of magnitude) than that in the coatings obtained by the pulsed discharge method.

The, anodic alumina films prepared by the pulsed discharge method have more uniform surface structure and electrical properties and are less dependent on the initial surface condition than those prepared by the conventional anodisation. In the pulsed films, the embedded charges locate in narrower defect layers bordering the film interfaces. In this respect, the pulsed discharge alumina films appear to have better barrier properties than the respective anodic films produced by the conventional methods.

The thickness of the oxide films prepared by high-voltage powerful pulsed discharge oxidation method can go up to 200-250 nm, depending on metal. After a certain thickness, the whole volume of the film cannot be completely ionized, and the mechanism of growth becomes similar to that in PEO process, what results in change of the properties of the film.

The detailed results and discussion are presented in chapters 4.1 and 4.2. The corresponding papers ("Impedance behavior of anodic $TiO_2$ films prepared by galvanostatic anodisation and powerful pulsed discharge in electrolyte" and "Anodic alumina films prepared by powerful pulsed discharge oxidation") were published[5, 127].

**Study of the conditions (applied voltage, electrolyte concentration) that influence the characteristics of the obtained films.**

Influence of the electrolyte concentration and applied voltage on the properties of the obtained films were studied. It was shown that increasing the phosphoric acid concentration in the electrolyte results in higher number of defects concentration in the film. Also, it is found that the maximum thickness of the anodic film on aluminium obtained in deionised water increases with the rise of the applied voltage, but at voltages over 1800 V oxide films cannot be formed by both methods due to film breakdown. The concentration of dopant atoms in the films prepared by the high-voltage powerful pulsed discharge oxidation method is higher in comparison with those, obtained by the conventional galvanostatic method. At the same time the number of structure defects (dislocations, pores etc.) in such films are significantly less. Varying the concentration of electrolyte, the electronic properties of resulting titania films and the kinetics of their growth can be tuned for specific applications. The results are presented in chapters 4.3 and 4.4., that correspond to papers "Titania films obtained by powerful pulsed discharge oxidation in phosphoric acid electrolytes" and "Aluminium anodisation in deionised water as electrolyte" already published 119-120. Two more papers ("Aluminium and titanium-aluminium nanorods encapsulated into oxide matrix by powerful pulsed discharge method" and "Powerful pulsed discharge oxidation of aluminium and titanium in hydrogen peroxide and distilled water") are currently under submission.

**Investigation of the film growth kinetics under action of discharge.**

Investigation of the film growth kinetics under action of discharge was performed in the frame of this part. Only 10% of the capacitor charge is consumed during the first microsecond (which corresponds to a current fall by more than 90% of the peak value) as follows from analysis of the discharge profile. The remaining 90% of charge is used during subsequent stage which lasts up to 0.5 s (depending on the thickness of the film). Thus, a pulsed discharge anodisation process can be conventionally divided into two stages where the first one (fast) is about 1 μs long, with the characteristic current magnitude of several kA/cm$^2$. It is believed that the main process during the first stage is ionization of an oxide film (either native film or that formed by previous oxidation). During the second long stage, a new layer grows. In comparison to the conventional anodisation processes this growth occurs in much higher electrical field and a higher total charge is transferred in unit time. Studies of current evolution with time for different concentrations of electrolyte show that the shape of the current profile does not depend on the electrolyte conductivity. The main role in the discharge profile is played by the dopant concentration in the oxide film. Oxides with lower concentration of dopants have well defined stages of ionization and film growth, while in the case of films with a higher dopant concentration, the two stages merge. The growth of the oxide also occurs with a higher rate for the films with a higher concentration of dopants. Studies of kinetics of the discharge process on the metal-filled porous titania and alumina electrodes show that the shape of temporal current evolution profile does not depend on the oxide matrix composition. Increasing the applied voltage results in a current increment without changing the profile shape. Analysis of the current vs time plots show that only minor part of the charge is spent for the oxide growth and the only process is ionization of the oxide with its further melting. The results are presented in chapters 4.3 and 4.4. The corresponding papers (“Titania films obtained by powerful pulsed discharge oxidation in phosphoric acid electrolytes” and “Aluminium anodisation in deionised water as electrolyte”) were published 119-120.

**Preparation of the films and structures by high voltage methods that could not be obtained by conventional anodisation.**

Preparation of titania and alumina were performed in deionised water, distilled water and hydrogen peroxide. In all electrolytes formation of the film by conventional electrochemical anodisation is impossible, due to high resistance of the media. However, it was found that formation of the films by application of high voltage is possible. The films prepared by high voltage anodisation methods in impurity-free electrolytes have very similar structure to those obtained in conventional solution. These films can be interesting as a reference point for further research of thin oxides on aluminium and titanium and possibly also on other metals.

Also encapsulated metal nanostructures were obtained. It was shown that under action of the discharge with voltages less than 1600V, the top part of the porous coating melts, resulting in closing of the bulk of pores. Closing the titania nanotubes by this method is possible irrespective of the pore content. In the case of alumina nanoporous layer, only minor part of the pores can be sealed if they are empty. The results are presented in chapters 4.4, 4.5 and 4.6. Two papers (“Aluminium and titanium-aluminium nanorods encapsulated into oxide matrix by

powerful pulsed discharge method” and “Powerful pulsed discharge oxidation of aluminium and titanium in hydrogen peroxide and distilled water”) are currently under submission.

# 6 Further work

In the frame of current work anodisation of titanium and aluminium by powerful pulsed discharge oxidation was studied. However, many questions about the properties of the films obtained by this method, their potential and structure are still not answered.

Further work will be divided in the following points:

1) Study of films obtained on different valve and non-valve substrates.
2) Anodisation in non-aqueous media, such as ionic liquids and deep eutectic solutions.
3) Preparation of the coatings with embedded capsules and studies of pores sealing.

In the first point, different valve and non-valve metals such as tantalum, zirconium, nickel and iron including their industrially important alloys will be tested as substrates for preparing the anodic films. The choice of these metals will be determined by their wide application in industry and medicine. Different parameters of the pulsed anodizing process such as applied voltage, injected charge, anode-to-cathode surface area ratio, and the composition of electrolyte will be changed to obtain anodic films with tailored properties. Different electrolytes (inorganic and organic acids, alkalis and inorganic salts) will be tested to prepare individual oxide and composite anodic films can be prepared according to point 3.

Anodisation in non-aqueous media (point 2) can help to reveal the influence of the native oxide on the metals in the obtained films. Also, it is possible to create dense films on materials which are not stable in aqueous electrolytes. Finally, studies of the pore sealing in non-aqueous media can help to create complex coatings with encapsulated active metals which are not stable in air.

Moreover, the PPDO technique allows to create other complex coatings. Thin oxide film deposition with certain properties without influence of the bulk substrate is a promising way of modification of material properties. The metal deposited on the surface of semiconductors or insulators by different physical and physical-chemical methods will be oxidized by high-voltage pulsed anodizing. The influence of the ratio of metal film oxidized and anodic film thickness will be studied. The chemical and physical properties of such anodic oxides prepared by high-voltage pulse and conventional galvanostatic methods will be compared.

Application of high-voltage pulse to the porous oxide results in melting of the top layer of the pores and formation of a complex porous film with closed pores. Different materials can be deposited into pores: mesoporous silica, layered double hydroxides, magnetic materials and metals. Deposition into pores can be carried out by several methods: mechanical injection of the particles from the solution (different oxides, hydroxides or nanocontainers containing corrosion inhibitors), chemical synthesis of the oxides in the pores, electrochemical metal deposition in the pores from aqueous and nonaqueous solutions and vacuum deposition. Afterwards the pores can be sealed by high voltage pulsed discharge, resulting in their closure and capsules formation.

# 7 List of papers published or under submission included in the thesis.

Lisenkov, A. D.; Salak, A. N.; Poznyak, S. K.; Zheludkevich, M. L.; Ferreira, M. G. S., Anodic Alumina Films Prepared by Powerful Pulsed Discharge Oxidation. Journal of Physical Chemistry C 2011, 115, 18634-18639.

Poznyak, S. K.; Lisenkov, A. D.; Ferreira, M. G. S.; Kulak, A. I.; Zheludkevich, M. L., Impedance Behaviour of Anodic Tio 2 Films Prepared by Galvanostatic Anodisation and Powerful Pulsed Discharge in Electrolyte. Electrochimica Acta 2012, 76, 453-461.

Lisenkov, A. D.; Poznyak, S. K.; Montemor, M. F.; Carmezim, M. J.; Zheludkevich, M. L.; Ferreira, M. G. S., Titania Films Obtained by Powerful Pulsed Discharge Oxidation in Phosphoric Acid Electrolytes. Journal of the Electrochemical Society 2014, 161, D73-D78.

Lisenkov, A. D.; Poznyak, S. K.; Zheludkevich, M. L.; Ferreira, M. G. S., Aluminium Anodisation in Deionised Water as Electrolyte. Journal of The Electrochemical Society 2016, 163, C364-C368.

Lisenkov, A. D.; Poznyak, S. K.; Zheludkevich, M. L.; Ferreira, M. G. S., Aluminium and titanium-aluminium nanorods encapsulated into oxide matrix by powerful pulsed discharge method (under submission)

Lisenkov, A. D.; Poznyak, S. K.; Zheludkevich, M. L.; Ferreira, M. G. S., Powerful pulsed discharge oxidation of aluminium and titanium in hydrogen peroxide and distilled water (under submission)

# 8 List of other papers published in which author is marked as “co-author”.

S.A. Ulasevich, S.K. Poznyak, A.I. Kulak, A.D. Lisenkov, M. Starykevich, E.V. Skorb, Photocatalytic Deposition of Hydroxyapatite onto a Titanium Dioxide Nanotubular Layer with Fine Tuning of Layer Nanoarchitecture, Langmuir (2016).

S.A. Ulasevich, A.I. Kulak, S.K. Poznyak, S.A. Karpushenkov, A.D. Lisenkov, E.V. Skorb, Deposition of hydroxyapatite-incorporated TiO2 coating on titanium using plasma electrolytic oxidation coupled with electrophoretic deposition, RSC Advances 6(67) (2016) 62540-62544.

M. Starykevich, A.N. Salak, D.K. Ivanou, A.D. Lisenkov, M.L. Zheludkevich, M.G.S. Ferreira, Electrochemical deposition of zinc from deep eutectic solvent on barrier alumina layers, Electrochimica Acta 170 (2015) 284-291.

Andrei N. Salak, Oleg V. Ignatenko, Aliaksandr L. Zhaludkevich, Aleksey D. Lisenkov, Maksim Starykevich, Mikhail L. Zheludkevich, Mário G. S. FerreiraHigh-pressure zinc oxysulphide phases in the ZnO–ZnS system Physica Status Solidi (A) Applications and Materials 04/2015; 212(4). DOI:10.1002/pssa.201431820

Andrei N. Salak, Aleksandr L. Zhaludkevich, Oleg V. Ignatenko, Aleksey D. Lisenkov, Aleksey A. Yaremchenko, Mikhail L. Zheludkevich, Mário G. S. Ferreira High-pressure induced phase formation in the CuGaS2–CuGaO2 chalcopyrite–delafossite system physica status solidi (b) 06/2014; 251(6). DOI:10.1002/pssb.201451013

Andrei N. Salak, Aleksey D. Lisenkov, Mikhail L. Zheludkevich, Mário G. S. Ferreira Carbonate-Free Zn-Al (1:1) Layered Double Hydroxide Film Directly Grown on Zinc-Aluminum Alloy Coating ECS Electrochem. Lett. 2014 volume 3, issue 1, C9-C11 doi: 10.1149/2.008401eel

Maksim Starykevich, Aleksey D. Lisenkov, Andrei N. Salak, Mario G. S. Ferreira, Mikhail L. Zheludkevich Electrodeposition of Zinc Nanorods from Ionic Liquid into Porous Anodic Alumina ChemElectroChem 07/2014; DOI: 10.1002/celc.201402130

Tedim, J., Zheludkevich, M.L., Bastos, A.C., Salak, A.N., Lisenkov, A.D., Ferreira, M.G.S. Influence of preparation conditions of Layered Double Hydroxide conversion films on corrosion protection (2014) Electrochimica Acta, 117, pp. 164-171.

Salak, A.N., Zhaludkevich, A.L., Ignatenko, O.V., Lisenkov, A.D., Yaremchenko, A.A., Zheludkevich, M.L., Ferreira, M.G.S. High-pressure induced phase formation in the CuGaS2-CuGaO2 chalcopyrite-delafossite system (2014) Physica Status Solidi (B) Basic Research, 251 (6), pp. 1192-1196.

Tedim, J., Zheludkevich, M.L., Bastos, A.C., Salak, A.N., Carneiro, J., Maia, F., Lisenkov, A.D., Oliveira, A.B., Ferreira, M.G.S. Effect of surface treatment on the performance of LDH conversion films (2014) ECS Electrochemistry Letters, 3 (1), pp. C4-C8.

Ivanou, D.K., Starykevich, M., Lisenkov, A.D., Zheludkevich, M.L., Xue, H.B., Lamaka, S.V., Ferreira, M.G.S. Plasma anodized ZE41 magnesium alloy sealed with hybrid epoxy-silane coating (2013) Corrosion Science, 73, pp. 300-308.

Ivanou, D.K., Ivanova, Y.A., Lisenkov, A.D., Zheludkevich, M.L., Streltsov, E.A. Electrochemical deposition of lead and tellurium into barrierless nanoporous anodic aluminium oxide (2012) Electrochimica Acta, 77, pp. 65-70.

A.N. Salak, A.L. Zhaludkevich, B.V. Korzun, A.D. Lisenkov, M.L. Zheludkevich, A copper-deficient tetragonal phase derived from chalcopyrite $CuGaS_2$, J. Phys. Condens. Matter, 2013, V.25, P. 082204 – 1 – 4

J. Tedim, M. L. Zheludkevich, A. N. Salak, A. Lisenkov and M. G. S. Ferreira “Nanostructured LDH-container layer with active protection functionality”, J. Mater. Chem., 2011, 21, 15464

F. Maia, J. Tedim, A. D. Lisenkov, A. N. Salak, M. L. Zheludkevich, Mario G. S. Ferreira, “Silica nanocontainers for active corrosion protection”, Nanoscale, 2012, 4, 1287

M. L. Zheludkevich, J. Tedim, C. S. R. Freire, S. C. M. Fernandes, S. Kallip, A. Lisenkov, A. Gandini and M. G. S. Ferreira "Self-healing protective coatings with “green” chitosan based pre-layer reservoir of corrosion inhibitor" J. Mater. Chem., 2011, 21, 4805-4812

A. Lisenkov, M.L. Zheludkevich, M.G.S. Ferreira “Active protective Al–Ce alloy coating electrodeposited from ionic liquid”, Electrochemistry Communications, Volume 12, Issue 6, June 2010, Pages 729-732

Rabchinskij S.M., Lisenkov A.D, Streltsov E.A. Electrochemical formation of photosensitive CdTe films on Ti substrates. // Vesti NAN Belorusi. 2007. Ser.him.nauk. № 2. 56-61 (in russian).

Rabchinskij S.M., Lisenkov A.D, Streltsov E.A., Kosyachenko L.A. Influence of the deposition potential to the photoelectrochemical properties of the CdTe films.// Vesti NAN Belorusi. 2007. Ser.him.nauk. № 3. 33-37 (in russian).

# References


1. Engell, H.; Young, J. L., Anodic Oxide Films, Academic Press London Und New York 1961. 377 Seiten Mit Bildern. Preis: 70 S. *Zeitschrift für Elektrochemie, Berichte der Bunsengesellschaft für physikalische Chemie* **1962**, *66*, 282-282.
2. Cigada, A.; Cabrini, M.; Pedeferri, P., Increasing of the Corrosion-Resistance of the Ti6al4v Alloy by High Thickness Anodic-Oxidation. *J Mater Sci-Mater M* **1992**, *3*, 408-412.
3. Singh, P. K.; Kim, K.-W.; Rhee, H.-W., Electrical, Optical and Photoelectrochemical Studies on a Solid Peo-Polymer Electrolyte Doped with Low Viscosity Ionic Liquid. *Electrochem Commun* **2008**, *10*, 1769-1772.
4. Poznyak, S. K.; Talapin, D. V.; Kulak, A. I., Electrochemical Oxidation of Titanium by Pulsed Discharge in Electrolyte. *Journal of Electroanalytical Chemistry* **2005**, *579*, 299-310.
5. Poznyak, S. K.; Lisenkov, A. D.; Ferreira, M. G. S.; Kulak, A. I.; Zheludkevich, M. L., Impedance Behaviour of Anodic Tio 2 Films Prepared by Galvanostatic Anodisation and Powerful Pulsed Discharge in Electrolyte. *Electrochimica Acta* **2012**, *76*, 453-461.
6. Kasemo, B.; Lausmaa, J., Surface Science Aspects on Inorganic Biomaterials. *Journal Name: CRC Crit. Rev. Clin. Neurobiol.; (United States); Journal Volume: 4* **1986**, Medium: X; Size: Pages: 335-380.
7. Tengvall, P.; Lundström, I., Physico-Chemical Considerations of Titanium as a Biomaterial. *Clinical Materials* **1992**, *9*, 115-134.
8. Hervieu, M., The Surface Science of Metal Oxides. By V. E. Henrich and P. A. Cox, Cambridge University Press, Cambridge 1994, Xiv, 464 Pp., Hardcover, £ 55.00, Isbn 0–521–44389-X. *Advanced Materials* **1995**, *7*, 91-92.
9. Vermilyea, D. A., Anodic Oxide Films. L. Young. Academic Press, New York, 1961. Xiii + 377 Pp. Illus. $11. *Science* **1962**, *135*, 783-784.
10. Tafel, J., Polarization in Cathodic Hydrogen Evolution. *Zeitschrift fuer Physikalische Chemie* **1905**, *50*, 641-712.
11. Schmuki, P., From Bacon to Barriers: A Review on the Passivity of Metals and Alloys. *Journal of Solid State Electrochemistry* **2002**, *6*, 145-164.
12. Carter, V. E., *Metallic Coatings for Corrosion Control*; Newnes-Butterworths, 1977.
13. Sawunyama, P.; Yasumori, A.; Okada, K., The Nature of Multilayered Tio2-Based Photocatalytic Films Prepared by a Sol-Gel Process. *Materials Research Bulletin* **1998**, *33*, 795-801.
14. Zeman, P.; Takabayashi, S., Effect of Total and Oxygen Partial Pressures on Structure of Photocatalytic Tio2 Films Sputtered on Unheated Substrate. *Surface and Coatings Technology* **2002**, *153*, 93-99.
15. Mahé, E.; Devilliers, D.; Groult, H.; Pouilleau, J., Electrochemical Behaviour of Platinum-Coated Ta/Ta2o5 Electrodes. *Electrochimica Acta* **1999**, *44*, 2307-2315.
16. Carlin, R. T.; Osteryoung, R. A.; Wilkes, J. S.; Rovang, J., Studies of Titanium(Iv) Chloride in a Strongly Lewis Acidic Molten-Salt - Electrochemistry and Titanium Nmr and Electronic Spectroscopy. *Inorganic Chemistry* **1990**, *29*, 3003-3009.
17. Fadl-Allah, S. A.; El-Sherief, R. M.; Badawy, W. A., Electrochemical Formation and Characterization of Porous Titania (Tio2) Films on Ti. *Journal of Applied Electrochemistry* **2008**, *38*, 1459-1466.

18. Aladjem, A., Anodic Oxidation of Titanium and Its Alloys. *Journal of Materials Science* **1973**, *8*, 688-704.
19. Asahi, R.; Taga, Y.; Mannstadt, W.; Freeman, A. J., Electronic and Optical Properties of Anatase Tio2. *Phys Rev B* **2000**, *61*, 7459-7465.
20. Bondarenko, A.; Ragoisha, G., Variable Mott-Schottky Plots Acquisition by Potentiodynamic Electrochemical Impedance Spectroscopy. *Journal of Solid State Electrochemistry* **2005**, *9*, 845-849.
21. Carp, O.; Huisman, C. L.; Reller, A., Photoinduced Reactivity of Titanium Dioxide. *Prog Solid State Ch* **2004**, *32*, 33-177.
22. Delplancke, J. L.; Winand, R., Galvanostatic Anodization of Titanium—Ii. Reactions Efficiencies and Electrochemical Behaviour Model. *Electrochimica Acta* **1988**, *33*, 1551-1559.
23. Kudelka, S.; Schultze, J. W., Photoelectrochemical Imaging and Microscopic Reactivity of Oxidised Ti. *Electrochimica Acta* **1997**, *42*, 2817-2825.
24. Lausmaa, J.; Kasemo, B.; Mattsson, H.; Odelius, H., Multi-Technique Surface Charaterization of Oxide Films on Electropolished and Anodically Oxidized Titanium. *Applied Surface Science* **1990**, *45*, 189-200.
25. Ohtsuka, T.; Otsuki, T., The Influence of the Growth Rate on the Semiconductive Properties of Titanium Anodic Oxide Films. *Corrosion Science* **1998**, *40*, 951-958.
26. Schmidt, A. M.; Azambuja, D. S.; Martini, E. M. A., Semiconductive Properties of Titanium Anodic Oxide Films in Mcilvaine Buffer Solution. *Corrosion Science* **2006**, *48*, 2901-2912.
27. Delplancke, J. L.; Winand, R., Galvanostatic Anodization of Titanium—I. Structures and Compositions of the Anodic Films. *Electrochimica Acta* **1988**, *33*, 1539-1549.
28. Jilani, O.; Njah, N.; Ponthiaux, P., Corrosion Properties of Anodized Aluminum: Effects of Equal Channel Angular Pressing Prior to Anodization. *Corrosion Science* **2014**, *89*, 163-170.
29. Macak, J. M.; Tsuchiya, H.; Ghicov, A.; Yasuda, K.; Hahn, R.; Bauer, S.; Schmuki, P., Tio2 Nanotubes: Self-Organized Electrochemical Formation, Properties and Applications. *Current Opinion in Solid State and Materials Science* **2007**, *11*, 3-18.
30. Pawar, P. S.; Gogawale, S. V.; Kothari, D. C.; Narsale, A. M.; Prabhawalkar, P. D.; Raole, P. M., Study of Aluminum-Oxide Films Formed by Plasma Anodization. *Thin Solid Films* **1990**, *193*, 683-689.
31. Vermilyea, D. A., Stresses in Anodic Films. *Journal of The Electrochemical Society* **1963**, *110*, 345-346.
32. Memming, R., Processes at Semiconductor Electrodes. In *Comprehensive Treatise of Electrochemistry: Volume 7 Kinetics and Mechanisms of Electrode Processes*, Conway, B. E.; Bockris, J. O. M.; Yeager, E.; Khan, S. U. M.; White, R. E., Eds. Springer US: Boston, MA, 1983; pp 529-592.
33. Güntherschulze, A.; Betz, H., Die Bewegung Der Ionengitter Von Isolatoren Bei Extremen Elektrischen Feldstärken. *Zeitschrift für Physik* **1934**, *92*, 367-374.
34. Verwey, E. J. W., Electrolytic Conduction of a Solid Insulator at High Fields the Formation of the Anodic Oxide Film on Aluminium. *Physica* **1935**, *2*, 1059-1063.
35. Cabrera, N.; Mott, N. F., Theory of the Oxidation of Metals. *Reports on Progress in Physics* **1949**, *12*, 163.
36. Mott, N. F., The Theory of the Formation of Protective Oxide Films on Metals, Ii. *Transactions of the Faraday Society* **1940**, *35*, 472-483.

37. Dewald, J. F., A Theory of the Kinetics of Formation of Anode Films at High Fields. *Journal of The Electrochemical Society* **1955**, *102*, 1-6.
38. Vetter, K. J., *Electrochemical Kinetics : Theoretical and Experimental Aspects*; Academic Press: New York, N.Y, 1967.
39. Kudelka, S.; Michaelis, A.; Schultze, J. W., Effect of Texture and Formation Rate on Ionic and Electronic Properties of Passive Layers on Ti Single Crystals. *Electrochimica Acta* **1996**, *41*, 863-870.
40. Schultze, J. W.; Lohrengel, M. M.; Ross, D., Nucleation and Growth of Anodic Oxide Films. *Electrochimica Acta* **1983**, *28*, 973-984.
41. Larsson, C.; Thomsen, P.; Lausmaa, J.; Rodahl, M.; Kasemo, B.; Ericson, L. E., Bone Response to Surface Modified Titanium Implants: Studies on Electropolished Implants with Different Oxide Thicknesses and Morphology. *Biomaterials* **1994**, *15*, 1062-1074.
42. Larsson, C.; Thomsen, P.; Aronsson, B. O.; Rodahl, M.; Lausmaa, J.; Kasemo, B.; Ericson, L. E., Bone Response to Surface-Modified Titanium Implants: Studies on the Early Tissue Response to Machined and Electropolished Implants with Different Oxide Thicknesses. *Biomaterials* **1996**, *17*, 605-616.
43. Ask, M.; Lausmaa, J.; Kasemo, B., Preparation and Surface Spectroscopic Characterization of Oxide Films on Ti6al4v. *Applied Surface Science* **1989**, *35*, 283-301.
44. Serruys, Y.; Sakout, T.; Gorse, D., Anodic Oxidation of Titanium in 1m H2so4, Studied by Rutherford Backscattering. *Surface Science* **1993**, *282*, 279-287.
45. Lausmaa, J., Surface Spectroscopic Characterization of Titanium Implant Materials. *Journal of Electron Spectroscopy and Related Phenomena* **1996**, *81*, 343-361.
46. Nolan, N. T.; Seery, M. K.; Pillai, S. C., Spectroscopic Investigation of the Anatase-to-Rutile Transformation of Sol-Gel-Synthesized Tio2 Photocatalysts. *Journal of Physical Chemistry C* **2009**, *113*, 16151-16157.
47. Hu, Y.; Tsai, H. L.; Huang, C. L., Effect of Brookite Phase on the Anatase-Rutile Transition in Titania Nanoparticles. *Journal of the European Ceramic Society* **2003**, *23*, 691-696.
48. Gong, X. Q.; Selloni, A., First-Principles Study of the Structures and Energetics of Stoichiometric Brookite Ti O2 Surfaces. *Physical Review B - Condensed Matter and Materials Physics* **2007**, *76*.
49. Wisitsoraat, A.; Tuantranont, A.; Comini, E.; Sberveglieri, G.; Wlodarski, W., Characterization of N-Type and P-Type Semiconductor Gas Sensors Based on Niox Doped Tio2 Thin Films. *Thin Solid Films* **2009**, *517*, 2775-2780.
50. Hoffmann, M. R.; Martin, S. T.; Choi, W.; Bahnemann, D. W., Environmental Applications of Semiconductor Photocatalysis. *Chemical Reviews* **1995**, *95*, 69-96.
51. Wang, Y.; Huang, Y.; Ho, W.; Zhang, L.; Zou, Z.; Lee, S., Biomolecule-Controlled Hydrothermal Synthesis of C-N-S-Tridoped Tio2 Nanocrystalline Photocatalysts for No Removal under Simulated Solar Light Irradiation. *Journal of Hazardous Materials* **2009**, *169*, 77-87.
52. Schultze, J. W.; Tsakova, V., Electrochemical Microsystem Technologies: From Fundamental Research to Technical Systems. *Electrochimica Acta* **1999**, *44*, 3605-3627.
53. Davepon, B.; Schultze, J. W.; König, U.; Rosenkranz, C., Crystallographic Orientation of Single Grains of Polycrystalline Titanium and Their Influence on Electrochemical Processes. *Surface and Coatings Technology* **2003**, *169-170*, 85-90.
54. Yahalom, J.; Zahavi, J., Electrolytic Breakdown Crystallization of Anodic Oxide Films on A1, Ta and Ti. *Electrochimica Acta* **1970**, *15*, 1429-1435.

55. Marchenoir, J. C.; Loup, J. P.; Masson, J., Étude Des Couches Poreuses Formées Par Oxydation Anodique Du Titane Sous Fortes Tensions. *Thin Solid Films* **1980**, *66*, 357-369.
56. Ikonopisov, S., Theory of Electrical Breakdown During Formation of Barrier Anodic Films. *Electrochimica Acta* **1977**, *22*, 1077-1082.
57. Sul, Y.-T.; Johansson, C. B.; Jeong, Y.; Albrektsson, T., The Electrochemical Oxide Growth Behaviour on Titanium in Acid and Alkaline Electrolytes. *Medical Engineering & Physics* **2001**, *23*, 329-346.
58. Kasalica, B.; Petkovic, M.; Belca, I.; Stojadinovic, S.; Zekovic, L., Electronic Transitions During Plasma Electrolytic Oxidation of Aluminum. *Surf Coat Tech* **2009**, *203*, 3000-3004.
59. Zwilling, V.; Darque-Ceretti, E.; Boutry-Forveille, A.; David, D.; Perrin, M. Y.; Aucouturier, M., Structure and Physicochemistry of Anodic Oxide Films on Titanium and Ta6v Alloy. *Surf Interface Anal* **1999**, *27*, 629-637.
60. Schmuki, P.; Division, E. S. C.; Luminescence, E. S.; Division, D. M.; Meeting, E. S., *Pits and Pores Ii: Formation, Properties, and Significance for Advanced Materials : Proceedings of the International Symposium*; Electrochemical Society, Incorporated, 2001.
61. Fujishima, A.; Honda, K., Electrochemical Photolysis of Water at a Semiconductor Electrode. *Nature* **1972**, *238*, 37-+.
62. Frank, S. N.; Bard, A. J., Heterogeneous Photocatalytic Oxidation of Cyanide Ion in Aqueous Solutions at Tio2 Powder [41]. *Journal of the American Chemical Society* **1977**, *99*, 303-304.
63. O'Regan, B.; Graetzel, M., Low-Cost, High-Efficiency Solar Cell Based on Dye-Sensitized Colloidal Tio2 Films. *Nature* **1991**, *353*, 737.
64. Wang, R.; Hashimoto, K.; Fujishima, A.; Chikuni, M.; Kojima, E.; Kitamura, A.; Shimohigoshi, M.; Watanabe, T., Light-Induced Amphiphilic Surfaces [4]. *Nature* **1997**, *388*, 431-432.
65. Mills, A.; Le Hunte, S., An Overview of Semiconductor Photocatalysis. *Journal of Photochemistry and Photobiology A: Chemistry* **1997**, *108*, 1-35.
66. Testino, A.; Bellobono, I. R.; Buscaglia, V.; Canevali, C.; D'Arienzo, M.; Polizzi, S.; Scotti, R.; Morazzoni, F., Optimizing the Photocatalytic Properties of Hydrothermal Tio2 by the Control of Phase Composition and Particle Morphology. A Systematic Approach. *Journal of the American Chemical Society* **2007**, *129*, 3564-3575.
67. Cozzoli, P. D.; Comparelli, R.; Fanizza, E.; Curri, M. L.; Agostiano, A., Photocatalytic Activity of Organic-Capped Anatase Tio2 Nanocrystals in Homogeneous Organic Solutions. *Materials Science and Engineering: C* **2003**, *23*, 707-713.
68. Hoffman, A. J.; Carraway, E. R.; Hoffmann, M. R., Photocatalytic Production of H2o2 and Organic Peroxides on Quantum- Sized Semiconductor Colloids. *Environmental Science and Technology* **1994**, *28*, 776-785.
69. Emilio, C. A.; Litter, M. I.; Kunst, M.; Bouchard, M.; Colbeau-Justin, C., Phenol Photodegradation on Platinized-Tio2 Photocatalysts Related to Charge-Carrier Dynamics. *Langmuir* **2006**, *22*, 3606-13.
70. Tachikawa, T.; Fujitsuka, M.; Majima, T., Mechanistic Insight into the Tio2 Photocatalytic Reactions: Design of New Photocatalysts. *Journal of Physical Chemistry C* **2007**, *111*, 5259-5275.
71. Choi, W.; Termin, A.; Hoffmann, M. R., The Role of Metal Ion Dopants in Quantum-Sized Tio2: Correlation between Photoreactivity and Charge Carrier Recombination Dynamics. *Journal of Physical Chemistry* **1994**, *98*, 13669-13679.

72. Liqiang, J.; Yichun, Q.; Baiqi, W.; Shudan, L.; Baojiang, J.; Libin, Y.; Wei, F.; Honggang, F.; Jiazhong, S., Review of Photoluminescence Performance of Nano-Sized Semiconductor Materials and Its Relationships with Photocatalytic Activity. *Solar Energy Materials and Solar Cells* **2006**, *90*, 1773-1787.
73. Jeurgens, L. P. H.; Sloof, W. G.; Tichelaar, F. D.; Mittemeijer, E. J., Growth Kinetics and Mechanisms of Aluminum-Oxide Films Formed by Thermal Oxidation of Aluminum. *J Appl Phys* **2002**, *92*, 1649-1656.
74. Klootwijk, J. H., et al., Ultrahigh Capacitance Density for Multiple Ald-Grown Mim Capacitor Stacks in 3-D Silicon. *IEEE Electron Device Letters* **2008**, *29*, 740-742.
75. Robertson, J., High Dielectric Constant Gate Oxides for Metal Oxide Si Transistors. *Reports on Progress in Physics* **2006**, *69*, 327-396.
76. Hickmott, T. W., Electrolyte Effects on Charge, Polarization, and Conduction in Thin Anodic Al2o3 Films. I. Initial Charge and Temperature-Dependent Polarization. *J Appl Phys* **2007**, *102*, 093706.
77. Buff, H., Ueber Das Electrische Verhalten Des Aluminiums. *Justus Liebigs Annalen der Chemie* **1857**, *102*, 265-284.
78. Wheatstone, C., Lxxviii. On the Thermo-Electric Spark. *Philosophical Magazine Series 3* **1837**, *10*, 414-417.
79. Wöhler, F.; Buff, H., Ueber Eine Verbindung Von Silicium Mit Wasserstoff. *Justus Liebigs Annalen der Chemie* **1857**, *103*, 218-229.
80. Ducretet, E., Note Sur Un Rhéotome Liquide À Direction Constante, Fondé Sur Une Propriété Nouvelle De L'aluminium. *J. Phys. Theor. Appl.* **1875**, *4*, 84-85.
81. Norden, K., Über Den Vorgang an Der Aluminiumanode. *Zeitschrift für Elektrochemie* **1899**, *6*, 159-167.
82. Walkenhorst, W., Ein Einfaches Verfahren Zur Herstellung Strukturloser Trägerschichten Aus Aluminiumoxyd. *Naturwissenschaften* **1947**, *34*, 373-373.
83. Georgiev, A. M., *The Electrolytic Capacitor*; Technical Division, Murray Hill Books, Inc.: New York; Toronto, 1967.
84. Wood, G. C.; O'Sullivan, J. P., The Anodizing of Aluminium in Sulphate Solutions. *Electrochimica Acta* **1970**, *15*, 1865-1876.
85. Wood, G. C.; O'Sullivarv, J. P., Electron- Optical Examination of Sealed Anodic Alumina Films: Surface and Interior Effects. *Journal of The Electrochemical Society* **1969**, *116*, 1351-1357.
86. Xu, Y.; Thompson, G. E.; Wood, G. C.; Bethune, B., Anion Incorporation and Migration During Barrier Film Formation on Aluminium. *Corrosion Science* **1987**, *27*, 83-102.
87. Pullen, N. D., An Anodic Treatment for the Production of Aluminium Reflectors. *Journal of the Institute of Metals* **1936**, *151*.
88. Hussein, R. O.; Northwood, D. O.; Nie, X., The Effect of Processing Parameters and Substrate Composition on the Corrosion Resistance of Plasma Electrolytic Oxidation (Peo) Coated Magnesium Alloys. *Surface and Coatings Technology* **2013**, *237*, 357-368.
89. Behin, J.; Bukhari, S. S.; Dehnavi, V.; Kazemian, H.; Rohani, S., Using Coal Fly Ash and Wastewater for Microwave Synthesis of Lta Zeolite. *Chemical Engineering & Technology* **2014**, *37*, 1532-1540.
90. Walsh, F. C.; Low, C. T. J.; Wood, R. J. K.; Stevens, K. T.; Archer, J.; Poeton, A. R.; Ryder, A., Plasma Electrolytic Oxidation (Peo) for Production of Anodised Coatings on Lightweight Metal (Al, Mg, Ti) Alloys. *Transactions of the IMF* **2009**, *87*, 122-135.

91. Liu, Y.; Xu, J.; Gao, Y.; Yuan, Y.; Gao, C., Influences of Additive on the Formation and Corrosion Resistance of Micro-Arc Oxidation Ceramic Coatings on Aluminum Alloy. *Physics Procedia* **2012**, *32*, 107-112.
92. Voevodin, A. A.; Yerokhin, A. L.; Lyubimov, V. V.; Donley, M. S.; Zabinski, J. S., Characterization of Wear Protective Al · Si · O Coatings Formed on Al-Based Alloys by Micro-Arc Discharge Treatment. *Surface and Coatings Technology* **1996**, *86-87*, 516-521.
93. Yerokhin, A. L.; Voevodin, A. A.; Lyubimov, V. V.; Zabinski, J.; Donley, M., Plasma Electrolytic Fabrication of Oxide Ceramic Surface Layers for Tribotechnical Purposes on Aluminium Alloys. *Surface and Coatings Technology* **1998**, *110*, 140-146.
94. Bajat, J. B.; Vasilić, R.; Stojadinović, S.; Mišković-Stanković, V., Corrosion Stability of Oxide Coatings Formed by Plasma Electrolytic Oxidation of Aluminum: Optimization of Process Time. *CORROSION* **2013**, *69*, 693-702.
95. Barik, R. C.; Wharton, J. A.; Wood, R. J. K.; Stokes, K. R.; Jones, R. L., Corrosion, Erosion and Erosion–Corrosion Performance of Plasma Electrolytic Oxidation (Peo) Deposited Al2o3 Coatings. *Surface and Coatings Technology* **2005**, *199*, 158-167.
96. Matykina, E.; Arrabal, R.; Scurr, D. J.; Baron, A.; Skeldon, P.; Thompson, G. E., Investigation of the Mechanism of Plasma Electrolytic Oxidation of Aluminium Using 18o Tracer. *Corrosion Science* **2010**, *52*, 1070-1076.
97. Sreekanth, D.; Rameshbabu, N.; Venkateswarlu, K., Effect of Various Additives on Morphology and Corrosion Behavior of Ceramic Coatings Developed on Az31 Magnesium Alloy by Plasma Electrolytic Oxidation. *Ceramics International* **2012**, *38*, 4607-4615.
98. Matykina, E.; Arrabal, R.; Skeldon, P.; Thompson, G. E., Investigation of the Growth Processes of Coatings Formed by Ac Plasma Electrolytic Oxidation of Aluminium. *Electrochimica Acta* **2009**, *54*, 6767-6778.
99. Alanazi, N. M.; Leyland, A.; Yerokhin, A. L.; Matthews, A., Substitution of Hexavalent Chromate Conversion Treatment with a Plasma Electrolytic Oxidation Process to Improve the Corrosion Properties of Ion Vapour Deposited Almg Coatings. *Surface and Coatings Technology* **2010**, *205*, 1750-1756.
100. Shokouhfar, M.; Dehghanian, C.; Montazeri, M.; Baradaran, A., Preparation of Ceramic Coating on Ti Substrate by Plasma Electrolytic Oxidation in Different Electrolytes and Evaluation of Its Corrosion Resistance: Part Ii. *Applied Surface Science* **2012**, *258*, 2416-2423.
101. Zhang, X.; Zhang, Y.; Chang, L.; Jiang, Z.; Yao, Z.; Liu, X., Effects of Frequency on Growth Process of Plasma Electrolytic Oxidation Coating. *Materials Chemistry and Physics* **2012**, *132*, 909-915.
102. Hussein, R. O.; Zhang, P.; Nie, X.; Xia, Y.; Northwood, D. O., The Effect of Current Mode and Discharge Type on the Corrosion Resistance of Plasma Electrolytic Oxidation (Peo) Coated Magnesium Alloy Aj62. *Surface and Coatings Technology* **2011**, *206*, 1990-1997.
103. Lee, J.; Kim, Y.; Chung, W., Effect of Ar Bubbling During Plasma Electrolytic Oxidation of Az31b Magnesium Alloy in Silicate Electrolyte. *Applied Surface Science* **2012**, *259*, 454-459.
104. Chen, M.-a.; Liu, S.-y.; Li, J.-m.; Cheng, N.; Zhang, X.-m., Improvement to Corrosion Resistance of Mao Coated 2519 Aluminum Alloy by Formation of Polypropylene Film on Its Surface. *Surface and Coatings Technology* **2013**, *232*, 674-679.
105. Yerokhin, A. L.; Snizhko, L. O.; Gurevina, N. L.; Leyland, A.; Pilkington, A.; Matthews, A., Discharge Characterization in Plasma Electrolytic Oxidation of Aluminium. *Journal of Physics D: Applied Physics* **2003**, *36*, 2110.

106. Xu, D.; Xu, Y.; Chen, D.; Guo, G.; Gui, L.; Tang, Y., Preparation of Cds Single-Crystal Nanowires by Electrochemically Induced Deposition. *Advanced Materials* **2000**, *12*, 520-522.
107. Jacobs, H. O.; Knapp, H. F.; Muller, S.; Stemmer, A., Surface Potential Mapping: A Qualitative Material Contrast in Spm. *Ultramicroscopy* **1997**, *69*, 39-49.
108. Nonnenmacher, M.; O'Boyle, M. P.; Wickramasinghe, H. K., Kelvin Probe Force Microscopy. *Applied Physics Letters* **1991**, *58*, 2921-2923.
109. Berger, R.; Butt, H. J.; Retschke, M. B.; Weber, S. A., Electrical Modes in Scanning Probe Microscopy. *Macromol Rapid Commun* **2009**, *30*, 1167-78.
110. Sakai, Y., Surface Properties of Cement Paste Evaluated by Scanning Probe Microscopy. *Open Journal of Civil Engineering* **2016**, *06*, 643-652.
111. Koley, G.; Spencer, M. G., Surface Potential Measurements on Gan and Algan/Gan Heterostructures by Scanning Kelvin Probe Microscopy. *J Appl Phys* **2001**, *90*, 337-344.
112. Kelvin, L., V. Contact Electricity of Metals. *Philosophical Magazine* **1898**, *46*, 82-120.
113. Rohwerder, M.; Turcu, F., High-Resolution Kelvin Probe Microscopy in Corrosion Science: Scanning Kelvin Probe Force Microscopy (Skpfm) Versus Classical Scanning Kelvin Probe (Skp). *Electrochimica Acta* **2007**, *53*, 290-299.
114. Yee, S.; Oriani, R. A.; Stratmann, M., Application of a Kelvin Microprobe to the Corrosion of Metals in Humid Atmospheres. *Journal of The Electrochemical Society* **1991**, *138*, 55-61.
115. Yasakau, K. A.; Zheludkevich, M. L.; Lamaka, S. V.; Ferreira, M. G., Mechanism of Corrosion Inhibition of Aa2024 by Rare-Earth Compounds. *J Phys Chem B* **2006**, *110*, 5515-28.
116. Zheludkevich, M. L.; Yasakau, K. A.; Poznyak, S. K.; Ferreira, M. G. S., Triazole and Thiazole Derivatives as Corrosion Inhibitors for Aa2024 Aluminium Alloy. *Corrosion Science* **2005**, *47*, 3368-3383.
117. Schmutz, P.; Frankel, G. S., Characterization of Aa2024- T3 by Scanning Kelvin Probe Force Microscopy. *Journal of The Electrochemical Society* **1998**, *145*, 2285-2295.
118. Lambert, J.; Guthmann, C.; Ortega, C.; Saint-Jean, M., Permanent Polarization and Charge Injection in Thin Anodic Alumina Layers Studied by Electrostatic Force Microscopy. *J Appl Phys* **2002**, *91*, 9161.
119. Hickmott, T. W., Polarization and Fowler–Nordheim Tunneling in Anodized Al–Al2o3–Au Diodes. *J Appl Phys* **2000**, *87*, 7903-7912.
120. Yasakau, K. A.; Salak, A. N.; Zheludkevich, M. L.; Ferreira, M. r. G. S., Volta Potential of Oxidized Aluminum Studied by Scanning Kelvin Probe Force Microscopy. *The Journal of Physical Chemistry C* **2010**, *114*, 8474-8484.
121. Jørgensen, M. J.; Mogensen, M., Impedance of Solid Oxide Fuel Cell Lsm/Ysz Composite Cathodes. *Journal of The Electrochemical Society* **2001**, *148*, A433-A442.
122. Suzuki, T.; Jasinski, P.; Petrovsky, V.; Dogan, F.; Anderson, H. U., The Microstructure Effect on the Electrical and Optical Properties of Undoped and Sr-Doped Smcoo3 Thin Films. *Solid State Ionics* **2004**, *175*, 437-439.
123. Macdonald, J. R., Impedance Spectroscopy. *Annals of Biomedical Engineering* **1992**, *20*, 289-305.
124. Macdonald, J. R., *Impedance Spectroscopy*; Vol. 11.
125. Zoltowski, P., On the Electrical Capacitance of Interfaces Exhibiting Constant Phase Element Behaviour. *Journal of Electroanalytical Chemistry* **1998**, *443*, 149-154.
126. Hirschorn, B.; Orazem, M. E.; Tribollet, B.; Vivier, V.; Frateur, I.; Musiani, M., Determination of Effective Capacitance and Film Thickness from Constant-Phase-Element Parameters. *Electrochimica Acta* **2010**, *55*, 6218-6227.

127. Lisenkov, A. D.; Salak, A. N.; Poznyak, S. K.; Zheludkevich, M. L.; Ferreira, M. G. S., Anodic Alumina Films Prepared by Powerful Pulsed Discharge Oxidation. *Journal of Physical Chemistry C* **2011**, *115*, 18634-18639.
128. Lisenkov, A. D.; Poznyak, S. K.; Montemor, M. F.; Carmezim, M. J.; Zheludkevich, M. L.; Ferreira, M. G. S., Titania Films Obtained by Powerful Pulsed Discharge Oxidation in Phosphoric Acid Electrolytes. *Journal of the Electrochemical Society* **2014**, *161*, D73-D78.
129. Long, M.; Rack, H. J., Titanium Alloys in Total Joint Replacement—a Materials Science Perspective. *Biomaterials* **1998**, *19*, 1621-1639.
130. Miller, K.; Nalwa, K. S.; Bergerud, A.; Neihart, N. M.; Chaudhary, S., Memristive Behavior in Thin Anodic Titania. *IEEE Electron Device Letters* **2010**, *31*, 737-739.
131. Strukov, D. B.; Snider, G. S.; Stewart, D. R.; Williams, R. S., The Missing Memristor Found. *Nature* **2008**, *453*, 80-83.
132. Piazza, S.; Calá, L.; Sunseri, C.; Di Quarto, F., Influence of the Crystallization Process on the Photoelectrochemical Behaviour of Anodic Tio2 Films. *Berichte der Bunsengesellschaft für physikalische Chemie* **1997**, *101*, 932-942.
133. Diamanti, M. V.; Pedeferri, M. P., Effect of Anodic Oxidation Parameters on the Titanium Oxides Formation. *Corrosion Science* **2007**, *49*, 939-948.
134. Blackwood, D. J.; Peter, L. M., The Influence of Growth-Rate on the Properties of Anodic Oxide-Films on Titanium. *Electrochimica Acta* **1989**, *34*, 1505-1511.
135. Shibata, T.; Zhu, Y. C., The Effect of Film Formation Conditions on the Structure and Composition of Anodic Oxide Films on Titanium. *Corrosion Science* **1995**, *37*, 253-270.
136. Ohtsuka, T.; Nomura, N., The Dependence of the Optical Property of Ti Anodic Oxide Film on Its Growth Rate by Ellipsometry. *Corrosion Science* **1997**, *39*, 1253-1263.
137. Mikula, M.; Blecha, J.; Čeppan, M., Photoelectrochemical Properties of Anodic Tio2 Layers Prepared by Various Current Densities. *Journal of The Electrochemical Society* **1992**, *139*, 3470-3474.
138. Kozlowski, M. R.; Tyler, P. S.; Smyrl, W. H.; Atanasoski, R. T., Photoelectrochemical Microscopy of Oxide Films on Metals: Ti/Tio2 Interface. *Surface Science* **1988**, *194*, 505-530.
139. Suay, J. J.; Giménez, E.; Rodríguez, T.; Habbib, K.; Saura, J. J., Characterization of Anodized and Sealed Aluminium by Eis. *Corrosion Science* **2003**, *45*, 611-624.
140. Bonnel, K.; Le Pen, C.; Pébère, N., E.I.S. Characterization of Protective Coatings on Aluminium Alloys. *Electrochimica Acta* **1999**, *44*, 4259-4267.
141. Girginov, A.; Popova, A.; Kanazirski, I.; Zahariev, A., Characterization of Complex Anodic Alumina Films by Electrochemical Impedance Spectroscopy. *Thin Solid Films* **2006**, *515*, 1548-1551.
142. Bardwell, J. A.; McKubre, M. C. H., Ac Impedance Spectroscopy of the Anodic Film on Zirconium in Neutral Solution. *Electrochimica Acta* **1991**, *36*, 647-653.
143. Di Quarto, F.; Piazza, S.; Sunseri, C., Amorphous Semiconductor—Electrolyte Junction. Impedance Study on the a-Nb2 O5—Electrolyte Junction. *Electrochimica Acta* **1990**, *35*, 99-107.
144. Blackwood, D. J., Influence of the Space-Charge Region on Electrochemical Impedance Measurements on Passive Oxide Films on Titanium. *Electrochimica Acta* **2000**, *46*, 563-569.
145. Pan, J.; Thierry, D.; Leygraf, C., Electrochemical Impedance Spectroscopy Study of the Passive Oxide Film on Titanium for Implant Application. *Electrochimica Acta* **1996**, *41*, 1143-1153.

146. Marsh, J.; Gorse, D., A Photoelectrochemical and Ac Impedance Study of Anodic Titanium Oxide Films. *Electrochimica Acta* **1998**, *43*, 659-670.
147. Birch, J. R.; Burleigh, T. D., Oxides Formed on Titanium by Polishing, Etching, Anodizing, or Thermal Oxidizing. *Corrosion* **2000**, *56*, 1233-1241.
148. Souza, M. E. P.; Ballester, M.; Freire, C. M. A., Eis Characterisation of Ti Anodic Oxide Porous Films Formed Using Modulated Potential. *Surface and Coatings Technology* **2007**, *201*, 7775-7780.
149. Jaeggi, C.; Kern, P.; Michler, J.; Zehnder, T.; Siegenthaler, H., Anodic Thin Films on Titanium Used as Masks for Surface Micropatterning of Biomedical Devices. *Surface and Coatings Technology* **2005**, *200*, 1913-1919.
150. Mantzila, A. G.; Prodromidis, M. I., Development and Study of Anodic Ti/Tio2 Electrodes and Their Potential Use as Impedimetric Immunosensors. *Electrochimica Acta* **2006**, *51*, 3537-3542.
151. Ibriş, N.; Mirza Rosca, J. C., Eis Study of Ti and Its Alloys in Biological Media. *Journal of Electroanalytical Chemistry* **2002**, *526*, 53-62.
152. González, J. E. G.; Mirza-Rosca, J. C., Study of the Corrosion Behavior of Titanium and Some of Its Alloys for Biomedical and Dental Implant Applications. *Journal of Electroanalytical Chemistry* **1999**, *471*, 109-115.
153. Fonseca, C.; Barbosa, M. A., Corrosion Behaviour of Titanium in Biofluids Containing H2o2 Studied by Electrochemical Impedance Spectroscopy. *Corrosion Science* **2001**, *43*, 547-559.
154. Hodgson, A. W. E.; Mueller, Y.; Forster, D.; Virtanen, S., Electrochemical Characterisation of Passive Films on Ti Alloys under Simulated Biological Conditions. *Electrochimica Acta* **2002**, *47*, 1913-1923.
155. Silva, T. M.; Rito, J. E.; Simões, A. M. P.; Ferreira, M. G. S.; da Cunha Belo, M.; Watkins, K. G., Electrochemical Characterisation of Oxide Films Formed on Ti · 6a1 · 4v Alloy Implanted with Ir for Bioengineering Applications. *Electrochimica Acta* **1998**, *43*, 203-211.
156. Schneider, M.; Schroth, S.; Schilm, J.; Michaelis, A., Micro-Eis of Anodic Thin Oxide Films on Titanium for Capacitor Applications. *Electrochimica Acta* **2009**, *54*, 2663-2671.
157. Simons, W.; Hubin, A.; Vereecken, J., The Role of Electrochemical Impedance Spectroscopy (Eis) in the Global Characterisation of the Reduction Kinetics of Hexacyanoferrate on Anodised Titanium. *Electrochimica Acta* **1999**, *44*, 4373-4381.
158. Gnedenkov, S. V.; Sinebryukhov, S. L.; Sergienko, V. I., Electrochemical Impedance Simulation of a Metal Oxide Heterostructure/Electrolyte Interface: A Review. *Russian Journal of Electrochemistry* **2006**, *42*, 197-211.
159. Van Gils, S.; Mast, P.; Stijns, E.; Terryn, H., Colour Properties of Barrier Anodic Oxide Films on Aluminium and Titanium Studied with Total Reflectance and Spectroscopic Ellipsometry. *Surface and Coatings Technology* **2004**, *185*, 303-310.
160. Piazza, S.; Cala, L.; Sunseri, C.; DiQuarto, F., Influence of the Crystallization Process on the Photoelectrochemical Behaviour of Anodic Tio2 Films. *Ber Bunsen Phys Chem* **1997**, *101*, 932-942.
161. Blondeau, G.; Froelicher, M.; Froment, M.; Hugot-Le Goff, A., On the Optical Indices of Oxide Films as a Function of Their Crystallization: Application to Anodic Tio2 (Anatase). *Thin Solid Films* **1977**, *42*, 147-153.

162. Kozlowski, M.; Smyrl, W. H.; Atanasoska, L.; Atanasoski, R., Local Film Thickness and Photoresponse of Thin Anodic Tio2 Films on Polycrystalline Titanium. *Electrochimica Acta* **1989**, *34*, 1763-1768.
163. McAleer, J. F.; Peter, L. M., Photocurrent Spectroscopy of Anodic Oxide Films on Titanium. *Faraday Discussions of the Chemical Society* **1980**, *70*, 67.
164. Stimming, U., Photoelectrochemical Studies of Passive Films. *Electrochimica Acta* **1986**, *31*, 415-429.
165. Láng, G.; Heusler, K. E., Remarks on the Energetics of Interfaces Exhibiting Constant Phase Element Behaviour. *Journal of Electroanalytical Chemistry* **1998**, *457*, 257-260.
166. Hsu, C. H.; Mansfeld, F., Technical Note:Concerning the Conversion of the Constant Phase Element Parameter Y0into a Capacitance. *Corrosion* **2001**, *57*, 747-748.
167. Quarto, F. D.; Sunseri, C.; Piazza, S., Amorphous Semiconductor-Electrolyte Junction. A New Interpretation of the Impedance Data of Amorphous Semiconducting Films on Metals. *Berichte der Bunsengesellschaft für physikalische Chemie* **1986**, *90*, 549-555.
168. da Fonseca, C.; Guerreiro Ferreira, M.; da Cunha Belo, M., Modelling of the Impedance Behaviour of an Amorphous Semiconductor Schottky Barrier in High Depletion Conditions. Application to the Study of the Titanium Anodic Oxide/Electrolyte Junction. *Electrochimica Acta* **1994**, *39*, 2197-2205.
169. Badawy, W. A., Electrochemical and Photoelectrochemical Behaviour of Passivated Niobium Electrodes During Hydrogen Evolution. *Journal of Applied Electrochemistry* **1990**, *20*, 139-144.
170. de-Sá, A. I.; Rangel, C. M.; Skeldon, P.; Thompson, G. E., Semiconductive Properties of Anodic Niobium Oxides. *Portugaliae Electrochimica Acta* **2006**, *24*, 305-311.
171. Metikoš-Huković, M.; Omanović, S.; Jukić, A., Impedance Spectroscopy of Semiconducting Films on Tin Electrodes. *Electrochimica Acta* **1999**, *45*, 977-986.
172. Sikora, J.; Sikora, E.; Macdonald, D. D., The Electronic Structure of the Passive Film on Tungsten. *Electrochimica Acta* **2000**, *45*, 1875-1883.
173. Schultze, J. W.; Stimming, U.; Weise, J., Capacity and Photocurrent Measurements at Passive Titanium Electrodes. *Berichte der Bunsengesellschaft für physikalische Chemie* **1982**, *86*, 276-282.
174. Lee, E.-J.; Pyun, S.-I., Analysis of Nonlinear Mott-Schottky Plots Obtained from Anodically Passivating Amorphous and Polycrystalline Tio2 Films. *Journal of Applied Electrochemistry* **1992**, *22*, 156-160.
175. Allard, K. D.; Ahrens, M.; Heusler, K. E., Wachstum Und Auflösung Anodisch Erzeugter Oxidschichten Auf Titan. *Materials and Corrosion* **1975**, *26*, 694-699.
176. Zane, D.; Decker, F.; Razzini, G., Characterization of Electrodeposited Tio2 Films. *Electrochimica Acta* **1993**, *38*, 37-42.
177. Khan, S. U. M.; Schmickler, W., The Capacity of Thin Passive Films. *Journal of Electroanalytical Chemistry and Interfacial Electrochemistry* **1980**, *108*, 329-334.
178. McAleer, J. F., Instability of Anodic Oxide Films on Titanium. *Journal of The Electrochemical Society* **1982**, *129*, 1252.
179. Hurlen, T.; Hornkjøl, S., Anodic Growth of Passive Films on Titanium. *Electrochimica Acta* **1991**, *36*, 189-195.
180. Leitner, K., Photoelectrochemical Investigations of Passive Films on Titanium Electrodes. *Journal of The Electrochemical Society* **1986**, *133*, 1561.

181. Habazaki, H.; Uozumi, M.; Konno, H.; Shimizu, K.; Skeldon, P.; Thompson, G. E., Crystallization of Anodic Titania on Titanium and Its Alloys. *Corrosion Science* **2003**, *45*, 2063-2073.
182. Thompson, G. E.; Xu, Y.; Skeldon, P.; Shimizu, K.; Han, S. H.; Wood, G. C., Anodic Oxidation of Aluminium. *Philosophical Magazine Part B* **1987**, *55*, 651-667.
183. Despić, A.; Parkhutik, V. P., Electrochemistry of Aluminum in Aqueous Solutions and Physics of Its Anodic Oxide. In *Modern Aspects of Electrochemistry*, J. O'M. Bockris, R. E. W., B. E. Conway Ed. 1989; Vol. 20, pp 401-503.
184. Ozawa, K.; Majima, T., Anodization Behavior of Al, and Physical and Electrical Characterization of Its Oxide Films. *J Appl Phys* **1996**, *80*, 5828-5836.
185. Uchi, H.; Kanno, T.; Alwitt, R. S., Structural Features of Crystalline Anodic Alumina Films. *Journal of The Electrochemical Society* **2001**, *148*, B17-B23.
186. Geiculescu, A. C.; Strange, T. F., Aluminum Oxide Thin Dielectric Film Formation under Elevated Gravity Conditions. *Thin Solid Films* **2006**, *503*, 45-54.
187. McCafferty, E., The Electrode Kinetics of Pit Initiation on Aluminum. *Corrosion Science* **1995**, *37*, 481-492.
188. Hausbrand, R.; Stratmann, M.; Rohwerder, M., The Physical Meaning of Electrode Potentials at Metal Surfaces and Polymer/Metal Interfaces: Consequences for Delamination. *Journal of The Electrochemical Society* **2008**, *155*, C369-C379.
189. Yasutake, M.; Aoki, D.; Fujihira, M., Surface Potential Measurements Using the Kelvin Probe Force Microscope. *Thin Solid Films* **1996**, *273*, 279-283.
190. Tanem, B. S.; Svenningsen, G.; Mardalen, J., Relations between Sample Preparation and Skpfm Volta Potential Maps on an En Aw-6005 Aluminium Alloy. *Corrosion Science* **2005**, *47*, 1506-1519.
191. Goodman, A. M., Photoemission of Holes and Electrons from Aluminum into Aluminum Oxide. *J Appl Phys* **1970**, *41*, 2176-2179.
192. Nakamura, R.; Shudo, T.; Hirata, A.; Ishimaru, M.; Nakajima, H., Nanovoid Formation through the Annealing of Amorphous Al2o3 and Wo3 Films. *Scripta Materialia* **2011**, *64*, 197-200.
193. Novikov, Y. N.; Vishnyakov, A. V.; Gritsenko, V. A.; Nasyrov, K. A.; Wong, H., Modeling the Charge Transport Mechanism in Amorphous Al2o3 with Multiphonon Trap Ionization Effect. *Microelectronics Reliability* **2010**, *50*, 207-210.
194. Luckey HA, K. F., *Titanium Alloys in Surgical Implants*; ASTM, 1983.
195. Pletcher, D.; Greff, R.; Peat, R.; Peter, L. M.; Robinson, J., 6 - Potential Sweep Techniques and Cyclic Voltammetry. In *Instrumental Methods in Electrochemistry*, Woodhead Publishing: 2010; pp 178-228.
196. Marino, C. E. B.; Mascaro, L. H., Eis Characterization of a Ti-Dental Implant in Artificial Saliva Media: Dissolution Process of the Oxide Barrier. *Journal of Electroanalytical Chemistry* **2004**, *568*, 115-120.
197. Qiu, J.; Dominici, J. T.; Lifland, M. I.; Okazaki, K., Composite Titanium Dental Implant Fabricated by Electro-Discharge Compaction. *Biomaterials* **1997**, *18*, 153-160.
198. Cámara, O. R.; de Pauli, C. P.; Vaschetto, M. E.; Retamal, B.; Aquirre, M. J.; Zagal, J. H.; Biaggio, S. R., Semiconducting Properties of Tio2 Films Thermally Formed at 400° C. *Journal of Applied Electrochemistry* **1995**, *25*, 247-251.

199. Park, J.-W.; Jang, J.-H.; Lee, C. S.; Hanawa, T., Osteoconductivity of Hydrophilic Microstructured Titanium Implants with Phosphate Ion Chemistry. *Acta Biomater* **2009**, *5*, 2311-2321.
200. Perre, E.; Taberna, P. L.; Mazouzi, D.; Poizot, P.; Gustafsson, T.; Edström, K.; Simon, P., Electrodeposited Cu2sb as Anode Material for 3-Dimensional Li-Ion Microbatteries. *Journal of Materials Research* **2010**, *25*, 1485-1491.
201. Matykina, E.; Arrabal, R.; Skeldon, P.; Thompson, G. E., Transmission Electron Microscopy of Coatings Formed by Plasma Electrolytic Oxidation of Titanium. *Acta Biomater* **2009**, *5*, 1356-66.
202. Park, D.; Kim, H., Electrochemical Etching of Aluminum through Porous Alumina. *Analytical Sciences/Supplements* **2001**, *17asia*, a73-a76.
203. Mokaddem, M.; Tardelli, J.; Ogle, K.; Rocca, E.; Volovitch, P., Atomic Emission Spectroelectrochemical Investigation of the Anodization of Aa7050t74 Aluminum Alloy. *Electrochem Commun* **2011**, *13*, 42-45.
204. Rogers, G. T.; Draper, P. H. G.; Wood, S. S., Anion Impurities in Anodic Oxide Films on Zirconium. *Electrochimica Acta* **1968**, *13*, 251-261.
205. Gileadi, E., *Electrode Kinetics for Chemists, Chemical Engineers, and Material Scientists. Von E. Gileadi. Vch Verlagsgesellschaft, Weinheim/Vch Publishers, New York, 1993. 597 S., Geb. 189.00 Dm. — Isbn 3-527-89561-2/1-56081-561-2*, 1994; Vol. 106, p 839.
206. Skeldon, P.; Skeldon, M.; Thompson, G. E.; Wood, G. C., Incorporation of Tungsten and Molybdenum into Anodic Alumina Films. *Philosophical Magazine Part B* **1989**, *60*, 513-521.
207. Chang, N.; Zhang, H.; Shi, M.-S.; Li, J.; Shao, W.; Wang, H.-T., Metal-Organic Framework Templated Synthesis of Tio2@Mil-101 Core-Shell Architectures for High-Efficiency Adsorption and Photocatalysis. *Mater Lett* **2017**, *200*, 55-58.
208. Krysiak, E.; Wypych-Puszkarz, A.; Krysiak, K.; Nowaczyk, G.; Makrocka-Rydzyk, M.; Jurga, S.; Ulanski, J., Core–Shell System Based on Titanium Dioxide with Elevated Value of Dielectric Permittivity: Synthesis and Characterization. *Synthetic Metals* **2015**, *209*, 150-157.
209. Maia, F.; Tedim, J.; Lisenkov, A. D.; Salak, A. N.; Zheludkevich, M. L.; Ferreira, M. G. S., Silica Nanocontainers for Active Corrosion Protection. *Nanoscale* **2012**, *4*, 1287-1298.
210. Park, J.-B.; Ham, J.-S.; Shin, M.-S.; Park, H.-K.; Lee, Y.-J.; Lee, S.-M., Synthesis and Electrochemical Characterization of Anode Material With titanium–Silicon Alloy Solid Core/Nanoporous Silicon Shell Structures for Lithium Rechargeable Batteries. *J Power Sources* **2015**, *299*, 537-543.
211. Zhao, L.; Sun, C.; Tian, G.; Pang, Q., Multiple-Shell Znse Core-Shell Spheres and Their Improved Photocatalytic Activity. *Journal of Colloid and Interface Science* **2017**, *502*, 1-7.
212. De Bonis, A.; Santagata, A.; Galasso, A.; Laurita, A.; Teghil, R., Formation of Titanium Carbide (Tic) and Tic@C Core-Shell Nanostructures by Ultra-Short Laser Ablation of Titanium Carbide and Metallic Titanium in Liquid. *Journal of Colloid and Interface Science* **2017**, *489*, 76-84.
213. Jiang, J.; Zhou, H.; Zhang, F.; Fan, T.; Zhang, D., Hydrothermal Synthesis of Core–Shell Tio2 to Enhance the Photocatalytic Hydrogen Evolution. *Applied Surface Science* **2016**, *368*, 309-315.
214. Kim, G. H.; Park, S. H.; Birajdar, M. S.; Lee, J.; Hong, S. C., Core/Shell Structured Carbon Nanofiber/Platinum Nanoparticle Hybrid Web as a Counter Electrode for Dye-Sensitized Solar Cell. *Journal of Industrial and Engineering Chemistry* **2017**, *52*, 211-217.

215. Poznyak, S. K.; Lisenkov, A. D.; Ferreira, M. G. S.; Kulak, A. I.; Zheludkevich, M. L., Impedance Behaviour of Anodic Tio2 Films Prepared by Galvanostatic Anodisation and Powerful Pulsed Discharge in Electrolyte. *Electrochimica Acta* **2012**, *76*, 453-461.
216. Liu, N.; Mirabolghasemi, H.; Lee, K.; Albu, S. P.; Tighineanu, A.; Altomare, M.; Schmuki, P., Anodic Tio2 Nanotubes: Double Walled Vs. Single Walled. *Faraday Discussions* **2013**, *164*, 107-116.
217. Endres, F.; MacFarlane, D.; Abbott, A., Electrodeposition from Ionic Liquids. John Wiley & Sons: 2008.
218. Tsuda, T.; Hussey, C. L.; Stafford, G. R.; Bonevich, J. E., Electrochemistry of Titanium and the Electrodeposition of Al-Ti Alloys in the Lewis Acidic Aluminum Chloride–1-Ethyl-3-Methylimidazolium Chloride Melt. *Journal of the Electrochemical Society* **2003**, *150*, C234.
219. Perre, E. Nano-Structured 3d Electrodes for Li-Ion Micro-Batteries. *Uppsala University*, Uppsala, 2010.
220. Perre, E.; Nyholm, L.; Gustafsson, T.; Taberna, P.-L.; Simon, P.; Edström, K., Direct Electrodeposition of Aluminium Nano-Rods. *Electrochem Commun* **2008**, *10*, 1467-1470.
221. Lisenkov, A. D.; Poznyak, S. K.; Zheludkevich, M. L.; Ferreira, M. G. S., Aluminum Anodization in Deionized Water as Electrolyte. *Journal of The Electrochemical Society* **2016**, *163*, C364-C368.

# 9 Attachments

Electrochimica Acta 76 (2012) 453–461

Contents lists available at SciVerse ScienceDirect

Electrochimica Acta

journal homepage: www.elsevier.com/locate/electacta

# Impedance behaviour of anodic $TiO_2$ films prepared by galvanostatic anodisation and powerful pulsed discharge in electrolyte

S.K. Poznyak[a,b,*], A.D. Lisenkov[a], M.G.S. Ferreira[a], A.I. Kulak[c], M.L. Zheludkevich[a]

[a] University of Aveiro, CICECO, Dep. Ceramics and Glass Eng., 3810-193 Aveiro, Portugal
[b] Research Institute for Physical Chemical Problems, Belarusian State University, 220030 Minsk, Belarus
[c] Institute of General and Inorganic Chemistry, National Academy of Sciences of Belarus, 220072 Minsk, Belarus

ARTICLE INFO

*Article history:*
Received 5 February 2012
Received in revised form 15 May 2012
Accepted 19 May 2012
Available online 29 May 2012

*Keywords:*
Anodic films
Titanium dioxide
Pulsed discharge
EIS
Photocurrent

ABSTRACT

Anodic titania films were prepared on titanium by novel powerful pulsed discharge technique which confers extremely high rates of the film growth. Electrochemical impedance spectroscopy (EIS) has been used as a main method to study the structure and semiconductive properties of the anodic oxide films grown in sulphuric acid electrolyte. The EIS results are supported with microscopic observations and photoelectrochemical measurements. For comparison, the properties of the anodic films prepared by the conventional galvanostatic anodisation in the same electrolyte were also examined. For modeling of the impedance spectra, different equivalent circuits taking into account the effects of space charge region and film structure were proposed. Thinner anodic films ($d \approx 25$ nm) prepared by both methods demonstrate a similar behaviour characteristic of amorphous barrier-type oxide, whereas a very significant difference in the properties of the films produced by the two different approaches was revealed for thicker films ($d = 70$–$120$ nm). The discharge-prepared films in this range of thickness are composed by one compact layer with a relatively low concentration of ionised donors ($N_d = (1–3) \times 10^{18}$ cm$^{-3}$) estimated from Mott–Schottky plots, whilst the conventional galvanostatic method leads to the development of two-layer films consisting of an inner compact layer and a nanoporous outer one. The latter samples exhibit a significantly reduced photocurrent response at short wavelengths and an essentially higher concentration of ionised donors as compared with the films obtained by the pulsed discharge method.


## 1. Introduction

Titanium and its alloys are widely used in different applications owing to their good mechanical properties and a high corrosion resistance in various media [1–3]. The latter is provided by a chemically stable oxide film which spontaneously forms on titanium. Electrochemical oxidation (anodisation) of titanium and its alloys provides thicker oxide layers demonstrating improved protective and functional properties [4,5]. Thin films of titania have very high potential to be used for fabrication of memristors [6]. The memristance arises naturally in nanoscale systems in which solid-state electronic and ionic transport are coupled under an external bias voltage [7]. The thickness and defect structure of the titania films has a significant effect on the memristance properties [6].

It has been shown that the properties of the anodic films on titanium depend greatly on the conditions at which the film is grown [8–16]. One of the important factors affecting the characteristics of the anodic films is their growth rate. Blackwood and Peter reported that the relative dielectric constant, $\varepsilon$, and defect concentration profiles in the oxide film depend markedly on the film growth rate [11]. Ohtsuka and Otsuki revealed that the $\varepsilon$ value increases and the ionised donor concentration decreases with increasing the growth rate of the anodic film on titanium [14]. The refractive index of the anodic $TiO_2$ films was also found to be smaller with the higher growth rate [13].

Recently we have demonstrated the application of the high-voltage pulsed discharge technique for creation of thin anodic films on titanium [17]. Under the action of single powerful electric discharges in electrolyte, extremely high rates (400–700 μm/s) of the oxide film growth were reached on the titanium anode. The growth rate is the fastest ever reported. The results of Auger depth profiling showed that the oxide films prepared by the pulsed discharge method are characterised by higher stoichiometry and more homogeneous distribution of basic elements (Ti and O) through the film thickness in comparison to the films grown by the conventional galvanostatic anodisation [17]. Moreover, enhanced photoelectrochemical activity was revealed for the pulse discharge-prepared films motivating their further investigation. Also preparation of oxide films on pure aluminium electrodes using the powerful

* Corresponding author. Permanent address: Research Institute for Physical Chemical Problems, Belarusian State University, 220030 Minsk, Belarus.
*E-mail addresses:* poznyak@bsu.by, poznyak@ua.pt (S.K. Poznyak).

0013-4686/$ – see front matter © 2012 Elsevier Ltd. All rights reserved.
http://dx.doi.org/10.1016/j.electacta.2012.05.064

pulsed discharge technique was studied [18]. It was found that dense one-layer alumina films with thicknesses up to 200 nm can be created on the Al surface. Scanning Kelvin Probe Force Microscopy (SKPFM) measurements showed that the anodic alumina films prepared by the pulsed discharge method have more uniform surface structure and electrical properties which are less dependent on the initial surface conditions than those of the films prepared by the conventional anodisation methods.

Electrochemical impedance spectroscopy (EIS) is a powerful technique for in situ characterisation of various oxide films on metal surfaces. This technique was successfully applied to examine anodic oxide films on different valve metals such as Al [19–21], Zr [22], Nb [23]. EIS was also used to characterise oxide films on titanium surface [24–40]. Blackwood [24] investigated the impedance response from very thin (several nanometers) passive oxide films on titanium and showed that the contribution of the space charge region (SCR) formed in the oxide layer must be taken into account when interpreting the impedance data. In a number of EIS studies [29,30,34], impedance spectra of thin anodic films on titanium exhibit a single time constant, which is indicative of a uniform compact layer, whereas thicker films tend to reveal a second time constant in the impedance spectra. In the latter case, the interpretation of the EIS data was based on a two-layer model of the oxide film composed by a thin intact inner layer and a porous outer layer [25,29–31,34,39,40].

In the present work, electrochemical impedance spectroscopy has been used as the main method for characterisation of the structural features and semiconductive properties of novel anodic oxide films formed on titanium at extremely high growth rates under the powerful pulsed discharges (hereafter referred to as PD films). For comparison reasons, impedance spectra recorded on the films grown by the conventional galvanostatic oxidation (hereafter referred to as GS films) are also discussed. The photoelectrochemical method as well as transmission electron microscopy (TEM) accompanied with electron diffraction were also applied for studying the anodic oxide films to support the selection of the equivalent circuits and the conclusions drawn from the EIS measurements.

## 2. Experimental

Titanium plates (8 mm × 70 mm; 99.8% Ti) used as working electrodes were polished mechanically and then chemically in HF:$HNO_3$ (1:3 by volume) mixture to mirror finish and finally rinsed with deionised water. Part of the surface was isolated with epoxy resin, giving an electrode working area of 6 $cm^2$. The electrochemical cell used for the pulsed discharge oxidation of Ti was constructed from high-impact polystyrene and consisted of a titanium anode placed in the centre of a cylindrical Ti cathode with 20 times larger surface area. 1 M $H_2SO_4$ aqueous solution ($T = 25 \pm 1$ °C) was used as an electrolyte. Electric discharges in the electrode system were generated using a low-inductive 100 μF capacitor bank charged to a definite voltage (1350 V) which was commutated with a low-inertial relay triggered by a synchronizing pulse. Duration of discharge was less than 20 μs. Conventional galvanostatic anodisation of the titanium electrodes was performed in the same cell at a current density of 10 mA $cm^{-2}$ using a controllable dc power supply.

The EIS measurements were performed using a Gamry FAS2 Femtostat with a PCI4 Controller in a $10^5$ down to $10^{-2}$ Hz frequency range with a step of 10 points per decade. Impedance spectra were recorded applying a 10 mV sinusoidal perturbation at open circuit potential or at different potentials in the range from 0.8 V to −0.4 V vs. SCE. The EIS measurements were carried out at room temperature in a conventional three-electrode cell consisting of a saturated calomel reference electrode (SCE), a platinum foil as the counter electrode and the working electrode with an exposed area of 1 $cm^2$. The cell was placed in a Faraday cage to avoid interferences with external electromagnetic fields. The working solution was 0.1 M acetate buffer (pH 6). To remove oxygen, the solution was purged with argon. Before the spectra recording, the system was allowed to attain a stable open circuit potential or a quasi-stationary current under potentiostatic polarisation. At least two samples prepared under the same conditions were tested to ensure reproducibility of the results. The impedance plots were fitted using different equivalent circuits by means of the Elchem Analyst software from Gamry Inc.

Photocurrent spectra were recorded in a quartz cell having an optical quality window. A setup equipped with a high-intensity grating monochromator, a 1000 W xenon lamp and a slowly rotating light chopper (0.3 Hz) was used for monochromatic irradiation of the working electrode. Photocurrent spectra were corrected for the spectral intensity distribution at the monochromator output measured by a calibrated thermocouple power meter.

TEM measurements were performed on a Hitachi H9000 transmission electron microscope at an acceleration voltage of 300 kV. Electron transparent sections for TEM with a thickness of 15 nm were cut using a Leica Reichert Supernova ultramicrotome. To prepare the samples, titanium electrodes with an oxide film were embedded into resin and polished from the metal side up to a thickness of 10–15 μm, and then they were re-embedded into resin. A cut with a width of 10 μm was then made using an ultramicrotome with a glass knife. Obtained microrod (10–15 μm × 10 μm × 3–4 mm, oxide is on the one of faces) was embedded once more into resin, perpendicular to the cut, and finally was sliced with a diamond knife (Diatome 45°).

## 3. Results and discussion

### 3.1. Anodic oxide film formation

Upon the action of powerful electric discharge on the electrode system, the extremely rapid growth of the oxide film on titanium anode surface is observed. An electric charge of 0.0225 C $cm^{-2}$ was passed through the Ti electrode–electrolyte interface during one discharge, resulting in the formation of 25 nm thick anodic film as shown in our previous work [17]. The subsequent discharges lead to step-wise increase in the film thickness visually observed as a characteristic change of the interference colour. The colour properties of anodic oxide films on titanium have been previously shown to originate from light interference [41]. The average thickness of the obtained anodic films was estimated by the depth profile analysis using Auger electron spectroscopy as described in detail in our previous work [17]. For relatively thick films (120–170 nm) the thickness values were also confirmed by TEM observations (Fig. 1). The films obtained by the discharge approach appear to be intact and uniform.

For comparison, the anodic films on titanium were also prepared by the conventional galvanostatic anodisation in the same electrolyte at a current density ($j$) of 10 mA $cm^{-2}$. The duration of the galvanostatic anodisation was chosen so that the thickness of the GS films was coincident with that of the PD films. This makes possible more correct comparison of the properties of the anodic films prepared by these two methods. The anodizing ratio (the ratio between the oxide film thickness, $d$, and the maximum film formation voltage, $U_{max}$) calculated for the galvanostatic growth of anodic $TiO_2$ films was about 2.78 nm/V and slightly decreased down to 2.65 nm/V for the films with $d > 120$ nm. This estimate is in a good agreement with the anodizing ratio values (2.5–3 nm/V) more commonly reported in literature for the titania anodic films grown in sulphuric acid solutions [8,10,37,41–43].

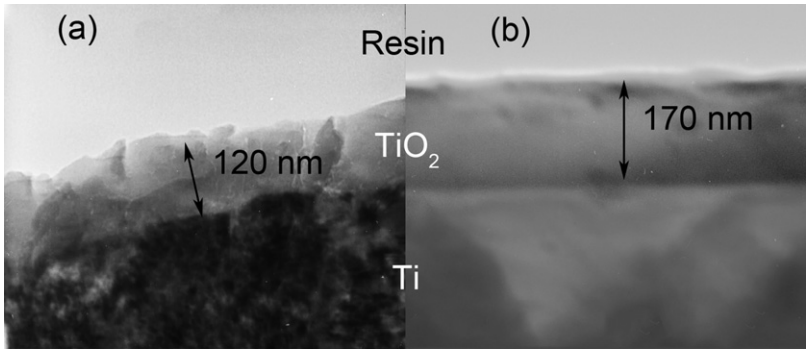


**Fig. 1.** Transmission electron micrographs of a cross section of the anodic $TiO_2$ films on titanium prepared by the powerful pulsed discharge method. Five (A) and ten (B) discharges ($U$ = 1350 V; $C$ = 100 μF) were passed through the electrode system.

### 3.2. EIS measurements

Fig. 2 shows the Bode plots obtained on the titanium electrodes covered with GS and PD anodic oxide films with different thickness. The impedance spectra presented in Fig. 2 were measured at anodic bias (0.6 V vs. SCE). In this potential region the EIS spectra of the anodic films, as will be shown below, are insignificantly changed with electrode potential. In a wide range of thickness, impedance spectra of the PD films exhibit an almost pure capacitive response (one time constant) illustrated by a phase angle close to −90° over a wide frequency range from $10^3$ to 0.1 Hz originated from capacitance of the formed titania film (Fig. 2a). Only at lower frequencies does the phase angle start to increase demonstrating the onset of the resistive response originated from the resistance of the oxide layer.

The Bode plot of the thinnest ($d \approx 25$ nm) anodic film produced by the conventional galvanostatic technique exhibits quite similar behaviour and impedance values as compared with those of the pulse discharge-prepared one with the same thickness (Fig. 2b). As the film thickness grows, a second time constant begins to appear in the EIS spectra of the GS films at intermediate frequencies. This relaxation process starts to be more pronounced and shifts gradually to higher frequencies with film thickening (Fig. 2b).

According to the literature [25,29–31,34], the first time constant can be assigned to the response from compact inner layer. Another time constant at intermediate frequencies is related to the outer porous layer. The formation of bilayer structure for the GS films is also supported using cross-sectional TEM analysis (Fig. 3). The bright field image (Fig. 3a) demonstrates a porous outer layer. Two layers are well distinct on the dark field (Fig. 3b): outer layer is composed almost completely by amorphous oxide, whilst clearly defined crystallites (bright spots) can be found in inner layer. These electron microscopy data are in good agreement with the TEM observations presented by Jaeggi et al. [29]. Taking into account this consideration, one may assume that the anodic films grown on titanium by the pulsed discharge method in a wide range of thickness is constituted by only one compact uniform oxide layer. This suggestion is confirmed by TEM as shown in Fig. 1.

It is known that titanium dioxide films prepared by anodisation are not simply a dielectric, but demonstrate well defined semiconductive behaviour [44,45]. Therefore, for these materials the influence of a space charge region (SCR) formed at the oxide–electrolyte interface on the electrochemical impedance spectrum can be appreciable [24,31,39,40]. To clarify this point for both PD and GS anodic films, the effect of the applied potential on the impedance spectra was studied. It is well known that polarisation of a semiconductive film leads to variation of its capacitance and, in turn, to modulation of the corresponding part of the impedance spectra. The modulation of the capacitance response under the variable polarisation is used as a proof of correct assignment of the corresponding part of the spectra to the SCR [39,40]. The impedance spectra for the films with different thicknesses were acquired in a potential range from −0.4 to 0.8 V for GS and PD films where the current values are very low ($\leq$1–2 μA cm$^{-2}$), moving from positive to negative potentials with a 0.2 V step.

The impedance spectra of 50 nm thick PD and GS anodic films taken at different potentials are shown in Fig. 4. The spectra depend slightly on the electrode potential in the region of positive bias. At potentials below 0 V vs. SCE, a distinct second time constant appears in the spectra of the PD films and a third time constant – in the spectra of the GS ones (Fig. 4). This additional time constant is gradually shifted to lower frequencies with increasing film thickness. It is important to notice that the variation of the impedance spectra with electrode potential is reversible, i.e. after negative polarisation similar spectra can be observed again at positive potentials. It is evident that this relaxation process modulated by the applied potential is originated from the SCR response.

In order to take into account the structure of the anodic oxide films formed on titanium and possible contribution of the space charge region, different equivalent electric circuits (EEC) were tested for fitting the experimental impedance spectra. When choosing an appropriate EEC describing the obtained impedance spectra with a minimum error and a minimum number of EEC elements, physical significance of the EEC parameters as well as their correct evolution with changing the electrode potential and $TiO_2$ film thickness were taken into consideration.

The whole set of EIS data for PD films can be satisfactorily fitted using the circuit (Fig. 5a) corresponding to the Voight model [46], where $CPE_{sc}$ and $CPE_b$ represent the space charge layer and bulk film constant phase elements and $R_{sol}$, $R_{sc}$ and $R_b$ – the resistances of electrolyte, space charge layer and bulk film, respectively. Impedance spectra of the GS films were fitted using a more complex EEC shown in Fig. 5b, where $CPE_{out}$ and $CPE_{in}$ represent the constant phase elements of the outer nanoporous layer and inner compact layer and $R_{out}$ and $R_{in}$ – the resistance of the outer nanoporous layer and inner compact layer of the film, respectively. These equivalent circuits were already reported in the literature as adequate for fitting the EIS spectra of anodic titania layers obtained at different conditions [39,40].

A constant phase element (CPE) instead of a capacitor was used in all fittings presented in the work. Such modification is needed when the phase angle of the capacitor is different from −90°. The physical origin of the CPE has been widely discussed in literature [47,48]. The impedance of the CPE, $Z_{CPE}$, depends on frequency, $\omega$, according to the following equation:

$$Z_{CPE} = [Q(j\omega)^n]^{-1} \quad (1)$$

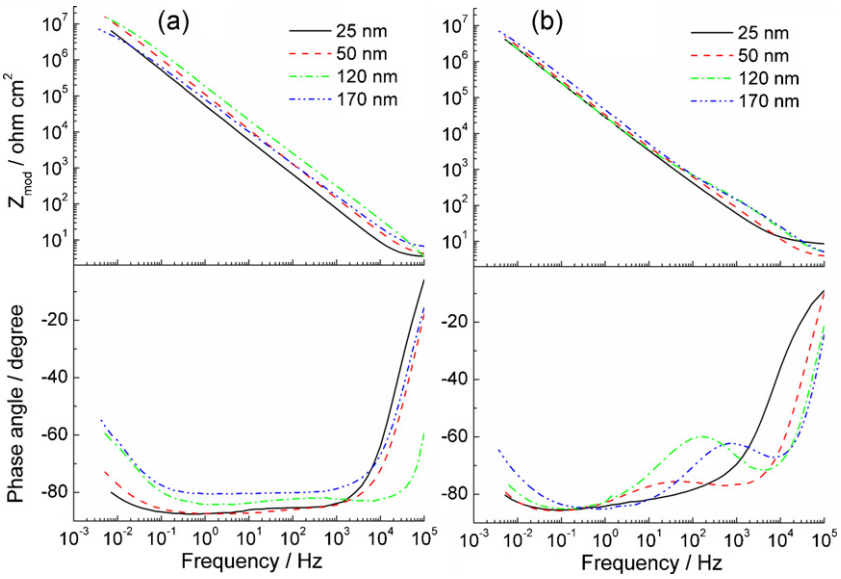


**Fig. 2.** Impedance spectra of the anodic oxide films with different thickness formed on titanium by pulsed discharge method (a) and galvanostatic anodizing (b). The spectra were measured at a potential of 0.6 V.

where $Q$ is a parameter numerically equal to the admittance ($|Z|^{-1}$) at $\omega = 1$ rad s$^{-1}$ and $n \leq 1$ is a power coefficient calculated as ratio of the phase angle at maximum of the corresponding time constant to $-90^{\circ}$. The capacitance values for the capacitive elements in the equivalent circuit were calculated as described previously [49].

As seen from Fig. 6, the fitting curves show good agreement with the experimental impedance spectra.

The representative results of impedance data fitting for different electrode potentials are presented in Tables 1 and 2 for 50 nm thick PD and GS films, respectively. These data show that all the elements of the equivalent circuits behave in a consistent manner. The resistance of the space charge region of both PD and GS films is highest and ranges from 10 to 70 MΩ cm$^2$ under positive bias, decreasing significantly at negative polarisation. The outer layer of the GS films has more than three orders of magnitude lower resistance, suggesting the porous structure of this layer. The capacitance of the outer and inner layers depend noticeably less on the applied potential in comparison with parameters of the space charge region. The electrolyte resistance (several Ω cm$^2$) remains constant over the whole potential range. The values of the exponent $n$ range from 0.8 to 1 (except $n_{in}$ for the GS film), conforming thereby mainly capacitive character of the CPE elements.

The main objective of the performed impedance analysis was to elucidate how the extremely fast growth of the titania films can influence the structure and semiconducting properties of the anodic layers. The results clearly show that PD films are constituted by a single layer whilst the conventional GS films are constituted of outer porous and inner dense oxide layers. The semiconductive properties of the anodic layers can be assessed by analyzing the impedance response from the space charge layer.

Fig. 7 presents the dependencies of the equivalent circuit parameters related to the SCR for the PD and GS anodic films with different thicknesses on the electrode potential. As seen from this figure, the values of SCR resistance and SCR capacitance decrease and increase, respectively, with decreasing electrode potential. As expected the sharpest variation of the $R_{sc}$ and $C_{cs}$ values is observed in the negative potential region near the flat band potential, $E_{fb}$, in accordance with the well known Mott–Schottky equation:

$$C_{sc}^{-2} = \left(\frac{2}{eN_d\varepsilon\varepsilon_o}\right)\left(E - E_{fb} - \frac{kT}{e}\right) \quad (2)$$

where $N_d$ is the ionised donor concentration for a n-type semiconductor, $\varepsilon$ the relative dielectric constant of the anodic film, $\varepsilon_o$ the

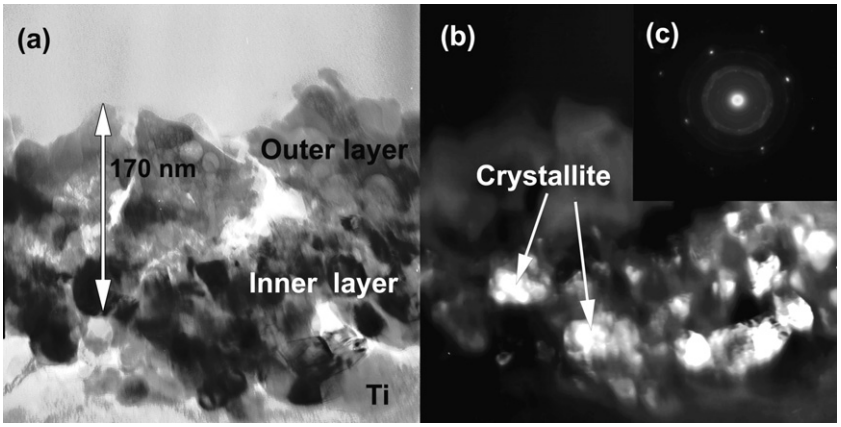


**Fig. 3.** Bright field (A) and dark field (B) transmission electron micrographs of a cross section of the anodic $TiO_2$ film prepared by galvanostatic anodizing ($U_{max}$ = 64 V). Bright parts on the dark field TEM image show $TiO_2$ nanocrystallites. The inset (C) shows electron diffraction pattern from the $TiO_2$ nanocrystallites.

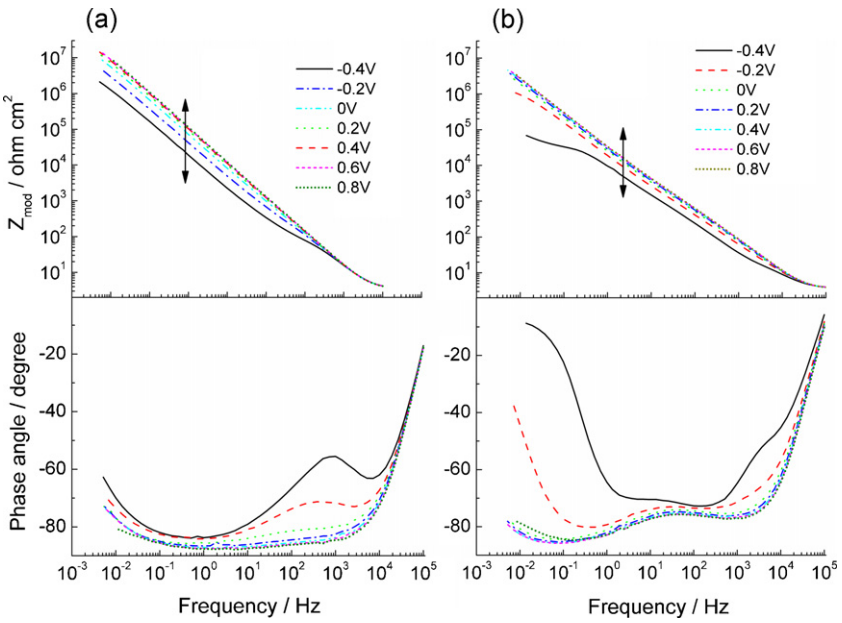


**Fig. 4.** Impedance spectra of the 50 nm thick anodic oxide films formed on titanium by pulsed discharge method (a) and galvanostatic anodizing (b). The spectra were measured at different potentials.

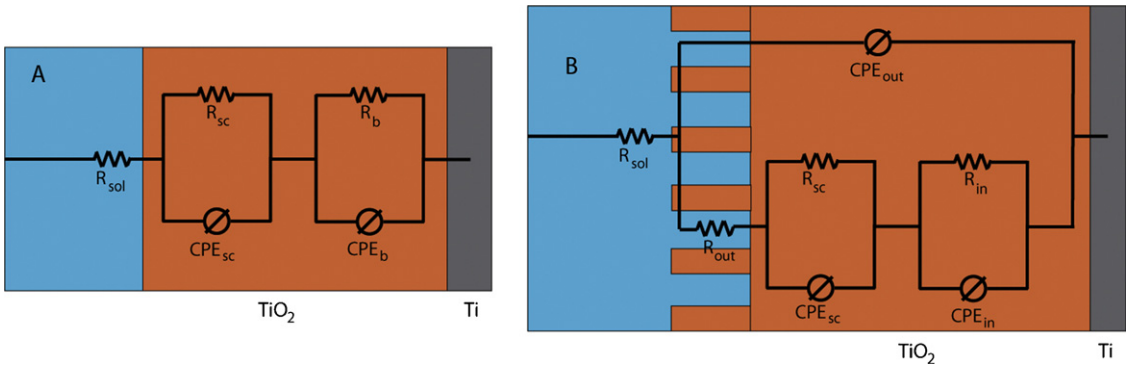


**Fig. 5.** Equivalent circuits used for fitting the impedance spectra of the anodic films formed on titanium by pulsed discharge method (a) and galvanostatic oxidation (b).

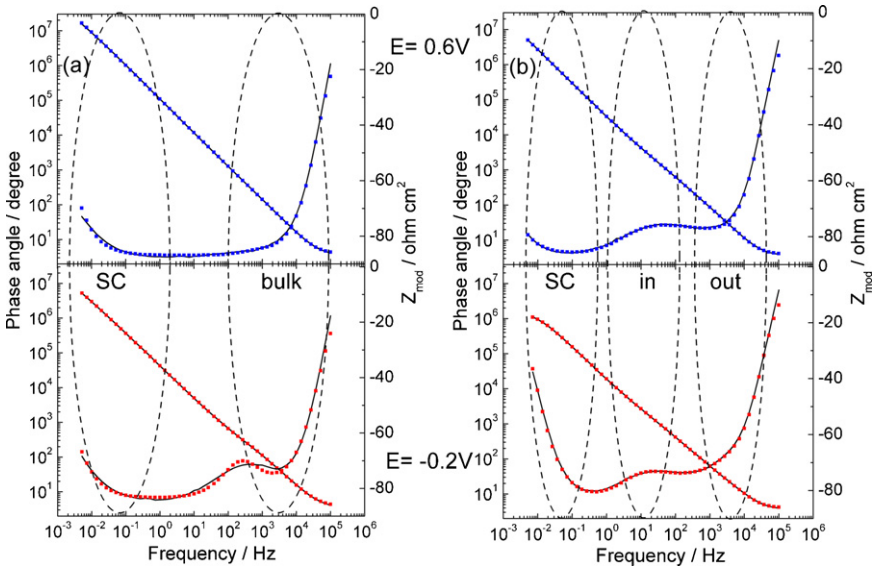


**Fig. 6.** Impedance spectra measured at electrode potentials of 0.6 and −0.2 V for 50 nm thick anodic titania films formed by pulsed discharge method (a) and galvanostatic anodizing (b). Symbols are the experimental points; lines present the fitting curves obtained using the equivalent circuits shown in Fig. 5. Dashed ovals indicate the positions of different time constants on the impedance spectra.

**Table 1**
Equivalent circuit parameters and respective errors (in percents) obtained after fitting the impedance spectra of 50 nm thick PD film (Figs. 4 and 6) polarised at different potentials. $n_{sc}$ and $n_b$ are the power coefficients for the constant phase elements of SCR and bulk layer, respectively.

| Applied potential[a] (V) | $R_{sol}$ ($\Omega$ cm$^2$) | $R_{sc} \times 10^{-6}$ ($\Omega$ cm$^2$) | $CPE_{sc} \times 10^6$ (S $s^n$ cm$^{-2}$) | $n_{sc}$ | $R_b$ ($\Omega$ cm$^2$) | $CPE_b \times 10^6$ (S $s^n$ cm$^{-2}$) | $n_b$ |
|---|---|---|---|---|---|---|---|
| −0.2 | 3.7 ± 2.4% | 18 ± 7.8% | 4.3 ± 0.70% | 0.92 ± 0.24% | 140 ± 9.3% | 9.2 ± 14% | 0.88 ± 1.7% |
| 0 | 3.8 ± 2.4% | 40 ± 9.5% | 2.4 ± 0.71% | 0.95 ± 0.24% | 110 ± 21% | 22 ± 31% | 0.87 ± 3.4% |
| 0.6 | 3.9 ± 2.1% | 56 ± 7.9% | 1.6 ± 0.69% | 0.97 ± 1.9% | 8.0 ± 11% | 27 ± 20% | 1.0 ± 19%[b] |

[a] Potential vs. SCE.
[b] High value of the error was obtained due to the limitation of the $n$. Maximum value of CPE exponent is 1, therefore higher values have no physical meaning.

**Table 2**
Equivalent circuit parameters and respective errors (in percents) calculated by fitting the impedance spectra of 50 nm thick GS film (Figs. 4 and 6) polarised at different potentials. $n_{sc}$, $n_{out}$ and $n_{in}$ are the power coefficients for the constant phase elements of SCR, outer nanoporous layer and inner compact layer, respectively.

| Applied potential[a] (V) | $R_{sol}$ ($\Omega$ cm$^2$) | $R_{out}$ ($\Omega$ cm$^2$) | $CPE_{out} \times 10^6$ (S $s^n$ cm$^{-2}$) | $n_{out}$ | $R_{in} \times 10^{-3}$ ($\Omega$ cm$^2$) | $CPE_{in} \times 10^6$ (S $s^n$ cm$^{-2}$) | $n_{in}$ | $R_{sc} \times 10^{-6}$ ($\Omega$ cm$^2$) | $CPE_{sc} \times 10^6$ (S $s^n$ cm$^{-2}$) | $n_{sc}$ |
|---|---|---|---|---|---|---|---|---|---|---|
| −0.2 | 4.0 ± 0.38% | 31 ± 9.4% | 1.6 ± 9.4% | 1.0 ± 7.3%[b] | 2.1 ± 17% | 37 ± 26% | 0.66 ± 5.5% | 1.5 ± 3.7% | 8.1 ± 1.9% | 0.92 ± 0.96% |
| 0 | 4.0 ± 0.45% | 36 ± 17% | 1.5 ± 12% | 1.0 ± 11%[b] | 3.7 ± 6.5% | 34 ± 32% | 0.60 ± 7.5% | 26 ± 2.4% | 5.6 ± 4.1% | 0.93 ± 0.84% |
| 0.6 | 3.9 ± 0.41% | 62 ± 9.4% | 1.5 ± 14% | 1.0 ± 8.2%[b] | 5.5 ± 6.6% | 28 ± 36% | 0.58 ± 8.4% | 41 ± 2.7% | 3.9 ± 3.8% | 0.95 ± 1.2% |

[a] Potential vs. SCE.
[b] High value of the error was obtained due to the limitation of the $n$. Maximum value of CPE exponent is 1, therefore higher values have no physical meaning.

permittivity of free space, $E$ the electrode potential, $k$ the Boltzmann constant, $T$ the temperature and e the charge of an electron.

It should be noted that the validity of the simple Mott–Schottky analysis is unambiguously confirmed only for classical single crystal or polycrystalline semiconductors. For thin anodic oxide films on valve metals, which are usually amorphous, the validity of this analysis is controversial [50,51]. Notwithstanding this fact, the Mott–Schottky relationship has been used by a great number of researchers for estimating semiconductive parameters of thin anodic oxide films on various valve metals such as titanium [11,14,24,31,37–40,44], niobium [52,53], tin [54], tungsten [55] and others. All things considered, in the present work we used the Mott–Schottky analysis for comparative reason to compare the semiconductive characteristics of the two types (GS and PD) of the anodic titania films having similar thickness.

As seen from Fig. 8, the calculated $C_{sc}^{-2} - E$ plots for both GS and PD films demonstrate a loss of linearity in the whole potential range studied, and some decrease in the slope is observed at higher potentials. Such nonlinearity of the Mott–Schottky plots has been previously found for titania anodic films and discussed by a number of researchers [8,11,14,37,38,56–59]. Different hypotheses have been proposed to rationalise this behaviour: uniform

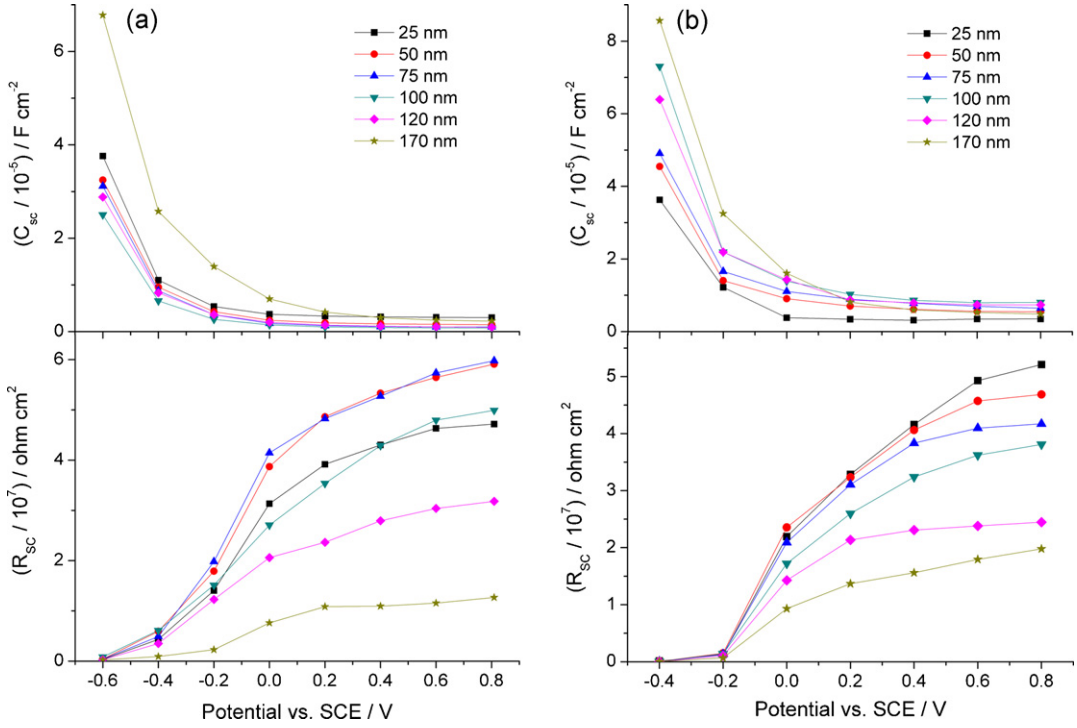


**Fig. 7.** Capacitance and resistance of the SCR for anodic titania films formed by pulsed discharge method (a) and galvanostatic anodizing (b) as a function of the electrode potential for different thicknesses of the films.

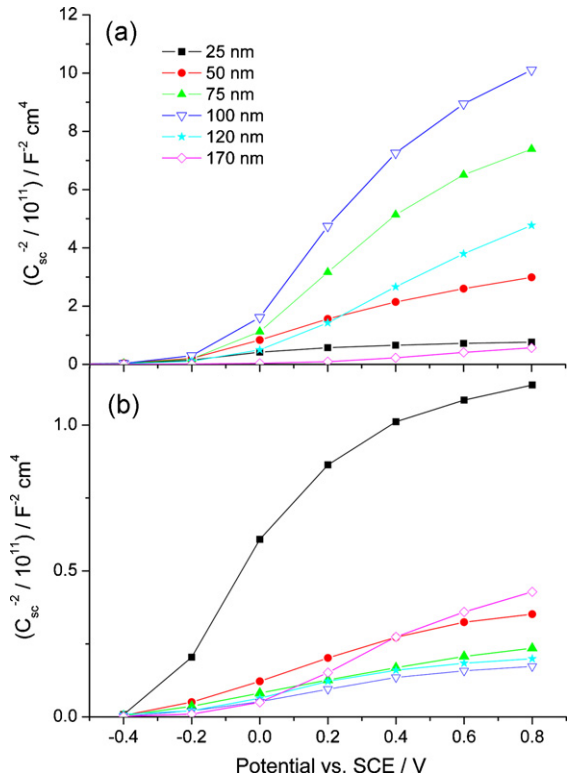


**Fig. 8.** Mott–Schottky plots, constructed from the data shown in Fig. 7, for anodic titania films formed by pulsed discharge method (a) and galvanostatic anodizing (b).

distribution of the donor concentration through the film thickness [11], existence of multiple donor levels within the bandgap of the oxide film [57] and field dependence of the relative dielectric constant of the oxide [58]. Moreover, at high positive potentials the passive film can be totally depleted of charge carriers when the space charge region becomes comparable with the film thickness [53,60]. Taking into account the heterogeneity and complexity of the electronic structure of anodic films on titanium, probably not a single, but several above-mentioned factors can be responsible for the nonlinearity of the Mott–Schottky plots.

For estimation of the ionised donor concentration we used a linear portion of the $C_{sc}^{-2} - E$ plots observed in the potential region from −0.2 to 0.4 V. It is worth to mention that the SCR capacitance values were obtained using analysis of the impedance spectra in a wide range of frequencies. Moreover, the non-ideality of the capacitance was taken into account employing the constant phase element approach. Fig. 9 summarises the $N_d$ values for the anodic titania films with different thicknesses, which was estimated from the Mott–Schottky plots assuming $\varepsilon = 57$ (the average of frequently reported $\varepsilon$ values for anodic oxide films on titanium [8,14,26,37,44,51,61]).

High $N_d$ values observed for galvanostatically grown $TiO_2$ films ($>10^{19}$ $cm^{-3}$) are in good agreement with the literature data [8,11,14,37,44,51,56–59,62]. The increase in the GS film thickness from 25 to 100 nm leads to some rise in the ionised donor concentration. On further thickening of these films the ionised donor concentration begins to decrease. An essentially different situation was revealed in the case of the anodic films prepared by the pulsed discharge method. Surprisingly the relatively thin PD films become less defective with increasing their thickness in contrast to the GS ones (Fig. 9). The ionised donor concentration for the 100 nm thick PD film is about two orders lower than that for the GS film with the same thickness. The further thickening of the PD films leads to

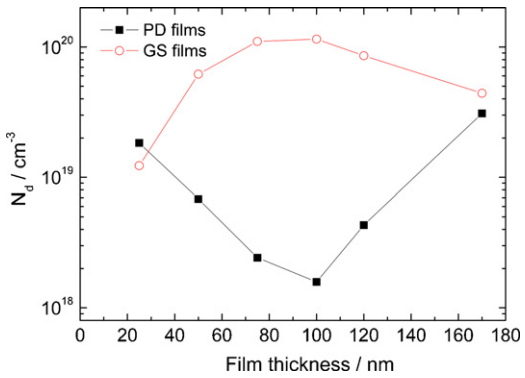


**Fig. 9.** Evolution of the ionised donor concentration, $N_d$, calculated from the Mott–Schottky plots, with thickness of the anodic oxide films prepared by the conventional galvanostatic oxidation and the pulsed discharge method.

the increase in $N_d$, which could correlate with the onset of the film crystallisation [17].

### 3.3. Photoelectrochemical spectroscopy measurements

Photocurrent spectroscopy is the other useful in situ technique which was repeatedly applied to examine semiconducting characteristics of titania anodic films [26,44,45] and can be used to support the conclusions drawn from EIS results. We applied this technique to gain complementary information on the structural and semiconducting properties of the PD and GS anodic oxide films under study. The photocurrent spectra recorded under anodic polarisation on two different types of the films are shown in Fig. 10.

For thinnest films, apart a small difference in the photocurrent density, the spectrum for the GS films is similar to that for the PD films exhibiting a peak at 260 nm. Further thickening of the GS film results in a significant drop of the photocurrent in the short-wavelength region of spectrum, and the photocurrent maximum is shifted to 325 nm (Fig. 10b). The similar short-wavelength decay in the photocurrent spectra was reported previously for anodic $TiO_2$ films [26,44,62,63] and associated with a sharp change in the film structure (so called “film breakdown”) occurring in a definite

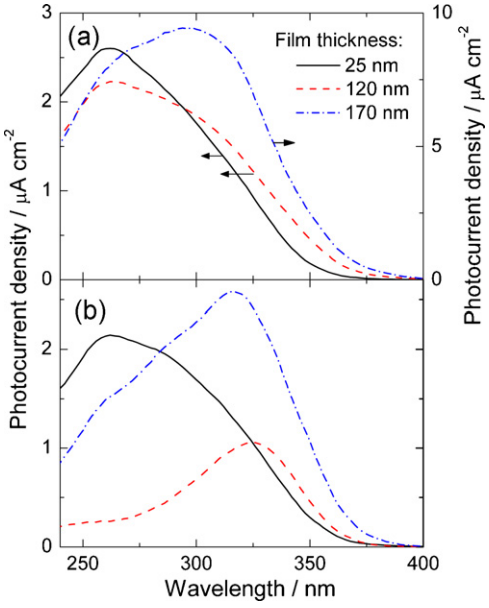


**Fig. 10.** Photocurrent spectra of the anodic oxide films with different thickness prepared by the pulsed discharge method (a) and conventional galvanostatic anodizing (b). Electrode potential: 0.8 V vs. SCE.

thickness range during the film growth on titanium [44,62]. Since short-wavelength light with high-energy photons is absorbed close to the film surface, the photocurrent drop in the short-wavelength region can be related to the increased rate of recombination and trapping of the photogenerated charge carriers in the more defective outer layer formed after the breakdown of the anodic film. In contrast to the GS films, the PD films demonstrate considerably smaller drop of photocurrent in the short-wavelength region of spectrum (260–300 nm) and the photocurrent peak remains at 260 nm (Fig. 10a). These results indicate that the PD films are essentially more uniform and less defective than the GS films, which is in good agreement with the EIS data.

For relatively thick GS films ($d \geq 170$ nm), the photocurrent increases considerably, especially in the short-wavelength region, and the photocurrent spectra again becomes to be similar to those of the PD films (Fig. 10). Crystallisation of thicker GS and PD films, which was previously evidenced by Raman measurements [17], and related transformation of their semiconductor properties may be responsible for this effect and for the observed changes of the EIS spectra. TEM measurements also testify that crystallisation of the anodic titania films occurs with increasing of their thicknesses (Fig. 3). On the dark field image (Fig. 3b) there are a lot of fine crystallites that appeared as a result of crystallisation of the amorphous oxide. According to the electron diffraction patterns (Fig. 3c) the crystalline phase is anatase. Habazaki et al. have reported that anatase crystallites develop in the inner anodic film region, formed by inward migration of oxygen species [64].

## 4. Conclusions

The EIS measurements on the titania anodic films prepared by novel high-voltage pulsed discharge method and the conventional galvanostatic anodisation have demonstrated that the impedance spectra are sensitive both to the space charge region developed in the oxide and to the anodic film structure changing with the film thickness. The pulsed discharge technique leads to the formation of single-layer compact anodic oxide films up to a thickness of 170 nm. In contrast, the EIS spectra of the anodic films grown by the conventional galvanostatic method exhibit several time constants under anodic polarisation for the film thickness above 25 nm, indicating a film with two layers: a dense inner layer and a nanoporous outer one. These films show a significantly lower photoelectrochemical activity at short wavelengths as compared with the films prepared in the pulsed regime. The concentration of the ionised donors estimated from Mott–Schottky plots for the relatively thin galvanostatically grown $TiO_2$ films (70–120 nm) is significantly higher (by two orders of magnitude) than that in the coatings obtained by the pulsed discharge method. Only at thickness above 170 nm, crystallisation of both types of the films leads to the fact that their semiconducting properties become similar.

The powerful pulsed discharge method can be considered as a very promising approach for preparation of thin anodic films on titanium offering lower defectiveness and enhanced photoelectrochemical response at short wavelengths.

## Acknowledgement

Financial support of FCT project PTDC/CTM/72223/2006 is gratefully acknowledged.

## References

[1] R.W. Schutz, D.E. Thomas, Corrosion of titanium and titanium alloys, in: J.R. Davis Sr. (Ed.), Metals Handbook, Corrosion, vol. 13, 9th ed., ASM, Materials Park, Ohio, 1987, p. 669.
[2] M. Long, H.J. Rack, Biomaterials 19 (1998) 1621.
[3] T.-L. Yau, Reactive and refractory alloys, in: R.H. Jones (Ed.), Environmental Effect on Engineered Materials, Marcel Dekker, New York, 2001, pp. 142–158 (Chapter 6).
[4] J. Lausmaa, B. Kasemo, H. Mattsson, H. Odelius, Applied Surface Science 45 (1990) 189.
[5] A. Cigada, M. Cabrini, P. Pedeferri, Journal of Materials Science: Materials in Medicine 3 (1992) 408.
[6] K. Miller, K.S. Nalwa, A. Bergerud, N.M. Neihart, IEEE Electron Device Letters 31 (2010) 737.
[7] D.B. Strukov, G.S. Snider, D.R. Stewart, R.S. Williams, Nature 453 (2008) 80.
[8] S. Piazza, L. Calà, C. Sunseri, F. Di Quarto, Berichte der Bunsen-Gesellschaft fur Physikalische Chemie 101 (1997) 932.
[9] M.V. Diamanti, M.P. Pedeferri, Corrosion Science 49 (2007) 939.
[10] J.-L. Delplancke, R. Winand, Electrochimica Acta 33 (1988) 1539.
[11] D.J. Blackwood, L.M. Peter, Electrochimica Acta 34 (1989) 1505.
[12] T. Shibata, Y.-C. Zhu, Corrosion Science 37 (1995) 253.
[13] T. Ohtsuka, N. Nomura, Corrosion Science 39 (1997) 1253.
[14] T. Ohtsuka, T. Otsuki, Corrosion Science 40 (1998) 951.
[15] M. Mikula, J. Blecha, M. Čeppan, Journal of the Electrochemical Society 139 (1992) 3470.
[16] M.R. Kozlowski, P.S. Tyler, W.H. Smyrl, R.T. Atanasoski, Surface Science 194 (1988) 505.
[17] S.K. Poznyak, D.V. Talapin, A.I. Kulak, Journal of Electroanalytical Chemistry 579 (2005) 299.
[18] A.D. Lisenkov, A.N. Salak, S.K. Poznyak, M.L. Zheludkevich, M.G.S. Ferreira, Journal of Physical Chemistry C 115 (2011) 18634.
[19] J.J. Suay, E. Giménez, T. Rodríguez, K. Habbib, J.J. Saura, Corrosion Science 45 (2003) 611.
[20] K. Bonnel, C. Le Pen, N. Pebere, Electrochimica Acta 44 (1999) 4259.
[21] A. Girginov, A. Popova, I. Kanazirski, A. Zahariev, Thin Solid Films 515 (2006) 1548.
[22] J.A. Bardwell, M.C.H. McKubre, Electrochimica Acta 36 (1991) 647.
[23] F. Di Quarto, S. Piazza, C. Sunseri, Electrochimica Acta 35 (1990) 99.
[24] D.J. Blackwood, Electrochimica Acta 46 (2000) 563.
[25] J. Pan, D. Thierry, C. Leygraf, Electrochimica Acta 41 (1996) 1143.
[26] J. Marsh, D. Gorse, Electrochimica Acta 43 (1998) 659.
[27] J.R. Birch, T.D. Burleigh, Corrosion 56 (2000) 1233.
[28] M.E.P. Souza, M. Ballester, C.M.A. Freire, Surface and Coatings Technology 201 (2007) 7775.
[29] C. Jaeggi, P. Kern, J. Michler, T. Zehnder, H. Siegenthaler, Surface and Coatings Technology 200 (2005) 1913.
[30] A.G. Mantzila, M.I. Prodromidis, Electrochimica Acta 51 (2006) 3537.
[31] N. Ibriş, J.C. Mirza Rosca, Journal of Electroanalytical Chemistry 526 (2002) 53.
[32] J.E.G. González, J.C. Mirza Rosca, Journal of Electroanalytical Chemistry 471 (1999) 109.
[33] C. Fonseca, M.A. Barbosa, Corrosion Science 43 (2001) 547.
[34] S.A. Fadl-Allah, R.M. El-Sherief, W.A. Badawy, Journal of Applied Electrochemistry 38 (2008) 1459.
[35] A.W.E. Hodgson, Y. Mueller, D. Forster, S. Virtanen, Electrochimica Acta 47 (2002) 1913.
[36] T.M. Silva, J.E. Rito, A.M.P. Simões, M.G.S. Ferreira, M. da Cunha Belo, K.G. Watkins, Electrochimica Acta 43 (1998) 203.
[37] M. Schneider, S. Schroth, J. Schilm, A. Michaelis, Electrochimica Acta 54 (2009) 2663.
[38] W. Simons, A. Hubin, J. Vereecken, Electrochimica Acta 44 (1999) 4373.
[39] S.V. Gnedenkov, S.L. Sinebryukhov, Russian Journal of Electrochemistry 41 (2005) 858.
[40] S.V. Gnedenkov, S.L. Sinebryukhov, V.I. Sergienko, Russian Journal of Electrochemistry 42 (2006) 197.
[41] S. Van Gils, P. Mast, E. Stijns, H. Terryn, Surface and Coatings Technology 185 (2004) 303.
[42] G. Blondeau, M. Froelicher, M. Froment, A. Hugot-Le Goff, Thin Solid Films 42 (1977) 147.
[43] M. Kozlowski, W.H. Smyrl, L.J. Atanasoska, R. Atanasoski, Electrochimica Acta 34 (1989) 1763.
[44] J.F. McAleer, L.M. Peter, Faraday Discussions 70 (1980) 67.
[45] U. Stimming, Electrochimica Acta 31 (1986) 415.
[46] D. Vladikova, G. Raikova, Z. Stoynov, H. Takenouti, J. Kilner, St. Skinner, Solid State Ionics 176 (2005) 2005.
[47] P. Zoltowski, Journal of Electroanalytical Chemistry 443 (1998) 149.
[48] G. Láng, K.E. Heusler, Journal of Electroanalytical Chemistry 457 (1998) 257.
[49] C.H. Hsu, F. Mansfeld, Corrosion 57 (2001) 747.
[50] F. Di Quarto, C. Sunseri, S. Piazza, Berichte der Bunsen-Gesellschaft fur Physikalische Chemie 90 (1986) 549.
[51] C. Fonseca, M.G. Ferreira, M.C. Belo, Electrochimica Acta 39 (1994) 2197.
[52] W.A. Badawy, Journal of Applied Electrochemistry 20 (1990) 139.
[53] A.I. de Sá, C.M. Rangel, P. Skeldon, G.E. Thompson, Portugaliae Electrochimica Acta 24 (2006) 305.
[54] M. Metikoš-Huković, S. Omanović, A. Jukić, Electrochimica Acta 45 (1999) 977.
[55] J. Sikora, E. Sikora, D.D. Macdonald, Electrochimica Acta 45 (2000) 1875.
[56] J.W. Schultze, U. Stimming, J. Weise, Berichte der Bunsen-Gesellschaft fur Physikalische Chemie 86 (1982) 276.

[57] E.-J. Lee, S.-I. Pyun, Journal of Applied Electrochemistry 22 (1992) 156.
[58] K.D. Allard, M. Ahrens, K.E. Heusler, Werkstoffe und Korrosion 26 (1975) 694.
[59] D. Zane, F. Decker, G. Razzini, Electrochimica Acta 38 (1993) 37.
[60] S.U.M. Khan, W. Schmickler, Journal of Electroanalytical Chemistry 108 (1980) 329.
[61] T. Hurlen, S. Hornkjol, Electrochimica Acta 36 (1991) 189.
[62] J.F. McAleer, L.M. Peter, Journal of the Electrochemical Society 129 (1982) 1252.
[63] K. Leitner, J.W. Schultze, U. Stimming, Journal of the Electrochemical Society 133 (1986) 1561.
[64] H. Habazaki, M. Uozumi, H. Konno, K. Shimizu, P. Skeldon, G.E. Thompson, Corrosion Science 45 (2003) 2063.

THE JOURNAL OF PHYSICAL CHEMISTRY C

ARTICLE

pubs.acs.org/JPCC

# Anodic Alumina Films Prepared by Powerful Pulsed Discharge Oxidation

Aleksey D. Lisenkov,[†] Andrei N. Salak,[†] Sergei K. Poznyak,[‡] Mikhail L. Zheludkevich,[*,†] and Mário G. S. Ferreira[†]

[†]Department of Ceramics and Glass Engineering/CICECO, University of Aveiro, 3810-193, Aveiro, Portugal

[‡]Institute for Physical Chemical Problems, Belarusian State University, 220050, Minsk, Belarus

**ABSTRACT:** A novel powerful pulsed discharge anodization technique has been applied to prepare dense, homogeneous oxide films of 16−180 nm thick on aluminum surface. The Volta potential difference (VPD) of the obtained films was studied by scanning Kelvin probe force microscopy. The VPD value was measured as a function of the film thickness and was compared with the similar dependences for the anodic alumina films prepared by the conventional galvanostatic and potentiostatic methods. The anodic films present polarization because of the embedded charges localized near the film interfaces. It was shown that despite the apparent differences in the respective anodization processes, the pulsed discharge films demonstrate the magnitude of polarization which is entirely comparable with that of the conventional anodic alumina films of the same thickness. At the same time, the pulsed discharge films are characterized by more uniform surface structure and electrical properties. The characteristic features of the films such as their fast growth and homogeneity have been considered in terms of the processes occurring at the powerful pulsed discharge.

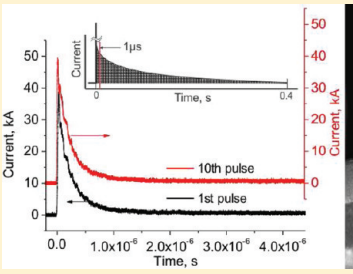


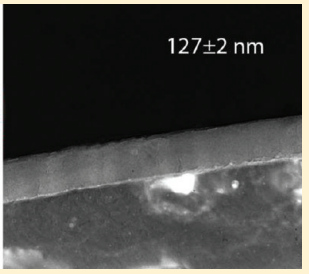


## 1. INTRODUCTION

Thin films of aluminum oxide have found important applications in electronic industry and corrosion protection because of their relatively high dielectric constant and ultralow conductivity as well as high corrosion resistance and good thermal and mechanical stability.[1] These properties also make aluminum oxide films promising for novel applications in microelectronics. Thin alumina layers are used as dielectrics in integrated capacitors with ultrahigh capacitance density.[2] Films of $Al_2O_3$ are also considered as replacements for $SiO_2$ in semiconductor devices.[3,4]

The conventional anodization methods allow production of alumina films of controlled thickness and quality.[5−7] In some cases, for example, in production of electrolytic capacitors and anticorrosion protection of aluminum and its alloys, anodization is combined with other oxidation methods.[8,9]

The relatively new electrochemical treatment technique being widely applied to lightweight metals is plasma electrolytic oxidation (PEO).[10] PEO operates at potentials above the breakdown voltage of an oxide film growing on the metal surface (typically, 120−350 V for aluminum). In the course of a PEO process, the multiple discharge channels, where the oxidation actually occurs, are created. Continuous formation and healing of pores and cracks (which are the natural discharge channels) is the essential feature of the process.[11,12] Therefore, the porous outer layer is the typical attribute of a PEO coating at any stage of its growth. Owing to the features of the technique, PEO coatings grow nonuniformly and are characterized by high roughness. Moreover, it was revealed from study of coating formed by PEO of aluminum that even the densest inner (next to the metal) alumina layer contains numerous defects.[13] PEO is certainly promising for corrosion and wear protection of aluminum and alloys and is inapplicable for production of thin (nanoscale) dielectric alumina films.

A new electrochemical technique of powerful pulsed discharge oxidation of metals has recently been reported.[14] In this technique, electrochemical reaction occurs at the metal−electrolyte interface under the action of single high-voltage (>1.3 kV) pulses. The most important difference of this technique from the conventional galvanostatic and potentiostatic anodization methods is an extremely high rate of the film growth. In principle, owing to plasma−thermochemical interactions at the electrode/electrolyte interface during a high-voltage electric discharge, both pure oxide films and doped ones can be easily produced (which is similar to the features of PEO). Only titania films prepared using the powerful pulsed discharge oxidation have been reported.[14] Since anodic $TiO_2$ is semiconductor and $Al_2O_3$ is dielectric, the surface properties of the respective films are expectedly different.

The potential measured on a metal surface is known to be an important characteristic of the covering oxide film since the potential reflects its physical properties.[15−18] The measured potential consists of the contact potential and that induced by embedded charges (induced potential). Opposite charges

**Received:** May 30, 2011
**Revised:** August 8, 2011
**Published:** August 22, 2011





dx.doi.org/10.1021/jp2050542 | *J. Phys. Chem. C* 2011, 115, 18634–18639

localized near the counter interfaces create polarization of a film. Character of the charge distribution and, as a result, the magnitude of polarization of anodic alumina films have been found to be affected by anodization conditions.[4,5,19−21] In particular, Hickmott has shown[4,19] that the charge contributing to the polarization depends on the nature of the anodizing electrolyte. Lambert et al.[20] associated a permanent polarization of thin anodic alumina layers with the charges trapped by the structural defects created during the anodization process. An electrostatic force microscope and a Kelvin probe were applied to measure the potential induced by these embedded charges.[20] It was found that application of potentiostatic stage to the layers prepared using galvanostatic anodization results in significant increase of their polarization. Scanning Kelvin probe force microscopy (SKPFM) has recently been used to study electrical properties of oxidized aluminum surface since changes in Volta potential difference (VPD) measured by SKPFM are caused by changes in the induced potential.[21]

SKPFM is a promising method to study surface electrical properties.[22,23] In comparison with the conventional scanning Kelvin probe (SKP), it combines capabilities of both SKP and atomic force microscopy and provides much higher resolution when mapping the local electrical properties of a surface. The Kelvin probe methods are based on measurement of VPD between a surface and a reference electrode. In the SKPFM technique, VPD corresponds to the voltage that nulls the oscillations of the cantilever, while in the SKP method, it is equal to the voltage applied to null inducted currents between electrode and surface.[17,24] It was shown[16,25−28] that the VPD distribution observed in some metals correlates with their corrosion potential. Thus, in spite of some restrictions of the technique related to impact of topography, probe−surface interactions, and others,[17,18] SKPFM is a valuable tool for nanoscale surface studies.

In the present work, thin oxide films on aluminum surface were prepared by the powerful pulsed discharge anodization. Peculiarities of the pulsed discharge process and their impact on the growth and the resulting properties of the alumina films were considered. Morphology and VPD of the films were characterized using transmission electron microscopy (TEM), electrochemical impedance spectroscopy (EIS), and SKPFM facilities. VPD measured as a function of the film thickness was analyzed in comparison with the VPD thickness dependences previously reported for the alumina films prepared using the conventional galvanostatic and potentiostatic methods.

## 2. EXPERIMENTAL SECTION

The electrochemical cell used for the pulsed discharge oxidation of aluminum was made of high-impact polystyrene and consisted of a plate Al anode (Goodfellow, 99.999%) with a working surface of 5 $cm^2$ placed inside a cylindrical Ti-foil cathode (Alfa Aesar, 99.7%) with 20 times larger surface area. Titanium was chosen as a cathode material because of its high strength and chemical stability. Both electrodes were mechanically polished using emery papers up to grid 4000. The titanium electrode was then chemically polished in a $HF:HNO_3$ (1:3 by volume) mixture, while the aluminum plate was electrochemically polished in a $C_2H_5OH:HClO_4$ (4:1 by volume) electrolyte in potentiostatic regime at 20 V to mirror finish. After polishing, both electrodes were rinsed with deionized water.

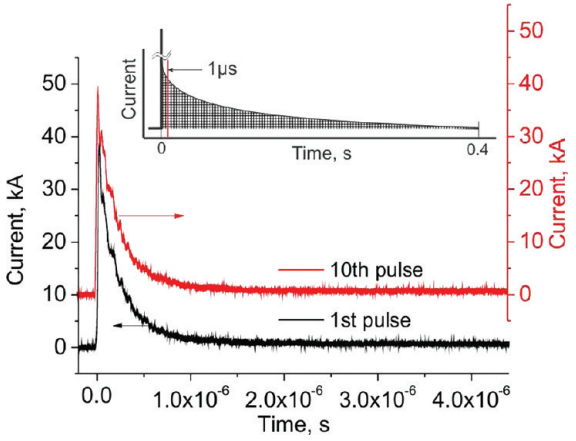


**Figure 1.** Time evolution of the current through aluminum electrode during the first 4 $\mu$s. The inset shows schematically a profile of the pulsed discharge as a whole. The dashed area represents the total charge passed through the electrode.

A 0.1 M ammonium pentaborate ($(NH_4)_2B_{10}O_{16}$) aqueous solution was used as the electrolyte for comparison reasons since alumina films prepared by the conventional anodization methods in that electrolyte are well-studied.[5,7,29,30] Electric discharges between the electrodes were generated using a low-inductivity 100 $\mu$F capacitor bank charged to a definite voltage (1400 V). The capacitor was commutated to the cell using a low-inertial relay triggered by a synchronizing pulse. To prepare the films with different thicknesses, the capacitor was discharged through the electrochemical cell from 1 to 15 times. Time−current characteristics of discharges were recorded using a Tektronix DPO7054 oscilloscope connected to the system and were synchronized with trigger.

The EIS measurements were performed using a Gamry FAS2 femtostat with a PCI4 controller in a frequency range from $10^5$ to $10^{-3}$ Hz with seven points per decade. The measurements were carried out at room temperature in a conventional three-electrode cell consisting of a mercury−mercurous sulfate reference electrode, a platinum foil as the counter electrode, and the working electrode with an exposed area of 1 $cm^2$. Impedance spectra were recorded applying a 10 mV sinusoidal perturbation at the open-circuit potential. The cell was placed in a Faraday cage to avoid interference with external electromagnetic fields. The testing electrolyte was 0.1 M ammonium pentaborate. Before recording the spectra, the system was allowed to attain a stable open-circuit potential. At least two samples prepared at the same conditions were tested to ensure reproducibility of the results. The impedance plots were fitted using equivalent circuits by means of the Echem Analyst software from Gamry Inc.

Some of the anodized samples were annealed at 300 °C for 3 h followed by quenching in air down to room temperature. A heating rate of 5 °C/min was applied. SKPFM measurements were performed on all the samples both before and after heat treatment.

TEM study was carried out using a Hitachi H9000 transmission electron microscope at acceleration voltage of 300 kV. Electron transcendent sections of the samples for TEM were cut with a Leica Reichert Supernova ultramicrotome.

Digital Instruments Nanoscope III atomic force microscope with conductive Pt−Cr probes (Budget Sensors) was used for SKPFM measurements. The measurements were performed in

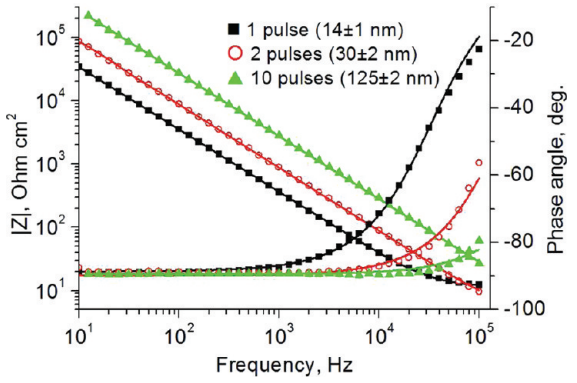


**Figure 2.** Bode plots of the oxide films formed on aluminum surface as a result of pulsed discharge anodization; solid lines represent the fitting results.

several areas of at least two samples of the same thickness. The obtained VPD values are presented versus the Volta potential values measured on Ni as a reference.

## 3. RESULTS

A series of samples with the pulsed discharge anodic alumina layers were prepared applying 1, 2, 3, 5, 10, and 15 pulses. A typical current pulse through the electrochemical cell during the discharge oxidation of aluminum is shown in Figure 1. As opposed to pulsed oxidation of titanium,[14] no change in the discharge profiles recorded during the first microseconds of each pulse is observed: the first and the following discharge peaks are essentially similar.

The thickness of the alumina films prepared by the pulsed discharge anodization was evaluated from EIS measurements. EIS spectra of the obtained films are shown in Figure 2. All the spectra demonstrate a broad relaxation process described by one time constant. This relaxation can be assigned to capacitance of the dielectric oxide films. The spectra were fitted using a simple equivalent circuit with one parallel R−C element for description of oxide film and an additional R element connected in series for the electrolyte resistance. A high-quality fit was achieved as seen in Figure 2. The thickness of the films was calculated using a plane capacitor model and the capacitance values derived from the EIS spectra. The dielectric constant value of alumina for the calculations was taken to be 9.[31]

It was found that the thickness ($d$) of the pulsed discharge films as a function of the number of applied pulses ($N$) obeys well an empirical equation

$$d = d_0 N^{\alpha} \quad (1)$$

where $d_0 = 16$ nm and $\alpha = 0.9$. A power law is known to describe a constant growth rate process: the relative increment $\Delta d/d$ of the film thickness is proportional (with a factor of 0.9) to the relative increase $\Delta N/N$ of the number of pulsed discharges.

The thickness values calculated from the EIS spectra were verified by the TEM measurements. Figure 3 shows the cross sections of the aluminum electrodes anodized by application of 3 and 10 discharge pulses. The obtained alumina films were measured to be 46 ± 2 and 127 ± 2 nm thick, respectively (cf. 45 ± 2 and 125 ± 2 nm found from the EIS data), and were uniform along the sections. It was also revealed from the TEM study that all the films obtained by high-voltage pulsed discharge

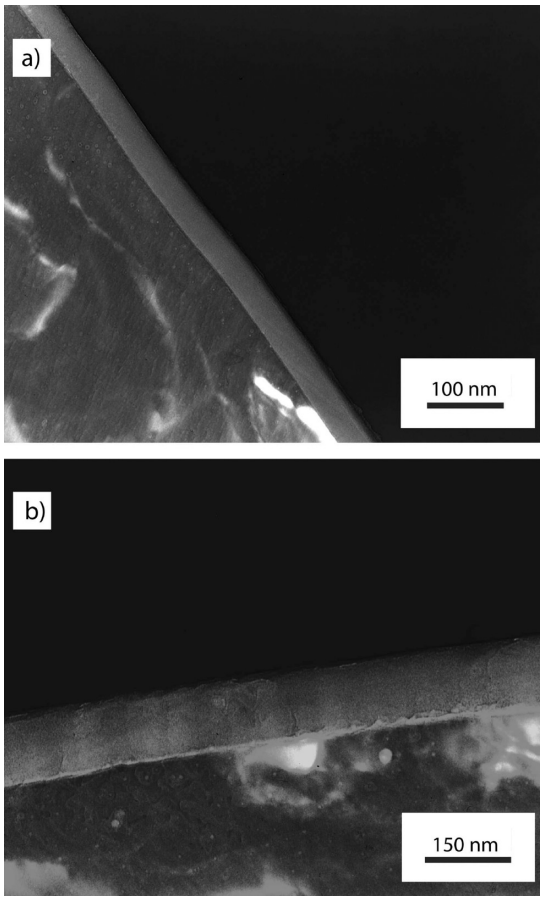


**Figure 3.** TEM cross sections of the aluminum samples anodized by application of (a) 3 and (b) 10 discharge pulses which resulted in formation of anodic alumina films of 46 ± 2 and 127 ± 2 nm thick, respectively.

anodization (1−15 pulses) were smooth, dense, and free of microdefects. However, attempts to produce thicker alumina films failed. The films formed by application of 18 and more pulsed discharges demonstrated typical signs of point electrical breakdown. In those points, the underlying aluminum surface was also affected. Thus, the maximal thickness of a dense and homogeneous alumina film which can be produced using the pulsed discharge anodization method with the above-described conditions is about 200 nm.

Figure 4 shows typical surface topography and the VPD map of the aluminum sample before and after 10 pulsed discharges which correspond to a native alumina layer (about 1 nm thick) and an anodic film (~127 nm), respectively. One can see that no visible change of topography occurs as a result of the anodization process, while the average VPD increases from about −1.28 V to +6.33 V (hereafter versus a Ni reference). Also, scatter of the VPD values in the typical SKPFM scans of the alumina films prepared by pulsed discharge technique is generally smaller than that observed in the films produced by the conventional anodization methods.[21] This suggests that in spite of the discrete character of the deposition methods (layer by layer) the pulsed discharge films have uniform properties. Furthermore, it follows from comparison of both surface topography and VPD maps of the anodic alumina films prepared by different methods that in the case of the pulsed discharge anodization the resulting film

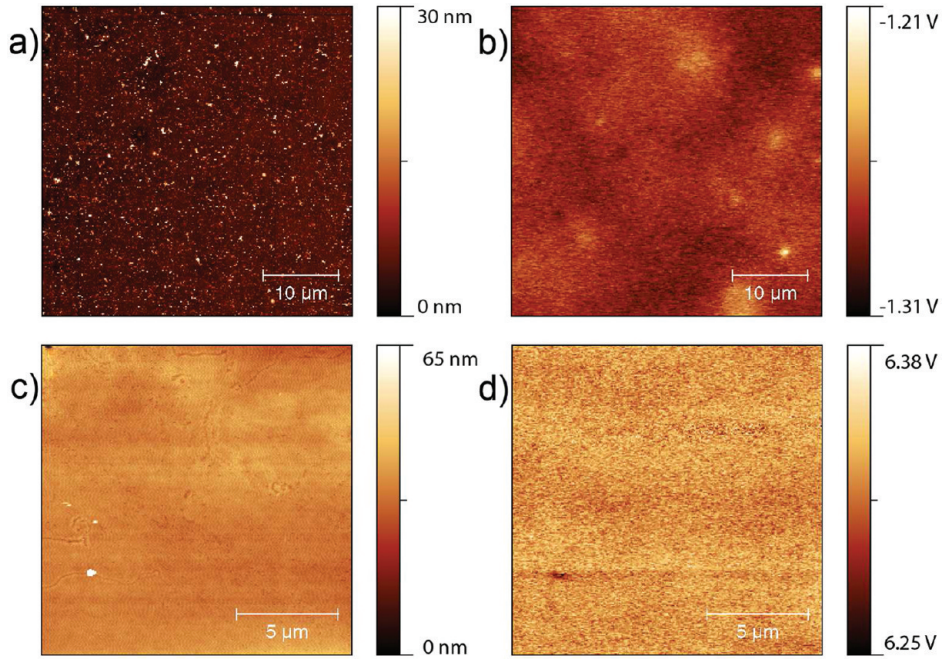


**Figure 4.** Maps of the surface topography (left) and Volta potential difference (right) of the aluminum sample (a, b) before and (c, d) after the pulsed discharge anodization procedure (10 pulses applied).

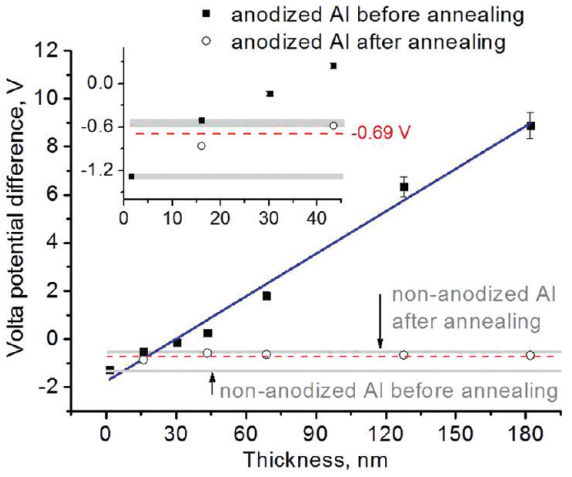


**Figure 5.** Volta potential difference versus thickness of the alumina films prepared by pulsed discharge anodization method before (solid squares) and after (open circles) annealing at 300 °C. The inset shows magnification of the plot for the thickness range of 1−45 nm. The reference levels corresponding to the measured VPD values for the untreated aluminum sample and the nonanodized sample thermally oxidized at 300 °C are indicated.

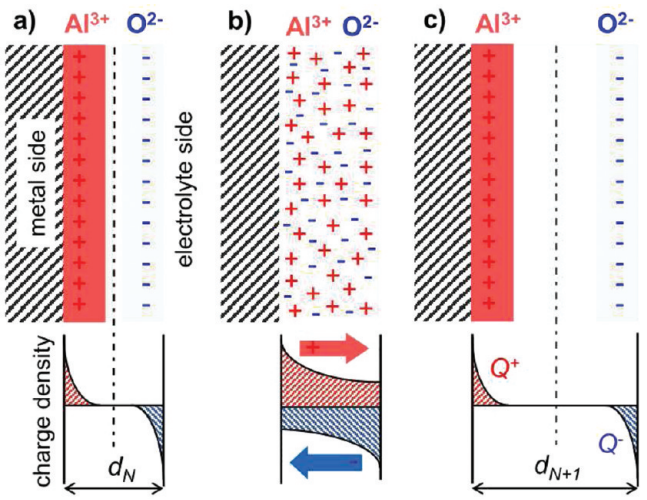


**Figure 6.** Schematic representation of charge distribution in alumina film polarized as a result of anodization: (a) after *N*th pulsed discharge, (b) during the first step of the discharge (in a field of ~$10^9$ V/cm), and (c) after ($N$ + 1)th pulsed discharge . Provided the same charge is embedded, the induced potential is proportional to the film thickness, $d$. Charge distribution in the pulsed discharge films is suggested to be essentially similar to that in the films produced by combination of the galvanostatic and potentiostatic methods.[21]

quality is less dependent on the initial state of aluminum surface. Pulsed discharges evidently smooth out imperfections of the charge distribution caused by surface defects.

Dependence of VPD on thickness of the pulsed discharge films is presented in Figure 5. As in the case of the anodic alumina films prepared by the conventional methods, this dependence is also described well with a linear function.[20,21] The slope value ($\Delta V/\Delta d$) obtained for the pulsed discharge, 0.059 ± 0.003 V/nm, is slightly higher than those previously found for the most polarized films produced by combination of the galvanostatic and potentiostatic methods (cf. ~0.052 and 0.055 V/nm reported by Lambert et al.[20] and Yasakau et al.,[21] respectively). However, taking into account a typical data spread of SKFPM measurements, all the above-mentioned values $\Delta V/\Delta d$ are equal within the limits of experimental error. Thus, the magnitude of polarization of the alumina films prepared by the pulsed discharge method is comparable with that observed in the conventional anodic films of the same thickness. It can be suggested that


dx.doi.org/10.1021/jp2050542 |*J. Phys. Chem. C* 2011, 115, 18634–18639

despite the apparent differences in the anodization methods their film growth mechanisms and hence the associated effects which result in the polarization of the films are inherently the same.

Because of the specificity of oxidation of a metal surface, the layers bordering the interfaces are characterized by structure imperfections: vacancies[4] and incorporated species (e.g., from electrolyte),[20] and thereby are the most defective regions of the oxide film. It has been accepted that polarization of an anodic film is caused by charge carriers (mainly by electrons and Al ions) trapped by these defects.[20,21] These defects and, accordingly, the embedded charges are distributed throughout a film with the maximal charge density near the metal/oxide and oxide/air interfaces as shown in Figure 6a, c.

Annealing of the as-prepared anodic alumina films was shown to lead to a release of their polarization owing to reduction of the number of defects[20] and to the relaxation of the charge.[32] It has recently been revealed[21] that on annealing, the measured VPD of the anodic films tends to the certain (equilibrium) level independent of the film thickness. This level is suggested to be the VPD value for an alumina film formed by thermal oxidation in air at the given annealing temperature. VPD of the pulsed discharge films annealed at 300 °C was found to be $-0.69 \pm 0.05$ V (Figure 5). Annealed films prepared by combination of the galvanostatic and potentiostatic methods demonstrated $-0.75 \pm 0.05$ V.[21] Thus, the VPD value of the annealed pulsed discharge films is closer to the equilibrium level (which is around $-0.55$ V) measured in the non-anodized aluminum sample annealed at 300 °C than that of the conventionally prepared anodic films annealed at the same temperature. It was suggested[21] that the equilibrium level is not reached because of residual defects (which do not disappear after annealing). When the concentration of defects in some anodic films is higher or when their distribution is wider, the number of residual defects is also higher. Correspondingly, the VPD value of this film after annealing will be further from the equilibrium level at the given annealing temperature.

## 4. DISCUSSION

The presented results demonstrate certain differences in properties between the alumina films formed using the pulsed discharge anodization and the respective anodic films prepared by the conventional methods. Their characteristic features are likely to result from specificity of the used anodization method. Thus, the pulsed discharge anodization process certainly needs to be considered in more detail.

Only 10% of the capacitor charge is consumed during the first microsecond (which corresponds to a current fall of more than 90% of the peak value) as follows from an analysis of the discharge profile (see inset in Figure 1). The remaining 90% of charge is used during the subsequent stage which lasts up to 0.5 s (depending on the thickness of the film). Thus, a pulsed discharge anodization process can be conventionally divided into two stages where the first one (fast) is about 1 $\mu$s long with the characteristic current magnitude of several kA/cm$^2$. It is believed that the main process during the first stage is ionization of an oxide film (either native film or that formed by previous oxidation). During the second (long) stage, a new layer grows. In comparison to the conventional anodization processes, this growth occurs in a much higher electrical field and a higher total charge is transferred in unit time. That is why at the pulsed discharge anodization the film growth rate is higher than in the case of any conventional method.

It seems reasonable to suggest that the discharge profile is determined by the electrical conduction of a growing anodic oxide film. In particular, the discharge can be expected to terminate faster in the case of a more conductive layer. Typical duration of the second stage at pulsed discharge anodization of titanium (anodic $TiO_2$ is a semiconductor) was found to be several times shorter[14] than that observed when preparing the respective anodic alumina (which is dielectric). Thus, during the second stage, the pulsed discharge alumina film is likely to have a significant impedance, which suggests a low concentration of the point defects and the trapped charge carriers in at least the inner part of the film.

No boundary between the layers formed by subsequent pulsed discharges has been observed by TEM (Figure 3). The films were found to be homogeneous regardless whether they were obtained by application of one or a number of pulses. The respective EIS spectra characterized by one time constant (Figure 2) confirm uniformity of the properties across the film suggesting no separation to internal sublayers. Thus, the prehistory (amount of the previous pulsed discharges which is equal to the number of the deposited layers) seems to be inessential (Figure 6) when the film thickness is below the maximal value (~200 nm). To assume a state of the film at the first stage of the pulsed discharge, energy of the electrostatic field in the film and its ionization energy were compared. The density of the electrostatic energy ($U_E$) in a film can be calculated using the expression

$$U_E = \frac{1}{2}\varepsilon_0\varepsilon E^2 = \frac{\varepsilon_0\varepsilon V^2}{2d^2} \quad (2)$$

where $E$ is the electric field strength, $V$ is an applied voltage, $d$ is the film thickness, $\varepsilon$ is the dielectric constant of the film, and $\varepsilon_0$ is the permittivity of the free space. The capacitor voltage and the dielectric constant of alumina mentioned previously in the text were used as the values of $V$ and $\varepsilon$ in the calculations.

The $U_E$ value found from eq 2 was compared with the value of ionization energy (per a volume unit) in the form of $(\rho N_A W_t)/(M)$, where $\rho$ (2.8−3.0 g/cm$^3$)[33] and $W_t$ (1.5 eV)[34] are density and (molecular) thermal ionization energy of amorphous alumina, respectively, $M$ is molar weight of $Al_2O_3$, and $N_A$ is Avogadro's number. According to the estimations, when the film thickness does not exceed the value of an order of $10^2$ nm, the energy of electrostatic field in the first stage of pulsed discharge is enough to ionize the film over the whole volume (Figure 6b). Hence, at the first stage of the pulsed discharge anodization, the existing defects and polarization do not matter since new defects are to be formed over again and consequently the respective polarization is to be induced during the second longer stage.

A pulsed discharge film of about 200 nm thick represents already a substantial insulator. High-voltage discharge breaks down this insulator creating weakened paths within. This action destroys the film and makes further growth impossible. In a PEO process, such a breakdown (a powerful arc) also results in a coating damage.[10] It seems that a pulsed discharge film with the thickness close to the maximal value can be hardly made thicker by means of subsequent PEO since such a film is low-defect. High concentration of defects over the whole growing coating is certainly essential for PEO since this allows multiple discharges (soft sparking[13]) at a relatively low voltage. Defectness of PEO coatings can be suggested to hamper their possible polarization.

The potential induced in an oxide film and measured by SKPFM is a function of both the total embedded charge and its distribution profile.[21] Provided the same charge is embedded, the bigger spacing is between positive and negative charges (i.e., the narrower the charge distribution profile and/or the thicker the film (cf. Figure 6a and c), the larger the respective polarization.

The VPD values measured in as-prepared pulsed discharge films are comparable with that of the films of the same thickness obtained by the conventional anodization methods. At the same time, the VPD value of the annealed pulsed discharge films is closer to the equilibrium level. This suggests that their measured potential is contributed by a smaller amount of the embedded charges located in narrower defect layers bordering the film interfaces. Thus, the pulsed discharge films are less defective in their inner layers than the respective alumina films produced by the conventional anodization methods.

## 5. CONCLUSIONS

A novel powerful pulsed discharge oxidation method allows the production of homogeneous low-defect anodic films up to ~200 nm thick on an aluminum surface. The thickness values estimated by independent methods (EIS and TEM) are in excellent agreement which suggests a good homogeneity of these films.

A pulsed discharge anodization process can be conventionally divided into two stages: ionization and growth of a film. Ionization of the film over the whole volume during the first microsecond of the process is an essential feature of the pulsed discharge anodization as it causes fast film growths and homogeneity. The film thickness can be controlled during the anodization process since this parameter is a power function of the number of applied pulses with a scaling exponent 0.9.

It was found from SKPFM measurements that the anodic alumina films prepared by the pulsed discharge method have more uniform surface structure and electrical properties which are less dependent on the initial surface condition than those of the films prepared by the conventional anodization methods. The pulsed discharge films demonstrate the magnitude of polarization comparable with those of the conventional anodic films of the same thickness. At the same time, in the pulsed films, the embedded charges locate in narrower defect layers bordering the film interfaces. In this respect, the pulsed discharge alumina films appear to have better barrier properties than the respective anodic films produced by the conventional methods.

## AUTHOR INFORMATION

### Corresponding Author

*Tel.: +351-234-370-255; fax: +351-234-425-300; e-mail: mzheludkevich@ua.pt.

## ACKNOWLEDGMENT

Financial support of the Portuguese Foundation for Science and Technology (FCT-Portugal) through the project PTDC/CTM/72223/2006 is gratefully acknowledged.

## REFERENCES

(1) Jeurgens, L. P. H.; Sloof, W. G.; Tichelaar, F. D.; Mittemeijer, E. J. *J. Appl. Phys.* **2002**, *92*, 1649–1656.

(2) Klootwijk, J. H.; Jinesh, K. B.; Dekkers, W.; Verhoeven, J. F.; van den Heuvel, F. C.; Kim, H.-D.; Blin, D.; Verheijen, M. A.; Weemaes, R. G. R.; Kaiser, M.; Ruigrok, J. J. M.; Roozeboom, F. *IEEE Electron Device Lett.* **2008**, *29*, 740–742.

(3) Robertson, J. *Rep. Prog. Phys.* **2006**, *69*, 327–396.

(4) Hickmott, T. W. *J. Appl. Phys.* **2007**, *102*, 093706.

(5) Thompson, G. E.; Xu, Y.; Skeldon, P.; Shimizu, K.; Han, S. H.; Wood, G. C. *Philos. Mag.* **1987**, *B55*, 651–667.

(6) Despic, A.; Parkhutik, V. P. In *Modern Aspects of Electrochemistry*; Bockris, J. O. M., White, R. E., Conway, B. E. S., Eds.; Plenum Press: New York, 1989; Vol. 20, pp 401−504.

(7) Ozawa, K.; Majima, T. *J. Appl. Phys.* **1996**, *80*, 5828–5836.

(8) Uchi, H.; Kanno, T.; Alwitt, R. S. *J. Electrochem. Soc.* **2001**, *148*, B17–B23.

(9) Geiculescu, A. C.; Strange, T. F. *Thin Solid Films* **2006**, *503*, 45–54.

(10) Yerokhin, A. L.; Nie, X.; Leyland, A.; Matthews, A.; Dowey, S. J. *Surf. Coat. Technol.* **1999**, *122*, 73−93.

(11) Yerokhin, A. L.; Lyubimov, V. V.; Ashitkov, R. V. *Ceram. Int.* **1998**, *24*, l–6.

(12) Sundararajan, G.; Rama Krishna, L. *Surf. Coat. Technol.* **2003**, *167*, 269–277.

(13) Matykina, E.; Arrabal, R.; Skeldon, P.; Thompson, G. E. *Electrochim. Acta* **2009**, *54*, 6767–6778.

(14) Poznyak, S. K.; Talapin, D. V.; Kulak, A. I. *J. Electroanal. Chem.* **2005**, *579*, 299–310.

(15) McCafferty, E. *Corros. Sci.* **1995**, *37*, 481–492.

(16) Schmutz, P.; Frankel, G. S. *J. Electrochem. Soc.* **1998**, *145*, 2285–2295.

(17) Rohwerder, M.; Turcu, F. *Electrochim. Acta* **2007**, *53*, 290–299.

(18) Hausbrand, R.; Stratmann, M.; Rohwerder, M. *J. Electrochem. Soc.* **2008**, *155*, C369–C379.

(19) Hickmott, T. W. *J. Appl. Phys.* **2000**, *87*, 7903–7912.

(20) Lambert, J.; Guthmann, C.; Ortega, C.; Saint-Jean, M. *J. Appl. Phys.* **2002**, *91*, 9161–9169.

(21) Yasakau, K. A.; Salak, A. N.; Zheludkevich, M. L.; Ferreira, M. G. S. *J. Phys. Chem. C* **2010**, *114*, 8474–8484.

(22) Jacobs, H. O.; Knapp, H. F.; Muller, S.; Stemmer, A. *Ultramicroscopy* **1997**, *69*, 39–49.

(23) Yasutake, M.; Aoki, D.; Fujihira, M. *Thin Solid Films* **1996**, *273*, 279–283.

(24) Yee, S.; Oriani, R. A.; Stratmann, M. *J. Electrochem. Soc.* **1991**, *138*, 55–61.

(25) Yasakau, K. A.; Zheludkevich, M. L.; Lamaka, S. V.; Ferreira, M. G. S. *J. Phys. Chem. B* **2006**, *110*, 5515–5528.

(26) Tanem, B. S.; Svenningsen, G.; Mardalen, J. *Corros. Sci.* **2005**, *47*, 1506–1519.

(27) Zheludkevich, M. L.; Yasakau, K. A.; Poznyak, S. K.; Ferreira, M. G. S. *Corros. Sci.* **2005**, *47*, 3368–3383.

(28) Jonsson, M.; Thierry, D.; LeBozec, N. *Corros. Sci.* **2006**, *48*, 1193–1208.

(29) Nguen, T. N.; Foley, R. T. *J. Electrochem. Soc.* **1982**, *129*, 27–32.

(30) Skeldon, P.; Skeldon, M.; Thompson, G. E.; Wood, G. C. *Philos. Mag. B* **1989**, *60*, 513–521.

(31) Sullivan, J. P.; Barbour, J. C.; Dunn, R. G.; Son, K. A.; Montes, L. P.; Missert, N.; Copeland, R. G. In *Proceedings of the Symposium on Critical Factors in Localized Corrosion III*; Kelly, R. G., Natishan, P. M., Frankel, G. S., Newman, R. C., Eds.; The Electrochemical Society Proceedings: Boston, MA, 1998.

(32) Goodman, A. M. *J. Appl. Phys.* **1970**, *41*, 2176–2179.

(33) Nakamura, R.; Shudo, T.; Hirata, A.; Ishimaru, M.; Nakajima, H. *Scr. Mater.* **2011**, *64*, 197–200.

(34) Novikov, Yu. N.; Vishnyakov, A. V.; Gritsenko, V. A.; Nasyrov, K. A.; Wong, H. *Microelectron. Reliab.* **2010**, *50*, 207–210.

*Journal of The Electrochemical Society*, **161** (1) D73-D78 (2014)
0013-4651/2014/161(1)/D73/6/$31.00 © The Electrochemical Society


# Titania Films Obtained by Powerful Pulsed Discharge Oxidation in Phosphoric Acid Electrolytes

**Aleksey D. Lisenkov,[a,z] Sergey K. Poznyak,[b] M. Fátima Montemor,[c] M. J. Carmezim,[c] Mikhail L. Zheludkevich,[a] and Mário G. S. Ferreira[a,*]**

[a]*Department of Materials and Ceramic Engineering/CICECO, University of Aveiro, 3810-193 Aveiro, Portugal*
[b]*Institute for Physical Chemical Problems, Belarusian State University, 220050 Minsk, Belarus*
[c]*ICEMS, Instituto Superior Técnico, Universidade Técnica de Lisboa, 1049-001 Lisboa, Portugal*

Thin $TiO_2$ films were prepared on the titanium surface using the powerful pulsed discharge oxidation method (PPDO) in phosphoric acid based electrolytes. The obtained films were characterized with electrochemical impedance spectroscopy (EIS), photocurrent spectroscopy, scanning Kelvin probe force microscopy (SKPFM), and Mott-Schottky plot analysis. The potential dependence of the space charge layer capacitance has demonstrated that the ionized donor concentration in the oxide is strongly influenced by the electrolyte concentration used during the pulsed anodization. It is also shown that the main factor influencing the kinetics of the oxide film growth is the concentration of point defects which, in turn is determined by the composition of electrolyte. SKPFM results show a non-linear evolution of the Volta potential of the anodized surface with the film thickness reaching a plateau after film thickness exceeds 100 nm. The results obtained clarify the mechanisms of titania film formation under high-voltage pulses and allow tuning the semiconductive properties of thin oxide layers on titanium surfaces.
 [DOI: 10.1149/2.085401jes] 

Manuscript submitted September 6, 2013; revised manuscript received November 5, 2013. Published December 6, 2013.

Titanium and its alloys are materials widely used in many industrial applications such as aerospace and automotive industries, as well as in medicine due to their high corrosion resistance, hardness, high melting point and biomedical capability.[1–9] Titanium dioxide film which forms spontaneously on the metal surface brings high resistance against corrosion although is very thin (about 3–5 nm).[10] However additional surface modifications, such as injection of dopants, increasing the dense oxide layer thickness, forming porous layers are often needed to meet requirements of particular applications. Anodization of titanium is an attractive method that can be used for surface modification giving additional corrosion resistance, higher affinity to biological tissues, and advanced electronic properties when compared to the native thin oxide films.[11–14] The anodic films formed on Ti surface can have various morphologies from dense barrier layers to porous deposits composed by separated nanotubes[15,16]

Titanium anodization can be performed in different electrolytes including mineral acids. There are a number of publications, where anodization has been carried out in phosphoric acid.[17,18] The corrosive attack of phosphoric acid to titanium and its alloys is relatively mild probably due to the adsorption of phosphate ions on the surface of the native metal oxide.[19–21] Incorporation of phosphate ions in titanium oxide can result not only in an increase of corrosion stability in biological environment, but also in improved compatibility with biological tissues.

Recently a new electrochemical technique, namely powerful pulsed discharge oxidation (PPDO) of metals, has been suggested.[22–24] In this technique, electrochemical reaction occurs at the metal-electrolyte interface under the action of single high-voltage (>1 kV) pulses. Growth of the film under these conditions occurs at much higher rates than in the case of conventional galvanostatic or potentiostatic methods.[22] This results in the formation of oxide films with properties different of those obtained by conventional approaches. For example the anodic films prepared by the pulsed discharge method on Ti in sulfuric acid electrolytes are constituted by a single uniform dense amorphous oxide, while films of the same thickness prepared by the conventional galvanostatic method present more complex structure consisting of two layers: an inner crystalline and an outer amorphous one.[24–26]

Powerful pulsed discharge method was also used to produce anodic films on the aluminum substrate. The main difference of the anodization processes that occurring on these two metals originates from different electronic properties of the respective oxides. The oxide prepared on aluminum shows well pronounced dielectric properties, while the titania demonstrates typical semiconductor properties. In the case of aluminum the structure of the anodic films prepared by both the pulsed discharge technique and by the galvanostatic/potentiostatic method is rather similar. However PPDO films are less dependent on the starting metal surface conditions and show very uniform dielectric properties as demonstrated by the even distribution of Volta potential along the entire surface.[23] In this work a new two-stage mechanism of film growth under powerful discharge was also suggested. The full ionization of entire anodic film occurs in a first step during a few microseconds followed by a slower anodic faradaic process of film formation. The fact that the entire film is fully ionized during the first step leads to vanishing out the difference between different zones on the surface and confers creation of a very uniform layer.

However some mechanistic details of the processes which occurring on Ti during the anodization pulse and the main factors affecting the process are not clear yet. In the present paper the titania anodic films on titanium were prepared by the powerful pulsed discharge method in phosphoric acid solutions with different concentration. A set of electrochemical methods was used to clarify the effect of electrolyte concentration on the kinetics of anodization processes and on the electronic properties of the obtained film. This information is important for optimization of the PPDO method helping to predict the influence of the electrolyte and other experimental conditions on the final properties of the obtained films.

## Experimental

The electrochemical cell used for the pulsed discharge oxidation of titanium was made of high-impact polystyrene and consisted of a Ti anode plate (Goodfellow, 99.999%, dimensions: 100 × 0.8 × 1 mm) with a working surface of 4.4 $cm^2$ placed inside a cylindrical Ti cathode (Alfa Aesar, 99.7%) with about 20 times larger surface area. Titanium was chosen as a cathode material due to its high strength and chemical stability. Both electrodes were mechanically polished using abrasive papers up to grid 4000. Then the titanium electrodes were chemically polished in a HF:$HNO_3$ (1:3 by volume) mixture to mirror finish and finally rinsed with deionized water.

The anodization of titanium in phosphoric acid electrolytes with different concentrations (1, 2 and 4M) was performed. Electric discharges between the electrodes were generated using a low-inductance 100 μF capacitor bank, charged to a definite voltage (1400 V). The capacitor was commutated to the cell using a low-inertial relay triggered by a synchronizing pulse. In order to prepare films with different

*Electrochemical Society Active Member.
[z]E-mail: lisenkov@ua.pt

thicknesses, the capacitor was discharged through the electrochemical cell between 1 to 5 times. The thickness of the films was found to be a near linear function of the number of pulses with increment of 25 nm/pulse. Time-current responses of discharges were recorded using a Tektronix DPO7054 oscilloscope connected to the system and synchronized with trigger.

The electrochemical impedance spectroscopy (EIS) measurements were performed using a Gamry FAS2 Femtostat with a PCI4 Controller in a frequency range from $10^5$ to $10^{-3}$ Hz with 7 points per decade. The measurements were carried out at room temperature in a conventional three-electrode cell consisting of a mercury–mercurous sulfate reference electrode, a platinum foil as a counter electrode and the working electrode with an exposed area of 1 $cm^2$. Impedance spectra were recorded applying a 10 mV (RMS) sinusoidal perturbation at an open circuit potential. The cell was placed in a Faraday cage to avoid interferences with external electromagnetic fields. The electrolyte used for EIS measurements was 0.1 M acetic buffer solution (pH = 6.03). Before recording the spectra, the system was allowed to attain a stable open circuit potential. At least two samples prepared in the same conditions were tested to ensure reproducibility of the results. The impedance plots were fitted using equivalent circuits by means of the Elchem Analyst software from Gamry Inc.

In the photoelectrochemical study the working electrode was illuminated through a quartz window with monochromatic light (beam area 0.12 $cm^2$). The optical instrumentation consisted of a 150 W Xe lamp (Oriel 6254), a 250 mm f18 monochromator (Oriel 77200), a stepper motor to control the wavelength and a mechanical chopper. The photocurrent was obtained by connecting the current output of the potentiostat (EG&G 273) to a lock-in amplifier (Brookdeal EG&G 5210) and recording the voltage output due to the signal at 19 Hz (the chopping frequency). The recorded values were then worked out to calculate the photocurrent and the quantum efficiency values using a spreadsheet software package.

TEM studies carried out using a Hitachi H9000 transmission electron microscope at an acceleration voltage of 300 kV. Electron transparent sections of the samples for TEM were cut with a Leica Reichert Supernova ultramicrotome. The main problem during preparation of the titania samples was low stability of the oxide layer under high energy beams (especially ion milling). The high energy can lead to recrystallization of titania and misleading results. Taking into account that crystallization is an important part of this work, ultramicrotomy was chosen since it does not induce change in the crystallinity of the oxides. However titanium is known to react with the material of a diamond knife leading causing its degradation. To reduce the damaged area of the knife, small bars of the metal with oxide (less than 1 × 0.05 × 0.05 mm) were cut from the electrodes and embedded into resin. Then the typical procedures of trimming were performed resulting in locating the sample bar in the middle of the pyramid perpendicularly to the cutting-off side. Finally sectioning with diamond knife was performed. The sample thickness was about 15–20 nm.

Digital Instruments Nanoscope III atomic force microscope with conductive Pt-Cr probes (Budget Sensors) was used for SKPFM measurements. The measurements were performed in several areas in at least two samples with identical oxide thickness. The obtained Volta potential difference (VPD) values are presented versus the Volta potential values measured on a pure Ni as a reference.

## Results and Discussion

*TEM characterization.*— Figure 1 shows a cross-section TEM image of titanium oxide film prepared by the high voltage pulse oxidation method in solution of 1M phosphoric acid on the titanium substrate. After 5 pulses a uniform oxide film with a thickness about of 120 nm is formed. Neither crystallites nor different layers can be observed in this film. The structure of the obtained film is similar to the one produced in sulphuric acid electrolyte as reported elsewhere.[24]

*Mott- Schottky analysis and photocurrent measurements.*— Impedance measurements provide essential information about physical properties of oxide films measuring the electrochemical response in a wide frequency range. In the case of semiconductive surfaces the responses of the space charge region and the capacitance of bulk oxide can result in appearance of respective relaxation processes on the spectra.[24] However these time constants are often overlapped and cannot be easily discriminated. Application of external polarization can help to separate response from capacitance of space charge region since only this component is influenced by the applied electrical field. Thus acquisition of impedance spectra under electrical polarization on the semiconductive electrode in this method can help to define the frequency ranges, corresponding to the different regions of the film (space charge region (SCR) and bulk oxide). In this way the capacitance of SCR can be accurately estimated and used for Mott-Schottky analysis to estimate electronic properties of the formed oxide layers. This approach accounts for the shifts of corresponding time constant in frequency domain conferring more adequate estimation of capacitance value when compared to conventional single frequency measurements.

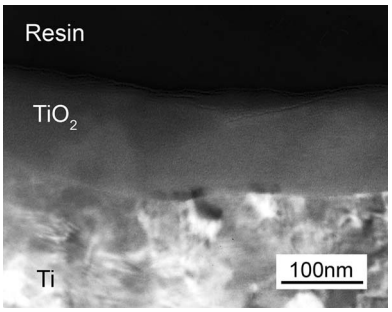


**Figure 1.** Cross-section TEM image of the anodic film on titanium prepared by high voltage method in 1M $H_3PO_4$ after 5 discharges (thickness of the film is about 120 nm).

A constant phase element (CPE) instead of a capacitor was used in all fittings presented in the work. Such modification is needed when the phase angle of the capacitor is different from −90 degrees. The impedance of the CPE, $Z_{CPE}$, depends on frequency, ω, according to the following equation:

$$Z_{CPE} = [Q\,(j\omega)^n]^{-1} \quad [1]$$

where Q is a parameter numerically equal to the admittance ($|Z|^{-1}$) at ω = 1 rad $s^{-1}$ and $n \leq 1$ is a power coefficient calculated as ratio of the maximum phase angle of the corresponding time constant to −90 degrees. The detailed description of the fitting on a similar system was previously discussed.[24]

The impedance spectra of the titania film with two different thicknesses and obtained under different polarization values are presented in Fig. 2. The frequency range $10^{-2}$–$10^0$ Hz corresponds to one time constant which can be interpreted as the space charge region (SCR) of the semiconductor film. The second time constant appears at frequencies $10^1$–$10^3$ Hz, describing the bulk part of the film. The high-frequency range of the spectra is not changed significantly under polarization, showing that single frequency measurements (which are usually performed at $10^3$ Hz for Mott- Schottky analysis) cannot be directly related to semiconductive properties of the film. This fact is especially noticeable on the sample with 120 nm thickness (Fig. 2b).

At the first impression the EIS spectra of the 70 nm thick film seem to be composed by only one time constant. However detailed analysis of the spectra reveals an asymmetry in the phase angle plot which can be interpreted as the presence of a second relaxation process. The reason why this response is not well defined is that the space charge region in this case occupies almost all volume of the film leaving only a thin layer of bulk titania with a low resistance and a capacitance significantly higher than that of the SCR layer. In this situation the response of the bulk film is almost fully overlapping with the dominating low-frequency time constant. Fitting of these spectra (Fig. 3b) with two time constants model (Fig. 3a) results in a rather

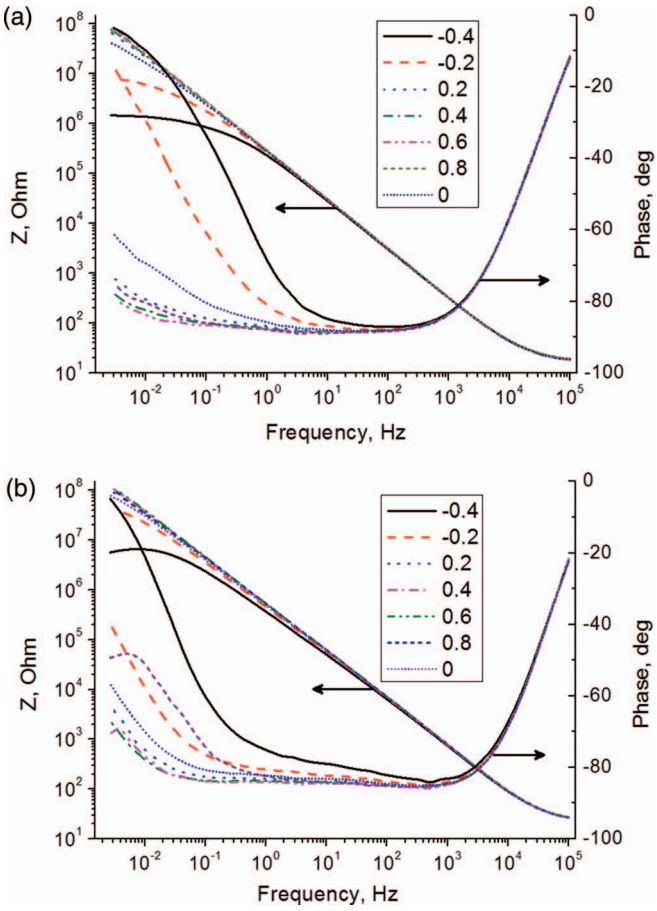


**Figure 2.** EIS spectra of $TiO_2$ films prepared in 2M $H_3PO_4$ solution recorded at different polarizations (from +0.8 V to −0.4 V vs. $Hg/HgSO_4$ reference electrode with step 0.2 V) with thicknesses of the oxide films 70 nm (a) and 120 nm (b).

accurate estimation of RC parameters for space charge (error is less than 10%). It is worth to notice that the fitting with one time constant equivalent circuit model gives a lower accuracy (error about 15–20%).

The second time constant is better defined in the region from 10 Hz to 1000 Hz in the case of thicker films (Fig. 2b). The reason for this is that for thicker films the contribution of the bulk part of the coating becomes more important, resulting in a well-separated response. Fitting with two time constant model (Fig. 3a) gives relatively good results (Table I, Fig. 3c) while use of one RC equivalent circuit can be considered as unjustifiable oversimplification in this case. Calculation of the capacitance from the constant phase element was previously described.[24]

The SCR capacitance for all studied samples at different potentials was calculated and used for the constructing Mott- Schottky analysis (Fig. 4). A correction for the Helmholtz layer and bulk region capacitance is not required in this situation, since fitting gives values of pure capacity of the space charge region. The obtained Mott-Schottky plots

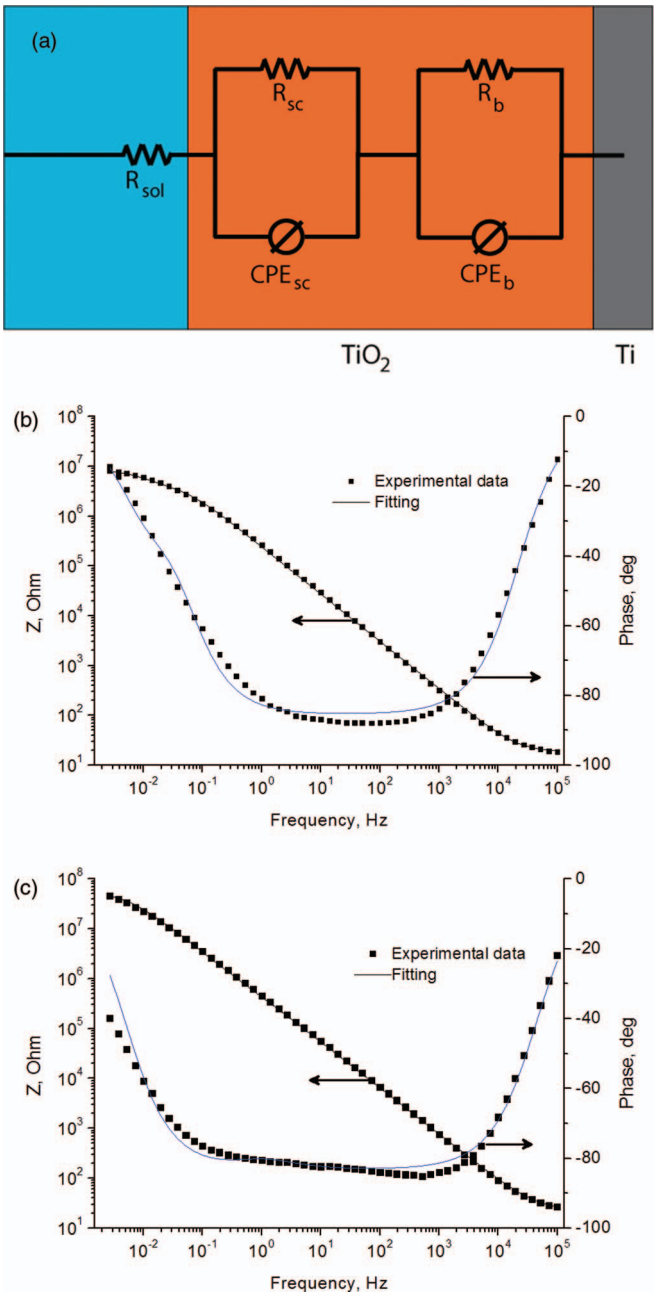


**Figure 3.** Model (a) and fitting results of 70 nm (b) and 120 nm (c) titanium oxide films under −0.2 V polarization.

are typical for such systems and a linear part of the plots was used for calculation the ionized donor concentration.

Figure 5a shows the dependence of the calculated ionized donor concentration on the film parameters. The $N_d$ increasing with the

**Table I. Equivalent circuit parameters and respective errors (in%) obtained for fitting the impedance spectra of 120 nm thick film (Fig. 3c) polarized at different potentials. $n_{sc}$ and $n_b$ are the power coefficients for the constant phase elements of SCR and bulk layer, respectively.**

| Applied potential (V) | $R_{sol}$ (Ohm cm$^2$) | $R_{sc} \times 10^{-7}$ (Ohm cm$^2$) | $CPE_{sc} \times 10^6$ (S s$^n$ cm$^{-2}$) | $n_{sc}$ | $R_b \times 10^{-6}$ (Ohm cm$^2$) | $CPE_b \times 10^3$ (S s$^n$ cm$^{-2}$) | $n_b$ |
|---|---|---|---|---|---|---|---|
| −0.2 | 24 ± 1.4% | 6.2 ± 2.7% | 6.2 ± 0.51% | 0.93 ± 0.14% | 3.6 ± 7.4% | 1.1 ± 8.1% | 0.92 ± 1.1% |
| 0 | 24 ± 1.8% | 18 ± 2.9% | 4.9 ± 0.44% | 0.94 ± 0.22% | 4.1 ± 8.9% | 1.5 ± 9.0% | 0.93 ± 6.1% |
| 0.6 | 25 ± 1.9% | 58 ± 2.9% | 4.6 ± 0.45% | 0.95 ± 0.91% | 2.9 ± 8.8% | 3.8 ± 8.9% | 1.0 ± 14%* |

*High value of error was obtained due to the limitation of the n. Maximum value of CPE exponent is 1, so higher values have no physical meaning.

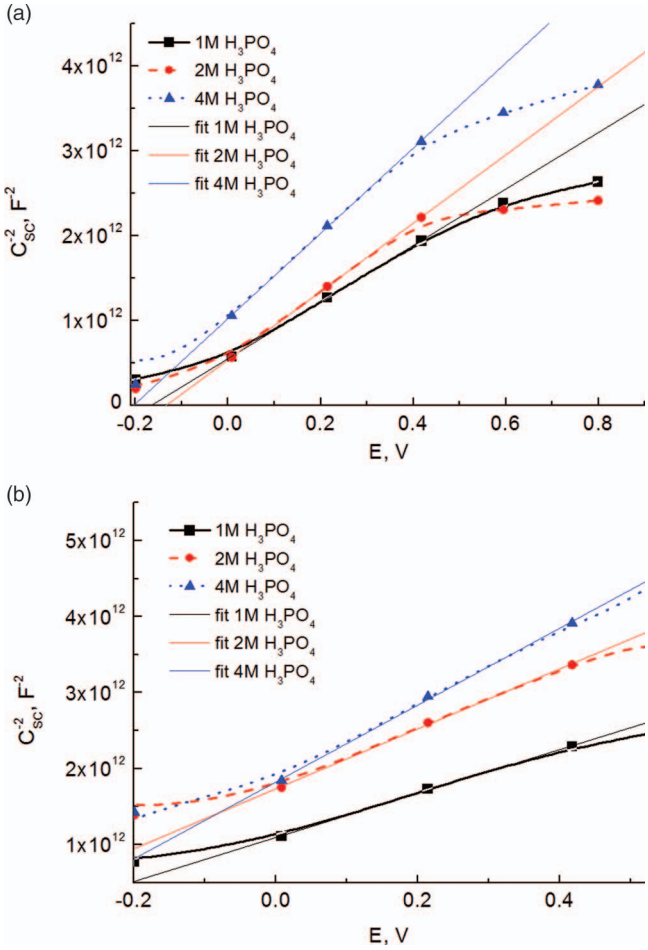


**Figure 4.** Mott-Schottky plots calculated from the SCR capacitance on titania films (with thickness 70 nm (a) and 120 nm (b)) obtained in electrolytes with different concentrations.

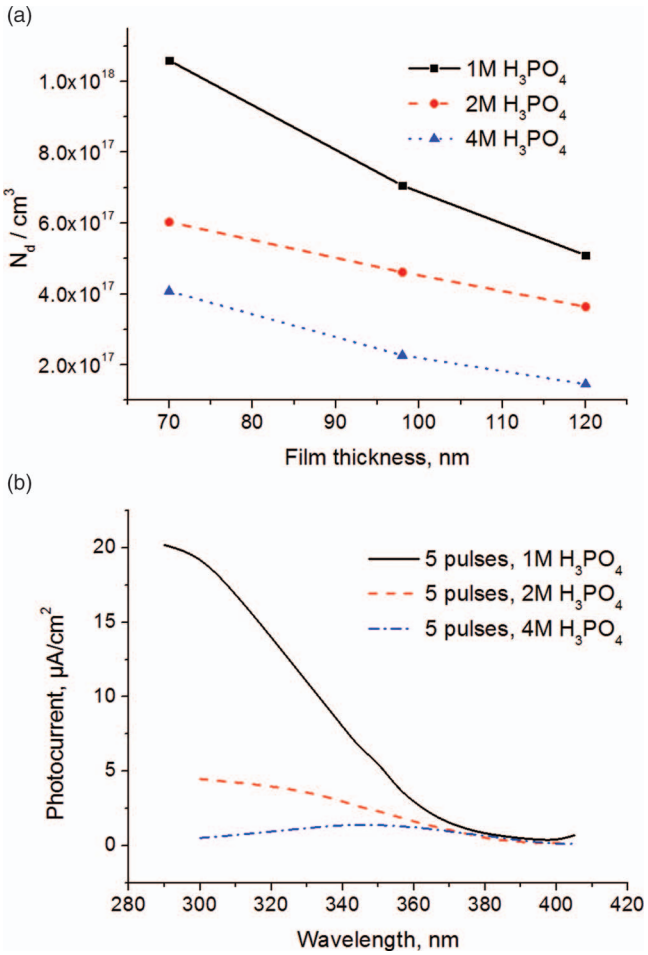


**Figure 5.** Ionized donor concentration, $N_d$ (a), and photocurrent spectra (b) of $TiO_2$ films prepared in $H_3PO_4$ solutions with different concentrations.

film thickness and with the electrolyte concentration. This can be explained by the fact that the increase of electrolyte concentration leads to a higher density of electron traps.

The photocurrent spectroscopy can be used as a complementary tool to characterize the obtained films for better understanding of their electronic structure. In the present work a qualitative analysis of the photocurrent response obtained from the electrodes 120 nm thick in the $H_3PO_4$ electrolytes with different concentrations are presented in Fig. 5b. The general observed trend shows a decrease in the photocurrent with increasing the electrolyte concentration. Taking into account that phosphor creates electron traps in titanium oxide, the drop of photocurrent response with $H_3PO_4$ concentration increment seems to be consistent (Fig. 5b). Higher concentration of phosphors should exist in the film grown in the more concentrated electrolytes, thus a higher number of electron traps are formed in the film. It is also important to notice that the titania films prepared by PPDO in phosphoric acid have a lower photoresponse in comparison to those prepared in sulfuric acid.[24]

*Volta potential measurements.*— Scanning Kelvin probe force microscopy (SKPFM) was used as an effective method for studying the electrical properties of the films. It was previously shown,[23] that PPDO anodizing of aluminum results in a more smooth Volta potential map in comparison to conventional methods of anodization. Figure 6 shows the topography and surface potential maps of the titania films with a thickness of 95 nm (4 pulses) prepared in $H_3PO_4$ solutions of different concentrations. The titania films prepared by PPDO demonstrate a very smooth Volta potential distribution (VPD) on the oxide surface similarly to the alumina. It is worth to notice that different topology effects, such as grain boundaries and cavities originating from the polishing procedure have almost no influence on the VPD. Furthermore, the Volta potential distribution becomes smoother when electrolyte concentration increases. Thus, for the sample prepared in solution of 1M phosphoric acid, fluctuation of the VPD is ±1.5 mV, while on the sample prepared in 4 M solution, the average deviation is even lower.

Figure 7 demonstrates the evolution of the average Volta potential values for 1M, 2M and 4M electrolytes with the increment of the oxide thickness. The observed growth of surface potential on titania is not linear in contrast to the results obtained on aluminum.[23] This non-linearity can be explained by the semiconductive nature of the titania film, where surface charges can spread into volume of the film much more easily than on an insulator film like alumina, avoiding high charging of the film surface.

The shift of the VPD values to higher potentials for higher electrolyte concentration can be explained as a result of better charge separation originated from lower electrical conductivity of the films, prepared in more concentrated solutions. However, it was not possible to obtain oxide films on titanium, with Volta potential higher than 0.30 mV vs. Ni. Possible explanation of this fact can be that in semiconductive films a certain maximal charge can be achieved. Further charging is impossible because the stable charge separation is limited by the recombination processes. A similar effect was observed on aluminum samples, where after heat-treatment the potential was also established at certain limit because of temperature-induced recombination.[23] The titania film does not need thermal activation for

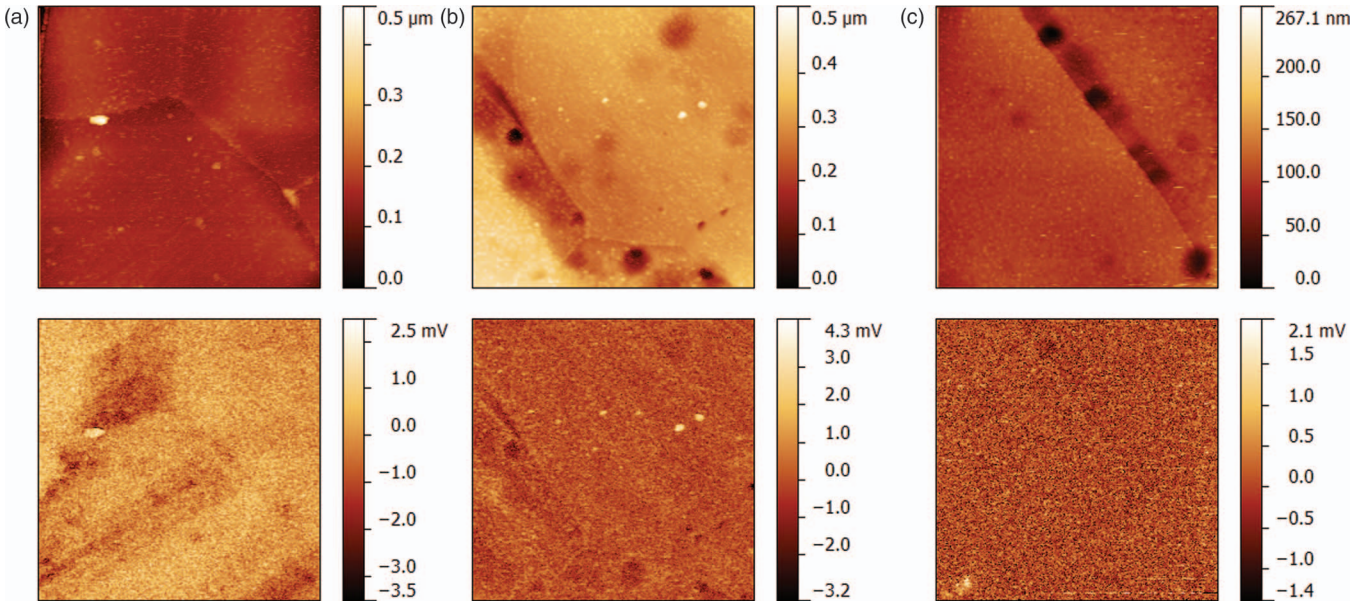


**Figure 6.** Topology (top) and measured potential distribution (bottom) on titania films with thickness 95 nm prepared by pulsed discharge anodization in phosphoric acid electrolytes with different concentrations (1M (a), 2M (b) and 4M (c)).

the charge recombination since mobility of charge carriers in the semiconductive film at room temperature is already sufficient. In contrast to the alumina films, it is also not possible to use the slope of the VPD vs. thickness plot for the characterization of the film electronic properties. However, values of the Volta potential for the same thickness can be used to compare films obtained in electrolytes with different concentrations. Thus, for all studied systems the VPD increases with the electrolyte concentration until the plateau is reached. The influence of the dopant type, its concentration and film preparation conditions on the Volta potential still needs to be further investigated.

*Discussion of the oxidation processes.*— In previous work[23] the mechanistic details of discharge on Al surface were investigated and growth model was proposed. In this section effect of the electrolyte concentration on the kinetics and mechanism of pulsed anodic film formation on Ti is discussed.

The pulsed discharge anodization process on aluminum can be conventionally divided into two stages where the first one (short) is about 1 µs long, with the characteristic current magnitude of several kA.[23] It has been proposed that ionization of an oxide film (either native film or formed by previous oxidation) is the main process during the first stage. In pulse discharge under action of high field, the resistive oxide film fully ionizes giving plasma. During the second (long) stage the growth of a new part of the layer occurs due to migration of ions inside the plasma or destabilized film. In comparison to the conventional anodization processes the oxide growth occurs in much higher electrical field and a higher total charge is transferred in an unit time leading to a higher film growth rate during the pulsed discharge anodization in comparison to the conventional method. Opposite to aluminum, in the titanium case there is no sharp distinction between the two stages (Fig. 8) and the border is blurred.

As shown above, the amount of defect centers in the film rise with increment of the electrolyte concentration. However, in the beginning of discharge, these dopant atoms can play a role of ionization centers, resulting in a higher ionization degree on the first stage. In the second stage these dopants increase of the film growth speed as they play a role of charge carriers rising mobility of ions in the destabilized film.

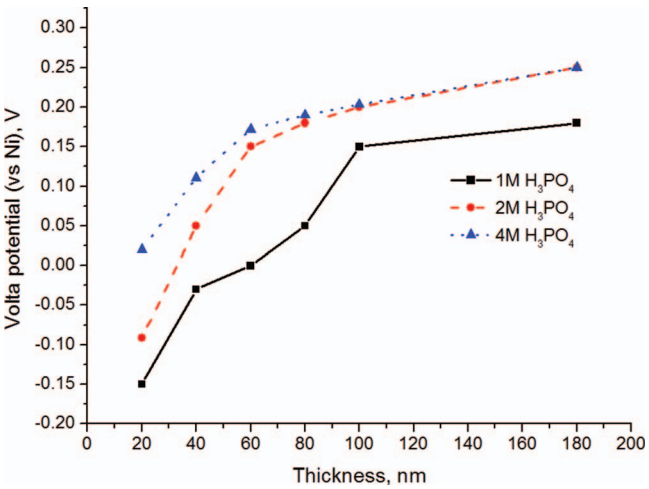


**Figure 7.** Volta potential measured on the titanium oxide films prepared by PPDO method in $H_3PO_4$ solutions with different concentrations.

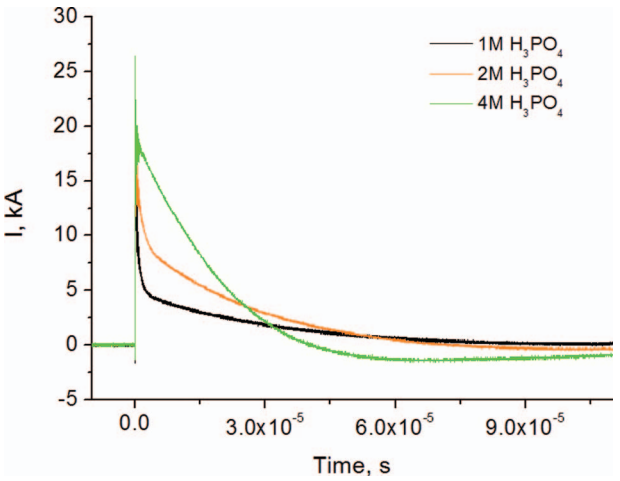


**Figure 8.** Influence of the concentration of $H_3PO_4$ on the current profiles during pulse oxidation.

As a result higher values of instantaneous current in the second stage are observed. Thus the main factor, which play role in pulse duration, is the concentration of dopant atoms in the oxide film.

In the first period of discharge, which corresponds to the oxide ionization, the difference between current profiles obtained in different electrolytes can be seen in Fig. 8. The highest current is observed for the electrode in 4M solution of $H_3PO_4$. In the second period, which corresponds to the ion migration and film growth, differences also can be also seen. After 50 μs the current between electrodes in the solution of 4M $H_3PO_4$ drops almost to zero, while in the solution of 2M it still has a value around 40A and in 1M phosphoric acid it is almost 50 A.

The lower currents at the beginning of discharge are observed for the anodic films grown in 1M phosphoric acid since the amount of defects in these films is lower in comparison to more concentrated electrolytes giving lower currents at the beginning of discharge. The first stage is better defined in this case being close to the situation obtained on aluminum. The ion transport also occurs with lower speed due to the low amount of the defects increasing duration of the second stage. In the case of current profile obtained in 4M solution, higher concentration of the defects results in higher currents in the first stage and also higher speed of film growth on the second one. These factors bring to superposition of both stages, so it is almost impossible to determine a border between two parts of the profile. In the other two electrolytes the effect of two phases superposition is not so evident.

It is known that solution conductivity becomes higher with increasing the phosphoric acid concentration. Taking into account that the current after the first stage is lower for the solutions with higher conductivity, we can consider that the solution conductivity doesn't play a main role in the discharge process.

## Conclusions

Powerful Pulsed Discharge Oxidation (PPDO) is a novel method of thin film preparation, which allows producing oxide films with tailored properties, quite different of those obtained by other conventional methods. Higher number of defects concentration in the film with increased of phosphoric acid concentration in electrolyte was confirmed by non-direct results, obtained from several complementary methods (Mott- Schottky analysis, photocurrent spectroscopy, SKPFM).

SKPFM studies show uniformity of charge distribution on the films prepared by PPDO. In contrast to the results obtained on aluminum, it was observed that the dependence of Volta potential on the film thickness is not linear, which can be explained by the semiconductive nature of the titanium oxide.

Studies of the time evolution of current on titanium electrodes in phosphoric acid solutions with different concentrations show that the shape of the current profile does not depend on the electrolyte conductivity. The main role in the discharge profile is played by the dopant concentration in the oxide film. Oxides with lower concentration of dopants have well defined stages of ionization and film growth, while in the case of films with a higher dopant concentration, the two stages merge. The growth of the oxide also occurs with a higher rate for the films with a higher concentration of dopants. Thus varying the concentration of electrolyte the electronic properties of resulting titatnia films and the kinetics of their growth can be tuned for specific applications.

## Acknowledgments

Financial support of FCT project PTDC/CTM/72223/2006 is gratefully acknowledged. Aleksey Lisenkov also acknowledges FCT grant SFRH/BD/78628/2011.

## References

1. R. W. Schutz and D. E. Thomas, in: J. R. Davis Sr. (Ed.), *Metals Handbook*, 9th ed., vol. 13: Corrosion, ASM, Materials Park, OH, 1987, p. 669.
2. M. Long and H. J. Rack, *Biomaterials*, **19**, 1621 (1998).
3. Te-Lin Yau and R. H. Jones (Ed.), *Environmental Effect on Engineered Materials*, Marcel Dekker, New York, 2001, Ch. 6.
4. H. Luckey and F. Kubli, Titanium Alloys in Surgical Implants, ASTM 796, 1981.
5. I. Gurrappa, *Mater. Characterization*, **51**, 131 (2003).
6. D. Pletcher and F. Walsh, *Industrial Electrochemistry*, Chapman and Hall, London, 1990.
7. L. D. Dorr, R. Bloebaum, J. Emmanual, and R. Meldrum, *Clin. Orthop.*, **261**, 82 (1990), http://www.dorrarthritisinstitute.org/pdf/bs-histologicalreport1.pdf.
8. G. Meachim and D. F. Williams, *J. Biomed. Mat. Res.*, **7**, 555 (1973).
9. C. E. B. Marino, E. M. de Oliveira, R. C. Rocha-Filho, and S. R. Biaggio, *Corr. Sci.*, **43**, 1465 (2001).
10. A. G. Mantzila and M. I. Prodromidis, *Electrochim. Acta*, **51**, 3537 (2006).
11. J. Qiu, J. T. Dominici, M. I. Lifland, and K. Okazaki, *Biomaterials*, **18**, 153 (1997).
12. J. W. Schultze and M. M. Lohrengel, *Electrochim. Acta*, **45**, 2499 (2000).
13. O. R. Camara, C. P. De Pauli, M. E. Vaschetto, B. Retamal, M. J. Aquirre, J. H. Zagal, and S. R. Biaggio, *J. Appl. Electrochem.*, **25**, 247 (1995).
14. J.-W. Park, J.-H. Jang, C. S. Lee, and T. Hanawa, *Acta Biomaterialia*, **5**, 2311 (2009).
15. E. Matykina, R. Arrabal, M. Mohedano, A. Pardo, M. C. Merino, and E. Rivero, *J. Mater. Sci.: Mater. Med.*, **24**, 37 (2013).
16. S. Berger, J. Kunze, P. Schmuki, A. T. Valota, D. J. LeClere, P. Skeldon, and G. E. Thompson, *J. Electrochem. Soc.*, **157**(1), C18 (2010).
17. J. E. G. Gonzales and J. C. Mirza-Rosca, *J. Electroanal. Chem.*, **471**, 109 (1999).
18. E. Krasicka-Cydzik, *Mater. Eng.*, **7**(2), 5 (2000).
19. A. Mazhar, *J. Appl. Electrochem.*, **20**, 494 (1990).
20. T. Shibata and Zhu Yao-Can, *Corros. Sci.*, **37**, 343 (1995).
21. E. Krasicka-Cydzik, *Corros. Sci.*, **46**, 2487 (2004)
22. S. K. Poznyak, D. V. Talapin, and A. I. Kulak, *J. Electroanal. Chem.*, **579**, 299 (2005).
23. A. D. Lisenkov, A. N. Salak, S. K. Poznyak, M. L. Zheludkevich, and M. G. S. Ferreira, *J. Phys. Chem. C*, **115**, 18634 (2011).
24. S. K. Poznyak, A. D. Lisenkov, M. L. Zheludkevich, A. I. Kulak, and M. G. S. Ferreira, *Electrochim. Acta*, **76**, 453 (2012).
25. J. Pan, D. Thierry, and C. Leygraf, *Electrochim. Acta*, **41**, 1143 (1996).
26. C. Jaeggi, P. Kern, J. Michler, T. Zehnder, and H. Siegenthaler, *Surf. Coat. Technol.*, **200**, 1913 (2005).

# Aluminum Anodization in Deionized Water as Electrolyte

**Aleksey D. Lisenkov,[a,*,z] Sergey K. Poznyak,[b] Mikhail L. Zheludkevich,[a,c] and Mário G. S. Ferreira[a,**]**

[a]*Department of Materials and Ceramics Engineering/CICECO, University of Aveiro, 3810-193 Aveiro, Portugal*
[b]*Institute for Physical Chemical Problems, Belarusian State University, 220050 Minsk, Belarus*
[c]*Institute of Materials Research, Helmholtz-Zentrum Geesthacht, 21502 Geesthacht, Germany*

Thin oxide films were prepared electrochemically on the aluminum surface using the high-voltage discharge and potentiostatic methods in deionized water as an electrolyte. The growth of continuous films occurred only at potentials lower than the breakdown potential. The films obtained by the discharge method are more uniform and can grow to a higher thickness in comparison to those formed by the potentiostatic mode, as demonstrated by electrochemical impedance spectroscopy (EIS), transmission electron microscopy (TEM), and scanning Kelvin probe force microscopy (SKPFM). The data herein obtained can be used as a reference to understand better the properties of the films produced in conventional electrolytes where apart from water other species are present.
 [DOI: 10.1149/2.0881607jes]


Manuscript submitted January 29, 2016; revised manuscript received April 11, 2016. Published April 21, 2016.

Anodizing treatment is widely used on aluminum and its alloys in industrial practice to enhance surface performance (corrosion resistance, hardness and wear resistance) and to modify physical and chemical properties of the metal surface.[1,2] Anodization is a convenient and important method of oxide film formation owing to low cost, flexibility and easiness.[3–7] There are several anodization processes that are currently used: conventional anodic oxidation (potentiostatic or galvanostatic) and plasma electrolytic oxidation (PEO).[3–5,7] The conventional anodization is well studied and allows growing oxide films of controlled thickness and quality.[5,7] The films can be partially hydrated.[5] The other method, PEO, which utilizes potentials above the breakdown voltage of the oxide film growing on the anode surface, makes possible to prepare well adherent, hard, ceramic-like coatings.[3,4] Both methods are currently applied in industry although they are still under investigation. One of the problems, which appears when studying the anodic oxides, is related to the impossibility of preparing a pure oxide film without foreign atoms apart from metal atoms of the substrate, oxygen and hydrogen atoms. In all electrolytes used for anodization, different ionic species are added to increase the conductivity of solution and the foreign atoms are trapped into the growing oxide.[8] According to the literature, the concentration of the foreign atoms during anodic oxidation usually does not exceed 1%,[9] however, impact of them on anodic film parameters, such as concentration of ionized donors, conductivity and photosensitivity, is significant. It was shown that the electrolyte concentration used for anodization influences the dopant content in the oxide[8] and even small amount of ionic species in solution results in changes of the film properties. Thus, in order to have a reference point for further research it is important to obtain an oxide film with minimal influence of foreign atoms. One of the electrolytes that can help to decrease the amount of entrapped foreign atoms in the oxide is anodization in hydroxide solutions. Although the concentration of extraneous elements is lower than the elements entrapped from the conventional electrolytes (such as ammonium pentaborate), even in this case foreign cations will be entrapped to the bulk of the film. Of course, impurity-free oxide on the metal surface can be prepared by other methods, such as oxidation in oxygen atmosphere at high temperature[1] or in boiling water,[10] but the properties of the obtained films will be different of those prepared by electrochemical oxidation. This motivates the present work where only deionized water was used as an electrolyte.

The properties of the films obtained in the present work were studied by scanning (SEM) and transmission electron microscopies (TEM), electrochemical impedance spectroscopy (EIS) and scanning Kelvin probe force microscopy (SKPFM). SKPFM allows simultaneous mapping of topography and Volta potential distribution on passive surfaces in air.[11,12] The Kelvin probe methods are based on measurement of Volta potential difference (VPD) between a surface and a reference electrode. Several factors can influence the Volta potential measurements, i.e. composition and structure of the oxide film covering the aluminum surface and intermetallics, tip–sample distance and adsorption of different molecules at the surface. Previously it was shown[10,13] that the VPD distribution observed on some metal surfaces correlates, for example, with their corrosion properties.

The main aim of the present work is to demonstrate the possibility of preparing impurity-free anodic oxide films on valve metals, particularly aluminum, by high-voltage anodization in deionized water. The current paper is the first part of a research focused on the preparation of impurity-free oxides by electrochemical methods.

## Experimental

The electrochemical cell used for anodization consisted of an aluminum (Alfa Aesar, 99.999%) anode with a working surface of 4 $cm^2$ and Ti cathode (Alfa Aesar, 99.7%) with about 20 times larger surface area. Titanium was chosen as a cathode material due to its high mechanical strength and chemical inertness. The electrodes were abraded using abrasive papers up to grit 4000. Then the Ti electrode was chemically polished in a $HF:HNO_3$ (1:3 by volume) mixture. Aluminum was electrochemically polished in $C_2H_5OH:HClO_4$ (4:1 by volume) electrolyte in potentiostatic regime at 20 V to a mirror finish. After polishing, both electrodes were thoroughly rinsed with deionized water.

Deionized water ($18 \times 10^6\ \Omega \cdot cm$) prepared from distilled water was used as an electrolyte for Al anodization. Preparation of the oxide film on Al was performed by two different ways: potentiostatic and high-voltage discharge methods. In the former, a constant voltage in the range from 1000 to 2000 V with 200 V step was applied to the electrodes using a Matsusada AU-3P400 high voltage power supply, and anodization was performed for different time intervals. The discharge method was another technique, in which a low-inductance 100-μF capacitor bank, with a measured internal resistance of $2.2 \times 10^3\ \Omega$, charged to the same voltages as in the potentiostatic mode, was then discharged to the cell. In order to prepare films with different thicknesses, the capacitor was discharged sequentially through the electrochemical cell between 1 and 30 times to the residual voltage of 100 V. The length of discharge varied in the range of 200–350 s depending on the film thickness. The thickness of the oxide film was controlled by two parameters: initial voltage and number of

*Electrochemical Society Student Member.
**Electrochemical Society Member.
[z]E-mail: lisenkov@ua.pt

discharges. In both methods, the resistance of the electrolyte plays a very important role. During anodization, the resistance of deionized water decreases from $8 \times 10^5$ Ω to $1 \times 10^5$ Ω, which could affect significantly the process. The electrolyte was replaced by fresh portions and all electrodes were carefully rinsed with deionized water after each two discharges or if the resistance of the water in the electrochemical cell, measured at the frequency of 1000 Hz, became lower than $6 \times 10^5$ Ω. To compare the properties of the obtained anodic oxides, anodization of Al was also performed in galvanostatic mode at a currant density of 10 mA/cm$^2$ followed by potentiostatic anodization in a 0.1 M ammonium pentaborate ($(NH_4)_2B_{10}O_{16}$) aqueous solution.

Determination of the potential distribution in the electrolyte plays an important role for this work. Theoretically, the potential drop can be estimated by dividing the applied potential by the distance between electrodes, but several parameters, such as potential drop on the electrode surfaces, edge effects and nonuniformity of the electrolyte will result in significant error. A better way is the measurement of the potential between the counter electrode and a neutral point in the electrolyte. In this case it is possible to determine non-uniformities of the electrolyte conductivity and avoid errors connected with processes on the electrode (the current between the counter electrode and tip is negligible). However, in this case the geometry plays a role (flat electrode vs. point tip), thus modelling and calculations become difficult. To avoid this problem two electrodes with platinum tips (10 μm in diameter) were placed in the electrolyte bulk between the cathode and the anode. In this case the geometry is not relevant (point tip vs. point tip). The distance between tips can be varied, and they can be placed in different parts of the electrolyte bulk to determine the field distribution. To determine the potential at the electrode surface, E, the cell geometry was taken as two parallel electrodes in high-resistance electrolyte. Over the main part of the surface the potential distribution is uniform. Due to the high resistivity of the electrolyte, the influence of the volume and distance to the walls of the cell can be ignored.

In highly resistive electrolytes, like deionized water, the anodic film thickness cannot be estimated by the applied voltage or by the charge passed through the cell during the discharge as in the case of the traditional anodization. Electrochemical impedance spectroscopy (EIS) is an effective tool to estimate the thickness of oxide films as well as to obtain information about their structure, for example, crystallinity and defects. In the present work, the thickness of the alumina films was evaluated using EIS measurements and confirmed by TEM. For the sake of comparison, thickness of the oxide was also estimated for the discharge-prepared films from the voltage vs time plots.

The EIS measurements were performed using a Gamry FAS2 Femtostat with a PCI4 Controller in a frequency range from $10^5$ to $10^{-2}$ Hz with 7 points per decade. The measurements were carried out at room temperature in a conventional three-electrode cell consisting of a mercury–mercurous sulfate reference electrode, a cylindrical platinum foil as a counter electrode and the working electrode with an exposed area of 1 cm$^2$. Impedance spectra were recorded by applying a 10 mV (RMS) sinusoidal perturbation at the open circuit potential. The cell was placed in a Faraday cage to avoid interferences with external electromagnetic fields. A 0.1 M ammonium pentaborate solution was used as the electrolyte for EIS measurements. At least five samples prepared in the same conditions were tested to ensure reproducibility of the results. The impedance plots were fitted using equivalent circuits by means of the Echem Analyst software from Gamry Inc.

Transmission electron microscopy (TEM) was carried out using a Hitachi H9000 microscope at an acceleration voltage of 300 kV. Electron transparent sections of the samples for TEM were cut with a Leica Reichert Supernova ultramicrotome. Investigation of the surface topography was performed using a Hitachi SU-70 SEM.

A Digital Instruments Nanoscope III atomic force microscope with conductive Pt-Cr probes (AppNANO) was used for SKPFM measurements. The obtained VPD values are presented versus the VPD measured for pure Ni as a reference.

## Results and Discussion

The results of Al anodization in deionized water under high-voltage potentiostatic and discharge modes with applied voltages between 1000 and 2000 V (Table I) showed that up to 1600 V in both cases oxide films with different properties can be obtained. For the first method the film thickness ranged from 5 to 12 nm (lower values are for lower voltages). Between 1000 and 1600 V the film was found to be uniform if anodization was performed during 1–2 minutes depending on the applied potential (Table I). In the case of the lower voltage range (1000–1200 V) it was possible to generate films up to 2 minutes of anodization. However, anodization for a period less than 1 minute resulted in formation of thin films, which thickness was comparable with natural oxide. In the case of the higher voltages (1400–1600 V) anodization was performed for 1 or 1.5 minute. The film thickness is limited by two parameters: the thickness of the natural oxide from the lower side and the breakdown of the film from the higher one. Longer anodization of the electrodes resulted in breakdown of the films. Application of potentials of 1800 and 2000 V in the potentiostatic method also resulted in breakdown of the film (Fig. 1A). For the discharge method, the film thickness was between 9 and 11 nm after 20 discharges and between 14 and 16 nm after 30 discharges for U = 1000–1200 V. When the voltage increased up to 1400–1600 V, the thickness rose to 15 nm after 10 discharges and 26 nm after 20 discharges. Under discharge mode the film still grew at 1800 V,

**Table I. Anodic film thickness, applied potential at the electrode after correcting for the ohmic drop in solution (E) and oxide growth parameters for aluminum anodized in deionized water at different applied voltages.**

| | | Potentiostatic method | | Discharge method | | |
|---|---|---|---|---|---|---|
| $U_0$/V | Time, min. | Thickness, nm | Number of discharges | Thickness, nm | Parameter $\beta \times 10^{-2}$ | E/ V |
| 1000 | 2 | 5 ± 3 | 20 | 9 ± 3 | 5,8 | 62 |
| | | | 30 | 14 ± 4 | | |
| 1200 | 2 | 6 ± 2 | 20 | 11 ± 3 | 5,3 | 75 |
| | | | 30 | 16 ± 4 | | |
| 1400 | 1,5 | 9 ± 4 | 10 | 14 ± 2 | 4,6 | 88 |
| | | | 20 | 24 ± 2 | | |
| 1600 | 1 | 12 ± 4 | 10 | 15 ± 2 | 4,4 | 100 |
| | | | 20 | 26 ± 2 | | |
| 1800 | - | Breakdown occurs from the beginning of the process. | 5–7 | 16 ± 2 | 4,9 | 115 |
| 2000 | - | Breakdown occurs from the beginning of the process. | - | Breakdown occurs after the first discharge. | | 130 |

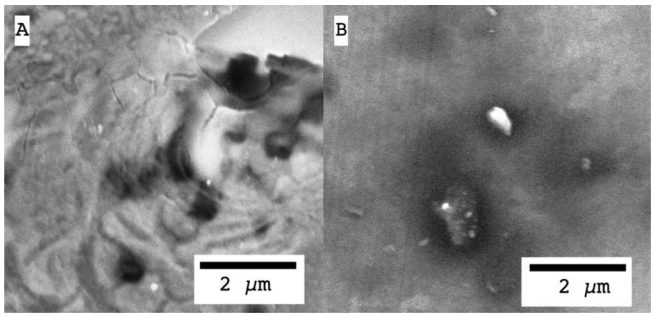


**Figure 1.** SEM images of the film breakdown on the oxides prepared at applied voltage of 2000 V by the potentiostatic (A) and discharged (B) methods.

reaching a maximum thickness of 16 nm after 5–7 discharges. At 2000 V the oxide film cannot be prepared by either methods, since breakdown occurred (Fig 1B). It should be noted, that in the case of the high-voltage potentiostatic method, the results show very poor reproducibility of breakdown events: even small fluctuations of parameters such as resistivity and amount of gases (oxygen and nitrogen) in the electrolyte, preparation and purity of the electrode surface can influence the process.

In contrast to the high-voltage discharge anodization in highly conductive electrolytes,[14–16] the process in deionized water cannot be explained by the same mechanism and has a significant difference in duration. As it was shown previously[15] in highly conductive electrolytes, such as 0.1 M ammonium pentaborate, the full discharge takes less than 0.5 s. In deionized water the applied voltage decays down to 100 V over a period of more than 100 s (Fig. 2). In deionized water, the measurements do not reveal the presence of plasma since besides the time elapsed, the current is low compared to previous works.[8,15] This is due to a large potential drop in the electrolyte bulk. In the conventional electrolyte, a plasma layer is formed on the anode surface and the oxide growth occurs in this layer.[8,15] Taking into account the growth rate of the films, their composition and structure, it can be suggested that the growth mechanism is similar to that obtained in potentiostatic method in conventional solutions where plasma is not similarly formed during film growth.[10]

In highly conductive solutions such as potassium hydroxide, an increase of the voltage to values higher than 100 V usually results in the formation of oxide film by PEO process, where a breakdown of the oxide followed by formation of plasma discharges and rapid growth of the porous anodic film occurs. However, in deionized water due to its high resistivity, no faradaic processes take place up to voltages of 1000 V. Further increment of the voltage to higher values leads to the formation of a thin oxide film. The growth of the oxide under such conditions is limited to the range of 1000 kV–1800 kV (Table I). At a certain voltage applied to the electrode, breakdown occurs only when a certain thickness of the oxide is reached. The same happens if the film is thick enough, but the voltage is lower than that required for filament formation (this voltage is the border between conventional anodization and PEO). In the case of potentiostatic oxidation, a constant potential is applied to the electrode, resulting in breakdown of the oxide when the thickness is enough (critical thickness) for the filament formation. Thus the thickness of the oxide is a limiting factor for dense oxide growth in high voltage anodization.

Electron microscopy (TEM and SEM) examination of the Al samples anodized by the potentiostatic method demonstrates a nonuniform oxide thickness distribution across the electrode surface (Figs. 3A, 3C). However, the films prepared by the high-voltage discharge method were found to be more uniform, without defects and fluctuations of the thickness (Figs. 3B, 3D). The oxide structure in the latter case is similar to the films previously prepared by powerful pulsed oxidation in ammonium pentaborate.[15]

SKPFM measurements (Fig. 4A) on the Al surfaces treated in deionized water by potentiostatic oxidation demonstrate nonuniform charge distribution on the surface: the Volta potential changed across the film, rising in the most defected zones (up to +10 mV vs. Ni) and decreasing in the intact areas (down to −9.7 mV vs. Ni). These results are a consequence of the nonuniform thickness of the oxide in the different areas.[10,15] It was also observed that applying a constant high voltage to the electrochemical cell with deionized water (for periods longer than 1–2 min) led to the appearance of breakdown processes on the surface.

In contrast to the case of potentiostatically prepared samples, SKPFM studies of the discharge prepared ones (Fig. 4B) showed low fluctuation of the Volta potential. Furthermore, the surface potential rose as the oxide film thickness increased (Fig. 4C), which is in a good agreement with the observations reported previously.[10] In the case of this method, as the voltage was applied through discharge of a capacitor, the conditions for film breakdown were not met. The voltage applied to the electrodes was lower than the minimum needed for breakdown of the oxide film. Thus, the pulse method seems to be effective for preparing impurity free thin anodic oxide films in highly resistive electrolytes.

The current flowing through an electrode depends on the total overpotential, η, which can be divided[17] in the following components:

$$\eta = \eta_{res} + \eta_{conc} + \eta_{act} \quad [1]$$

where $\eta_{res}$ describes the resistance overpotential resulting from the ohmic drop in the bulk of the electrolyte, $\eta_{conc}$ is the concentration overpotential which is related to mass transfer and $\eta_{act}$ is the activation overpotential. Due to the high resistivity of deionized water, the overpotential $\eta_{res}$ should be significantly higher in comparison to the conventional electrolytes. In order to estimate the $\eta_{res}$ value, two platinum tips were placed in the middle part of the cell and the

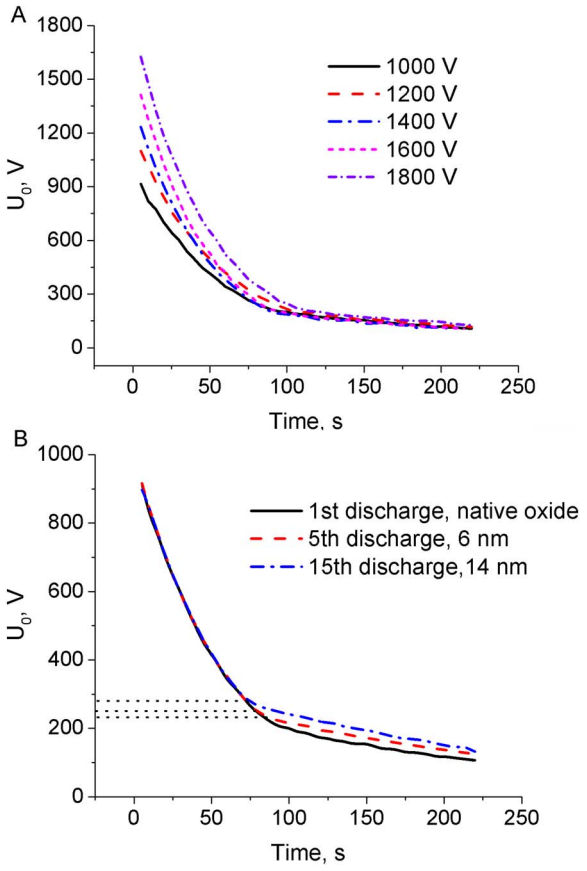


**Figure 2.** (A) Discharge plots for the aluminum anodization by discharge method at different potentials applied to the Al electrodes. (B) Discharge plots for the aluminum anodization by discharge method at 1000 V applied to the electrode covered with oxide film with different thicknesses.

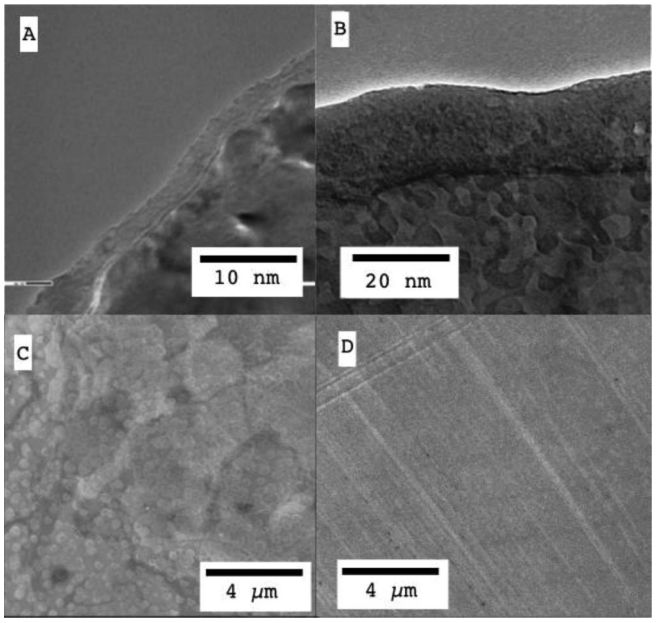


**Figure 3.** TEM cross sectional images (A, B) and SEM images (C, D) of aluminum oxide prepared by high-voltage potentiostatic (A, C) and discharge (B, D) methods.

voltage between them was measured. The distribution of the field in the bulk of the electrolyte was found to be uniform. The voltage available for the electrochemical process at the electrode for the initial voltage (time = 0):

$$E = U - \eta_{res} \quad [2]$$

can thus be estimated for the different applied potentials (Table I).

During the film growth some ions can be injected from the electrode into deionized water (even in small amount), resulting in local fluctuations of the solution resistance. In such regions, the electrode potential can change. The film growth occurs preferentially in these areas and the amount of charge used for the oxide film growth on the rest of the surface will be lower. In the case of the discharge method, the electrolyte can homogenize and the layer near the electrode can be restored due to the diffusion process between the discharges, resulting in more uniform film growth (Fig. 3).

To understand better the processes, that occur during the discharge anodization, the temporal evolution of the applied voltage was recorded (Figs. 2A, 2B). It was found that the discharge plot consisted of two parts, both of which can be described by the equation of capacitor discharge,[20] but with different resistance parameters:

$$U_t = U_0 \left( e^{-\frac{t}{\beta C}} \right) \quad [3]$$

where $U_t$ is the voltage after the time (s), $t$, from the beginning of the discharge, $U_0$ is the initial applied voltage, C is the capacitance and β is the resistance parameter. Both parts of the plots can be easily separated (Figs. 2A, 2B); the first part is highly influenced by the applied voltage and does not change with the oxide thickness, while the second part is displaced positively with the film thickness. Fitting the first part of the plots obtained at different applied voltages (Fig. 2A) using Equation 3, the parameter β can be estimated (Table I). In the second part, the faradaic process related to the oxide growth does not take place. The resistance between electrodes becomes significantly higher than the internal resistance of the capacitor and the only process that takes place, is self-discharge of the capacitor. Thus the film growth occurs only during the first period of the discharge and only depends on the initial voltage applied. The change in the voltage $U_0$ in the second part of the plot is linearly related to the thickness of the oxide formed. Thus it is possible to estimate the thickness of the film using the value of $U_0$ obtained from the fitting of this section of the discharge plot.

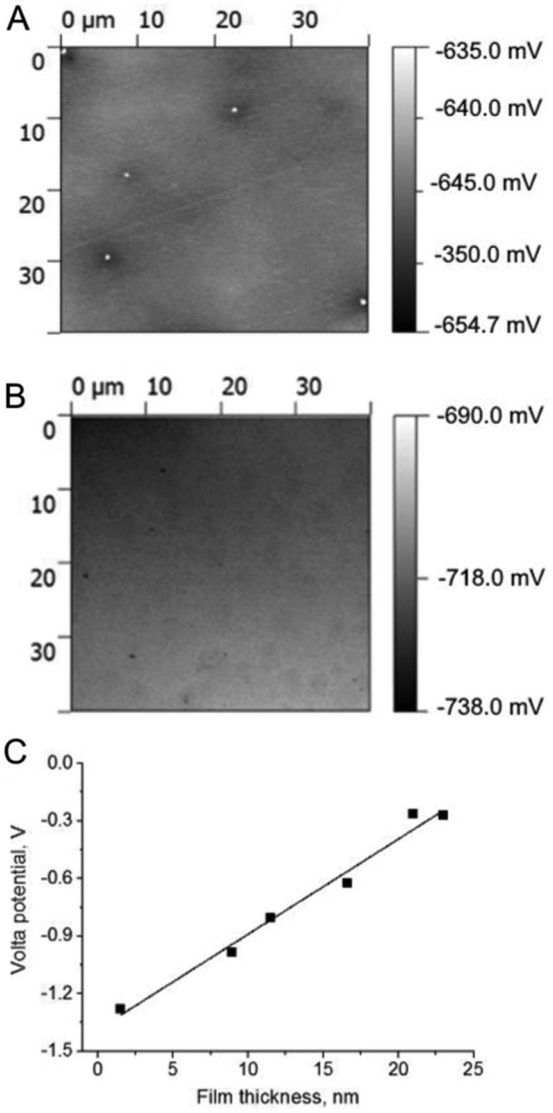


**Figure 4.** SKPFM images of aluminum samples with oxide thickness of 15 nm anodized by high-voltage anodization at applied voltage of 1600 V by potentiostatic (A) and discharge (B) methods. Volta potential difference versus thickness of the alumina films (different number of discharges) prepared by discharge method at an applied voltage of 1600 V (C).

Considering that the resistance parameter β is the same for all the films and very close to the values found for self-discharge of a capacitor ($2.2 \times 10^3$ Ω), it is possible to fit the second part of the plot using Equation 3 and reveal the parameter $U_0$. Estimated values of thickness were found to be in good agreement (less than 5%) with values in Table I obtained from EIS and TEM measurements.

EIS measurements of the anodized aluminum samples with an oxide thickness of 20 nm prepared by different methods are displayed in Fig. 5. The impedance values of the specimens prepared by high-voltage potentiostatic anodization (red dash line) are higher than those measured on the pure metal coated only by the native oxide (black solid line), but significantly lower in comparison with those prepared by the discharge method (dash dot green line) and conventional anodization in ammonium pentaborate solution (dot blue line). This last film was prepared for the sake of comparison by galvanostatic followed by potentiostatic anodization in solution of ammonium pentaborate. The advantages of the two-step method of anodization in comparison with pure galvanostatic are described in the literature.[10,18,19] Alumina films prepared in this way have been well studied and have a dense uniform structure.[10,15,18,19] According to the data from electron microscopy

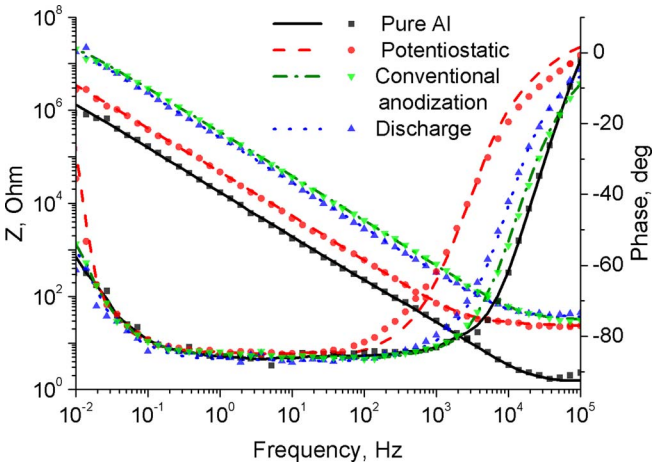


**Figure 5.** The impedance spectra recorded on as-polished Al with a native oxide film (black solid) and anodized aluminum in different conditions: Al with: 10 nm thick oxide prepared by potentiostatic method in deinonized water (red dashed line); oxide with thickness of 20 nm prepared by discharged method in deionized water (blue dotted line); oxide with thickness of 20 nm prepared by conventional anodization in ammonium pentaborate solution (green dash-dot). Experimental: points; Fitting: lines.

(Figs. 3B, 3D) and SKPFM (Fig. 4B), the topography of the films prepared by the discharge method is similar to those obtained by the conventional method.

The EIS spectra were fitted with a model, that consists of a constant phase element (CPE) in parallel with a resistor (R) corresponding to the oxide film, in series with an additional resistor element, which describes the electrolyte. The physical origin of the CPE has been widely discussed in the literature.[21] The impedance of the CPE, $Z_{CPE}$, depends on frequency, ω, according to the following equation:

$$Z_{CPE} = [Q(j\omega)n]^{-1} \quad [4]$$

where Q is a parameter numerically equal to the admittance ($|Z|^{-1}$) at $\omega = 1$ rad $s^{-1}$ and $n$ ($\leq 1$) is a power coefficient calculated as the ratio of the measured maximum phase angle and −90 degrees. The fitting of the spectra shows a high goodness ($<10^{-6}$ according to the Echem Analyst software) and low error ($< 1\%$ for all parameters) (Fig. 5). The value of effective capacitance, $C_{eff}$, was estimated by assuming a normal time-constant distribution through a surface layer by equation 5 derived by Hirschorn et al.:[22]

$$C_{eff} = Q^{1/n} R^{(1-n)/n} \quad [5]$$

The capacitances of all films prepared by the discharge method were higher by 5–10% than for the films prepared by conventional method. Capacitance, $C$, is related to thickness, $d$, by the following equation:

$$C = \varepsilon\varepsilon_0 \frac{S}{d} \quad [6]$$

where $S$ is the surface area and ε is the dielectric constant of the film and $\varepsilon_0$ is the vacuum permittivity ($8.854 \times 10^{-12}$ F · $m^{-1}$). Taking into account that the thickness of the samples prepared by both methods is similar (20 nm) and using Eq. 6 it was found that the aluminum oxide prepared by electrochemical oxidation of Al in deionized water has a dielectric constant of 9.3–9.9 with a mean value of 9.8. This value is slightly higher than the value obtained for the alumina (9.0) produced by conventional anodization.

## Conclusions

The formation of oxide films on the aluminum surface in deionized water was demonstrated in the current work by several methods: TEM, EIS, SKPFM. Images and properties of the films are in good agreement with those widely presented in literature for different conditions.

Discharge and potentiostatic methods were used to prepare thin oxide films on the surface of aluminum in deionized water. The maximum thickness of the anodic film increased with increasing the applied voltage, but at voltages over 1800 V oxide film cannot be prepared by either methods due to film breakdown. The maximum thickness of the film was 12 nm for the potentiostatic method and 26 nm for the discharge method. The alumina films obtained by the discharge method have also better uniformity in comparison to those prepared by the potentiostatic method. Both films have a dielectric constant comparable to that for the alumina films obtained in conventional electrolytes.

The data here obtained can be used as a reference for better understanding of the properties of anodic films prepared in conventional electrolytes. Further investigation allowing to obtain additional parameters, such as nature of defects, charge carriers concentration, etc., will be pursued.

## Acknowledgments

Financial support of FCT grants PTDC/CTM/72223/2006 and SFRH/BD/78628/2011 are gratefully acknowledged.

## References

1. L. P. H. Jeurgens, W. G. Sloof, F. D. Tichelaar, and E. J. Mittemeijer, *Journal of Applied Physics*, **92**, 1649 (2002).
2. J. Lausmaa, B. Kasemo, H. Mattsson, and H. Odelius, *Applied Surface Science*, **45**, 189 (1990).
3. P. S. Pawar, S. V. Gogawale, D. C. Kothari, A. M. Narsale, P. D. Prabhawalkar, and P. M. Raole, *Thin Solid Films*, **193**, 683 (1990).
4. B. Kasalica, M. Petkovic, I. Belca, S. Stojadinovic, and L. Zekovic, *Surf Coat Tech*, **203**, 3000 (2009).
5. M. Mokaddem, J. Tardelli, K. Ogle, E. Rocca, and P. Volovitch, *Electrochemistry Communications*, **13**, 42 (2011).
6. K. Ozawa and T. Majima, *Journal of Applied Physics*, **80**, 5828 (1996).
7. A. Cigada, M. Cabrini, and P. Pedeferri, *J Mater Sci-Mater M*, **3**, 408 (1992).
8. A. D. Lisenkov, S. K. Poznyak, M. F. Montemor, M. J. Carmezim, M. L. Zheludkevich, and M. G. S. Ferreira, *Journal of the Electrochemical Society*, **161**, D73 (2014).
9. G. T. Rogers, P. H. G. Draper, and S. S. Wood, *Electrochimica Acta*, **13**, 251 (1968).
10. K. A. Yasakau, M. L. Zheludkevich, S. V. Lamaka, and M. G. Ferreira, *J Phys Chem B*, **110**, 5515 (2006).
11. H. O. Jacobs, H. F. Knapp, S. Muller, and A. Stemmer, *Ultramicroscopy*, **69**, 39 (1997).
12. M. Yasutake, D. Aoki, and M. Fujihira, *Thin Solid Films*, **273**, 279 (1996).
13. B. S. Tanem, G. Svenningsen, and J. Mardalen, *Corrosion Science*, **47**, 1506 (2005).
14. S. K. Poznyak, D. V. Talapin, and A. I. Kulak, *Journal of Electroanalytical Chemistry*, **579**, 299 (2005).
15. A. D. Lisenkov, A. N. Salak, S. K. Poznyak, M. L. Zheludkevich, and M. G. S. Ferreira, *Journal of Physical Chemistry C*, **115**, 18634 (2011).
16. S. K. Poznyak, A. D. Lisenkov, M. G. S. Ferreira, A. I. Kulak, and M. L. Zheludkevich, *Electrochimica Acta*, **76**, 453 (2012).
17. E. Gileadi, *Angew Chem Int Ed Engl*, **106**, 839 (1994).
18. P. Skeldon, M. Skeldon, G. E. Thompson, and G. C. Wood, *Philosophical Magazine Part B*, **60**, 513 (1989).
19. A. Despić and V. P. Parkhutik, Electrochemistry of Aluminum in Aqueous Solutions and Physics of Its Anodic Oxide, in *Modern Aspects of Electrochemistry*, J. O'M. Bockris, R. E. W., and B. E. Conway ed., 1989, p. 401.
20. D. Landau, J. S. Bell, M. J. Kearsley, L. P. Pitaevskii, E. M. Lifshitz, and J. B. Sykes, *Electrodynamics of Continuous Media (2nd edition)*, Pergamon Press, 1980, 460.
21. P. Zoltowski, *Journal of Electroanalytical Chemistry*, **443**, 149 (1998).
22. B. Hirschorn, M. E. Orazem, B. Tribollet, V. Vivier, I. Frateur, and M. Musiani, *Electrochimica Acta*, **55**, 6218 (2010).